Veselin Milev, 4465873

Feasibility of Medium Span Steel- Timber Hybrid Bridges

A comparative study

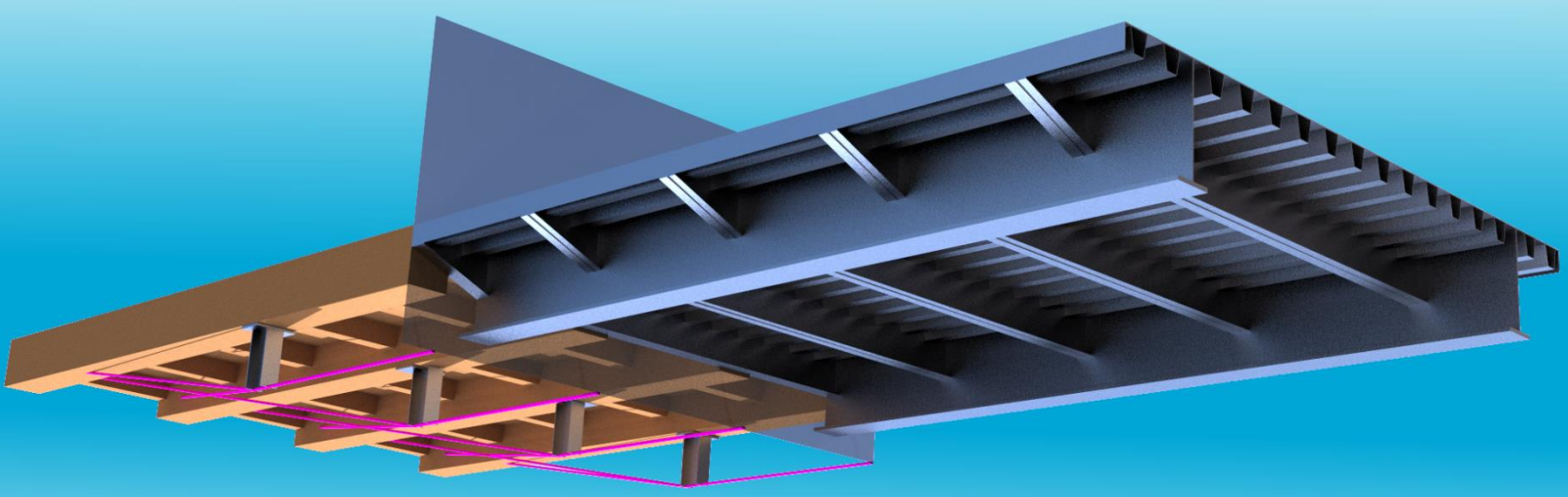

TU Delft

Iv-Infra

MSc Thesis

By

V. Milev, 4465873

in partial fulfilment of the requirements for the degree of

Master of Science

in Structural Engineering

at the Delft University of Technology,

to be defended publicly on Friday January 7, 2022 at 9:30 AM.

Thesis committee:

Prof. Dr. M. Veljkovic, TU Delft, Engineering Structures, Steel Structures

Dr.ir. G.J.P. Ravenshorst, TU Delft, Engineering Structures, Biobased Structures and Materials

Prof.dr.ir. J.W.G. van de Kuilen, TU Delft, Engineering Structures, Biobased Structures and Materials

Ir. B. van Aken, IV-Infra, Steel and Movable Bridges

Acknowledgments

The report presented marks the end of my studies as a structural engineering master student in Delft.

My gratitude goes out to all members of my thesis committee.
I would like to thank Prof. Veljkovic for providing me with academic insight through his feedback.
Much appreciation goes out to Dr. Ravenshorst for pulling me out of proverbial ruts and allowing me to continue the work on my thesis from perspectives I hadn't considered.
I would like to express my appreciation for Prof. van de Kuilen for his invaluable critical reviews of my work.
Ir. van Aken has my respect and admiration for enduring reading through and giving me feedback on numerous versions of my thesis.

The writing of this thesis, during these trying times of viral loads, has been made much more enjoyable by the company that took me under its wing, IV- Infra.
The team is full of knowledgeable people, who I've gotten to bond with over not only engineering topics, but a shared dislike of fish as a meal among other things.
Many thanks to you all for the useful, fun, and sometimes distracting conversations and many thanks to IV for providing me with a place among you and copious amounts of coffee.

To my family, thank you for your support during my entire academic carrier and before.
Without you, I wouldn't have gotten where I am today. My girlfriend, who somehow persevered through uncountable monologues about bridges, you've been nothing but impressive during the course of this thesis.

Lastly, I would like to express my gratitude towards the solid-state drive of my computer for enduring terabytes worth of write cycles. Many FE models were run, but you're still standing.

Vesko Milev

Leiden, January 2022

Abstract

Concrete and Steel are the materials with the largest market share in the construction industry and have been for a long time.
With environmental awareness increasing, timber is regaining popularity due to the potential for carbon neutral and even carbon negative construction.
Use of structural wood elements in bridges, however, is often limited to foot- and cycle bridges.
In this thesis, key aspects with regards to the design of heavy traffic bridges incorporating timber members are identified.

A fully steel bridge and an equivalent bridge, combining timber members with steel are designed within boundaries set by a case study. These designs are developed to a level sufficient for an adequate comparison of the bridges.
The basis on which the bridges are compared are laid out, followed by the conditions the bridges are subjected to. These are based on typical conditions found in an urban Dutch environment.

Analytic equations are automated, by way of python scripts, for the analysis and optimization of the steel bridge longitudinal dimensions under simplified ULS loading. After the optimization is complete, these initial bridge dimensions are verified with a 2D plate element model in SCIA engineer. The full loading for the bridge during utilization, save for accidental loading, is then modelled and the bridge dimensions are adapted in order to meet ULS, SLS, and fatigue conditions.

Several potential versions of a bridge with timber members are considered. Following this, a bridge with a mostly timber superstructure, supported by a self-anchored cable system is further worked out. For this, a SCIA model, with 1D elements and subjected to the same loads as its steel counterpart, is produced. The incompatible combination of 1D elements, thick cross sections, and surface loads is addressed by the use of connector elements (“dummy members”) and individual load panels per member.
After the global optimization of the bridge dimensions with regards to ULS and SLS, the connections are designed with a combination of detail 2D element FE models and analytic equations. The forces and support conditions of the connections follow from the global bridge design. A fatigue check is then run on the timber members of the bridge.

Subsequently, the durability and eco- costs of the bridges are computed. The data for the durability estimation of the steel bridge is based on experience within IV- Infra and the durability of the timber bridge is estimated using the RISE factor method. The eco- costs of the bridges are computed using the IDEMAT database.

The results from the analyses are discussed based on this.
Finally, aspects of relevance in the design of timber bridges are synthesized and recommendations for the application of bridges and further research are given.

Contents

1 Introduction

1.1 Problem Statement

The popularity of wood as a construction material is rising. This rise of material is well represented by new buildings using timber and timber based engineered materials in the Netherlands.
With regards to bridges, especially in the Netherlands, timber is mostly utilized in foot- and cycle bridges.
There is, however, a multitude of traffic bridges used in countries with a richer timber- building heritage.

This thesis aims to identify and critically discuss aspects of relevance in the design of (heavy traffic) bridges with timber members.

1.2 Research Questions

The purpose of the report is fulfilled through answering the following research questions:

- What are the specific limitations and challenges of timber in comparison to steel?
- What is the cause of these limitations?
- What incentives are there for the use of timber bridges as opposed to steel?

1.3 Methodology

In this report, engineering methods and guidelines are applied to design and optimize a conventional steel bridge superstructure and one combining timber and steel. The optimization of the designs is done to a level between predesign and definitive design; sufficient for a comprehensive comparison between the bridges.

Firstly, the grounds for this comparison are presented.
These are based on engineering guidelines and relevant state of art.
Boundary conditions, that need to be fulfilled by the bridges, are stipulated in the form of case study parameters.
In order to obtain base dimensions for the fully steel bridge version, analytic equations are used.
Python scripts are used to automate the formulas for quick iteration.
The steel bridge, with dimensions following from the analytic analysis, is then modelled using a plate element model in SCIA Engineer. The bridge dimensions are subsequently optimized, taking into account ULS, SLS, and fatigue loading.
Then wood as a material is discussed and a choice for the wood to be used in the bridge is made.
Afterwards, timber bridge design options are considered. From these, a choice is made for a design to further develop. The optimization of the members is done through a SCIA FE model with 1D elements, using the built- in Eurocode checking function.
From the global bridge model, forces needing to be transferred are obtained. On the basis of these forces, the connections are developed through a combination of finite element modelling and analytic equations. A fatigue verification, according to EC 5-2 is then performed on the bridge members.
Finally, the steel and steel- timber are compared on their estimated durability and sustainability.
The results from these comparisons and the performed structural analyses are discussed.
On the basis of this discussion, conclusions are drawn and recommendations for future research are given.

1.4 Report Outline

- Chapter 1 covers the global introduction; the problem statement, research questions and methodology.

- Chapter 2 sets the grounds for comparison of the bridges, along with the explanation of the guidelines used to obtain the needed results.

- Chapter 3 outlines the boundary conditions for the bridge in the form of a case study and details the loading conditions the bridge is subjected to. The exact norms and guidelines used are also listed in this chapter.

- Chapter 4 covers the analytic calculation of the longitudinal direction of the steel bridge for simplified ULS conditions

- In Chapter 5 the steel bridge dimensions from the previous chapter are verified against results obtained from a SCIA 2D element model and subsequently optimized for the full ULS and SLS loading conditions, as well as fatigue loading

- In chapter 6 the wood material is described and a choice for the wood species used in the timber bridge design is made. Different timber bridge design options considered. A select few of them are then roughly worked out to aid in the choice for the final timber bridge design.

- Chapter 7 addresses the bottlenecks following from the rough calculation performed in the previous chapter. After this, the final timber bridge concept is explained and globally calculated. This is then followed by the modelling and analysis of the full global bridge system for ULS and SLS. From the global model, forces on the connections are obtained, which are then calculated. Finally, a fatigue validation of the timber bridge members is performed.

- In chapter 8, the final steel and timber bridges are compared with regards to their durability prediction and sustainability. Additional designs, disregarding the boundary conditions and design choices previously adhered to, are produced and roughly analyzed. This is done in order to weigh the drawbacks inherent to the set conditions.
  The results obtained are then discussed.

- Chapter 9 presents the conclusions and provides recommendations for future work.

2 Basis for Comparison

In this chapter the grounds on which the bridges are to be judged are listed.
This is accompanied by the methods with which the quantification of different points will be performed.

2.1 Strength

The ultimate limit state describes the maximum loading under which a structure may not collapse. This loading is resisted by the strength of the structure.

Steel Bridge

The steel bridge strength is determined according to the Eurocodes relating to steel and steel bridges (EN 3 series). These norms offer sufficient depth to design a safe structure.

Timber Bridge

The design of the timber bridge with regards to ULS is mostly done according to the Eurocodes for the material (EN 5 series). Some design aspects are not covered within this series of norms.
For those cases, the book “Timber Engineering [1] by Blaß and Sandhaas, is referred to.

2.2 Serviceability

The serviceability limit state describes the maximum loading under which a structure is considered to be no longer usable due to it no longer being able to fulfil its purpose or it being uncomfortable to utilize. For bridges, within the design stage considered in this thesis, the SLS requirements relate to deflections of the bridge members.

Steel and Timber Bridge

There are no deflection limits set for steel bridges in the relevant Eurocode. Due to this, the steel bridge will be subjected to the same SLS requirements as its timber counterpart.

2.3 Fatigue

A structure may experience forms of failure when subjected to loads lower than those in the ultimate limit state if they are applied statically. The phenomenon of fatigue has a pronounced effect on bridges, which are subjected to traffic loading.

Steel Bridge

The steel bridge fatigue design is covered by EC 3-1-9 and the Dutch national annex to EC 3-2. This is done by S-N curves and detail categories. The combination of these relates the magnitude of stress cycles a detail experiences to the number of those cycles until the detail's failure.

Stress cycles with a low enough magnitude, entail no fatigue damage. The limit for the stress cycle magnitude is the "cut-off limit". If a detail experiences stress cycles of a single magnitude, a higher stress range may be applied without fatigue damage occurring. The limit range for this type of loading is called the "constant amplitude fatigue limit".

The damage resulting from different stress ranges can be summed up to obtain the total fatigue damage, following Miner's rule.

Timber Bridge

A validation method for the fatigue of timber is provided in EC 5-2. This method relies on stress cycles for relatively low magnitudes, under which the wood is assumed to be able to experience an infinite number of cycles. This is the endurance limit.

For stress ranges higher than the endurance limit, a reduction factor must be applied to the material strength for the type of loading. This reduced strength is then compared to the maximum stress resulting from the fatigue loading.
The reduction factor depends on the type of loading and the number of cycles, the bridge member or detail experiences, multiplied by its required service life.

2.4 Durability

The durability, in this specific context, relates to how well the bridges can resist degradation due to environmental influences. This is dependent on the resistance of the material and its exposure to adverse effects.

Steel Bridge

Steel degradation is given in loss of material due to rusting; this is normalized with corrosivity categories in ISO 12944-2. The corrosivity categories are dependent on the environment and correspond to a certain amount of material loss per a set unit of time. Steel preservation can be done painting, relevant paint system specifications are provided in ISO 12944-5.

The paint system used on the bridge will be chosen based on reference projects of IV- Infra.

Timber Bridge

The sensitivity of wood due to degradation depends on the wood species and its treatment.
This is shown in EN 350 in terms of durability classes. As stated, the durability is dependent on the environmental influences as well. For wood, the distinction between various levels of negative environmental effects is shown in EN 335 in terms of use classes.

Methods for quantification of timber exist as well. One of these is the RISE method, as defined in [9]. In it, the durability is separated into resistance and exposure. The resistance depends on the wood species and whether it is treated by preservation methods, its unit is days. The exposure depends on the macroclimate, which takes into account the amount of rainfall, the relative humidity and the temperature. It is quantified by a dose of exposure, which is given in days per year.
The resistance and exposure are related through tests on sample specimen.
The effects of detailing are taken into account by factors, which modify the exposure dose depending on the local conditions and detailing.

The RISE method will be used to predict the durability of the timber bridge details.

2.5 Environmental Impact

The Environmental cost indicator translates the impact a product or process has, with regards to the environment, to a monetary value.

The ECI can be calculated according to a multitude of impact categories as defined in EN 15804, annex C.

The eco- costs of a product or process are the monetary costs needed to compensate for its negative environmental effects, when invested in relevant measures [48].

The ECI can be a part of a larger life cycle analysis or LCA. In such an analysis, the impact of a product is assessed for its entire lifetime. The ECI of a structure can then account for stages A to D as defined in EN 15804 and illustrated in figure 1.1.

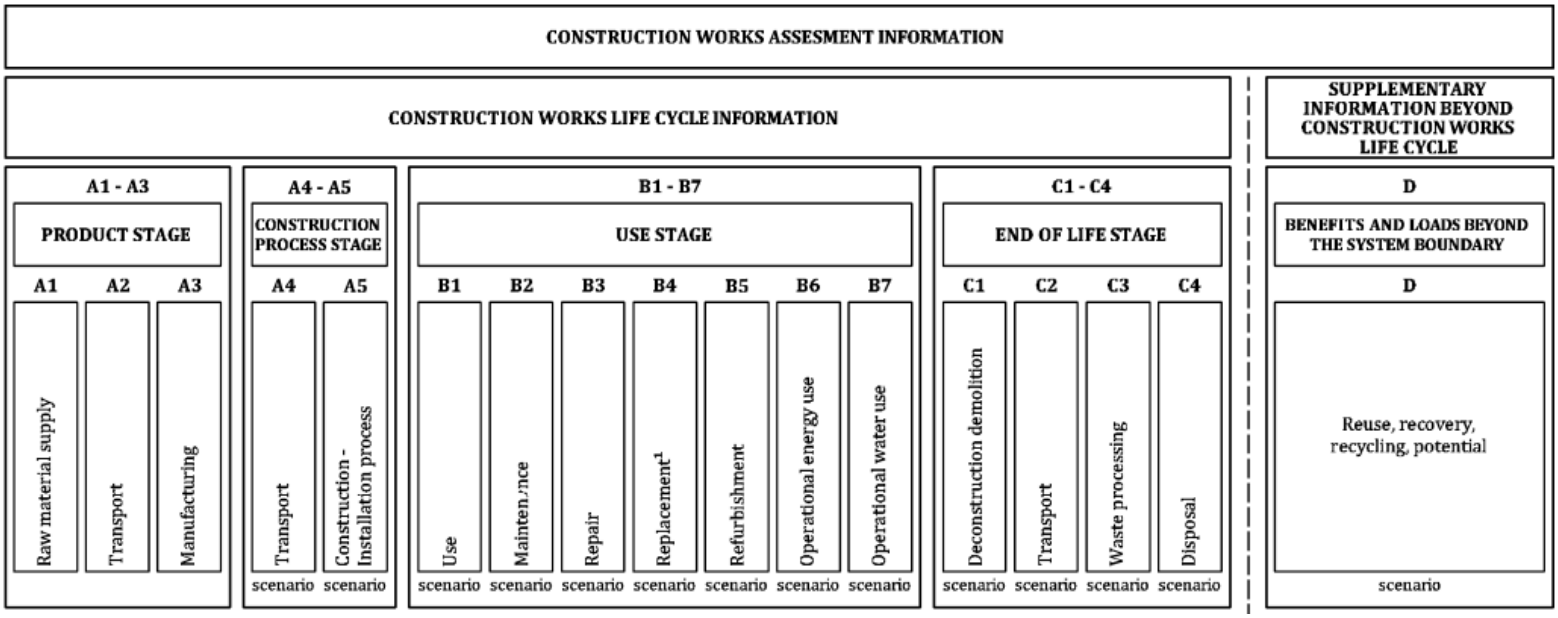

Figure 1.1: Defined stages in LCA, from [EN 15804, p.17]

2.5.1 Scope and Data

- The analysis will be limited to the production stage and use stage.
- Only the items that differ between the two designs will be compared (e.g., superstructure without the wearing layer)

- The IDEMAT 2022 database [48] will be used.
  IDEMAT is based on the EcoInvent 3.6 database. It is further expanded upon with research performed or reviewed by the sustainability platform of the Industrial Design Engineering faculty of TU Delft.
  The dataset includes eco costs for all impact categories from EN 15804, table C.1 and C.3

3 Case Study and Loading

In this chapter, the case study is detailed. Some background is provided with regards to the bridge location and the requirements for the timber following from it.

The norms and software, used in the case study, are be specified, alongside material properties and partial factors.

Loads and combination are then specified.

3.1 Case Study

The designs produced are based on a real- world river crossing and are therefore limited by the assumed conditions at the site.

3.1.1 Background

The main connections between the southern parts of the A4 and A44 highways currently run through highly built-up areas. In particular, the link of the two highways that goes through the city of Leiden (N206), is a substantial bottleneck for traffic. The “Rijnlandroute” project addresses this by way of creating a new connecting road and expanding of the current road system capacity.

A part of that expansion is the new “Trekvlietbrug” bridge along the N206.

The “Trekvlietbrug”, in its current, movable form, is to be decommissioned and replaced with a non-movable higher bridge. The bridge spans 25 meters and is subjected to heavy traffic.

In its current shape, the bridge consists of 4 traffic lanes and additional cycle and footpaths on either side. It has a width of 20 meters.

As a part of a new nation-wide policy, Leiden will no longer allow trucks with a fossil fuel powered engines within the city, starting in the year 2025. This is expected to increase the need for supplying businesses in the city by waterway. Currently there is discussion about the form of the new bridge, in particular its clearance height is highly debated.

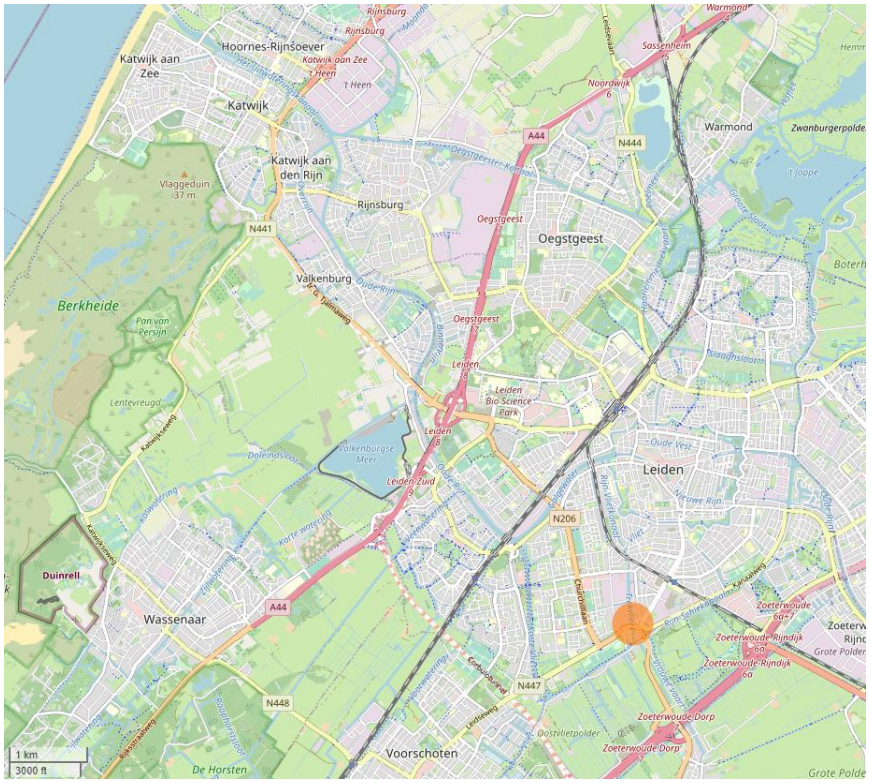

Figure 3.1: Location "Trekvlietbrug", from openstreetmap.org

Figure 3.2: Current "Trekvlietbrug", from maps.google.com

Figure 3.3: Current "Trekvlietbrug", from nl.wikipedia.org

3.1.2 Bridge Requirements and Boundary Conditions

The case study will be limited to the superstructure of the bridge.

- Developed as new. No footpaths, only theoretical traffic lanes in order to provide maximum flexibility for potential changes of layout in future.
- Span is taken equal to the river bank to river bank distance, 25 meters. Currently the supports extend into the waterway, this form of the bridge is disregarded.
  The larger span is to allow for higher waterway traffic.
- Total width is currently 20 meters. This is to be split into two bridges with a width of 10 meters. An efficient steel bridge for a 25-meter span is a girder bridge. A dual girder bridge is to be applied as opposed to a multi girder one. This is done in order to avoid rising of the middle girder(s) due to thermally imposed loads or necessitate hinged connections in the transverse direction of the structure.
- A limited construction depth of 2 meters for the superstructure. This depth is set to limit the access road inclination and accommodate the waterway traffic.
- The bridge has a design service life of 100 years and is within consequence class 3.

3.1.3 Environment

Steel Design

The environmental influences need to be considered in the design of the bridge variants.
Global and local climate effects are of importance.
Steel directly exposed to the elements is classified in corrosivity category C3, according to ISO 12944-2; this constitutes a loss of material of 2,5 to 5 mm per 100 years for unprotected steel.

Timber Design

The use class of wood according to EN 335 can be considered to be either class 2 or 3. Class 3 will be assumed as more conservative.
The annual exposure dose for the Netherlands, according to the Durable Timber bridges guidelines [9], is 43 days.

3.1.4 Traffic category

The bridge is a part of a trunk road (N weg in Dutch). According to the Dutch NA to 1991-2, it falls within category 2, which entails a yearly heavy lorry traffic, $N_{obs,a,sl}$ of $0{,}5 * 10^6$.

3.1.5 Norms Used

The bridge variants will be designed according to the following norms:

- NEN-EN 1990: Eurocode: Basis of structural design & Dutch NA to EN 1990
- NEN-EN 1991-1-1: Actions on structures- Part 1-1: General actions- densities, self-weight, imposed loads for buildings & Dutch NA to EN 1991-1-1
- NEN-EN 1991-1-4: Actions on structures- Part 1-4: General actions- Wind actions & Dutch NA to EN 1991-1-4
- NEN-EN 1991-1-5: Actions on structures- Part 1-5: General actions- Thermal actions
- NEN-EN 1991-2: Actions on structures- Part 2: Traffic loads on bridges & Dutch NA to EN 1991-2
- NEN-EN 1993-1-1: Design of steel structures – Part 1- 1: General rules and rules for buildings & Dutch NA to EN 1993-1-1
- NEN-EN 1993-1-5: Design of steel structures- Part 1-5: Plated structural elements & Dutch NA to EN 1993-1-5
- NEN-EN 1993-1-8: Design of steel structures- Part 1-8: Design and calculation of connections & Amendments and Corrections
- NEN-EN 1993-1-9: Design of steel structures- Part 1-9: Fatigue
- NEN-EN 1993-2: Design of steel structures- Part 2: Steel bridges & Dutch NA to EN 1993-2
- NEN-EN-ISO 12944-2: Paints and varnishes- Corrosion protection of steel structures by protective paint systems- Part 2: Classification of environments
- NEN-EN-ISO 12944-5: Paints and varnishes- Corrosion protection of steel structures by protective paint systems- Part 5: Protective paint systems
- NEN-EN 1995-1-1: Design of timber structure- Part 1: Common rules and rules for buildings
- & Dutch NA to EN 1995-1-1
- NEN-EN 1993-2: Design of timber structures- Part 2: Bridges
- NEN-EN 1993-1-11: Design of steel structures- Part 1-11: Design of structures with tension components
- NEN-EN 12385-10: Steel wire ropes- Safety: Spiral ropes for general structural applications
- NEN-EN 335: Durability of wood and wood- based products- Use classes: definitions, application to solid wood and wood- based products
- RISE Durable Timber Bridges Final Report and Guidelines
- NEN-EN 14080: Timber structures- glued laminated timber and glued solid timber- Requirements

3.1.6 Software Used

- SCIA Engineer 20.0.2028 for FEM modelling
- Jupyter Notebook (Python 3) for a quick, iterative implementation of analytical formulas in a python coding environment
- Autodesk Autocad 2020 for drafting, 3D modelling, and quick determination of (effective) cross section properties
- MatrixFrame, for quick calculation of internal forces of statically (in)determinate structures.

3.1.7 Material Properties

Steel Variant

S355 steel is to be used for the steel design, material properties are taken according to EN 1993-1-1.

- Modulus of Elasticity E = 210.000 MPa
- Shear Modulus G = 81.000 MPa
- Elastic Poisson ratio ν = 0,3
- Linear thermal expansion coefficient α = $\frac{12*10^{-6}}{K}$ (For $T \leq 100\ °C$)
- Ultimate tensile strength f_u, for $t \leq 40\ mm$ = 490 MPa
- Ultimate tensile strength f_u, for $40\ mm < t$ = 470 MPa
- Yield strength f_y, for $t \leq 40\ mm$ = 355 MPa
- Yield strength f_y, for $40\ mm < t$ = 335 MPa

Timber Variant

GL 26h according to EN 14080 is to be used for the timber design.

- Bending strength $f_{m,g,k} = 26\ MPa$
- Tensile strength $f_{t,0,g,k} = 20{,}8\ MPa, f_{t,90,g,k} = 0{,}5\ MPa$
- Compression strength $f_{c,0,g,k} = 26\ MPa, f_{v,90,g,k} = 2{,}5\ MPa$
- Shear strength $f_{v,g,k} = 3{,}5\ MPa$
- Rolling shear strength $f_{r,g,k} = 1{,}2\ MPa$
- MOE $E_{0,g,mean} = 12100\ MPa, E_{90,g,0} = 10100\ MPa, E_{90,g,mean} = 300\ MPa, E_{90,g,05} = 250\ MPa$
- Shear modulus $G_{mean} = 650\ MPa, G_{g,05} = 540\ MPa$
- Rolling shear modulus $G_{r,g,mean} = 65, G_{r,g,05} = 54$
- Density $\rho_{g,k} = 405, \rho_{g,mean} = 445$

3.1.8 Material factors

Steel

Partial factors are gathered from the national annex to EN 1993-2.
Factors with respect to fatigue must be assumed according to safe life; high consequence for the main structure and low consequence for the OSD stiffeners, deck plate and the connection between stiffeners and cross beam. These factors follow from the Dutch NA to 1993-1-9.

- For exceeding yield strength $\gamma_{M0} = 1{,}0$
- For instability resistance $\gamma_{M1} = 1{,}0$
- For tension until rupture and connections in ULS: $\gamma_{M2} = 1{,}25$
- For slip resistance in ULS and SLS respectively $\gamma_{M3} = 1{,}25$, $\gamma_{M3,ser} = 1{,}10$
- Others $\gamma_{M4}, \gamma_{M5}, \gamma_{M6,ser} = 1{,}0$
- Pretensioned HSS bolts $\gamma_{M7} = 1{,}10$
- Fatigue $\gamma_{Mf} = 1{,}35 \text{ for main load carrying structure, } \gamma_{Mf} = 1{,}15 \text{ for OSD}$

Timber

Partial factors for timber in use in bridges are gathered from EN 1995-2.

- Service Class 3
- $K_{mod} = 0{,}9$, according to EN 1995-1-1, 3.1.3; dependant on load duration and climatic conditions, wind and traffic loads assumed as instantaneous.
- $K_{sys}\ (\text{Only for deck/ secondary main beams}) = 1{,}1$ can be set to a higher factor (up to 1,2 for deck) due to a high number of lamellas being subjected to actions. In a conservative assumption it is set to 1,1
- $K_{def} = 2$, no increase due to installation near fibre saturation point
- Material factor for Glulam $\gamma_M = 1{,}25$
- Material factor for Connections $\gamma_M = 1{,}3$
- Material factor for Fatigue $\gamma_{M,fat} = 1{,}0$

3.2 Loads and Combinations

The different bridge designs will be compared with regards to actions during their service life. Loads during execution will not be accounted for. Exceptional loads, such as explosions and collisions with ships also fall out of the scope of this study.

3.2.1 Permanent Loads

Self- weight

- Steel: 78,5 kN/m^3, conservatively following from EN 1991-1-1, table A.4
- GL 26h: 445 $kg/m^3 \approx$ 4,37 kN/m^3, from EN 14080, table 5

Dead loads

Dead loads, such as railings and sidewalks, are considered by assuming an oversized layer (15 cm) of waterproof asphalt.

- Waterproof asphalt: 25 kN/m^3, from EN 1991-1-1, table A.6
  Thus $25 * 0{,}15 = 3{,}75\ kN/m^2$

3.2.2 Variable Loads

Traffic Loads- Load Model 1

For a bridge loaded by less than 2 million heavy lorries per year, the Dutch NA to EN 1991-2 specifies reduction factors to the given loads, these however are negligible for bridges loaded by 0,5 million lorries per year and will therefore be taken into account.

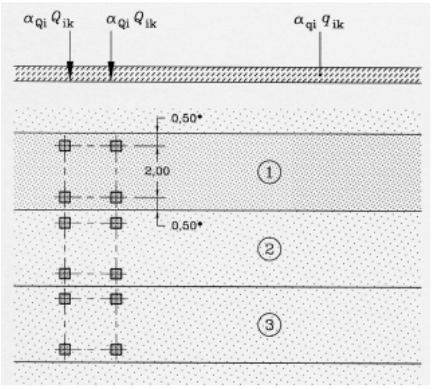

Positie	Tandemstelsel *TS*	Gelijkmatig verdeelde belasting (GVB)
	Aslast Q_{ik} (kN)	q_{ik} (of q_{rk}) (kN/m^2)
Rijstrook nummer 1	300	9
Rijstrook nummer 2	200	2,5
Rijstrook nummer 3	100	2,5
Overige rijstroken	0	2,5
Resterende oppervlakte (q_{rk})	0	2,5

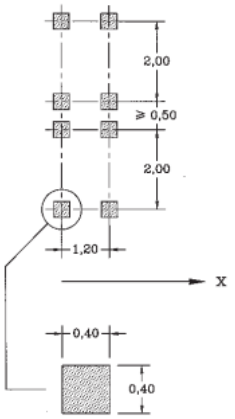

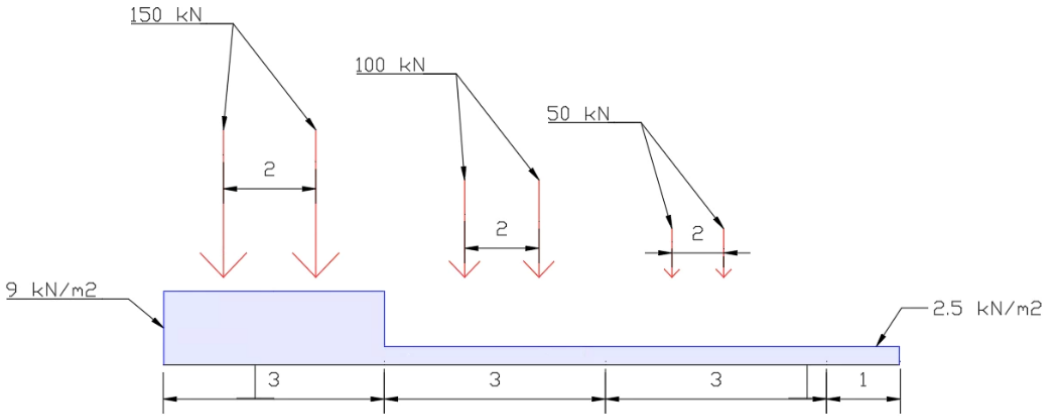

Figure 3.4: Load Model 1 (EN 1991-2) applied on the bridge

Traffic Loads- Load Model 2

Load model 2 consists of a single tandem system or a single wheel, where relevant, with a tire size of 0,35 x 0,6 m and an axle load of 400 kN, with the long direction of the tyre patch perpendicular to the longitudinal direction of the bridge.

The load is applied at a random location on the roadway.

This model is used for local verifications only.

Braking and acceleration forces

Horizontal braking and acceleration forces are done according to EN 1991-2. The national annex limits the value to a maximum of 800 kN, as opposed to the 900 kN, following from the norm.

$$Q_{lk} = 0{,}6\alpha_{Q1}(2Q_{1k}) + 0{,}10\alpha_{q1}q_{1k}w_l L$$

$$180\alpha_{Q1}\ (kN) \leq Q_{lk} \leq 900\ (kN)$$

$$0{,}6 * 2 * 300 + 0{,}10 * 9 * 3 * 25 = 427{,}5\ kN$$

Wind Loads

Wind loads are determined according to EN 1991-1-4 and the NA to the norm.

- Wind area II, built- up area
- Height of bridge: 3 meters
- Extreme wind pressure: 0,58 kN/m^2
- Span to depth ratio: 5, assuming the maximum height of 2 meters
- Structural factor ($c_s c_d$): 1
- Force coefficient ($c_{fx,0}$): 1,3
- Wind pressure perpendicular to span: $1{,}3 * 1 * 0{,}58 \approx 0{,}75\ kN/m^2$
- Coefficient for wind in z- direction ($c_{fx,0}$): 0,55
- Wind pressure in downward direction: $0{,}55 * 1 * 0{,}58 = 0{,}32\ kN/m^2$
- Wind pressure in longitudinal direction: $0{,}40 * 0{,}75 = 0{,}3\ kN/m^2$

Thermal Actions

Temperature actions on (steel) bridges have two possible effects:

- A constant temperature change in the entire bridge structure. This results in an extension or contraction of the structure, which must be accommodated by the supports and the interfaces between the bridge and the road it connects.
  If this extension is not restrained, no stresses will result from it.
  This effect will therefore be neglected.
- A difference of temperature over the depth of the structure.
  EN 1991-1-5 provides two approaches to consider such temperature effects: linear and non-linear.
  The linear approach, which considers the deck as having a temperature higher or lower than the rest of the structure, will be applied.

Following from tables 6.1 and 6.2 from EN 1991-1-5, the following temperature differences are obtained.

During heating up

$$\Delta T_{M,heat}\,(°C) * \; k_{sur} = 18 * 0{,}7 = 12{,}6°C$$

During cooling down

$$\Delta T_{M,heat}\,(°C) * \; k_{sur} = 13 * 1{,}2 = 15{,}6°C$$

Traffic Loads- Fatigue Load Model 3

FLM 3 is a single lorry model, which is used to obtain the minimum and maximum stress on elements and details as opposed to multiple stress spectra.
The axle loads are equal to 120 kN and are spaced as shown in figure 3.5

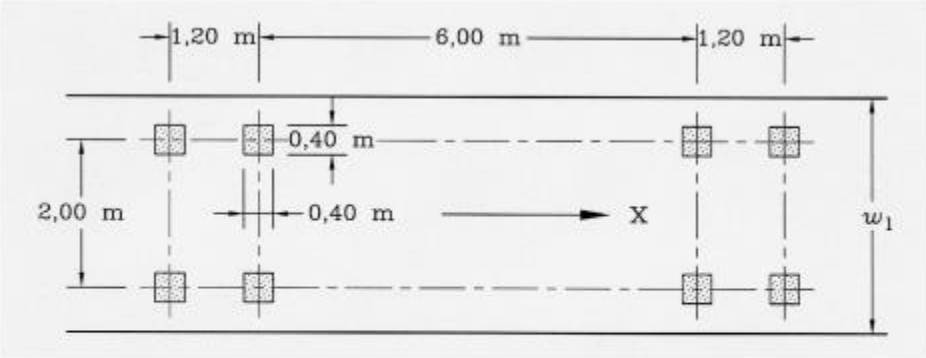

Verklaring

w_l : breedte van de rijstrook
X : lengterichting van de brug

Figure 3.5: FLM 3, wheel dimensions and spacings

Fatigue load models 1 through 4 must be multiplied by a magnification factor ($\Delta\varphi_{fat}$) in the vicinity of expansion joints. According to the national annex to EN 1991-2, 4.6.1, this factor equals 1,15 for high quality road surfaces. It must be applied when one or more axles are within 6 meters of the expansion joint.

3.2.3 Combinations

Load Combinations are assembled according to the EN 1990 and its Dutch NA.

For the ULS, the least favourable of equation 6.10a and 6.10b, from EN 1990, must be applied.

$$\sum_{j\geq 1}\gamma_{G,j}G_{k,j}\text{"+"}\gamma_P P\text{"+"}\gamma_{Q,1}\psi_{0,1}Q_{k,1}\text{"+"}\sum_{i>1}\gamma_{Q,i}\psi_{0,i}Q_{k,i} \qquad (6.10a)$$

$$\sum_{j\geq 1}\xi_j\gamma_{G,j}G_{k,j}\text{"+"}\gamma_P P\text{"+"}\gamma_{Q,1}Q_{k,1}\text{"+"}\sum_{i>1}\gamma_{Q,i}\psi_{0,i}Q_{k,i} \qquad (6.10b)$$

Figure 3.6: equations 6.10 a and b, from [EN 1990]

The Dutch national annex gives the following γ factors for the abovementioned equations.

Tabel NB.16 – A2.4(B) — Belastingsfactoren voor wegverkeersbruggen en bruggen voor langzaam verkeer en voetgangers- en fietsbruggen STR/GEO) (groep B)

Gevolgklasse	β	G			Verkeer (met $\psi = 1$)	Overig veranderlijk (met $\psi = 1$)
		$\gamma_{G,j,sup}$		$\gamma_{G,j,inf}$		
		6.10a	6.10b (incl. ξ)	6.10a en 6.10b		
CC1	3,3	1,20	1,10	0,9	1,20	1,35
CC2	3,8	1,30	1,20	0,9	1,35	1,5
CC3	4,3	1,40	1,25	0,9	1,5	1,65

$\gamma = 0$ voor gunstig werkende veranderlijke belastingen

Voor γ_P zie de aanbevelingen in de desbetreffende materiaalgebonden Eurocodes 1992 t/m 1999.

Voor de berekening van het effect van ongelijkmatige zettingen geldt dat $\gamma_{G,set} = 1{,}20$ in het geval van een lineaire berekening en $\gamma_{G,set} = 1{,}35$ in het geval van een niet lineaire berekening. Gunstig werkende zettingsverschillen worden niet in rekening gebracht. De grootte van de zettingen is bepaald op basis van de karakteristieke belastingscombinatie en de karakteristieke waarden voor de grondeigenschappen.

OPMERKING De factor K_{Fi} volgens B 3.3 is in de waarden van γ verwerkt; voor de zettingsberekening blijft de betrouwbaarheidsdifferentiatie achterwege.

Table 3.1: NB.16- A2.4(B), from [EN 1990, NA]

From preliminary calculations, it is evident that equation 6.10b leads to higher loads compared to 6.10a, therefore this is the equation to be applied.

The Dutch annex synthesizes all Ψ factors, that need to be applied to equation 6.10b, in table 3.2.

Tabel NB.19 — ψ-waarden voor belastingscombinaties STR – wegverkeersbruggen en bruggen voor langzaam verkeer

Belasting	Belastingscombinaties												
	gr1a	gr1b	gr2	gr3	gr4	gr5	W [b]		T [b]		S	A1 [a,b]	
TS	1	0	0,8	0	0	0,8	0,8	0,64	0,8	0,64	0	0,8	0,64
UDL	1	0	0,8	0	0	0,8	0,8	0,64	0,8	0,64	0	0,8	0,64
Enkele as	0	1	0	0	0	0	0	0	0	0	0	0	0
Horizontale belasting	0,8	0	1	0	0	0,8	0,64	0,8	0,64	0,8	0	0,64	0,8
Voetpaden	0,4	0	0,4	1	1	0	0,32	0,32	0,32	0,32	0	0,32	0,32
Mensenmenigte	0	0	0	0	1	0	0	0	0	0	0	0	0
Bijzondere voertuigen	0	0	0	0	0	1	0	0	0	0	0	0	0
Wind [c] F_{wk}	0,3	0	0,3	0	0	0,3	1	1	0,3	0,3	0	0	0
F^*_w	1	0	1	0	0	1	0	0	0	0	0	0	0
Temperatuur	0,3	0	0,3	0	0,3	0,3	0,3	0,3	1	1	0	0	0
Sneeuw	0	0	0	0	0	0	0	0	0,	0	1	0	0
Impact op of onder de brug	0	0	0	0	0	0	0	0	0	0	0	1	1
Aardbevingsbelasting	0	0	0	0	0	0	0	0	0	0	0	0	0

[a] A1 = aanrijding op of onder de brug en aanvaring.

[b] Bij deze combinaties is in eerste kolom gr1a × Ψ_0 en de tweede kolom gr2 × Ψ_0 .Voor de definitie van de groep verkeersbelasting gr1a en gr2 zie NEN-EN 1991-2+C1.

[c] Waar verkeersbelasting op (delen van) de brug aanwezig is, mag zijn gerekend met F^*_w in plaats van F_{wk}.

Table 3.2: NB.19, from [EN 1990, NA]

4 Steel Bridge Design Predesign – Hand Calculation

In this chapter, the bridge structure, in longitudinal direction, will be calculated according to the Eurocode. This will be done in a simplified manner, after which the results of this simplified calculation will be verified against those from a SCIA FE model.

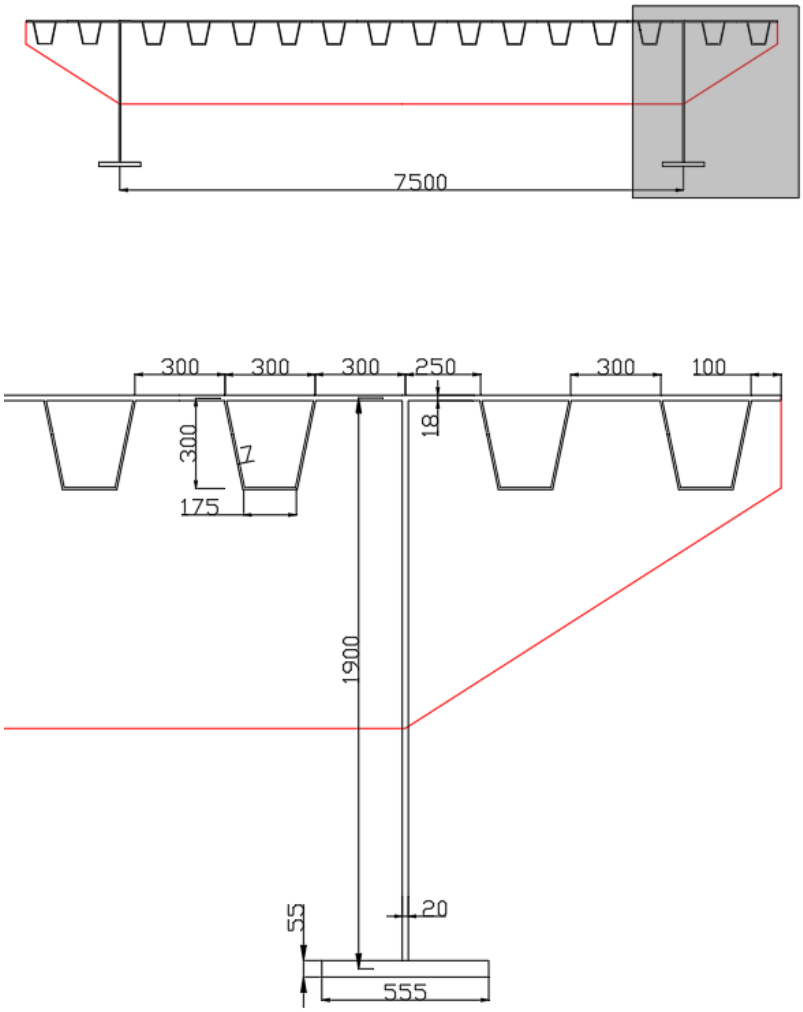

Figure 4.1: Steel Bridge Dimensions

A plated steel girder bridge can be seen as a large beam on global scale in the longitudinal direction. The bottom flanges of the main girders act as the bottom flanges of the beam, while the deck and trough combination act as the top flange.

On local scale, a single trough and the deck width belonging to it act as a beam, carrying the load from cross girder to cross girder.

In the transverse direction, loads are carried by the cross girder. The deck further acts as the top flange in the transverse direction.

4.1 Load Action Determination Analytic Calculation

4.1.1 Dead Loads

- Steel self-weight: $10{,}57\ m^3 * 78{,}5 \approx 813{,}67\ kN => 813{,}67 * \gamma_G = 813{,}67 * 1{,}25 = 1017{,}09\ kN$
  For the purpose of predesign the self-weight will not be accounted for. Instead of this, a lower UC will be aimed for during the optimization.
- Asphalt and other dead loads: $3{,}75 * \gamma_G = 3{,}75 * 1{,}25 = 4{,}6875\ kN/m^2$, when negatively affecting the analysed member. $3{,}75 * \gamma_G = 3{,}75 * 0{,}9 = 3{,}375\ kN/m^2$, when positively affecting the analysed member.

4.1.2 Vertical Traffic Loads

- Concentrated wheel loads:
  Lane 1: $150 * \gamma_Q = 150 * 1{,}5 = 225\ kN$
  Lane 2: $100 * \gamma_Q = 100 * 1{,}5 = 150\ kN$
  Lane 3: $50 * \gamma_Q = 50 * 1{,}5 = 75\ kN$
- Distributed loads:
  Lane 1: $9 * \gamma_Q = 9 * 1{,}5 = 13{,}5\ kN/m^2$
  Rest of deck: $2{,}5 * \gamma_Q = 2{,}5 * 1{,}5 = 3{,}75\ kN/m^2$

4.1.3 Load Effects

For the transverse load distribution, through the cross girders, a linear influence line, for the left girder, is assumed, as shown in figure 4.2.

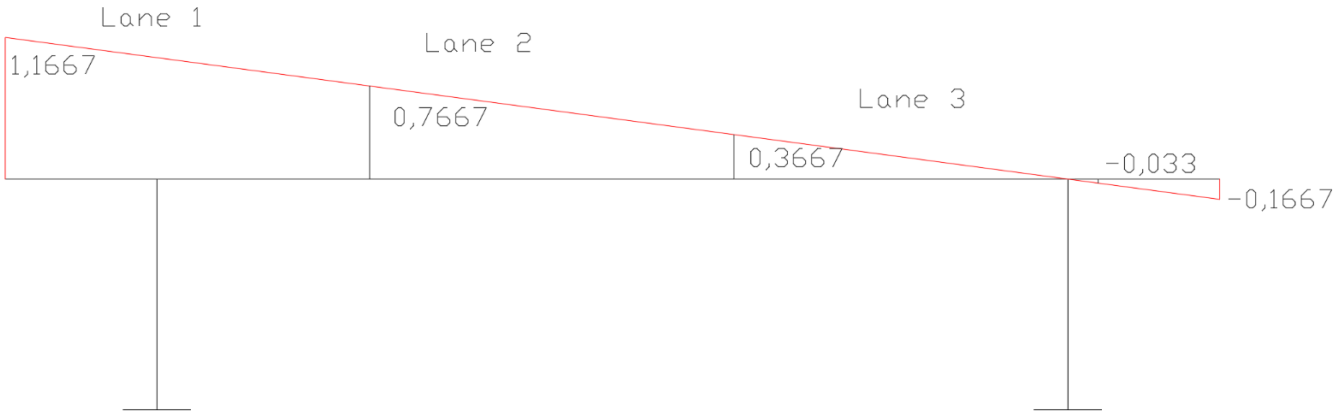

Figure 4.2: Transverse influence line

The global longitudinal bridge system is simply supported, maximum moments will occur in mid span, when the structure is loaded there and maximum shear forces will occur close to the supports.

Naturally, in reality, the exact stress distribution will depend on the placement of the cross girders and their stiffness, this will not be accounted for in the hand calculation.

Total forces on the left girder are as follows:

Concentrated Wheel Loads:

Front and rear axle have the same value, which is:

$$225 * 1{,}1 + 225 * 0{,}833 + 150 * 0{,}7 + 150 * 0{,}433 + 75 * 0{,}3 + 75 * 0{,}033 = 629{,}85\ kN$$

Distributed Load is:

$$0{,}9667 * 13{,}5 * 3 + 0{,}38 * 3{,}75 * 6{,}25 + 0{,}5833 * 4{,}6875 * 6{,}25\ - 0{,}0833 * 1{,}25 = 65{,}04 \frac{kN}{m}$$

Global Effects

The abovementioned concentrated loads are placed close to the supports to obtain the maximum shear stress and in mid span to obtain the maximum global bending moments.

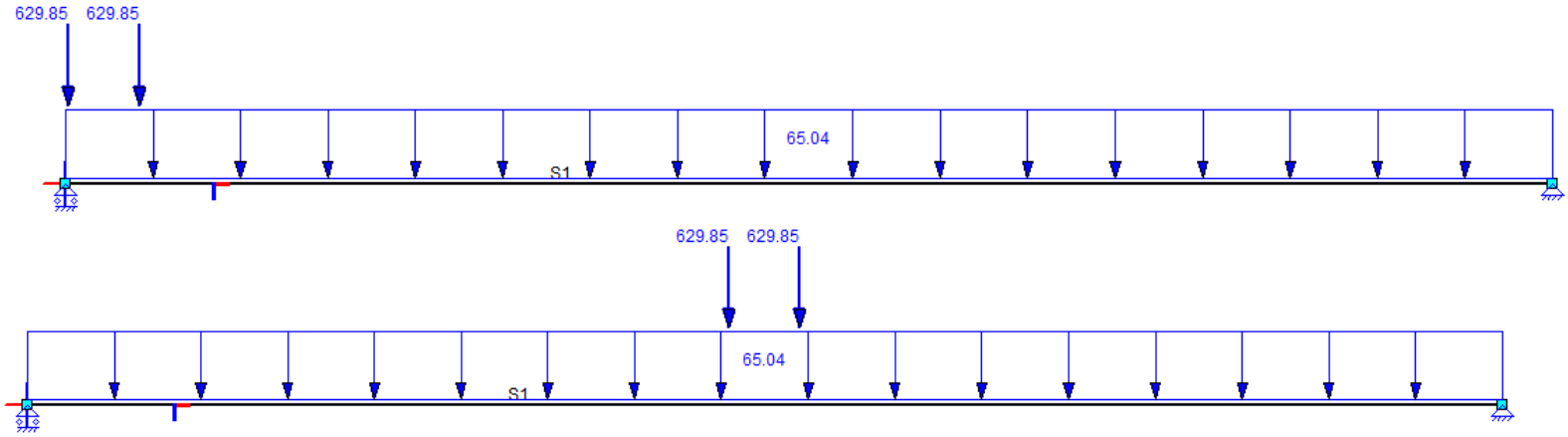

Figures 4.3a.and 4.3b: Load placement for maximum global shear and bending moment

With the concentrated loads placed in mid-span, the resulting moment is $Med = 12.576{,}47\ kNm$

With the concentrated loads close to the supports, the resulting shear force is $Ved = 2.036{,}70\ kN$

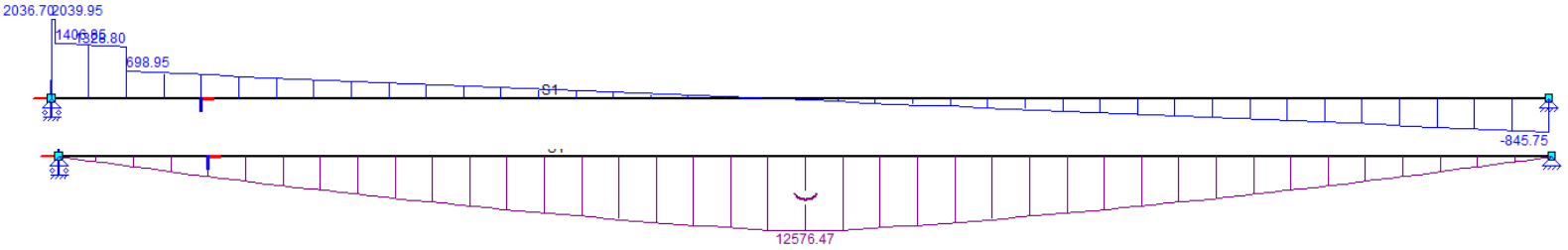

Figures 4.4a and 4.4b: Maximum global shear force and bending moments

Local Effects

The local action effects (between the cross girders), are dependent on the stiffness of the effective cross sections between various sections of the deck plate/ stiffener combination. Therefore, the aforementioned effective cross sections are determined prior.

4.2 Effective Cross Section Determination

4.2.1 Buckling of subpanels

For the global behaviour, the deck and troughs are assumed to work as the top flange of the longitudinal system. Given the simply supported nature of the bridge, this means that the panels can be assumed to be fully in compression.

Reduction of the stiffener webs as per EN 1993-1-5:

$$\psi = 1 \quad f_y = 355 => \epsilon = \frac{235}{355} = 0{,}81 \quad k_{sig} = 4$$

$$\lambda_{rel} = \frac{\frac{c}{t}}{28{,}4 * \epsilon * ksig^{0{,}5}} = \frac{\frac{308}{7}}{28{,}4 * 0{,}81 * 4^{0{,}5}} = 0{,}95 \qquad \rho = \frac{\lambda_{rel} - 0{,}55 * (3 + \psi)}{\lambda_{rel}^2} \approx 0{,}81$$

The reduction of the stiffener webs is 0,81.
The total and active cross section surface areas along with the total second moment of inertia are shown in figures 4.4a and b for the parts of the deck between the main girders (in) and the cantilever part (out).

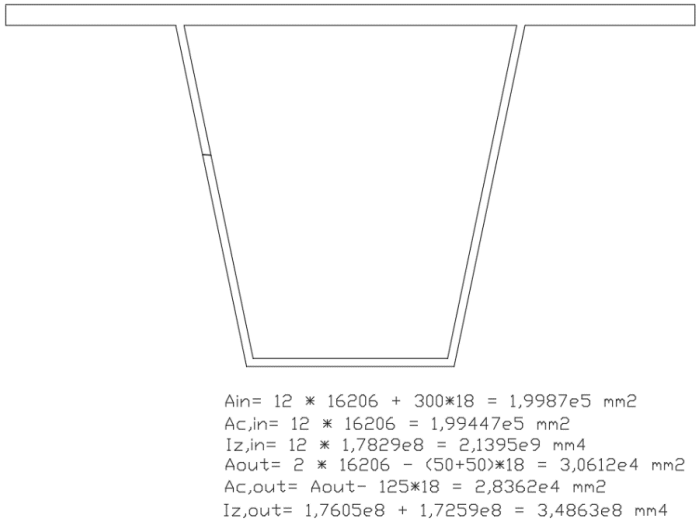

Figure 4.5a: Total and active properties of deck plate

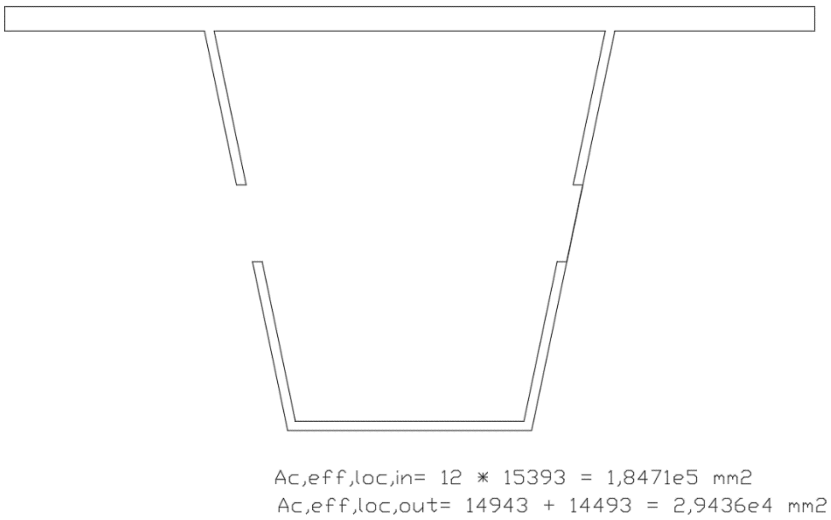

Figure 4.5b: Effective area of deck

***Note, line on right web reduction for easier use of "massprop" command in AutoCAD*

For Local behaviour, meaning bending in the cross section, the webs are classified as class 1, no reduction is applied. This is the case even if the neutral axis is assumed to be in the middle of the cross section; in reality it is much closer to the deck, resulting in a more favourable result.

$$\frac{308}{7} = 44 < 72 * 0{,}81 = 58{,}32 => Class\ 1$$

4.2.2 Plate-like Buckling behaviour

For plate-like buckling behaviour of the deck, it is assumed that the stiffeners are smeared out across the plate and the plate-stiffener system buckles as a whole.

This behaviour is largely governed by the aspect ratio of the considered plate, that being length divided by width.

Calculations are done following the equations in 1993-1-5, Annex A1.
These equations are meant to be used for plates supported on all four sides. This isn't the case with the cantilevering parts of the orthotropic steel deck.

In order to estimate the lack of support on one side, when it comes to the cantilever, it is assumed that the width of the plate there is twice its actual size. This entails an increase in the number of stiffeners as well. The equations used can be found in appendix A in python code form.

Both the inner and cantilevering parts require no reduction due to plate- like buckling.
Intermediate results for the plates are as follows:

	Inner plate (between main girders)	Outer plate (cantilever part)
Relative bending stiffness (γ)	534,1	522,2
Aspect Ratio (α)	0,476	1,428
Plate buckling coefficient ($k_{\sigma.p}$)	1592,7	172,5
Critical plate buckling stress ($\sigma_{cr,p}$)	1741,2 MPa	1697,1 MPa
Relative plate slenderness (λ_p)	0,560	0,469

Table 4.1: Plate- like Buckling intermediate results

4.2.3 Column-like Buckling behaviour

Column-like behaviour occurs when the stiffeners in an orthotropic plate buckle as separate columns. This buckling can be somewhat restrained by plate action, however for that to be possible, the critical buckling resistance for plate-like buckling must be higher than that for column-like buckling.
Column-like buckling depends on the reduction factor χ, which in term depends on the relative slenderness, the root of the second moment of inertia and the surface area, and the distance between the centroid of the column and either the plate or stiffener.
The latter is visualized in figures 4.6 a and b for the stiffeners belonging to the plate between the main girder.

Figures 4.6a, b: Full and reduced relevant inner stiffener properties

Relevant results for all differently placed stiffeners are shown below. A full calculation, for the inner stiffeners in python script form, can be found in appendix A.

	Inner stiffener	Outermost stiffener	Cantilever stiffener next to main girder
Critical stress	1788,1 MPa	1832,8 MPa	1816 MPa
Ratio $\frac{A_{sl,eff}}{A_{sl}}$, $(\beta_{A,c})$	0,95	0,95	0,91
Relative slenderness (λ_c)	0,423	0,428	0,423
Factor i	104,89 mm	106,2 mm	105,70 mm
Buckling factor α_e	0,448	0,443	0,445
Imperfection factor (φ)	0,647	0,642	0,639
Reduction factor (χ)	0,888	0,892	0,894

Table 4.2: Column- like Buckling behaviour intermediate results

4.2.4 Interaction of plate- and column- like behaviour

Both the outer and inner stiffeners have higher column- like buckling resistance compared to plate-like buckling. Therefore, no extra support from plate-like behaviour can be offered to the column-like resistance.

The inner part of the deck is thus reduced with a factor of **0,888**.
For the outer parts, reductions of **0,892** and **0,894** are obtained. To simplify calculations the average of the two, **0,893**, is taken. This is justified due to the negligible difference between the two and would not be done, had there been larger discrepancies between the two reduction factors.

The abovementioned reductions are without accounting for global shear lag effects.

4.2.5 Global shear lag

Shear lag effects are considered for mid-span and at the supports for simply supported systems in EC-3-1-5.
The largest moments, and thus normal forces in the deck, are expected at mid-span. This is why shear lag only in this area is to be expanded upon in this paragraph.
For the full reduction, with respect to shear lag, at mid- span and the supports, for the inner deck plate, see appendix A.

The results for shear lag for the inner and outer parts of the plate are shown below.

	Inner Plate	Outer Plate
b_0	3750 mm	1250 mm
α_0	1,256	1,217
κ	0,188	0,061
β	0,824	0,977
$\beta_{plastic}$	0,965	0,999

Table 4.3: Global shear lag intermediate results

4.2.6 Global effective cross section deck plate/ stiffeners

The global effects of buckling of the subpanels, plate- and column-like buckling, and shear lag are taken into account. The reduction is illustrated in figures 4.6 and 4.7, with the hatched areas being effective.

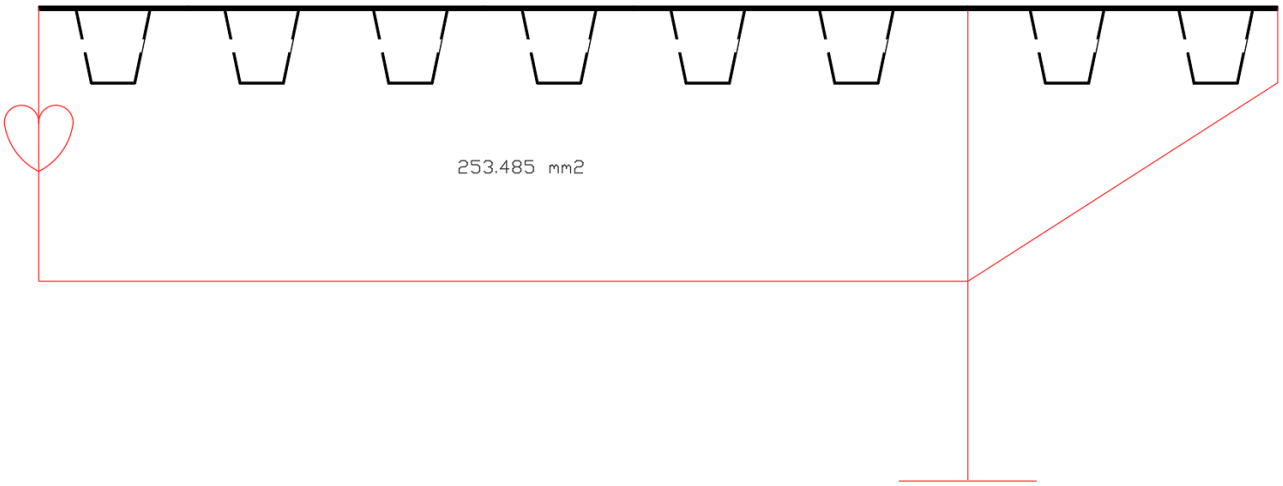

Figure 4.7: Effective cross section with regards to subpanel buckling

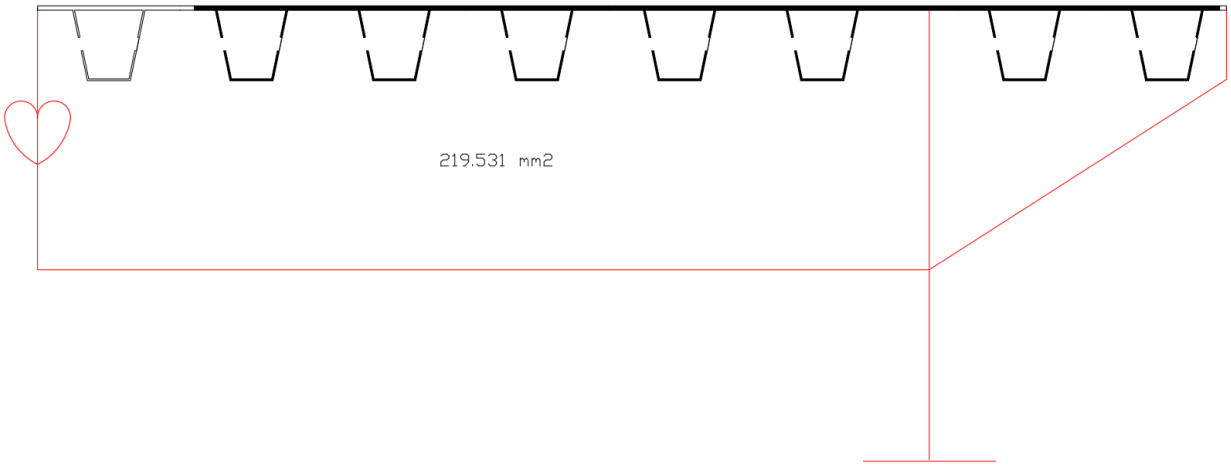

Figure 4.8: Effective cross section with regards to subpanel buckling and global shear lag effects.

The interaction between shear lag and the buckling of plates, according to paragraph 3.3 of EN 1993-1-5, results in a surface area of 220.562 mm^2 when assuming elastic shear buckling. This is higher than that of only shear lag and lower than if plastic shear buckling would be assumed. The maximally globally reduced cross section is taken as equal to 219,531 mm^2, which is only due to shear lag and local subpanel buckling.

4.2.7 Local shear lag

Local effects of shear lag on the deck plate are calculated in the same way as for global shear lag, save for the fact that the α_0 factor is set to 1 as there are no stiffeners on the plates that make up the trough.
For local effects, the deck plate and stiffener combination are seen as a beam over multiple supports.
A distinction is made between shear lag effects for an end span, a middle span, and over a support.

The results for an end span, a middle span, and those for support for the stiffeners between the main girders are shown in table 4.4.

	End Span Top	End Span Bottom	Middle Span Top	Middle Span Bottom	Support Top	Support Bottom
b_0	150 mm	87,5 mm	150 mm	87,5 mm	150 mm	87,5 mm
α_0	1	1	1	1	1	1
κ	0,0494	0,0288	0,06	0,035	0,084	0,049
β	0,9846	0,9947	0,9774	0,9922	0,6726	0,8007
$\beta_{plastic}$	0,9992	1,0	0,9986	1,0	0,9672	0,989
b_{eff}	147,69 mm	87,04 mm	146,62 mm	86,82 mm	100,89 mm	70,06 mm

Table 4.4: Local shear lag results 1

The cantilevering part of the stiffener combination differs in regards to the local cantilevering part of the deck and the deck part between the main girder and the first stiffener. The properties of the parts that differ are shown below, with the cantilevering part of the deck denoted with c and the inner part with “i”.

	End Span Top, c	Middle Span Top, c	Support Top, c	End Span Top, i	Middle Span Top, i	Support Top, i
b_0	100 mm	100 mm	100 mm	125 mm	125 mm	125 mm
α_0	1	1	1	1	1	1
κ	0,033	0,04	0,056	0,0412	0,05	0,07
β	0,9931	0,9899	0,7703	0,9893	0,9843	0,7176
$\beta_{plastic}$	1,0	1,0	0,985	1,0	1,0	0,9770
b_{eff}	99,31 mm	98,99 mm	77,03 mm	123,66 mm	123,03 mm	89,70 mm

Table 4.5: Local shear lag results 2

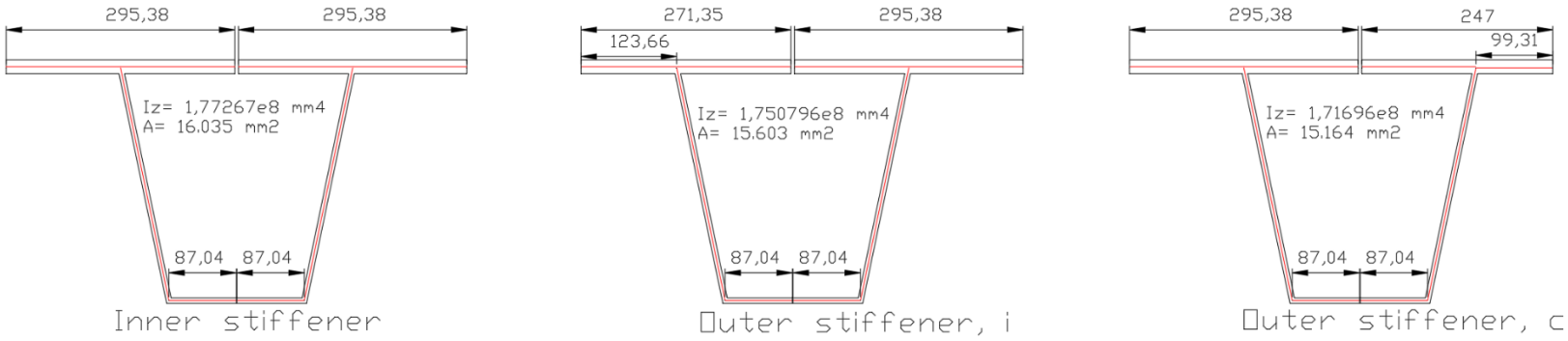

Figure 4.9: Effective local cross sections due to shear lag in the end span

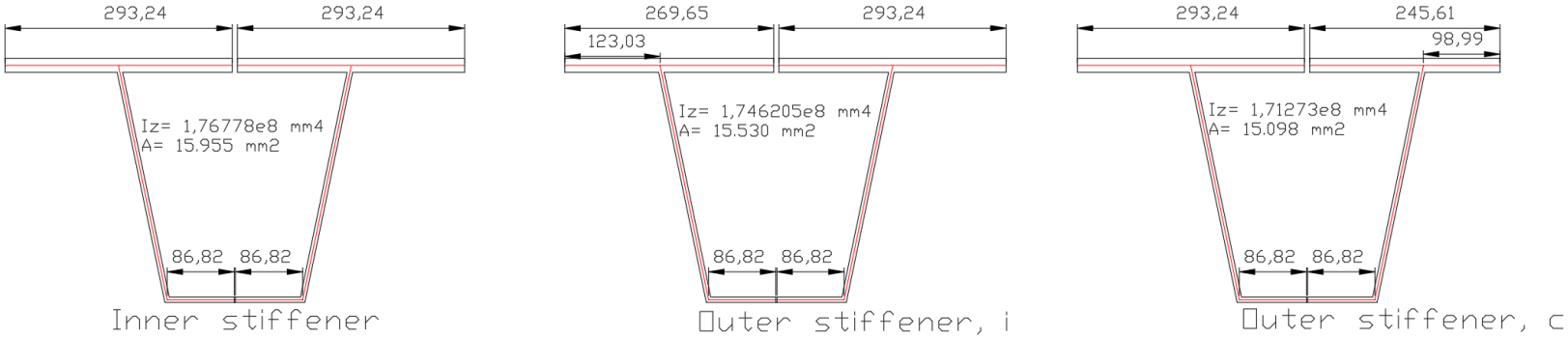

Figure 4.10: Effective local cross sections due to shear lag in a middle span

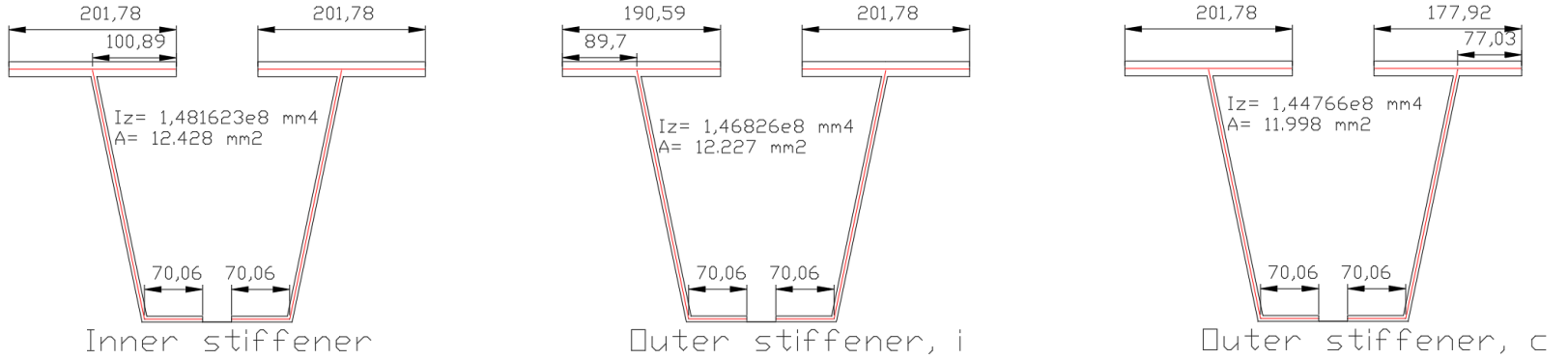

Figure 4.11: Effective local cross sections due to shear lag over cross beams

4.2.8 Effective Cross Section

The previously determined effective area of the deck and stiffeners due to shear lag and subpanel buckling are used to determine the effective cross section. This is shown for one longitudinal girder-deck combination.
Lengths are considered to be from centre to centre of plates. The effective cross section properties, of the elements outlined in black in figure 4.12, are determined with the autocad massprop function.

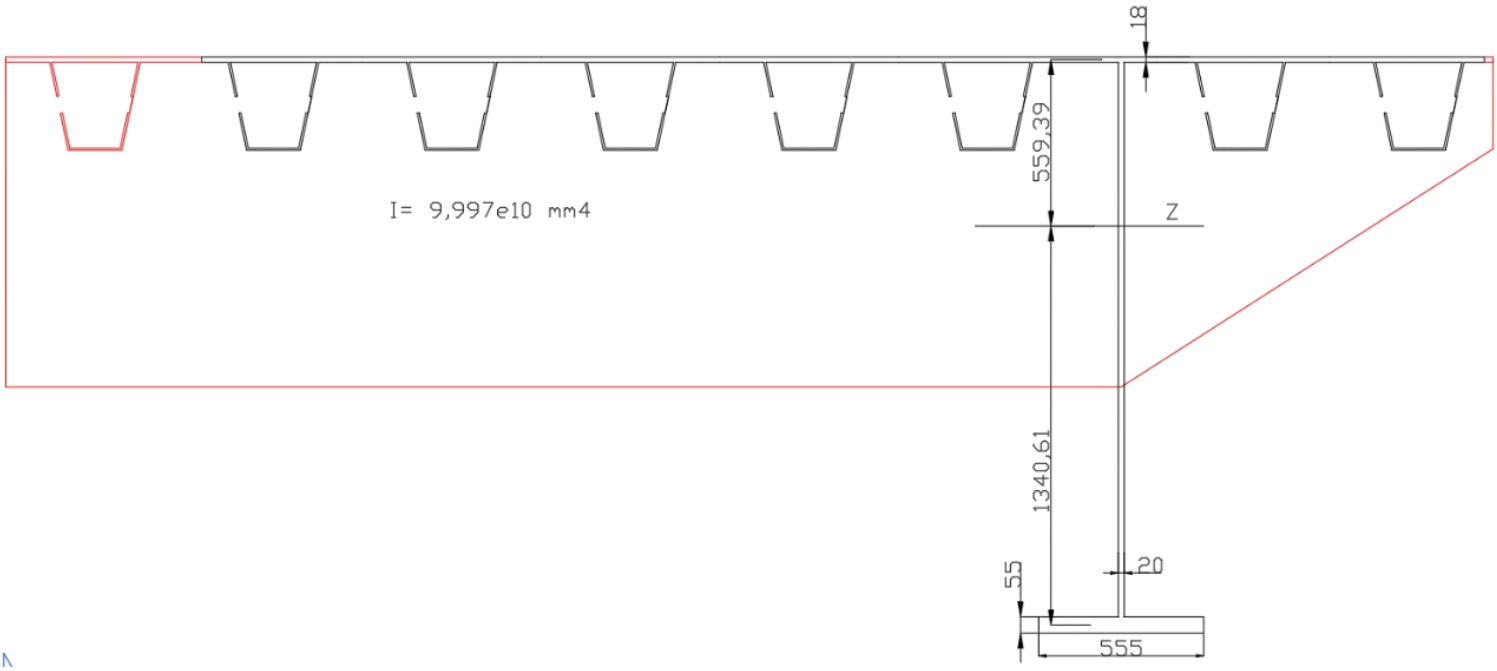

Figure 4.12: Effective global cross section

Cross section classification is done according to EN 1993-1-1, table 5.2.

$$\frac{c}{t} = \frac{1340{,}61 + 559{,}39 - 27{,}5 - 9}{20} = 93{,}175 < \frac{36 * \varepsilon}{\alpha} = \frac{36 * 0{,}81}{\left(\frac{559{,}39}{1340{,}61 + 559{,}39 - 27{,}5 - 9}\right)} = 97{,}21$$

Both the web and the flange of the main girder are classified as class 1, fully effective.

4.3 Verification

4.3.1 Longitudinal Direction – Global Bending

Top flange: $\sigma_{gl,tf} = \frac{M_{ED}}{I_{eff}} * z_{tf} = \frac{12.576{,}47e6}{9{,}997e10} * 559{,}39 = 70{,}37\ MPa < 345\ MPa$

Bottom flange: $\sigma_{gl,bf} = \frac{M_{ED}}{I_{eff}} * z_{bf} = \frac{12.576{,}47e6}{9{,}997e10} * 1340{,}61 = 168{,}66\ MPa < 335\ MPa$

4.3.2 Longitudinal Direction – Local and Combined Bending

To determine the local load distribution, stiffness differences between the various locations of the deck plate/ stiffener combination must be taken into account as, on the local level, it is a statically indeterminate structure.

The outer most stiffener will be considered as it has the smallest moment of inertia.

Stiffeners in a mid- and an end span have closely matching moments of inertia and will, for the purposes of this calculation, be considered equal. The smaller moment of inertia of the two will be used to ensure maximum distribution of the forces to the more critical area of the deck plate/ stiffener combination; over the supports.

The ratio between the moments of inertia is:

$$\frac{I_{support}}{I_{midspan}} = \frac{1{,}44766}{1{,}71273} = 0{,}845$$

To acquire the moment distribution, the conservative assumption, that the lesser effective cross section has a span of $0{,}25 * (3{,}5714 + 3{,}5714) = 1{,}7857\ m$ and the more effective cross section covers the rest of the span, meaning $1{,}7857\ m$ for an intermediate span and $2{,}6786\ m$ for an end span.

The deck above the outermost stiffener has a transverse span of 0,55 meters. This allows a single wheel load, along with the distributed traffic and dead loads to be placed over it.

The loads to be used for load model 1 are as follows:

$$Concentrated\ load: 225\ kN$$

$$Distributed\ load: (13{,}5 + 4{,}6875\ ) * 0{,}55 = 10\frac{kN}{m}$$

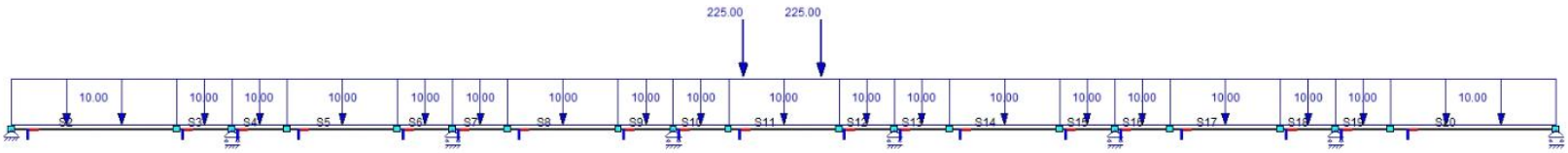

Figure 4.13: Local loading of stiffener, load in intermediate mid span

Figure 4.14: Bending moment diagram, resulting from imposed loads in intermediate mid span

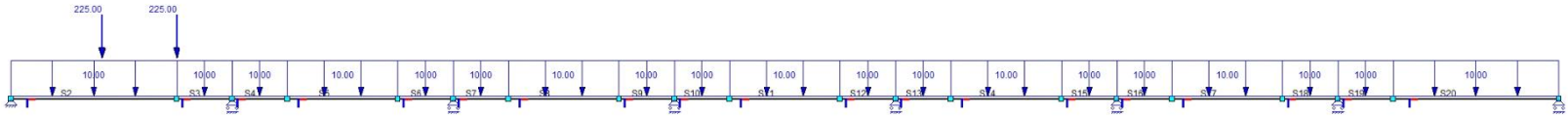

Figure 4.15: Local loading of stiffener, load placed for maximum bending hogging moment over side support

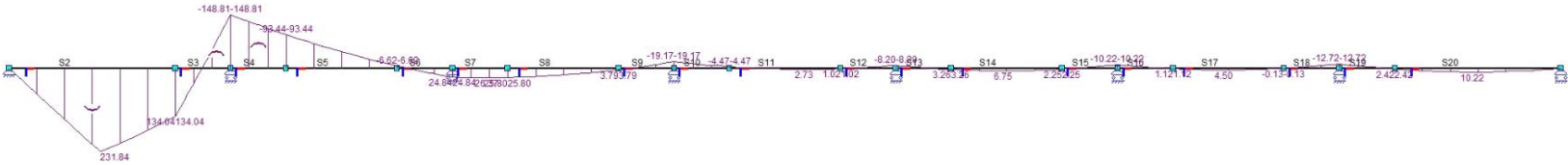

Figure 4.16: Bending moment diagram, resulting from loads placed in end span

The local sagging bending moments in the middle mid span are considered for local/ global interaction. This is done because the largest bending moment on global scale takes place in mid span.

The hogging moments over the local supports result in stresses opposing those from the global bending moment. Therefore, the most severe stresses due to local hogging moments are the ones where the global bending moments are of the smallest magnitudes; the local end spans.

Check at intermediate mid span

$$\sigma_{loc,bf} = \frac{M_{Ed}}{I_{eff}} * z_{bf} = \frac{161e6}{1{,}712373e8} * 235 = 220{,}95 \text{ MPa} < 355 \text{ MPa}$$

$$\sigma_{loc,tf} = \frac{M_{Ed}}{I_{eff}} * z_{tf} = \frac{161e6}{1{,}712373e8} * 67{,}29 = 63{,}27 \text{ MPa} < 345 \text{ MPa}$$

Interaction global/ local bending:

$$\sigma_{Ed,1} = \sigma_{gl,tf} + \psi * \sigma_{loc,tf} = 70{,}37 + 0{,}925 * 63{,}27 = 128{,}89 \text{ MPa} < 345 \text{ MPa}$$

$$\sigma_{Ed,2} = \psi * \sigma_{gl,tf} + \sigma_{loc,tf} = 0{,}925 * 70{,}37 + 63{,}27 = 128{,}36 \text{ MPa} < 345 \text{ MPa}$$

Check at end span, over support

Interaction between global and local bending at the end span is irrelevant. For the bottom flange, the moments are opposing; a conservative assumption of no interaction is applied.

$$\sigma_{loc,bf} = \frac{M_{Ed}}{I_{eff}} * z_{bf} = \frac{149e6}{1{,}44766e8} * 222{,}72 = 229{,}23 \text{ MPa} < 355 \text{ MPa}$$

$$\sigma_{loc,tf} = \frac{M_{Ed}}{I_{eff}} * z_{tf} = \frac{149e6}{1{,}712373e8} * 78{,}78 = 74{,}91 \text{ MPa} < 345 \text{ MPa}$$

Check at end span, mid span

$$\sigma_{loc,bf} = \frac{M_{Ed}}{I_{eff}} * z_{bf} = \frac{232e6}{1{,}712373e8} * 235 = 318{,}39{,}95 \text{ MPa} < 355 \text{ MPa}$$

4.3.3 Longitudinal Direction – Local Bending LM2

The same structural system and longitudinal load placement is applied as in the previous subparagraph. The loads are now changed to a single concentrated wheel load with a magnitude and dimensions as denoted in subparagraph 3.2.2 and a distributed load, only due to dead loads. The concentrated wheel load is placed at the edge of the bridge in transverse direction. This is done because any transverse force distribution can then be done only in one direction and thus the highest local effects are expected.

$$Concentrated\ load: \frac{0{,}55}{0{,}6} * 200 * 1{,}5 = 274{,}5\ kN$$

$$Distributed\ load: 4{,}6875 * 0{,}55 = 2{,}58\ kN/m$$

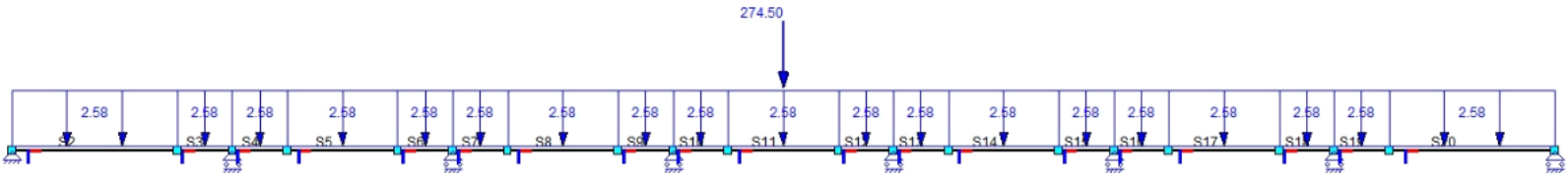

Figure 4.17: Local loading in stiffener, LM2, Single load

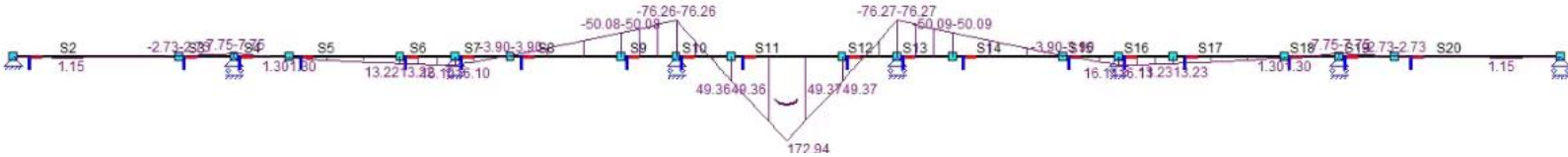

Figure 4.18: Bending moment diagram, resulting from local loading

$$\sigma_{loc,bf} = \frac{M_{Ed}}{I_{eff}} * z_{bf} = \frac{173e6}{1{,}712373e8} * 235 = 237{,}42\ \text{MPa} < 355\ \text{MPa}$$

4.3.4 Shear verification – Longitudinal direction

Shear in the main girder is checked. This is done at the location where shear the shear force is the largest; at the supports.

This is done according to EN 1993-1-5, paragraph 5 and Annex A.3

The Unity check without taking into account shear buckling is

$$UC = \frac{\tau_{Ed}}{f_y/(\gamma_{M0} * \sqrt{3})} = \frac{54{,}65}{345/(1 * \sqrt{3})} \approx 0{,}27$$

According to the Eurocode, shear buckling must be taken into account in this case, resulting in a resistance of $4715{,}58\ \text{kN} \gg 2037\ \text{kN}$, leading to a unity check of $\mathbf{0,43}$. The detailed calculation, leading to this UC, can be found in appendix A.

The latter UC is without the contribution of the flanges to the shear capacity. A negligible increase in shear capacity is obtained when the flanges are considered, namely less than $\mathbf{0,04}$ decrease in the unity check if moments aren't accounted for.

4.3.5 Optimization

Several iterations are run in order to obtain the optimal height of the longitudinal girder. This is done in the same way as detailed in the previous section. The results of the final iteration are detailed below.

The local behaviour is often governed by fatigue, therefore getting a UC close to 1 is not of great importance and the bridge will not be further optimized.

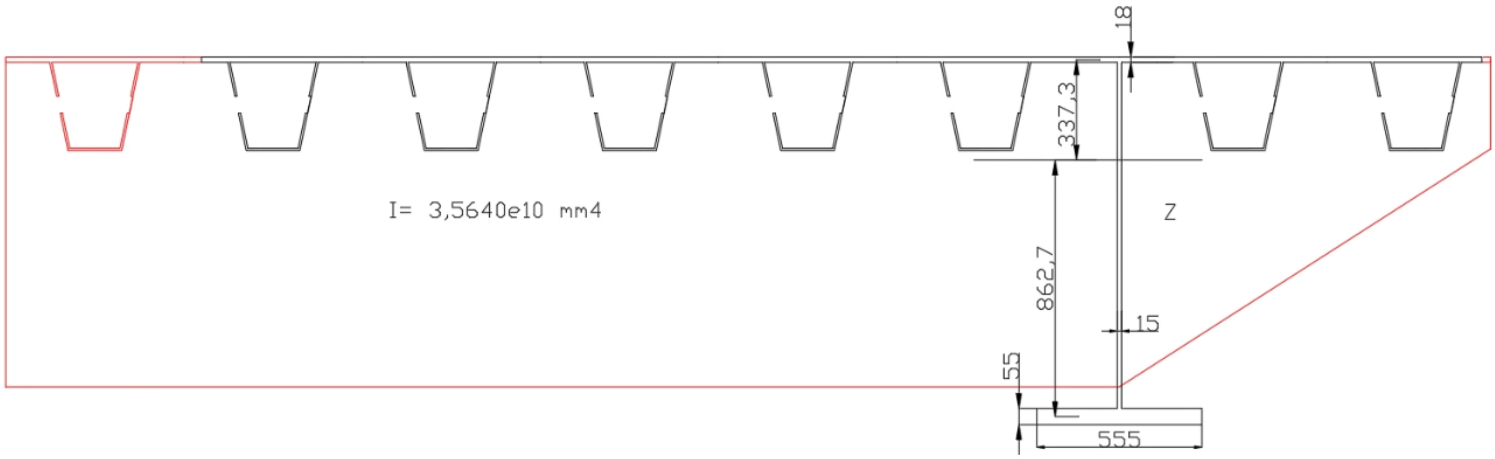

Figure 4.19: Optimized effective global cross section

4.3.6 Bending Verification – Longitudinal direction

Global

Top flange: $\sigma_{gl,tf} = \frac{M_{ED}}{I_{eff}} * z_{tf} = \frac{12576{,}41e6}{3{,}5640e10} * 337{,}3 = 119{,}02\ MPa < 345\ MPa$

Bottom flange: $\sigma_{gl,bf} = \frac{M_{ED}}{I_{eff}} * z_{bf} = \frac{12576{,}41e6}{3{,}5640e10} * 862{,}7 = \mathbf{304{,}42}\ MPa < \mathbf{335}\ MPa$

Local/ Global at Intermediate span

$$\sigma_{Ed,1} = \sigma_{gl,tf} + 0{,}7 * \sigma_{loc,tf} = 119{,}02 + 0{,}7 * 74{,}66 = 171{,}28\ MPa < 345\ MPa$$

$$\sigma_{Ed,2} = 0{,}7 * \sigma_{gl,tf} + \sigma_{loc,tf} = 0{,}7 * 119{,}02 + 74{,}66 = 124{,}262 MPa < 345\ MPa$$

Shear verification – Longitudinal direction

The web thickness of the longitudinal girder is reduced to 15 mm, leading to the following results:

The Unity check without taking into account shear buckling is $\frac{\tau_{Ed}}{f_y/(\gamma_{M0}*\sqrt{3})} = \frac{116{,}20}{355/(1*\sqrt{3})} \approx \mathbf{0,57}$

According to the Eurocode, shear buckling must be taken into account in this case, resulting in a resistance of $2690{,}68\ kN > 2037\ kN$, leading to a unity check of $\mathbf{0,76}$.

The latter UC is without the contribution of the flanges to the shear capacity. A sizeable increase in shear capacity is obtained when the flanges are considered fully available to take up shear, namely a decrease in the unity check of $\mathbf{0,10}$.

5 Steel Bridge Design With FEA

Firstly, the results obtained in the previous chapter is verified against the ones obtained from a SCIA FE calculation. Subsequently all load effects are taken into account and the structure is optimized.

5.1 Hand Calculation Verification

5.1.1 Models

The bridge, with dimensions as specified in chapter 4, is modelled in SCIA Engineer with the following parameters:

- 2D Kirchoff plate elements
- Average Mesh size: 5 cm, local mesh refinement of factor 10
- Nonlinearity Applied for potential local plasticity

Two models are made:

- Model A: Web height of transverse stiffeners: 800 mm, material nonlinearity only
- Model B: Web height of transverse stiffeners: 1200 mm, material nonlinearity only and 2nd / 3rd order geometric nonlinearity.

The different variants of model B are made to compare their results and establish the necessity or lack thereof of more time- consuming geometrically nonlinear calculations

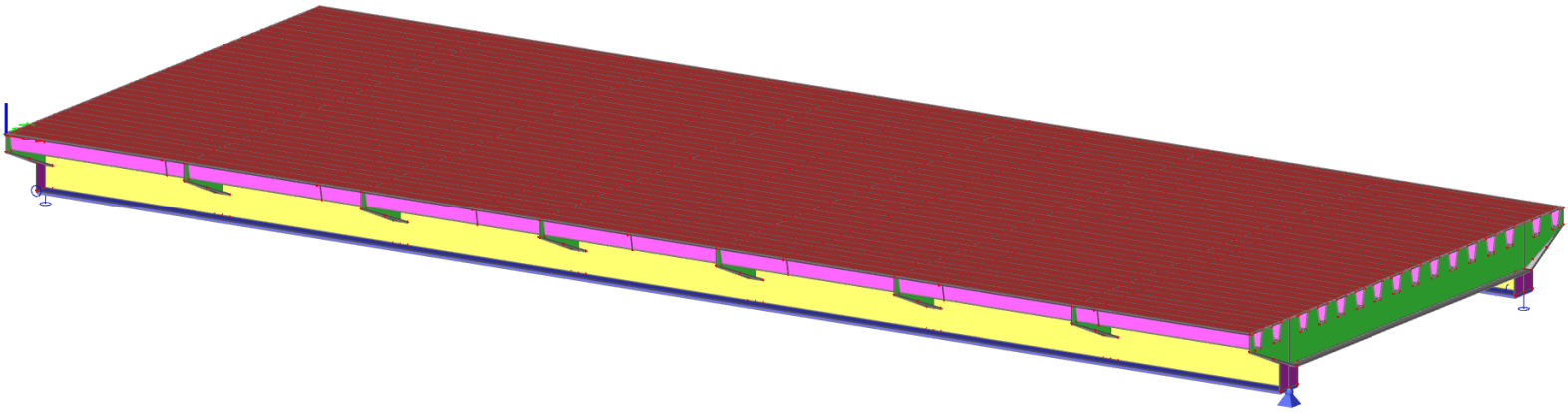

Figure 5.1: SCIA Model A, material nonlinear only

5.1.2 Loads and combinations

The loads and combinations applied are the same as for the hand calculation, some of these are visualized in figures 5.2 and 5.3

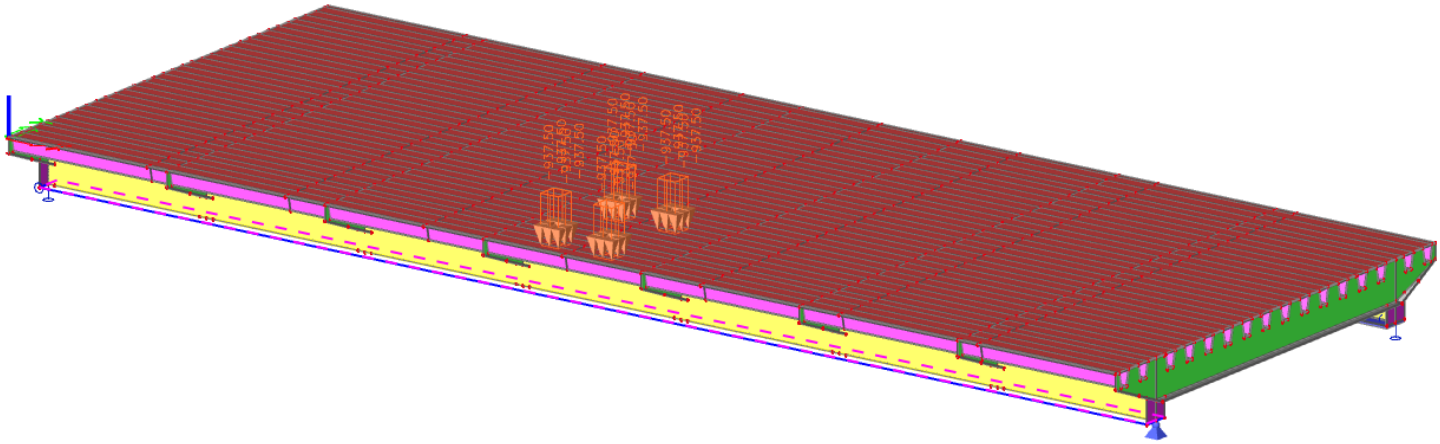

Figure 5.2: Load position of tandem system, mid span on first lane

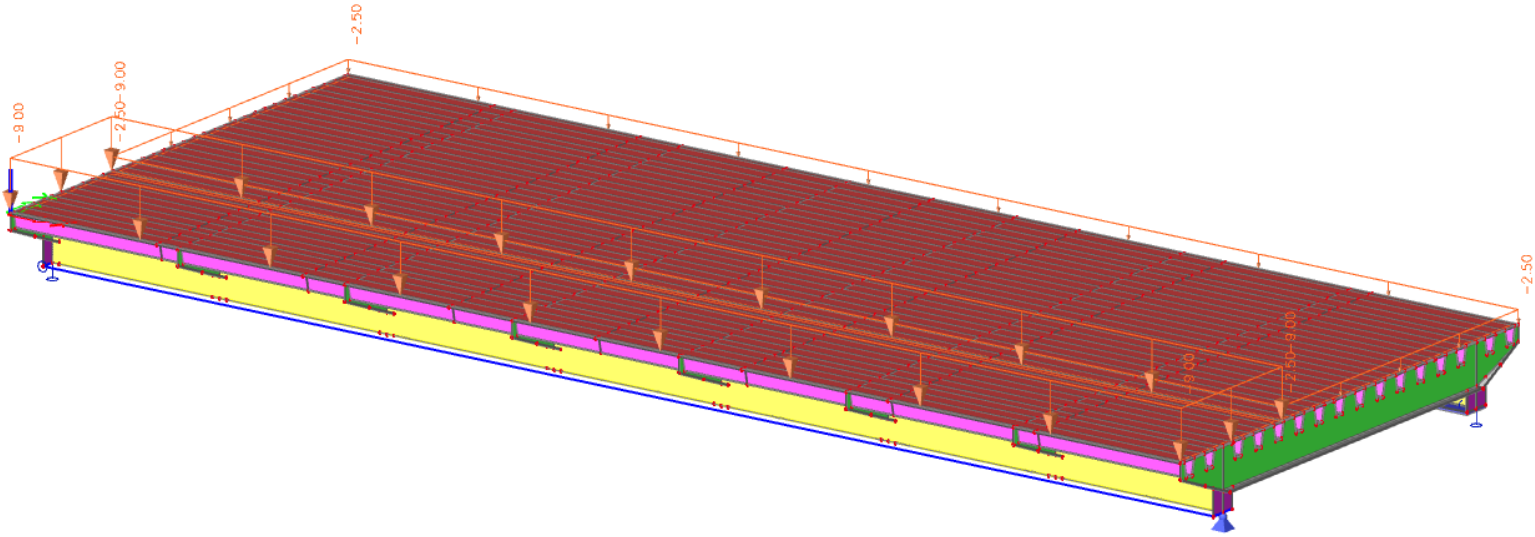

Figure 5.3: Load position of distributed load, LM 1

The tandem systems are applied at the centre of each lane. Five combinations for the tandem systems are considered:
- In mid span
- Over cross girder close to mid span
- Over one to last cross girder
- In mid span of last local span
- Close to end support

5.1.3 Results

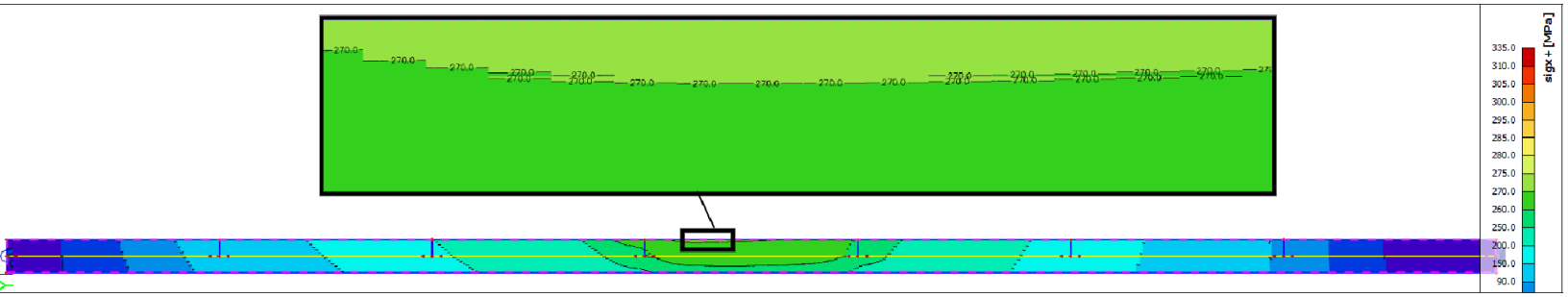

Figure 5.4: Model A, Normal stress bottom flange of heavily loaded main girder with tandem systems in mid span

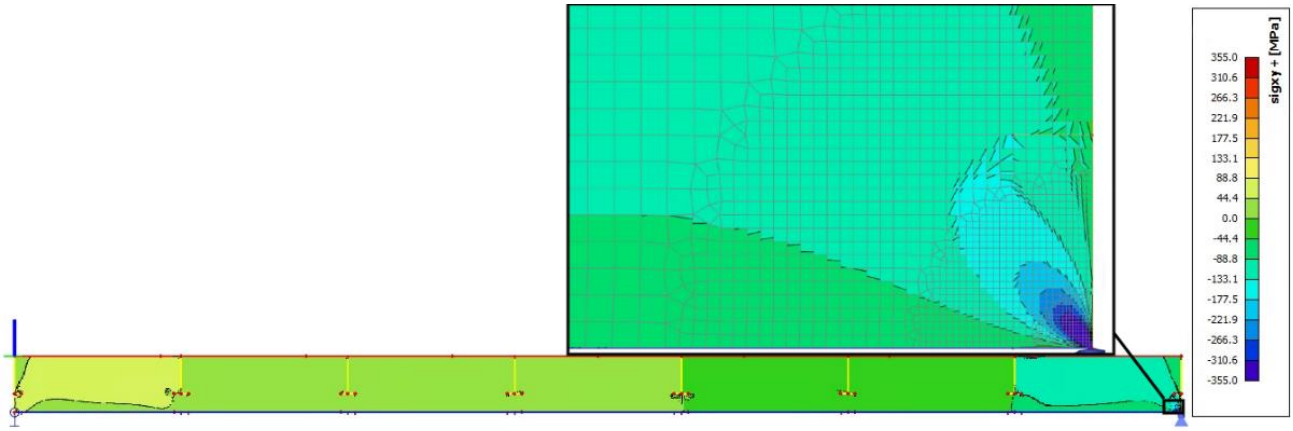

Figure 5.5: Model A, Shear stress web of heavily loaded main girder with tandem systems above one to last transverse girder.

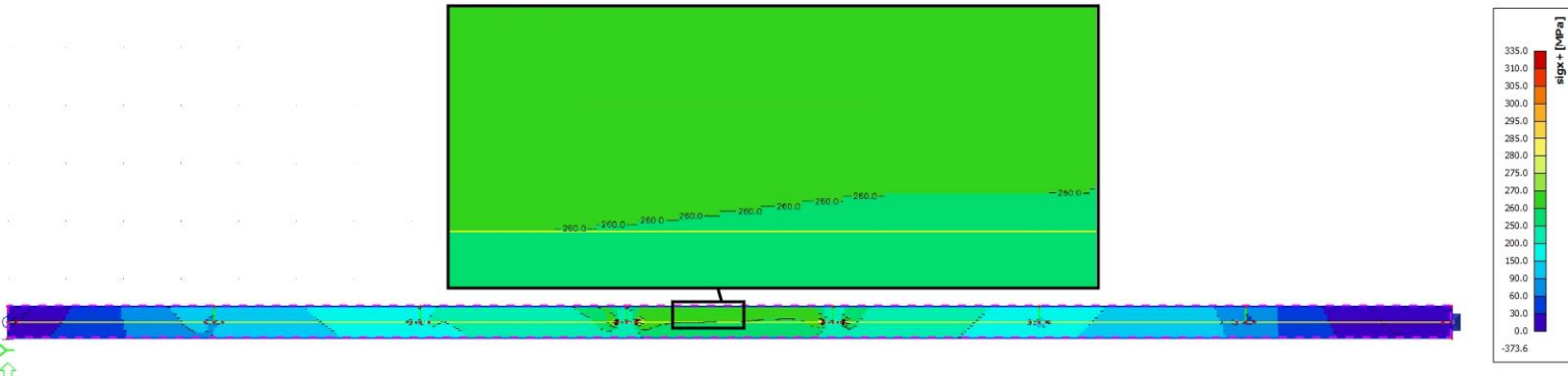

Figure 5.6: Model B, material nonlinear, Normal stress flange of heavily loaded main girder

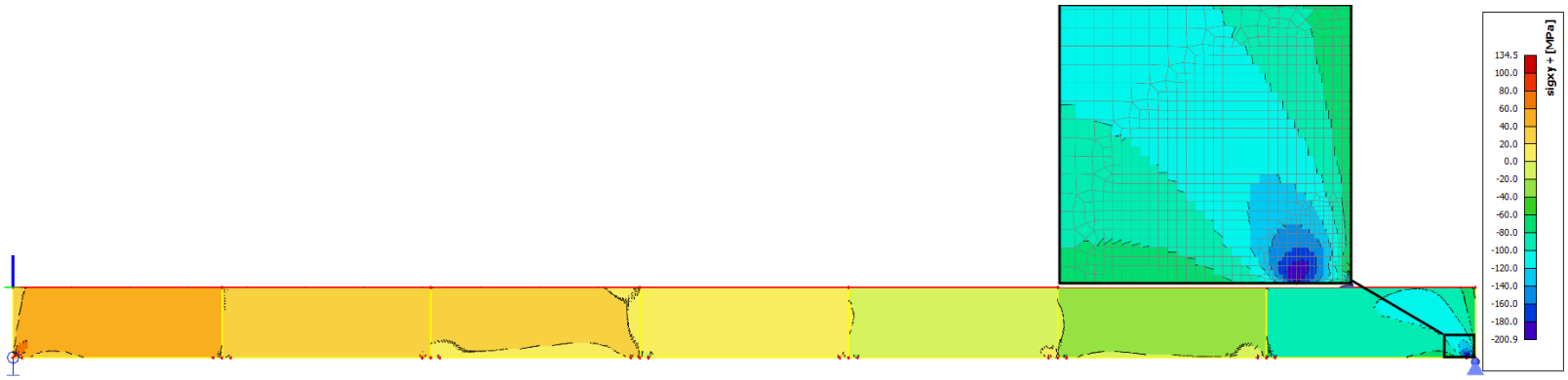

Figure 5.7: Model B, material nonlinear, Shear stress web of heavily loaded main girder

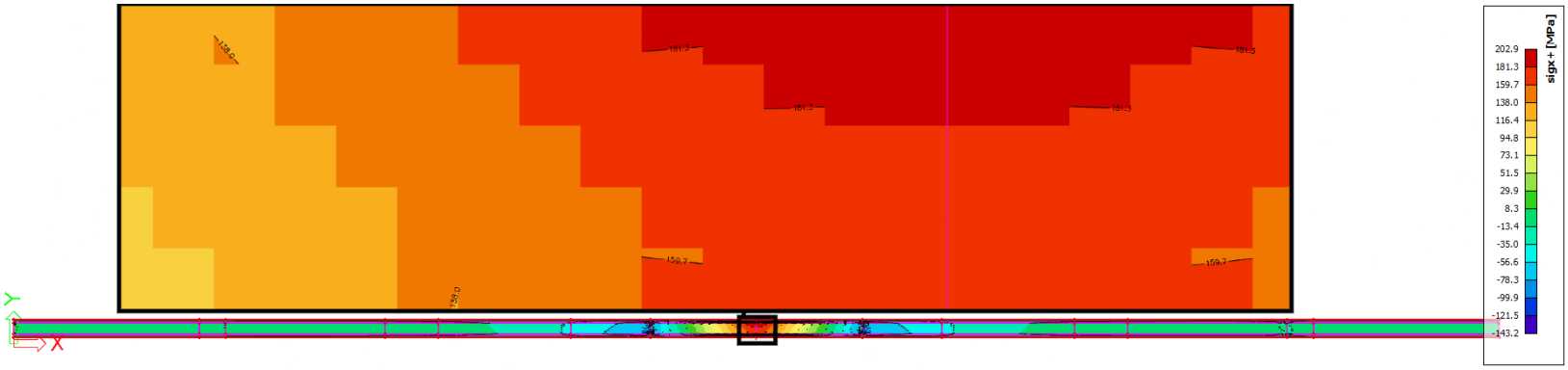

Figure 5.8: Model A, Normal stress lower flange of locally loaded trough.

5.1.4 Reflections and Conclusion

The stresses obtained from the analytical calculations and the ones from FE model are in line with each other. The differences between the analytical calculation and the FE calculation, alongside with the differences between the different FE models are addressed.

- The key difference between the FE model and the hand calculation is that the force distribution for the global model, in the hand calculation, is assumed to follow the linear transverse influence line throughout the span. This is a rough approximation of reality. The shape of the influence line heavily depends on the stiffness of the cross girder. Larger stresses in the more heavily loaded main girder are observed in the results of the model with a smaller and therefore less stiff cross girder, which is to be expected as the redistribution of applied forces is less efficient.

- The distributed loads applied in close proximity to the longitudinal girder can indeed be assumed as distributed loads acting on it, however those further away are mostly carried to the cross girders first and subsequently to the main girder. This results in a multitude of concentrated loads applied on the longitudinal girder instead of a distributed load. Because of this, stresses in the longitudinal beams differ between the hand calculation and the FE calculation.

- There are no substantial differences between the 2nd and 3rd order geometrical nonlinear analysis.
  In the case of bridge version B, there were no substantial differences between material nonlinear only and geometrically nonlinear solver options.
  Nonlinearity should nevertheless be applied when slender members are concerned.
  This is to be done in order to account for buckling phenomena and local yielding in ULS.
  No notable differences between the models were observed in the application of load model 2 for local verification.

- Both shear and normal stresses are smaller in the SCIA model, this is to be expected due to the abovementioned factors. Furthermore, the analytical equations from the Eurocode often result in overly conservative reductions of the cross sections. A relatively precise numerical solution is therefore expected to yield more favorable results. A difference in stresses of 10 to 15%, in favor of the numerical solution, is obtained when comparing resulting stresses from the analytical methods to those from SCIA.

From this, it can be concluded that SCIA engineer offers good results for the analysis of members. The full load combinations according to the Eurocode will be modelled in SCIA to obtain the bridge dimensions.

5.2 Complete Bridge Design

In this paragraph, all loads will be applied according to the combination following from table NB.19 of the Dutch NA to EN 1990. Efficient dimensions of the elements of the structure will be obtained according to the complete loading.

The modelling is done in the same fashion as in that of model B in the previous paragraph with 2nd order geometrical solver applied to account for potential buckling phenomena.

5.2.1 Bridge Dimensions

The global bridge dimensions remain the same. Plate thicknesses and detailing have been adapted. The bridge is extended on either longitudinal side, past the supports by 15 cm to accommodate the flanges of the final cross girders. The span between the supports remains 25 meters.
Vertical end plates are added in the longitudinal direction so that no cantilever originates past the final trough in transverse direction.

The end cross beams are executed in larger thickness than the inner ones to ensure the deformations at the supports remain within the limits as prescribed in the Dutch NA to EN 1993-2.

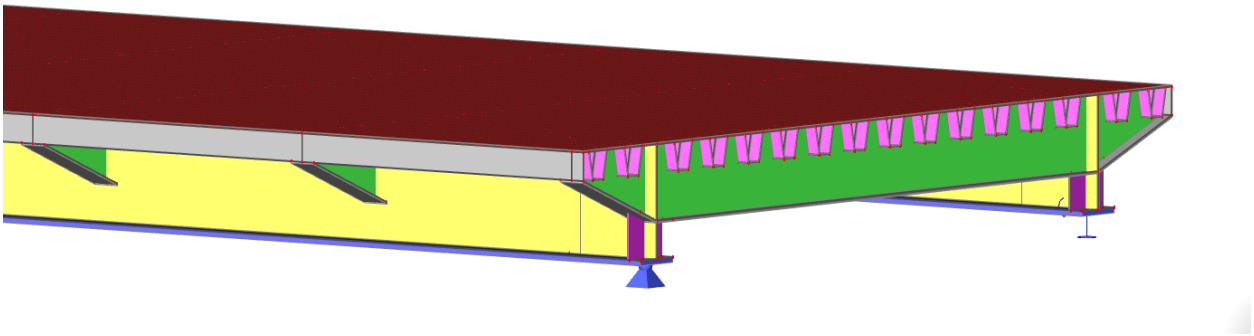

Figure 5.9: Bridge Model in SCIA

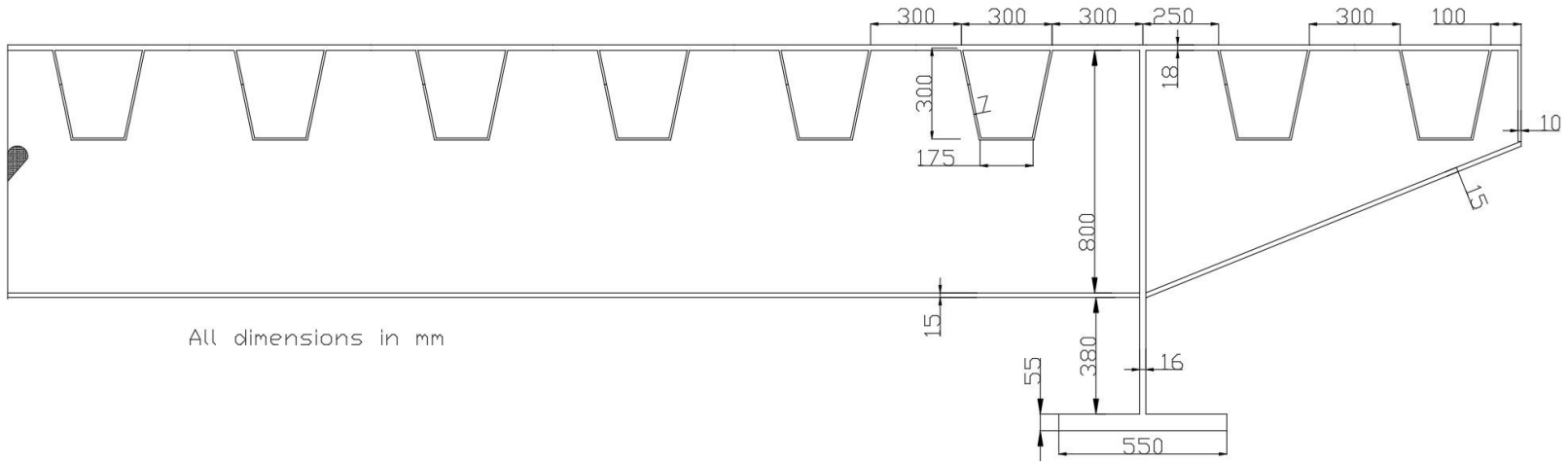

Figure 5.10: Transverse bridge cross section, mid span cross girder

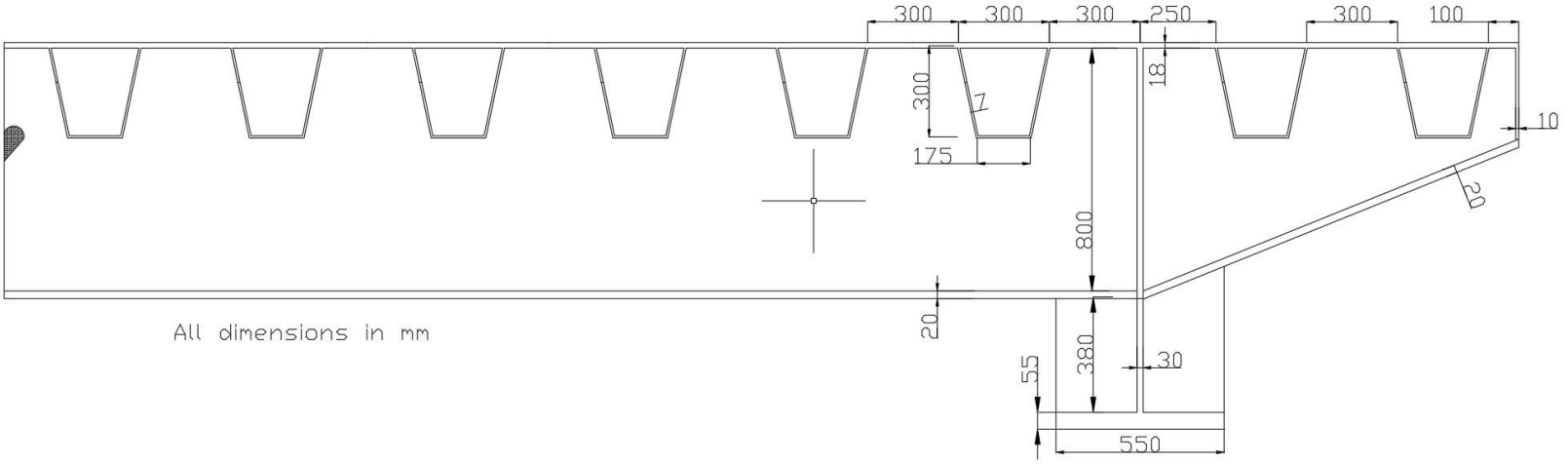

Figure 5.11: Transverse bridge cross section, end cross girder

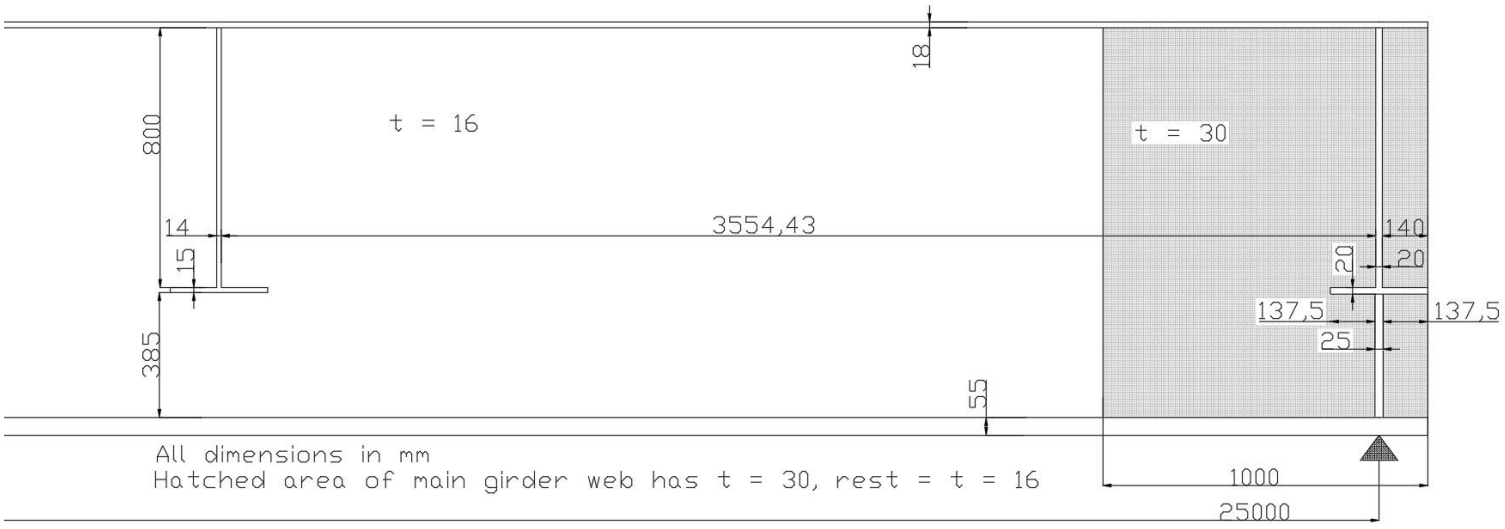

Figure 5.12: Longitudinal bridge cross section, right end span

5.2.2 Loads and combinations

Loads as specified in subparagraph 5.1.2 are applied to the structure. Alongside with the loads previously specified, temperature actions, self-weight, wind loads, and braking/ acceleration forces are applied. The latter are applied as a line load in the most heavily loaded lane.

Each load case, with a different placement of load model 1, is included in four combinations for ULS.
All these combinations include:

- All dead loads
- Load model 1
- Wind along the deck of the bridge in longitudinal and downward direction
- Temperature loads

The combinations differ in:

- Wind loads from either transverse direction
- Either positive or negative temperature differences of the deck.

SLS combinations are generated according to the frequent combination in EN 1990 (reversible limit states), with Ψ factors gathered from table NB.12- A2.1 from the Dutch NA.
The tandem systems are placed at:

- Mid span
- Over cross girder close to mid span
- Close to end support

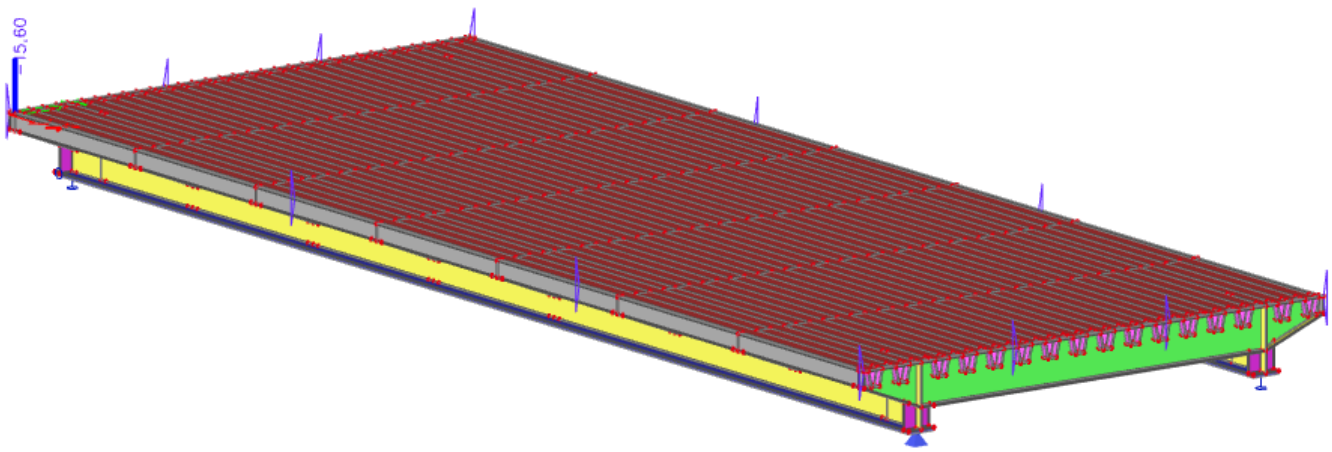

Figure 5.13: Negative temperature action applied to bridge deck.

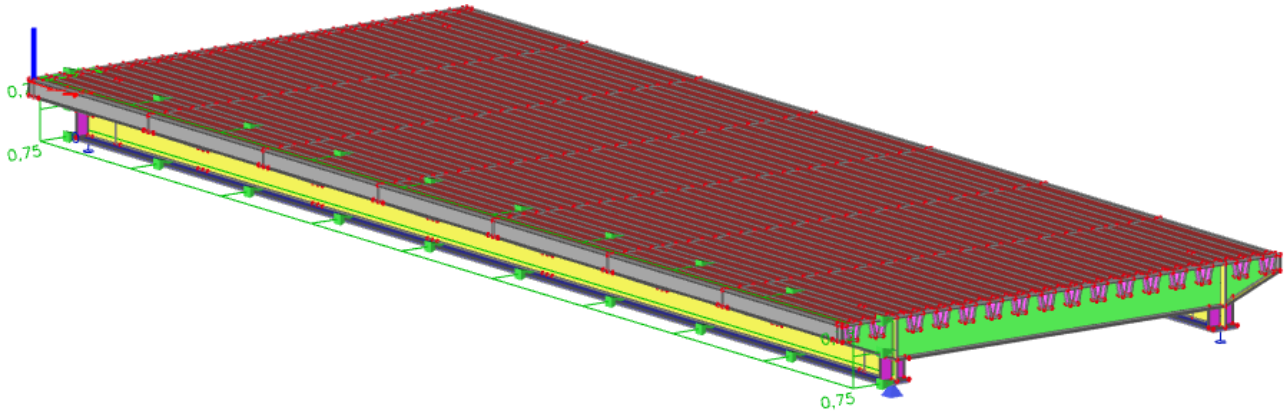

Figure 5.14: Transverse wind loads from one side applied to bridge

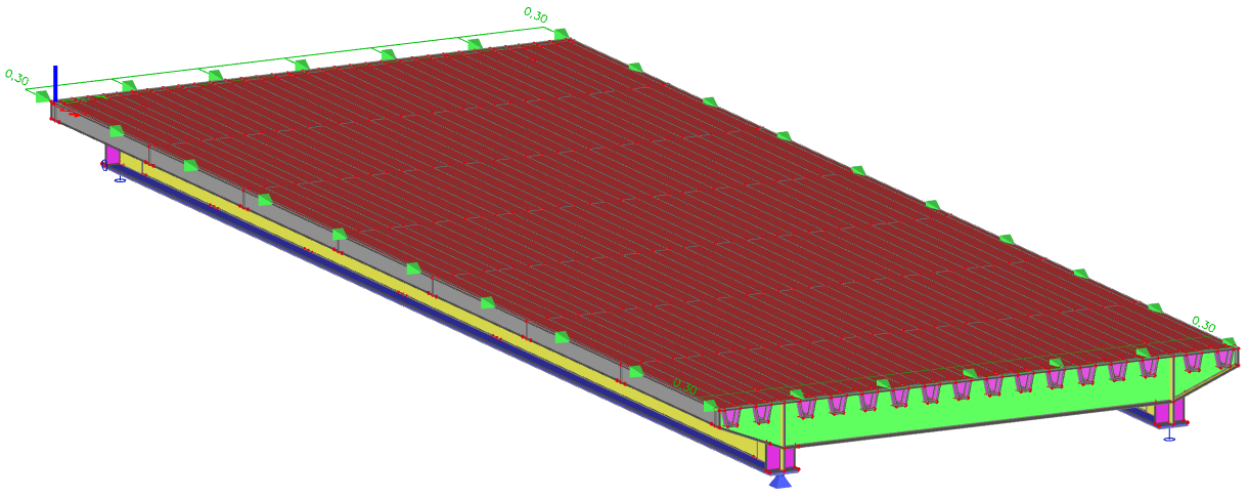

Figure 5.15: Longitudinal wind loads applied to bridge

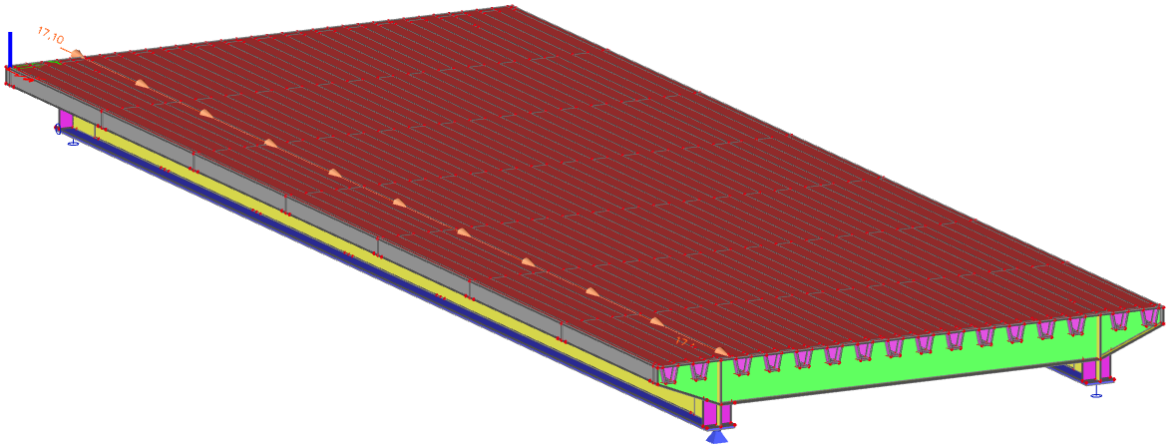

Figure 5.16: Braking and acceleration forces applied in Lane 1

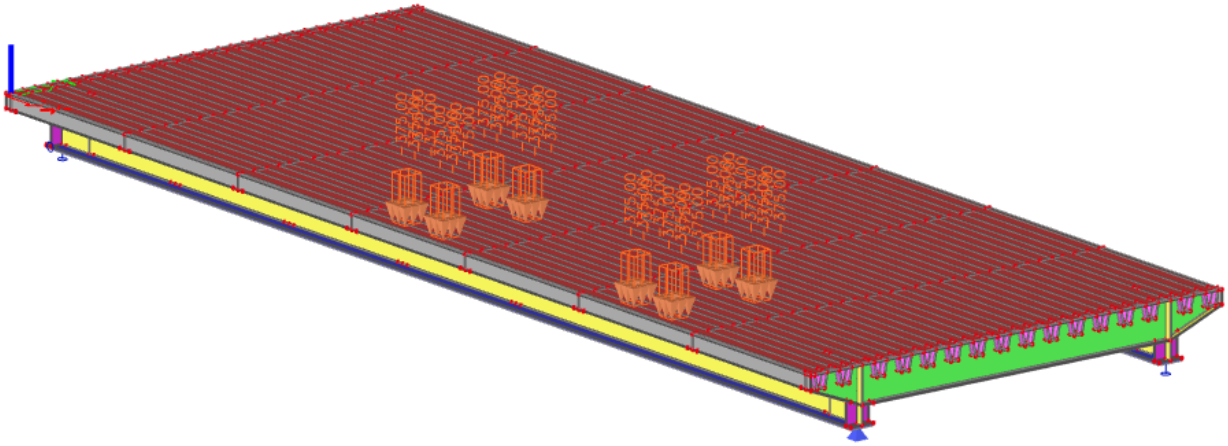

Figure 5.17: Fatigue Load model 3

5.2.3 ULS Results

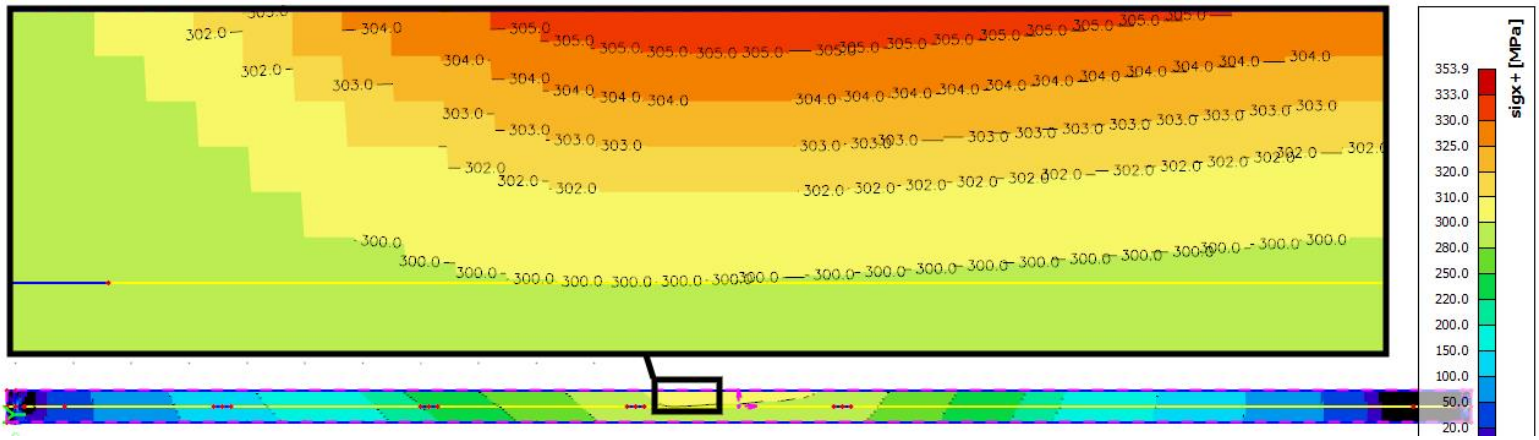

Figure 5.18: Normal stresses in bottom flange of heavily loaded main beam.

- Ultimate Normal Stress in Main beam bottom flange: 305 to 306 MPa
- At mid span of beam
- Under Combination: Tandem systems at mid span + Transverse wind acting on more heavily loaded beam, negative temperature difference of deck

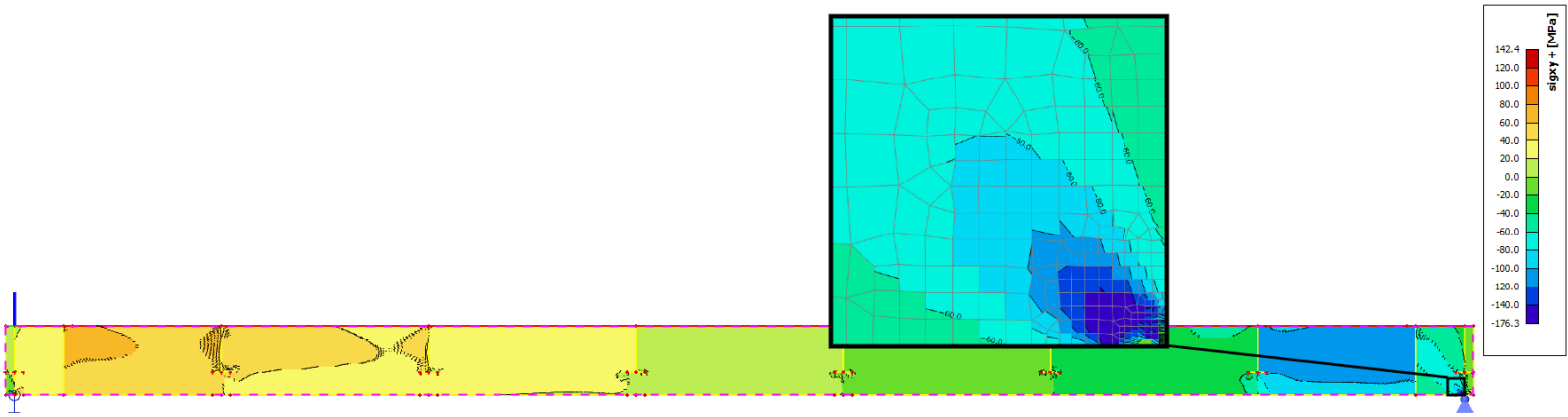

Figure 5.19: Shear stresses in web of heavily loaded girder.

- Ultimate shear stress in Main beam web: ≈ 120 MPa, excluding the nodes directly next to support
- Close to support
- Under Combination: Tandem systems over penultimate cross girder + transverse wind acting on more heavily loaded beam + negative temperature of the deck

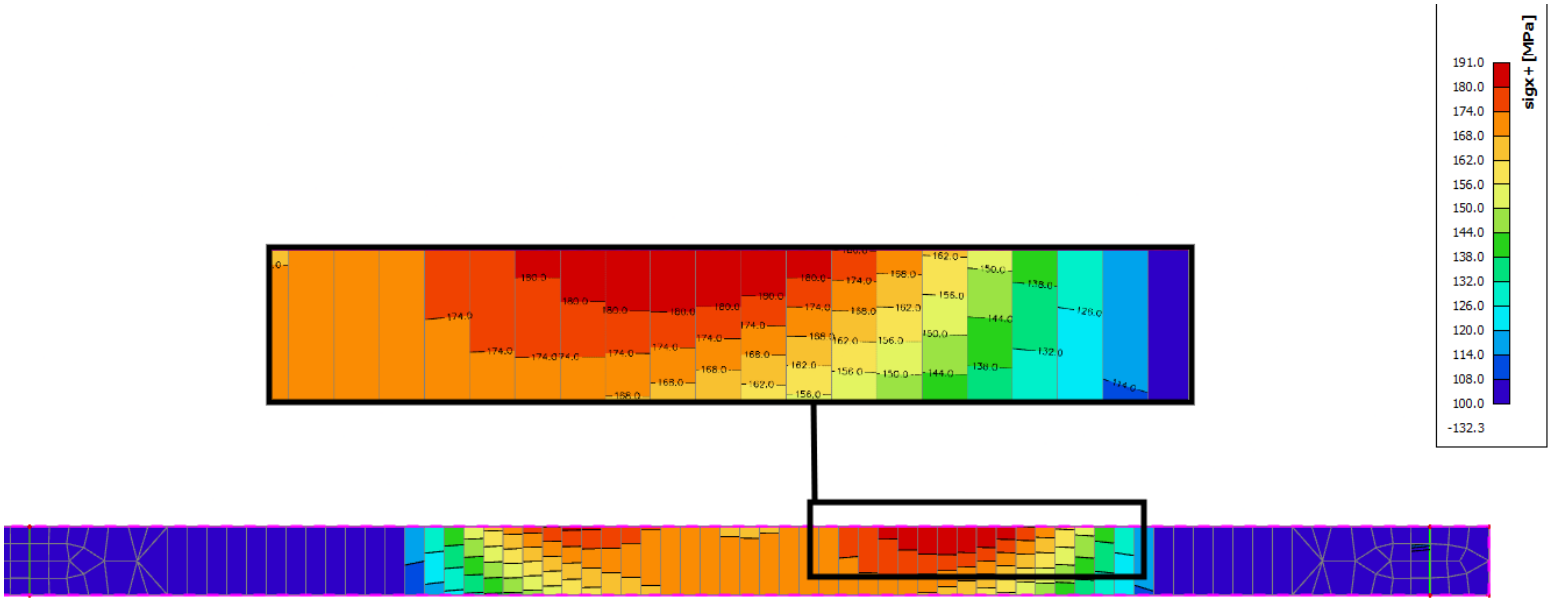

Figure 5.20: Normal stresses in bottom flange of most heavily loaded trough

- Ultimate Normal stress in bottom flange of most heavily loaded trough: 191 MPa
- At final local span
- Under Combination: Tandem systems at local end span + transverse wind load on the more heavily loaded main girder + positive temperature difference of the deck

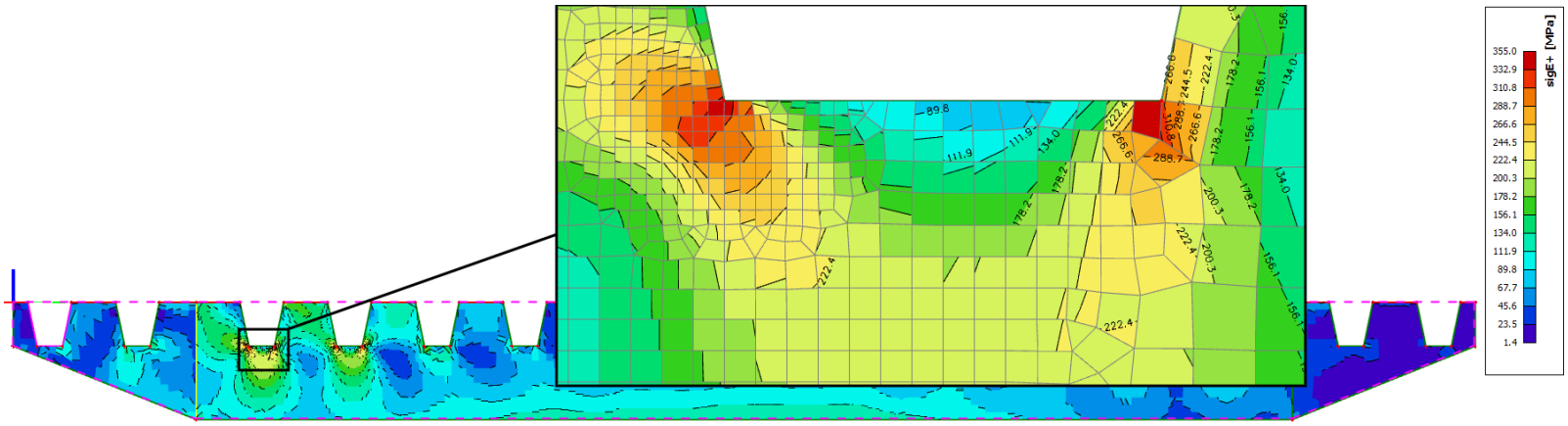

Figure 5.21: Von Mises stresses in closest to mid-span cross girder web

- Ultimate Von Mises stress in mid span cross beam: ≈ 355 MPa
- At cross beam- trough connection corner
- Under Combination: All combination in which LM1 tandem systems are positioned in middle local mid span

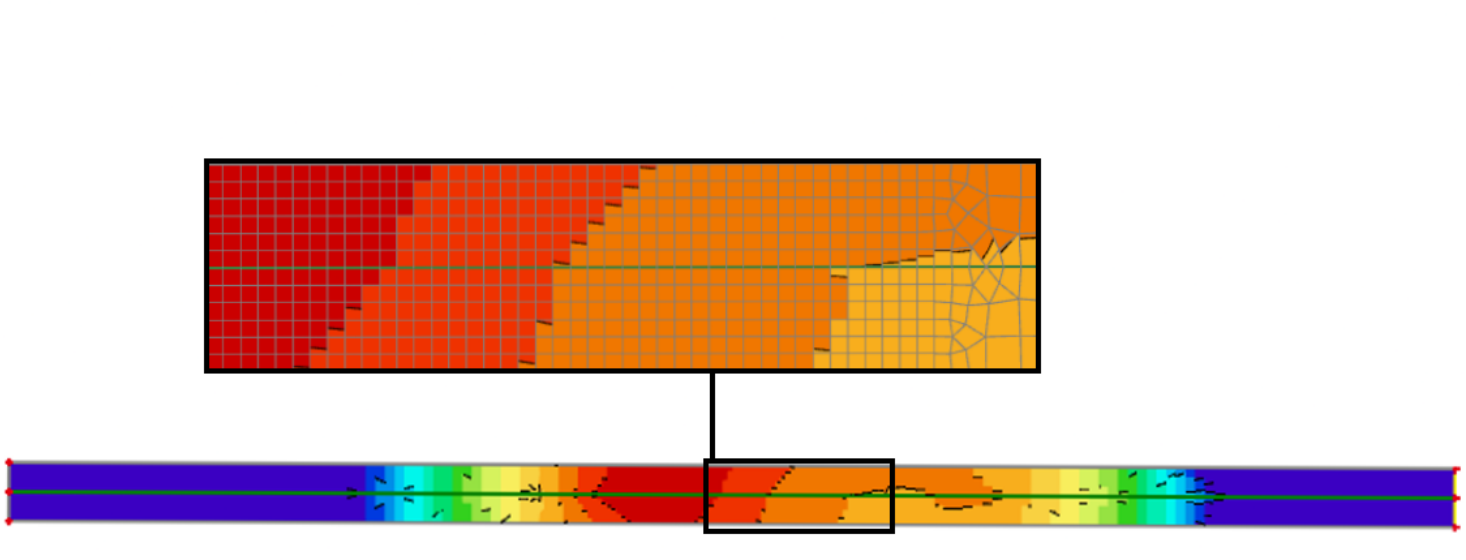

Figure 5.22: Normal stresses in closest to mid span cross girder flange

- Ultimate normal stress in cross girder flange: ≈ 161 MPa
- At mid span cross beam
- Under Combination: Tandem systems over mid span cross beam + transverse wind forces on less heavily loaded main girder + Negative temperature difference of the deck

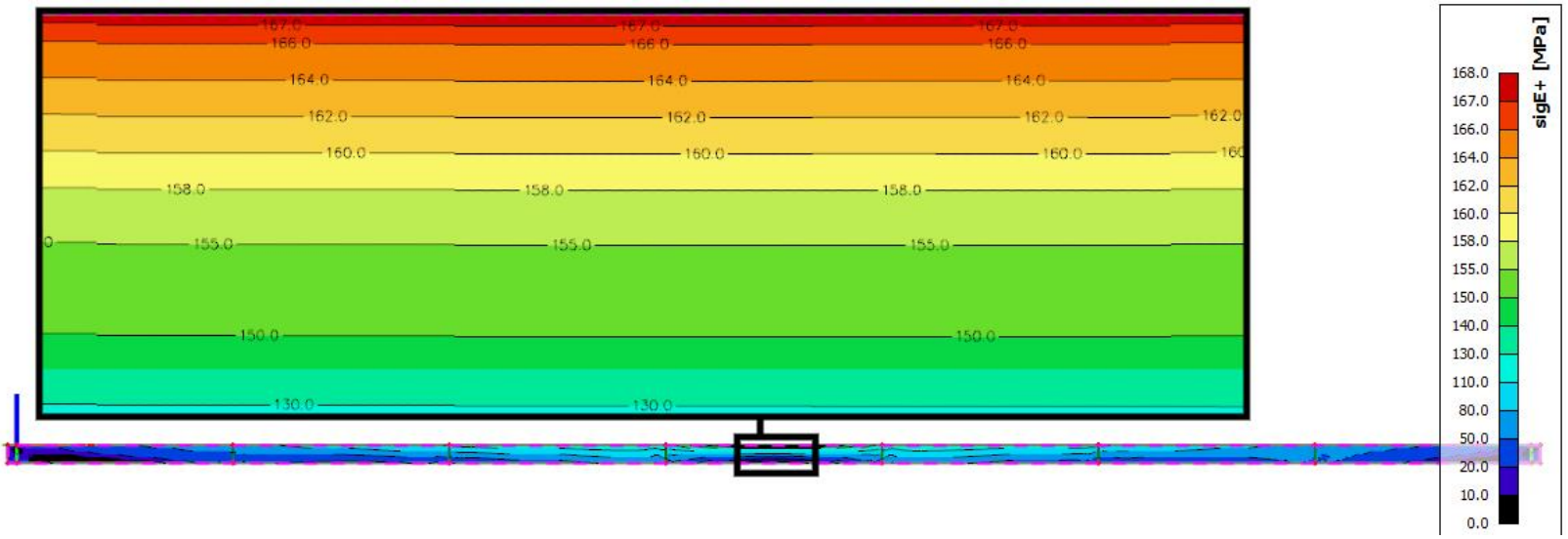

Figure 5.23: Von mises stresses in heavily loaded longitudinal end plate

- Ultimate Von Mises stress in heavily loaded end plate: 168 MPa
- At mid span of end plate
- Under Combination: Tandem system at mid span + wind load on more heavily loaded main beam + negative temperature difference of the deck

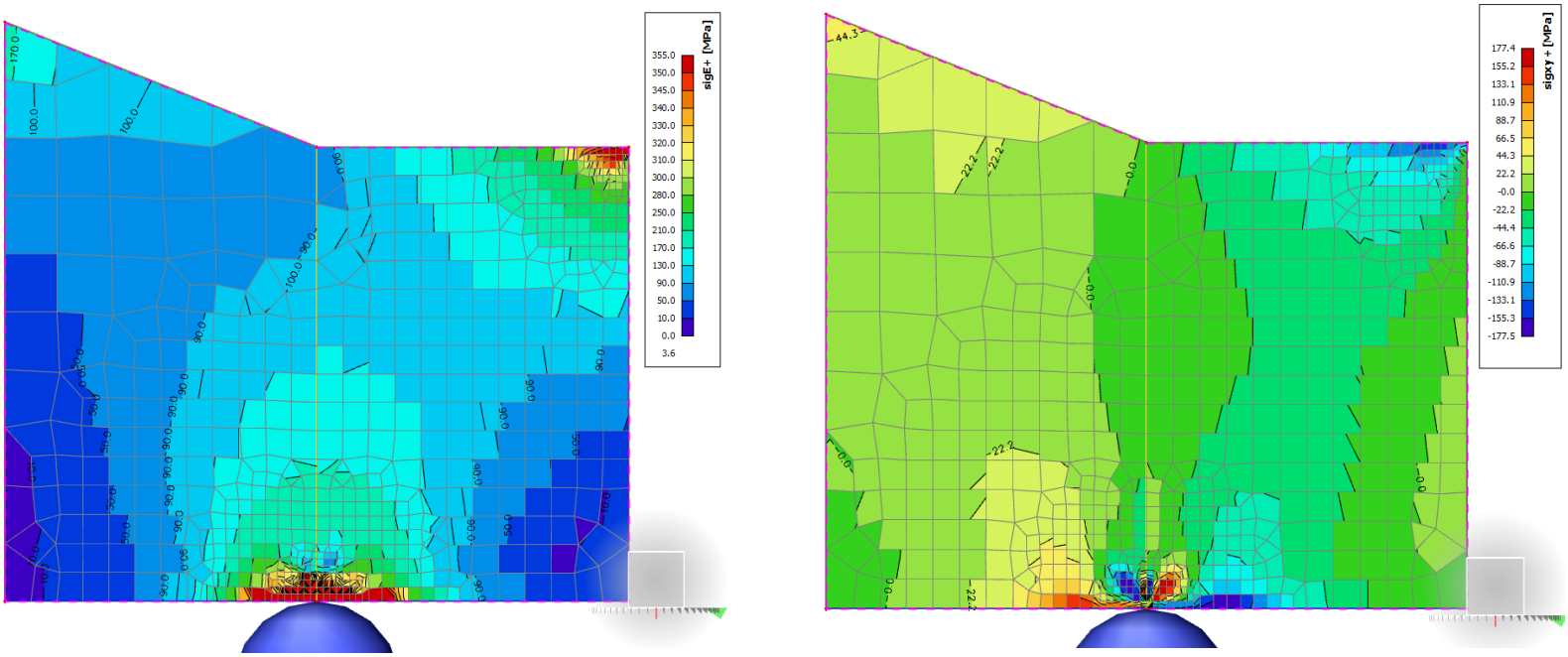

Figure 5.24: Von Mises and Shear stresses in shear stiffener over support of more heavily loaded main beam

- Ultimate Von Mises stress in shear stiffener: ≈ 355 MPa (Nodes next to support)
- Under Combination: All combinations with Tandem systems close to final cross beam and thus shear stiffener

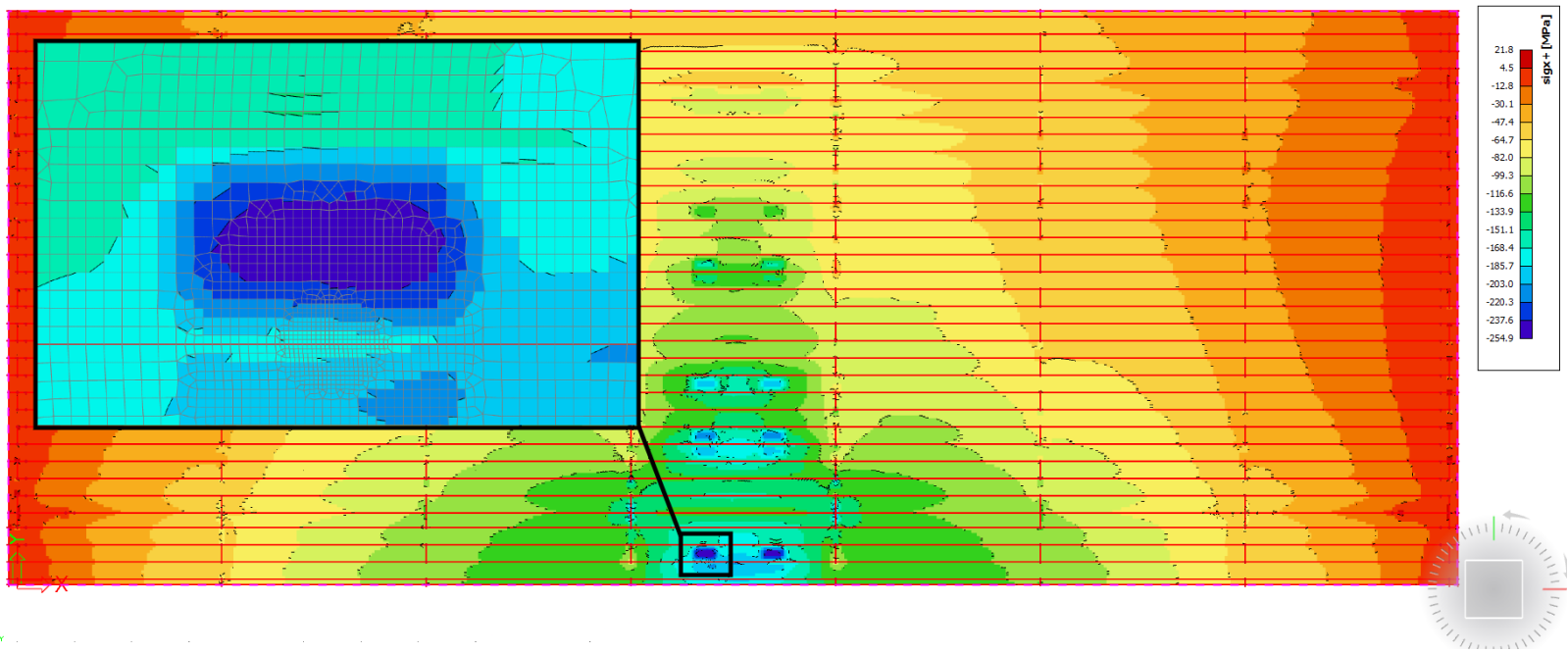

Figure 5.25: Normal stresses in deck plate

- Ultimate Normal stress in deck plate: -255 MPa
- At global mid span, lane 1
- Under Combination: Tandem systems at mid span + wind load on more heavily loaded main girder + positive temperature difference

5.2.4 SLS Results

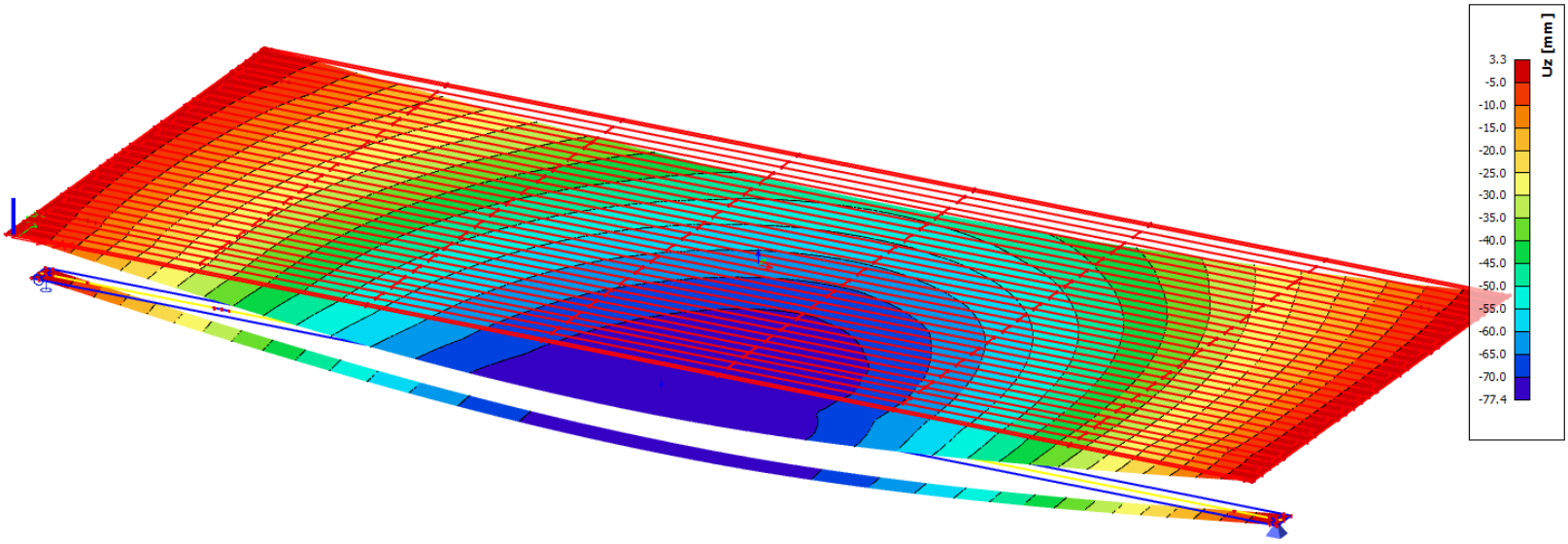

Figure 5.26: Z Displacement of heavily loaded main beam flange and deck

- Largest Displacement of Main girder flange: -75,3 mm (downwards)
- At mid span, more heavily loaded main beam

- Largest displacement of deck: -77,4 mm (downwards)
- At mid span, above more heavily loaded main beam

- Largest displacement of deck: 3,3 mm (upwards)
- Transverse edge of plate

- Under Combination: Tandem systems at mid span + Negative temperature difference of deck

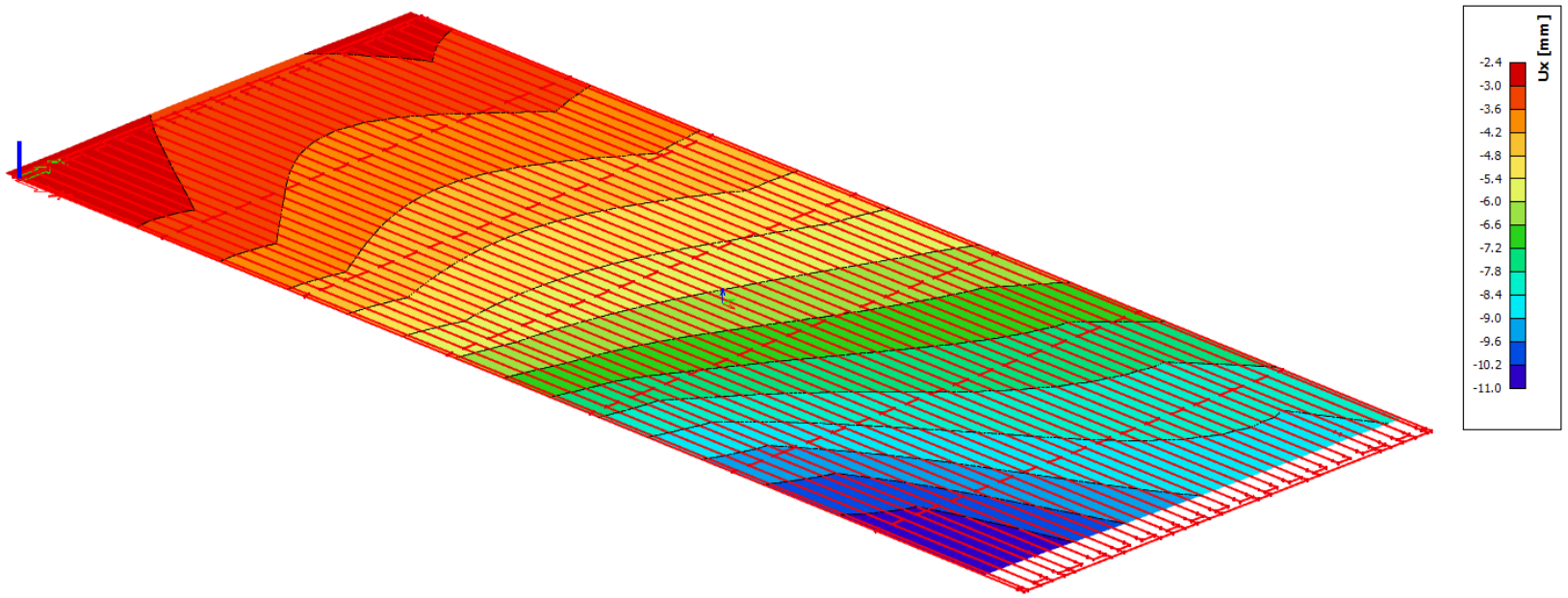

Figure 5.27: Maximum X Displacement of transverse deck edge

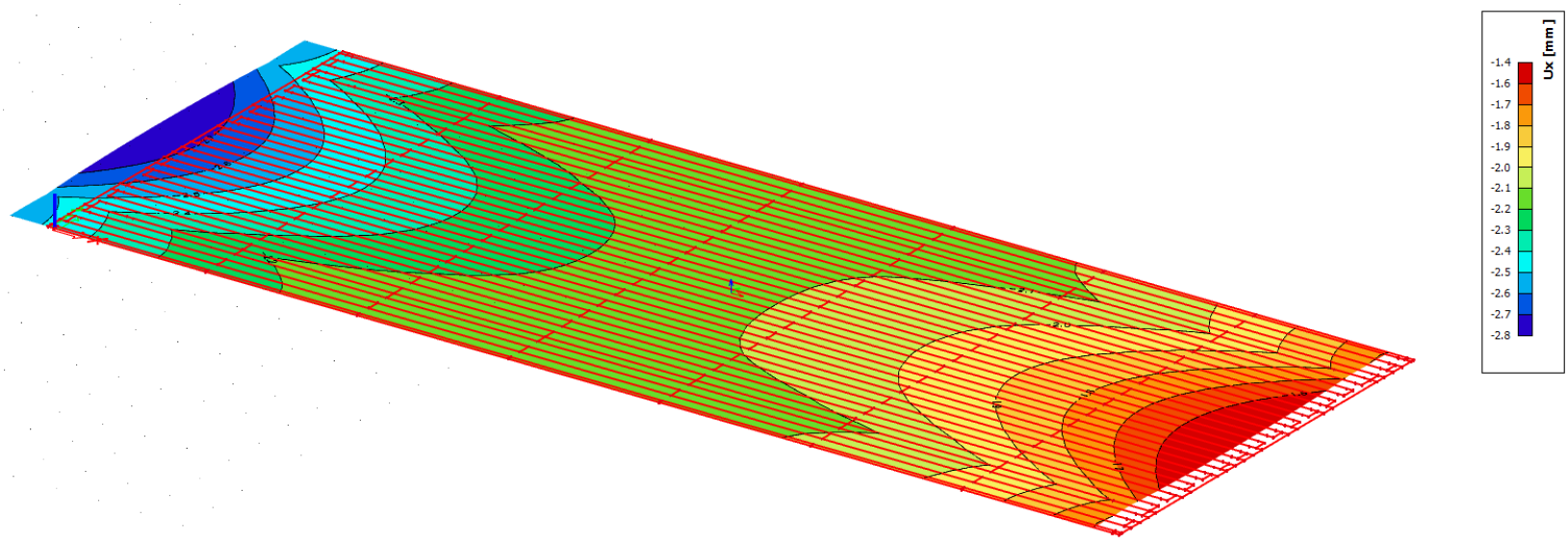

Figure 5.28: Minimum X Displacement of transverse deck edge

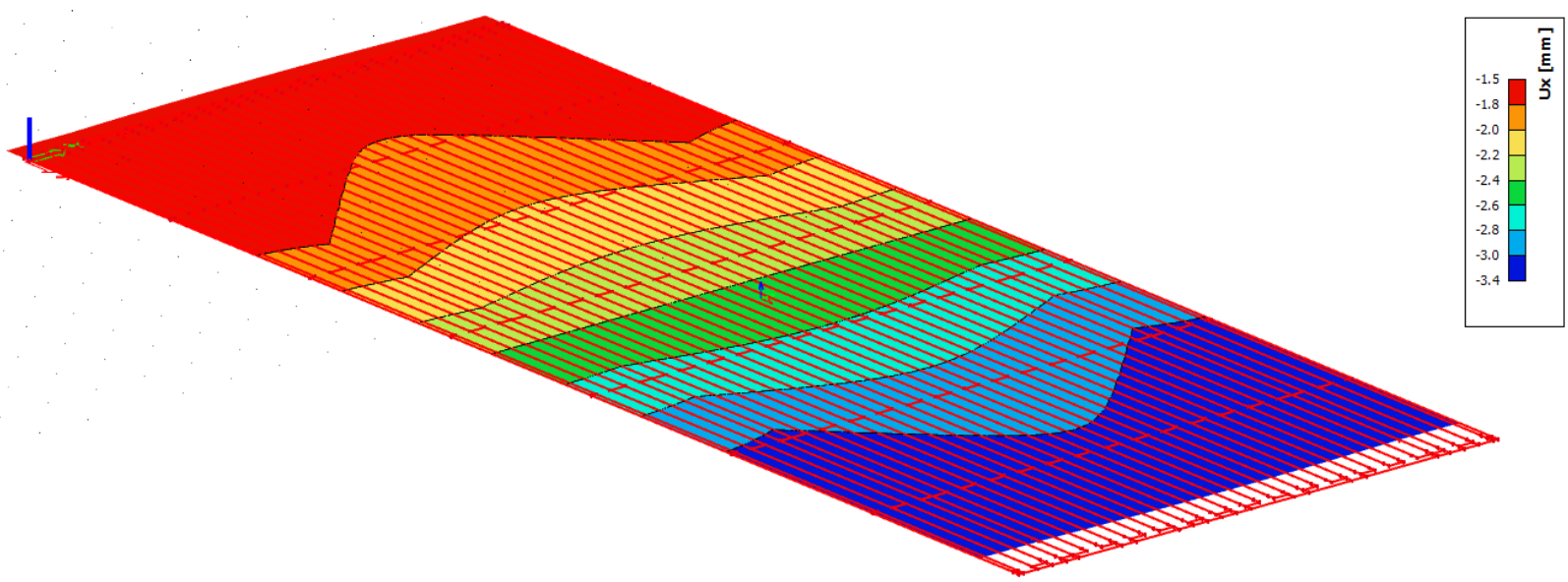

Figure 5.29: X Displacement of transverse edge under only dead loads

- Largest transverse displacement of deck edge in longitudinal direction (x direction): 11 mm
- Under Combination: Tandem systems at mid span + Negative temperature difference of deck

- Smallest transverse displacement of deck edge: 2,8 mm
- Under Combination: Dead loads + Positive temperature

- Deck edge displacement under only dead loads: 3,4 mm

5.2.5 ULS and SLS Discussion

ULS

- All members have sufficient strength and no buckling phenomena are observed. Stress concentrations occur in corners as expected.
  These stress concentrations are expected to be of importance for the fatigue life of the troughs.

- The inner corners of the shear stiffeners to final cross beam connection can be improved by applying a curved plate instead of having a sharp corner. Ultimate stresses in this part of the structure however remain under the ULS threshold, despite the sharp intersection.

- In the ULS criterium, only single elements reached the yield stress. This highly likely to be due to a singularity in the solving process or an insufficiently refined mesh. If this is not the case, very local plasticity may occur under ULS loading.

- In the model, plasticity occurs in the supports. The supports are modelled in a single node, this is therefore expected and very unlikely to happen in reality.

- Some elements are oversized when it comes to ULS. This is due to fatigue being the expected normative condition.
  The OSD dimensions are based on reference projects of IV Infra.

SLS

- When it comes to other over dimensioned elements, the SLS limits are normative. Although there are no limits on sag of steel bridges, they exist for timber ones in the Eurocode.

- The maximum sag of the deck is 77,4 mm in SLS. This corresponds to $\frac{L}{323}$.
  This sag is lower than the recommended $\frac{L}{300}$ in EN 1995-2

- Table NB.4 in the NA to EN 1993-2 recommends the value of the vertical gap at the end of the bridge to be equal to 0 and sets a maximum of 5 mm. The 3,3 mm obtained is less than the maximum value.

- For a horizontal gap a recommended value of 20 mm and a maximum value of 40 mm is given. The largest range of motion is $11 - 2{,}8 = \mathbf{8{,}2}\ mm$.
  If a gap of 20 mm is realized with only the dead loads and positive temperature load, it would grow to 28,2 mm when the maximum x displacement is achieved, staying within the limit of 40 mm.

- A potentially more desirable option would be having the 20 mm gap calibrated to only the dead loads, resulting in a maximum gap growth of $11 - 3{,}4 = \mathbf{7{,}6}\ mm$ or a gap of 27,6 mm and a minimum gap of $20 - (3{,}4 - 2{,}8) = \mathbf{19{,}4}\ mm$.
  This depends on which option would be seen as more desirable and on the expected frequency of the positive temperature action on the deck.
  Regardless, the structure is within the prescribed limits given in the Eurocode.

5.2.6 Fatigue Verification

Fatigue design is often governing when it comes to steel plate girder bridges. In order to produce a functional design, critical details will be verified.
A series of model iterations with different dimensions is produced and checked. The final bridge dimensions are shown. A single detail verification is worked out in detail in the main text, while the verifications of the other points of interest are shown in appendix C, with their results summarized in table 5.1.

Modelling

The lorry is modelled as “driving” over the bridge in all three lanes with a step of 1 meter maximum. EN 1993-2 specifies deviations from the centre of a lane for certain percentages of the total traffic. This is of importance for local deck details. However, due to the relatively thick surfacing and the large resulting spread, these deviations will not be accounted for.

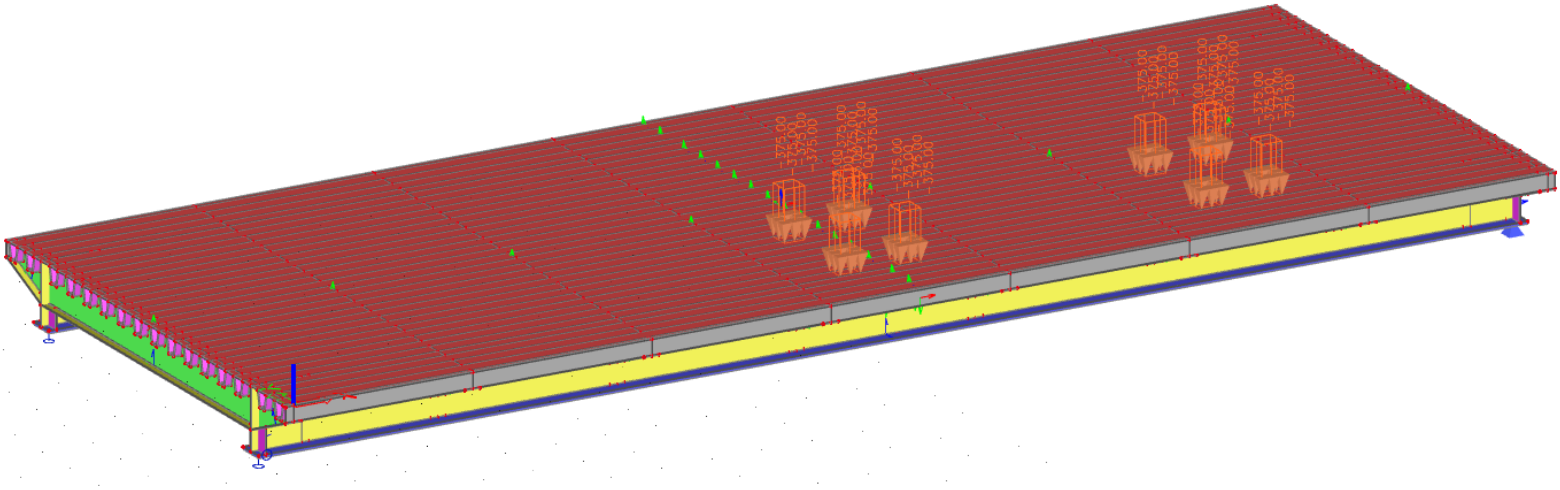

Figure 5.30: FLM 3 start position in Lane one

The mesh settings are the same as described in the previous paragraphs. A local mesh refinement with a factor constitutes a minimum mesh size of 5 mm.

Equivalent damage factors

When applying FLM 3 on steel bridges, the stresses obtained from the model, must be multiplied by the, so called, equivalent damage factors.

The equivalent damage factors are calculated according to EN 1993-2, 9.5.2.

The factors λ_i, with i from 1 to 4 account for respectively:

- The damage factor due to traffic, dependent on the influence area
- The factor due to traffic volume
- The factor due to the design service life of the bridge
- The factor account for the fact that a load carrying member is subjected to effects of multiple lanes

$$For\ normal\ stresses\ in\ main\ girder: \lambda_1 = 2{,}55 - 0.7 * \frac{25-10}{70} = 2{,}4$$

$$For\ shear\ stresses\ in\ main\ girder: \lambda_1 = 2{,}55 - 0.7 * \frac{0{,}4 * 25 - 10}{70} = 2{,}55$$

$$For\ normal\ stresses\ in\ cross\ girder\ midfield: \lambda_1 = 2{,}55 - 0.7 * \frac{0{,}7 * 7{,}5 - 10}{70} = 2{,}6 > 2{,}55$$

$Reduced\ to\ 2{,}55$

$$For\ normal\ and\ shear\ stresses\ in\ cross\ girder\ at\ support: \lambda_1 = 2{,}0 - 0.3 * \frac{0{,}15 * 7{,}5 - 10}{20} > 2{,}0$$

$Reduced\ to\ 2{,}0$

$$\lambda_2 = \frac{Q_{m1}}{Q_0} * \left(\frac{N_{Obs}}{N_0}\right)^{\frac{1}{5}} = \frac{4 * 120}{480} * \left(\frac{0{,}5 * 10^6}{0{,}5 * 10^6}\right)^{\frac{1}{5}} = 1$$

$$\lambda_3 = \left(\frac{t_{Ld}}{100}\right)^{\frac{1}{5}} = \left(\frac{100}{100}\right)^{\frac{1}{5}} = 1$$

$$\lambda_4 = 1, traffic\ on\ the\ bridge\ is\ in\ one\ direction\ only, a\ single\ heavy\ traffic\ lane\ is\ assumed$$

$$\lambda = \lambda_1 * \lambda_2 * \lambda_3 * \lambda_4 < \lambda_{max}$$

In all cases the factor λ_1 exceeds the maximum given value λ_{max}, which is capped at $2{,}5 - 0{,}5 * \frac{25-10}{15} = 2$ for mid span checks and $1{,}8$ for checks over supports.

λ is therefore set to 2.

Fatigue Resistant Bridge Dimensions

The bridge dimensions obtained from the fatigue design are detailed.

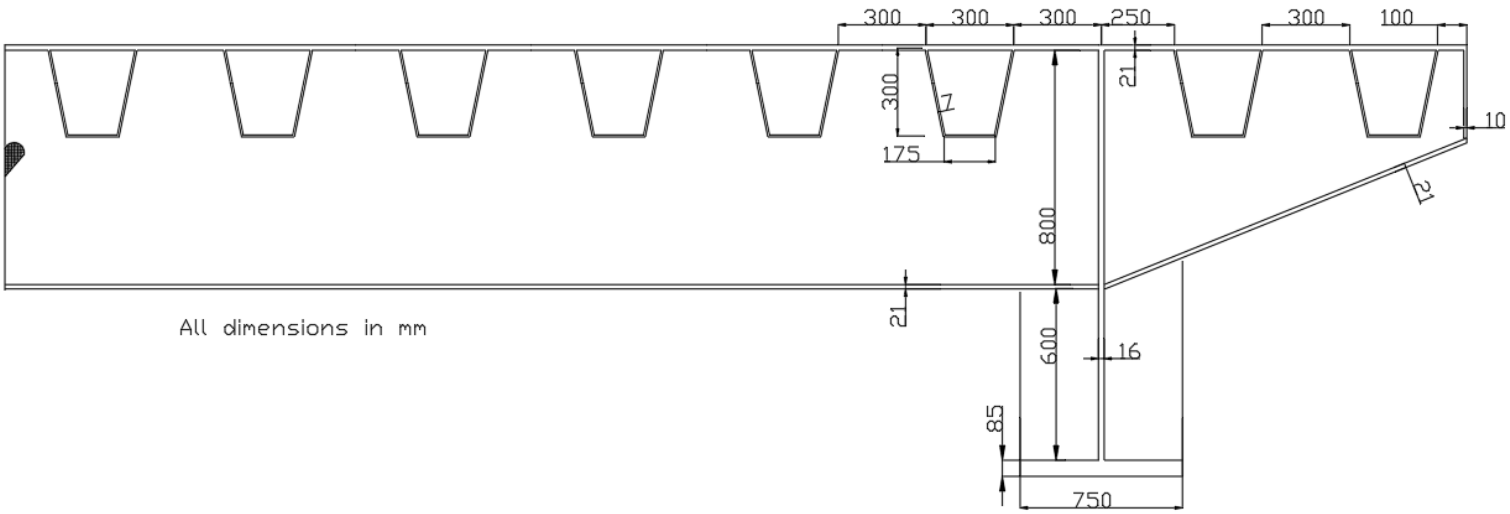

Figure 5.31: Transverse bridge cross section, mid span cross girder

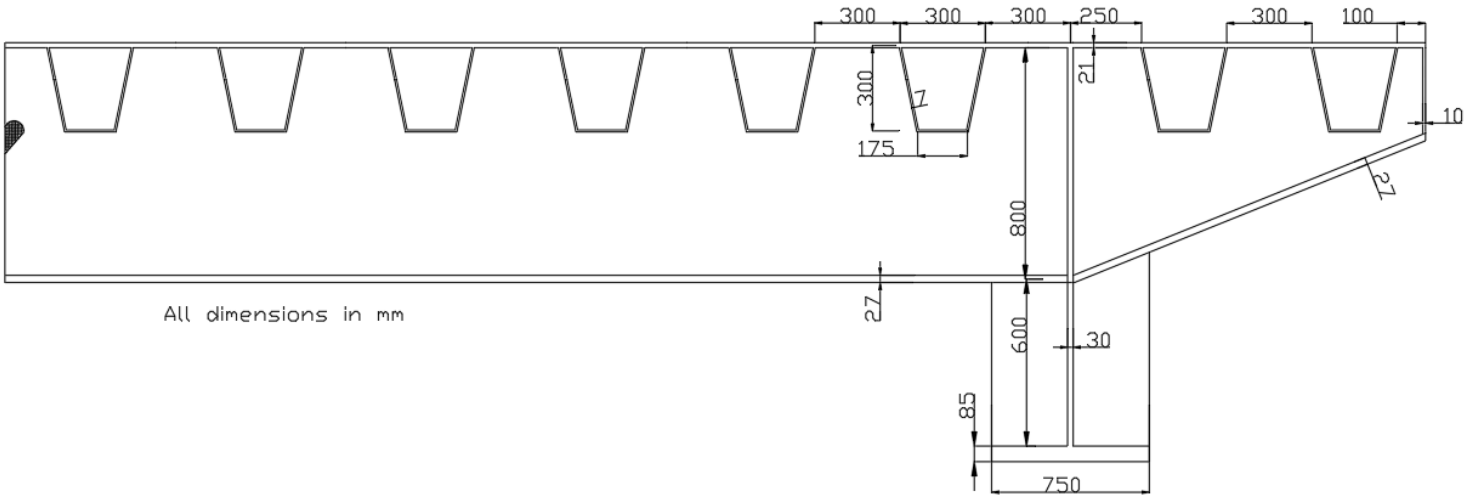

Figure 5.32: Transverse bridge cross section, end span cross girder

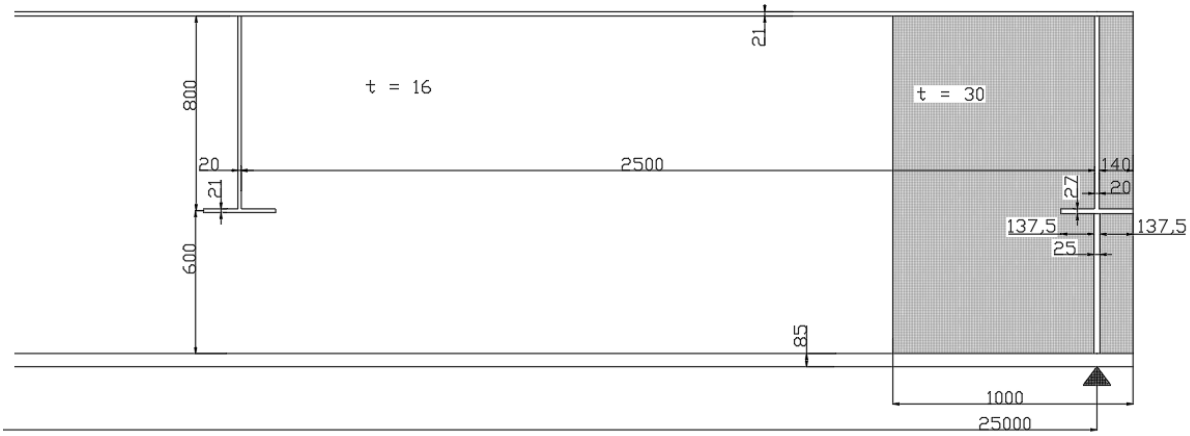

Figure 5.33: Longitudinal bridge cross section, right end span

Fatigue Details of Interest and Calculation

The areas of interest, along with the detail class according to EN 1993-1-9 (unless otherwise specified) are shown in figure 5.30.

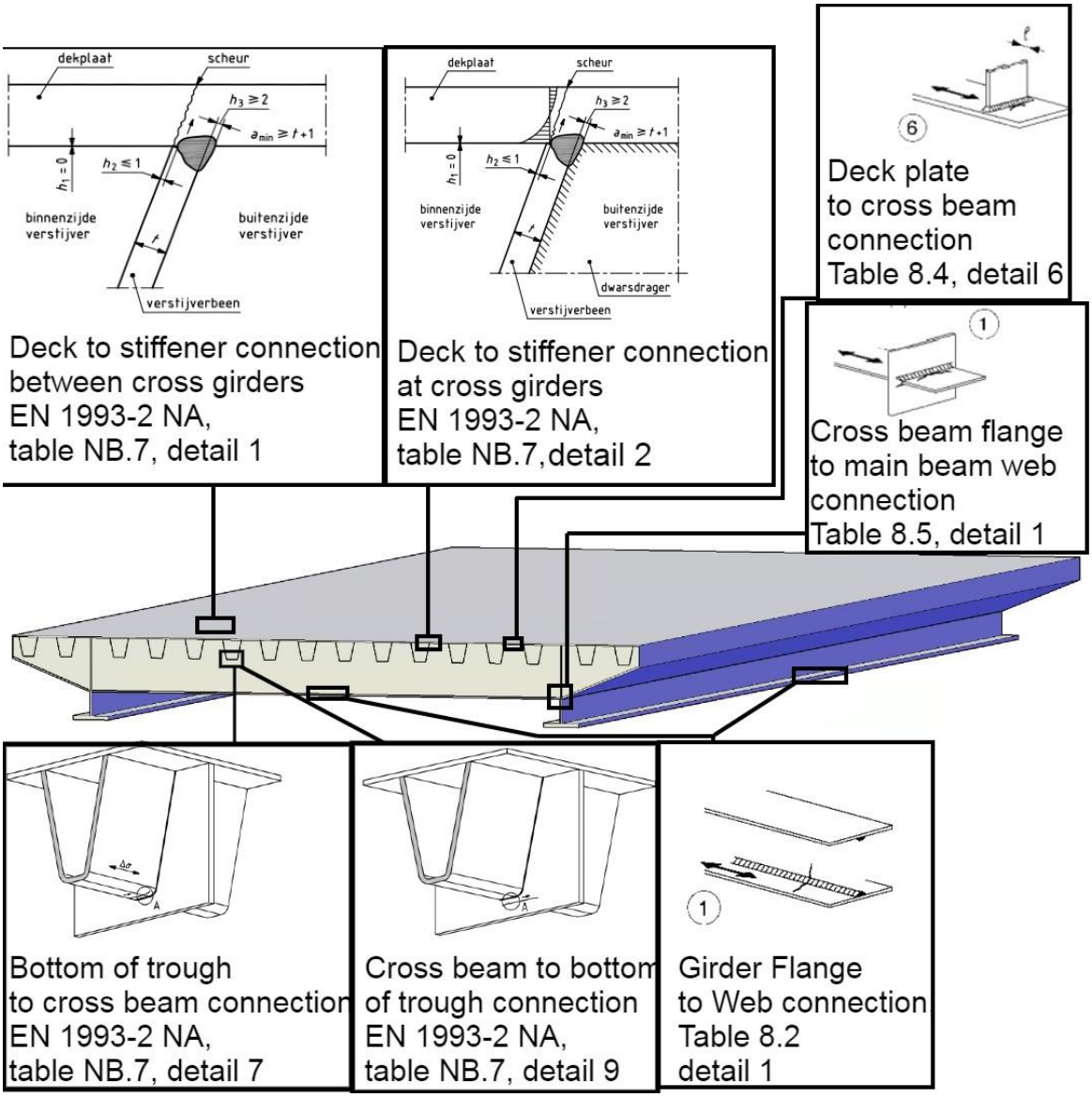

Figure 5.34: Fatigue details of interest

Detail 2 from EN 1993-2 must be verified according to the hot spot stress method. The other details, as shown in figure 5.34 are based on the nominal stress method.

The calculation for the normative deck to stiffener connection above a cross girder is performed. The calculation for the other details is done in the same fashion, with the only difference being the reading of the stresses according to the simpler nominal stress method as opposed to HSS. The calculations alongside with the detail classes of all details can be found in appendix C.

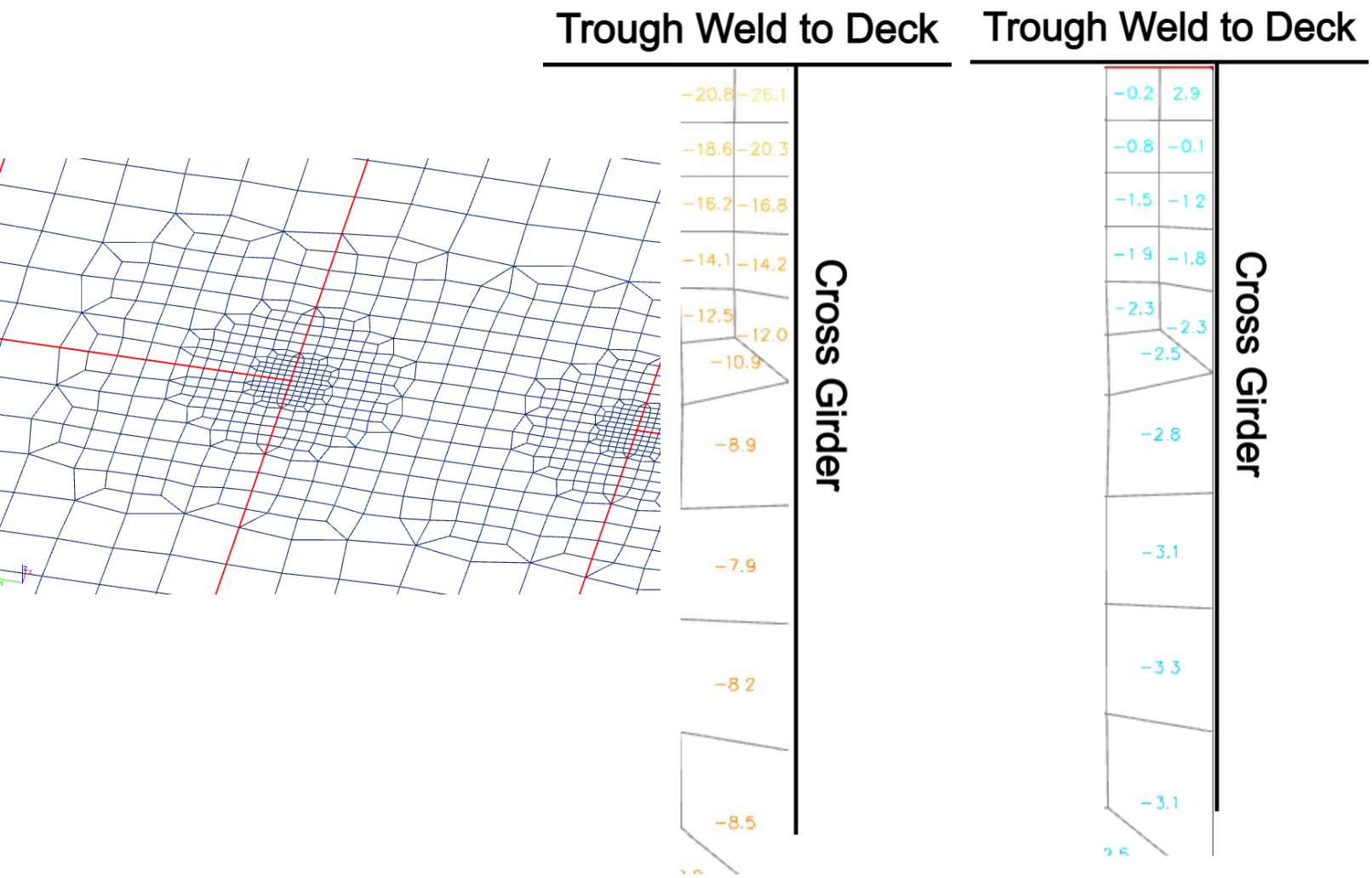

Figures 5.35a, b, c: Mesh used at trough to deck check, minimum and maximum stresses underside of deck

Spacings at which stresses are obtained for this verification are 0,5 and 1,5t of the member as specified by the IIW [14] for a “rough” mesh.

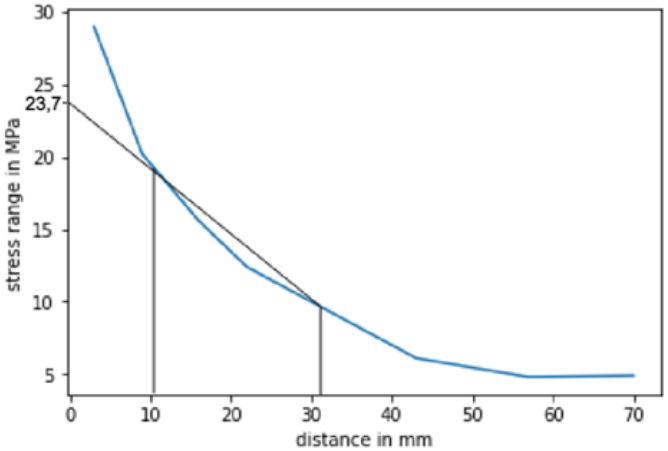

Figure 5.36: Stress range from trough weld and hot spot stress

$$\Delta\sigma_C = 125\ MPa \qquad \gamma_{Mf,OSD} = 1{,}15 \qquad \lambda = 2 \qquad \Delta\sigma_R = 23{,}7\ MPa$$

$$\Delta\sigma_D = \Delta\sigma_C * 0{,}737 = 125 * 0{,}737 = 92{,}125\ MPa$$

$$\frac{\Delta\sigma_D}{\lambda * \gamma_{Mf}} = \frac{92{,}125}{2 * 1{,}15} \approx 40{,}05\ MPa$$

$$40{,}05 = \Delta\sigma_D > \Delta\sigma_R = 23{,}7$$

$$N_r = \left(\frac{\frac{\Delta\sigma_D}{\lambda * \gamma_{Mf}}}{\Delta\sigma_R}\right)^{m2} * N_D = \left(\frac{40{,}05}{23{,}7}\right)^5 * 5e6 = 68{,}85e6\ cycles$$

$$UC = \frac{N_{obs}}{\mathrm{N}_r} = \frac{50e6}{68{,}85e6} = 0{,}73$$

Fatigue Results and Discussion

The unity checks of the fatigue details shown in figure 5.34. Subsequently discussion points raised by the fatigue validation are handled.

Fatigue Detail	Unity Check
Cross Beam to Stiffener Connection, EN 1993-2 NA, Table NB.7, detail 9	0,97
Bottom of Stiffener at Cross Beam, EN 1993-2 NA, Table NB.7, detail 7	0,83
Deck, between Cross Girders, EN 1993-2 NA, Table NB.7, detail 1	Below cut-off limit
Deck, above Cross Girder, EN 1993-2 NA, Table NB.7, detail 2	0,73
Main Beam- Flange to Web Connection, EN 1993-1-9, Table 8.2, detail 1	0,78
Cross Beam- Flange to Web Connection, EN 1993-1-9, Table 8.2, detail 1	Mid Cross beam: 0,88 Outer Cross beam: 0,99
Cross Beam Flange to Main Beam Web Connection, EN 1993-1-9, table 8.5, detail 1	Below cut-off limit
Deck to Cross Beam Connection, EN 1993-1-9, table 8.5, detail 6	Below cut-off limit

Table 5.1: Fatigue check results

The bridge element dimensions have drastically increased due to fatigue. Spacing between the cross girders has decreased as well. Because of this, it is not expected that ULS or SLS will be governing for this design and will therefore not be checked.

- FLM 3: Fatigue load model 3 is used. FLM 4 offers more accurate results and a range of stresses, resulting from different lorries. The application of it, however, is very time consuming; verifying a bridge, like the one presented, would constitute a work amount warranting a thesis by itself. FLM 3 is considered to be sufficiently accurate and the dimensions obtained for the bridge elements are reasonable.

- Verified details: The verified details are the ones which are expected to be governing and the ones which constitute a substantial use of material. For this reason, the shear stiffeners aren't validated for fatigue; an increase in thickness and thus decrease of stresses and stress ranges would not result in a notably larger material use.

- Unity check discrepancies: Some details have high unity checks, while others have relatively low ones.
  This is inherent when using a non-varying thickness for members.
  For example, the deck has a relatively high unity in detail 2 from the NA to EC 3-2, table NB.7, but an infinite lifetime for its connection to the cross beam.
  The same can be said about the cross-beam flange connection to the cross-beam web and its connection to the main beam web.

- Unity check values: A small decrease in thickness can result in notably higher stress ranges for fatigue and drastically decrease fatigue life. The current normative unity check for the deck is 0,73. A decrease in thickness of 1 millimetre brings this value above 1.

6 Wood Bridge Orientation

In this chapter, wood is described and a choice for the timber used in the bridge is made based on the use conditions.
Subsequently, various timber bridge design options are considered. A selection of these is then worked out to aid with the choice for a final design.

6.1 Wood as a Material

6.1.1 Wood Build-up

Wood is a naturally occurring, anisotropic material; its physical and mechanical properties differ per direction. This is due to differences in cell types, their shape, size, and orientation.
The mechanical properties of wood strongly depend, among other factors, on growth irregularities.

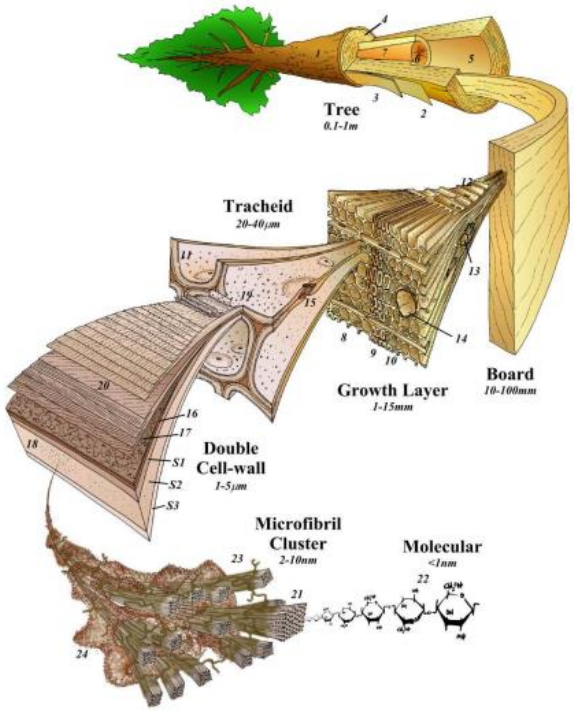

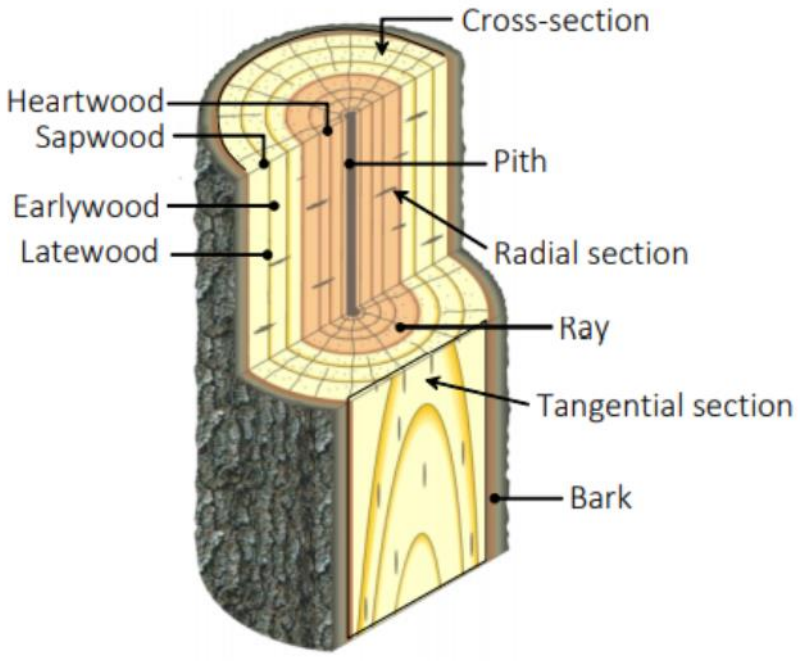

Figure 6.1: Softwood schematic, from [23, p.2]

Figure 6.2: Macroscopic structure of wood, from [20, p.24]

The tree stem is used for structural applications. In nature, its main function is that of supporting the crown of the tree and transporting nutrients and water to and from it. To serve this purpose, most cells are orientated along the tree stem. Due to this, the stem has a much larger strength in the axial direction when compared to the radial or tangential directions. Ray cells have a radial orientation; they ensure transport of nutrients and water in that direction.

The stem is divided into heartwood and sapwood. The heartwood is made up of older, dead cells and stabilizes the tree, while the sapwood transports and stores nutrients. Upon formation, heartwood closes its pits, preventing transport of nutrients. Due to this, it is more durable dan sapwood.
It must be noted, that the oldest rings of the heartwood, around the pith, have lower mechanical properties. This area is known as juvenile wood, while the material further out is known as mature wood.

The tree grows in girth from the Cambium. This is a thin layer between the bark and the sapwood. Annual growth rings are formed each year. Starting in the spring, the tree must transport water and nutrients with a large flow, forming large canals, which results in less dense wood than when compared to wood grown in the winter. This is known as earlywood and generally has a light color. Latewood is formed in the winter; less to no water and nutrients are transported then and thus canals are smaller and the density is higher in latewood compared to earlywood.
The formation of early- and latewood therefore depends on the climatic conditions and the tree type; some species have clearly visible growth rings, while others have nearly indistinguishable latewood and earlywood. The growth rate and differences in density impact the strength of the wood, with slower growth and relatively more latewood ensuring higher strength.

When the tree is subjected to forces perpendicular to its orientation, it forms reaction wood.
In hardwoods, this is tension wood, while in softwoods, it is compression wood. These parts of a stem have different properties to the rest of the stem and entail fiber deviations. Branches make for local fiber deviations in structural timber in the form of knots.

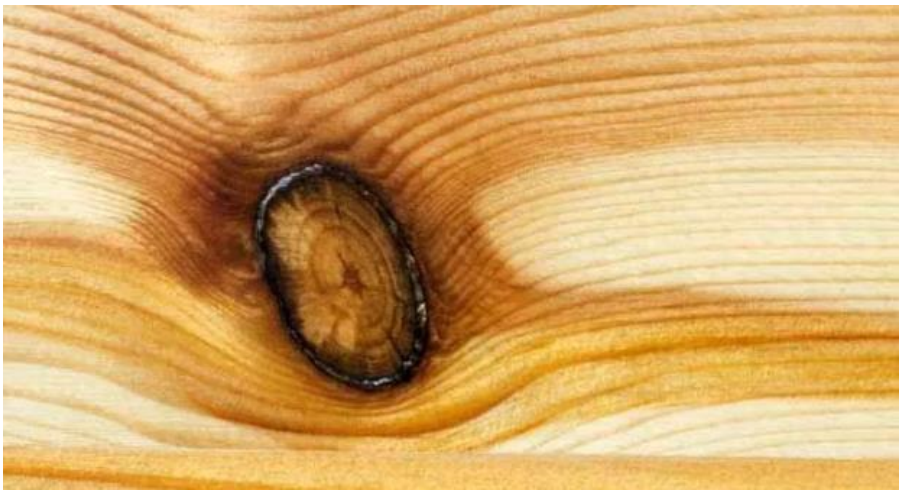

Figure 6.3: Knot in wood, from [The Pros and Cons of Knots in Wood - Wagner Meters]

Timber with large global fiber deviations and/ or a large number of knots has reduced mechanical properties and is graded accordingly. [20] [23]

6.1.2 Wood Behaviour

Wood is a hygroscopic material; it is susceptible to water infiltration. The higher the amount of water in timber, the lower the values of its mechanical and durability properties are.
The magnitude of water sorption depends on the wood porosity. Denser wood types are generally less porous and thus less prone to pronounced hygroscopic behaviour.
Softwoods are usually more prone to water infiltration than hardwoods.
The amount of water sorption further depends on the environment; high relative humidity or contact with water, especially when combined with high temperature make for more moisture adsorption.

A higher amount of water also brings with it swelling of the timber. This happens until the fibre saturation point; above this point, free water is present in cell cavities and the mechanical properties of the timber no longer change. Underneath this point, water is bonded to -OH groups in the cell walls.
The fibre saturation point is taken as an average of 28%.

Due to the anisotropic nature of the material, this swelling differs in radial, tangential and longitudinal direction.

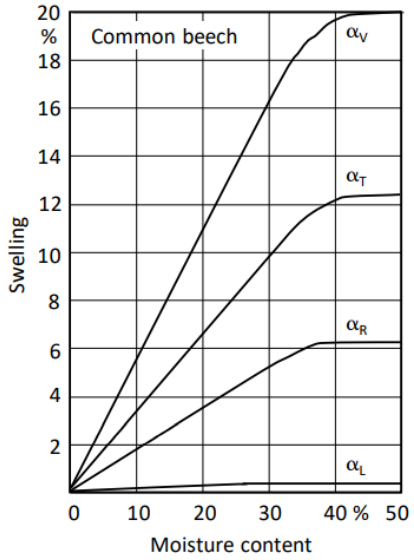

Figure 6.4: Swelling in tangential (T), radial (R), longitudinal (L) direction, and total volume (V) of beech, from [20, p.42]

Depending on the location of the wood cut from a log, various distortions can happen in a sample.
Higher amounts of water in wood also make for a favourable environment for (deteriorating) fungi.

Wood has time dependant properties. Creep takes place under continuous loading, it depends on the type of loading and the environment the structure is located in.
Under relaxation, stresses in timber due to constant loads reduce. This is especially of relevance for prestressed elements, where prestressing force is lost. [20]

6.1.3 Wood Durability

Wood is sensitive to degradation. This degradation can be caused by insects, such as termites, or wood destroying fungi. Fungal deterioration is especially of relevance in temperate climates.

Wood fungi grow best in moisture contents of between 30 and 60% and temperatures between -2,5 and 40°C. The harshness of environments is treated with “use classes” as defined in EN 335, with lower numbered classes representing less harsh environments.

The durability of various wood species can be found in EN 350-2. Classification against fungi is done only for heartwood, sapwood is considered prone to fungal attack.
Tropical hardwoods are generally more durable against pests, they contain higher amounts of extractives compared to temperate woods.

The durability of wood species prone to degradation can be improved with chemical treatment or modification. Creosote treatment has been widely applied in the past, but due to health and environmental reasons, it’s been all but banned across most of the world.

Modifying the wood structure so that it does not bind with water is a more accepted option.
Heat treatment destroys -OH groups, preventing water from bonding to the wood structure.
It also lowers the mechanical properties of the timber and is therefore undesirable for most structural applications.
Occupying hydroxyl groups does not notably change the timber’s mechanical properties.
This is done by furfurylation (impregnating the wood with furfuryl alcohol) or acetylation (using acetic acid to occupy hydroxyl groups). The latter process is done on a commercial scale to radiata pine timber, creating what is known as Accoya.

Figure 6.5: Accoya Bridge, close to Sneek, from [https://www.shr.nl/case-studies/houten-brug-bij-sneek-voor-de-zwaarste-verkeersklasse]

The rate of effectiveness of these techniques is dependent on the susceptibility of a wood species to be impregnated. Some species are more suitable for that than others, treatability per species should therefore be considered.

The most effective way of ensuring the durability of wood is design:

- Keeping the elements as dry as possible, away from direct rain or splashing water
- Water drainage and ventilation must be ensured
- Use fitting fasteners; stainless steel bolts and such if in an environment which stimulates corrosion
- Cover end grain

[9], [20]

6.1.4 Glulam

Glulam is an engineered timber product. It consists of multiple planks of wood (lamellas) glued together. Lamellas are glued on top of each other, but can also be joined at their ends with finger joints to create longer beams. By doing this, large spans can be achieved without the need for dowel connections.
Glulam can be joined into large very large cross sections, making it competitive to steel and concrete. Block glued glulam consists of multiple glulam members joined together, creating various cross sections; monolithic and box sections are common. The current European standard, EN 14080, only considers rectangular block glued glulam cross sections.

Figure 6.6: Curved Block glued Glulam Member, from [24]

6.2 Wood in the Context of Bridges

“Instead of thinking of ways how to maximize wood biomass use, the more critical question is how to minimize the environmental impacts of construction and maximize the needs of a society in a holistic way by combining different materials and exploiting their best properties” [18].

Relatively small amounts of wood are necessary for construction. However, replacing more environmentally taxing products with timber brings with it added value.
According to a book published by CEI-Bois [21], the substitution of other building materials with wood results in an average of 2 tons of CO2 per cubic meter being saved, if the CO2 stored in wood is considered.

Most heavy traffic bridges in Western Europe are built with traditional materials. The use of timber, in the load bearing structure of bridges, is often limited to pedestrian and cycle bridges.

Low-capacity traffic bridges, made from wood can be seen throughout European countries with a more pronounced timber building heritage. Many of these bridges can be found in Scandinavian and Germanic countries.

Figure 6.7: Lohmar Höngersberg bridge, from https://www.ib-miebach.de/en/projects/timber-bridges/arch-bridges-made-from-timber/long-span-timber-arch-bridge-hoengesberg-de.html

The Miebach engineering firm in Germany has produced several timber arch bridges as can be seen in figure 6.7.

Figure 6.8: Flisa bridge, from https://structurae.net/en/structures/flisa-bridge

The Flisa bridge in Norway, is an arch truss bream with 3 spans, the largest of which is 70.5 meters. The load over this span is carried by a truss arch.
The bridge has two lanes and a raised footpath.

Figure 6.9: Pieter Smitbrug, from [22]

Recently, the longest cycling bridge in Europe was completed in Groningen. This bridge is made from azobé, a tropical hardwood.

6.3 Timber Choice for case study

6.3.1 Wood Requirements

The requirements for the wood are shown, with the reasoning behind them.

- European sourced for ensuring shorter transportation distances.
- Glulam for allowing the use of large cross sections without dowelled connections.
- Commercially available in order for the structure to be representative of reality as much as possible.
- Fitted for outside use: Dimensionally stable and durable.

6.3.2 Douglas Fir

Douglas fir is a softwood tree species, native to the pacific northwest in America. It was introduced to Europe in 1827 by David Douglas. From then on, the species has been cultivated throughout Europe and currently makes up 0,4% of the European forest area [25].

The countries with the largest stocks of Douglas fir in Europe are France and Germany. In terms of relative coverage, the Netherlands and Belgium, have the highest share of Douglas fir.

Public perception of Douglas fir differs per region. In France, the stock of this species has an age of 21 to 40 years and is grown for timber production. There, the species is mostly grown in monocultures for commercial use and is widely accepted by the public.

In Germany, the species is often considered as invasive and its planting was temporarily banned for a period of time in the 1940s due to a pathogen, which was later exterminated [25].

Invasiveness

Different definitions of invasiveness have been considered and different conclusions have been drawn in various studies. Some of these are summarized by Bindewald and Michiels in [26]. The conclusion of this research is that, currently, Douglas fir regeneration is low in both managed and unmanaged forests, with the exception of patches, where it is the dominant species.
A case study on Douglas fir in Freiburg [27] concludes that the species regenerates well with medium sun exposure, but not under tight canopies.

A set of simulations were run by B. Eberhard, et al. [28]. These show that Douglas fir is very sensitive to competition, especially from Beech. They conclude that Douglas fir is not an invasive species. The results from these simulations agree with previous real-world findings.

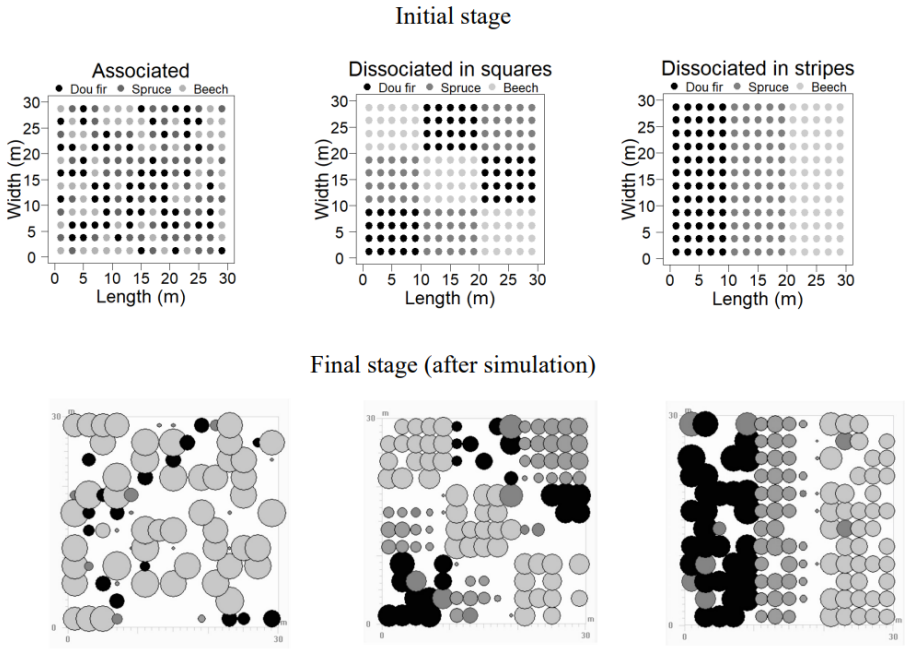

Figure 6.10: 50-year simulation of mixed species stands, from [28]

Growing Conditions

There are two predominant varieties of Douglas fir, the coastal and the interior. The coastal variety has faster growth and reaches larger sizes, while the interior variety is more resistant to cold climates and requires less sun exposure.

The coastal variety is of interest. It thrives in temperate coastal climates. Young Douglas fir trees are sensitive to frost in the spring.
Douglas fir has exhibited larger tolerance to drought compared to Norway Spruce, but a recent study by M. Vejpustková and T. Čihák [29], described an increased sensitivity for droughts in European forests.

In a study by the U.S. Forest service [30], genetical discrepancies were found between various Douglas fir trees. Trees originating from more extreme climates; dryer summers and colder winters had higher drought tolerance. This implies that seeds can be selectively sourced, in order to grow trees with the desired properties.
Some populations of the observed trees retained a fast growth rate, alongside drought resistance. Nevertheless, drought is the largest point of attention for Douglas fir. A. Sergent et al. [31] found that especially older trees were very susceptible to drought damage. This was observed after the 2003 drought in France.

This is combated by planting stands with seeds from fitting origins. Southern European countries import seeds from California and Douglas fir plantations in Europe are shifting further North due to the warming climate.

Figure 6.11: Natural variety of coastal (green) and interior Douglas fir (black), from [25, p. 34]

Durability

Douglas fir is widely considered more durable than other temperate softwood species. It is usually classified in use class 3 or 4 according to EN 350-2.
M. Kutnik [32], conducted a review of buildings and bridges made from Douglas fir in France.
It was found that elements not directly exposed to driving rain exceeded expectations of service life.

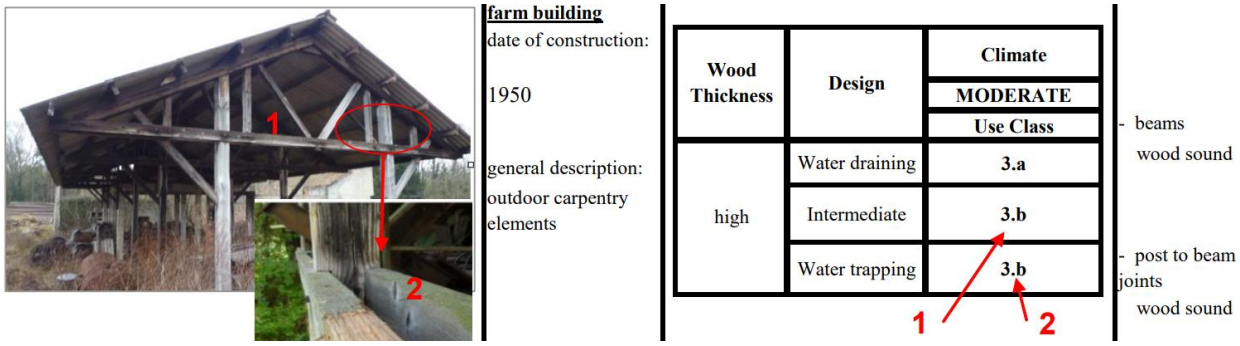

Figure 6.12: Douglas fir barn, from [32]

In this study, Douglas fir was classified with a potential service life of 10 to 50 years under use class 3.1. Given the results obtained, this can be considered a conservative classification.

T. Highley [33] conducted an experiment in which inclined timber beams and joints of various wood sorts were exposed to the elements for 20 years. No significant deterioration was found in the inclined Douglas fir beams, while L- joints of the same material had deteriorated after 9 years.

The relatively high durability of Douglas fir is corroborated in the RISE guidelines [9].
It is more durable than most European softwood species, with a material resistance of 1716 days.
For comparison, Norway spruce has a resistance of 325 days and teak, a resistance of 3027 days.

Dimensional stability

Douglas fir has a low permeability. This has the negative effect of making the species unsuitable for preservative treatments, but entails a high natural durability and dimensional stability.

The low permeability is demonstrated by E. Wang, et al. [34]. Radiata pine and Douglas fir clear wood samples were compared and it was found that the maximum swelling of Douglas fir, under bath conditions, was reached after more than 48 hours, while it took less than 24 hours for radiata pine.

Observed distortions of Douglas fir were also much smaller than those of Radiata pine.

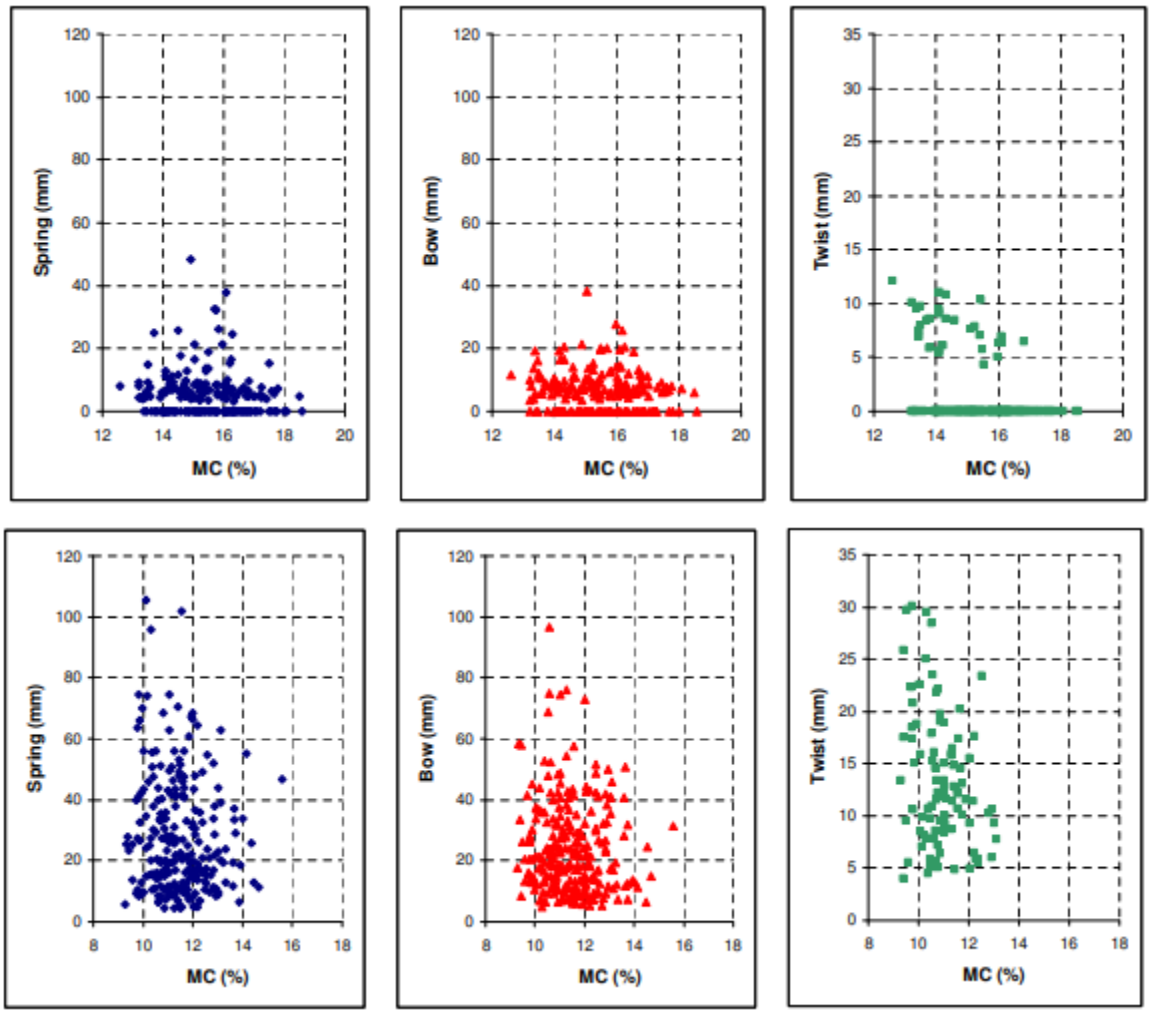

Figures 6.13a and 6.13b: Distortions of Douglas fir and Radiata pine, from [34]

Strength and classification

J. Henin, et al. [35] explored the effect of growth rate on the mechanical properties of Douglas fir in Belgium. It was found that for the outer wood, growth rate doesn't affect the strength properties in a notable way and some samples reached grade C30.
Core wood samples, on the other, hand proved to be sensitive to growth rate.

If core wood in products for structural use is kept to a minimum, shorter rotation periods for Douglas fir stands would be acceptable.

In a grading report by Brookhuis Applied Data Intelligence [41], it can be seen that Douglas fir with an origin from France, Germany, the Netherlands and Italy can be classified from C18 to C40.
Solid timber class C40 corresponds with class T24, as per table 1 from EN 14080.
Table 3 from the same norm specifies that homogeneous glued laminated timber made up from T24 lamellas is to be classified in class GL 32h.

The France Douglas catalogue [36], specifies grades of up to GL 28h to be available for purchase, albeit at long delivery times. Grades up to GL 24h are readily available.

6.4 Timber Bridge Orientation

6.4.1 Steel – Timber Limitations

Wood and steel have vastly different expansion behaviours.
Wood swells with changes in its moisture content, which is heavily dependent on the relative humidity in the air. Furthermore, the swelling of wood also differs in the longitudinal, tangential and radial direction. This swelling behaviour differs per species as well.

The expansion behaviour of steel is highly dependent on the temperature. As clarified in subparagraph 3.2.2, the Eurocode requires a difference in temperature between the deck and the rest of the superstructure to be taken into account during the steel bridge design.

In order to combine timber and steel, the difference in expansion behaviours must be accounted for. The environmental conditions can be somewhat controlled indoors, thus the expansion behaviours of the materials as well. This isn't the case in an outdoor application such as a traffic bridge.
This holds true for large lengths over which composite behaviour is desirable.
The lack of timber- steel composites used in practice is summarized by Riola-Parada in [2];
in the state of the art, it is noted that high production costs, combined with incompatibility of expansion/ contraction coefficient are, among other factors, the main reasons for the lack of application of steel- timber composites.

Dietsch [7] investigated steel reinforcement perpendicular to the grain. He found that a moisture reduction of 3% could lead to cracking of the wood, when continuously reinforced by threaded rods. The likelihood of cracking increased with higher members, thus longer reinforced lengths, and more reinforcing elements applied close to each other.

Numerical simulations from the same study showed that decreasing the angle of the reinforcement from 90° to 45° decreased the shrinkage stresses perpendicular to the grain drastically.

Wood Swelling in Set Conditions

Historical records of the average daily relative humidity at the location of the bridge are available through the Dutch Meteorological Institute (KNMI) [51].

This data is visualized in figure 6.14

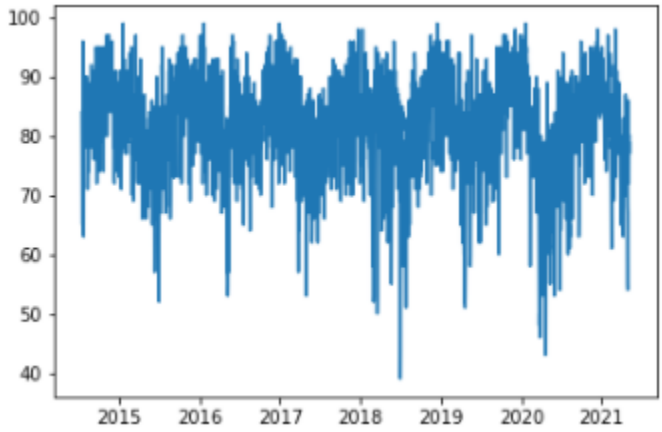

Figure 6.14: Relative Humidity vs year, weather station Voorschoten, data from [51]

Sorption Isotherms for Douglas fir are provided by Hedlin [52] and Bergman [53]. The values from both are in good agreement.

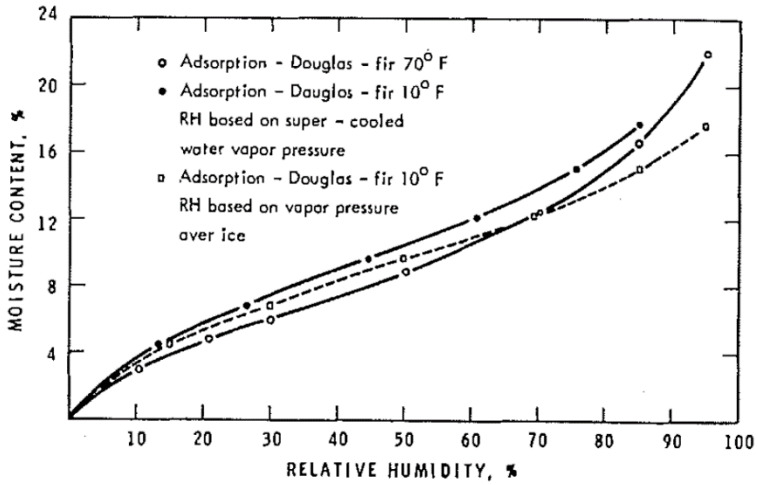

Figure 6.15: Adsorption Isotherms for Douglas fir, from [52]

Naturally, it takes time for the relative humidity to be reflected in the moisture content of a timber element. This is especially the case for Douglas fir, as it is a relatively difficult species to penetrate.

Nonetheless, a moisture content difference of 5% throughout the year is a reasonable assumption. This is conservatively based on a range of persistent relative humidity from 65% to 90% and a corresponding moisture content of 11% and 16% under the respective RH values.

Nguyen, et al. [53] measured the swelling coefficients (α) of Douglas fir heartwood to be respectively 0,14 %/%, 0,20 %/%, and 0,02 %/% for the radial, tangential and longitudinal directions.

Over a beam length of 25 m (the bridge span), the needed room for expansion in longitudinal direction would be:

$$0{,}0002 * 5 * 2500 = 2{,}5\ cm$$

If the beams would be reinforced by steel across their whole length, this expansion would be hindered in the proximity of the reinforcement.
The reinforcement can be attached to the wood using individual fasteners or can be glued to the element. Both options entail stresses local to the fastening location.

With regards to gluing, a ductile adhesive would be better able to accommodate the displacements than a less ductile, more brittle adhesive. A more ductile adhesive would however be more prone to creeping.
It is possible that ductility in the timber would be sufficient for the accommodation of expansions, with either individual fasteners or a glue line.

6.4.2 Bridge Concepts and Qualitative Analysis

By replacing steel elements by timber ones, fatigue details present in steel are negated.

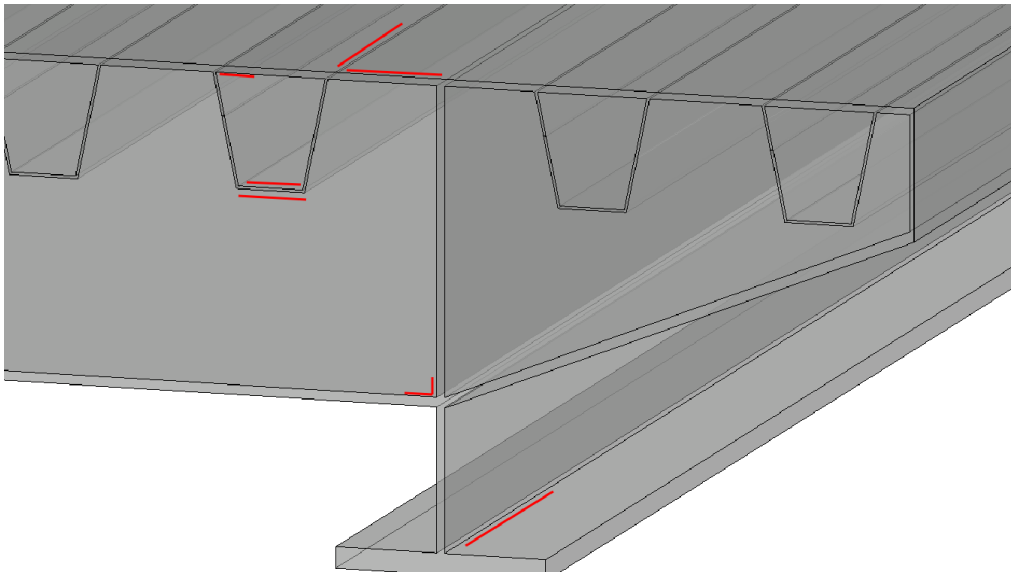

Figure 6.16: Location of relevant fatigue details in steel plate girder bridge with an OSD

Several timber bridge variants are presented in the following subparagraphs. Two of those are subsequently verified according to EC 5, with the help of SCIA Engineer. The critical checks are then reflected upon and an optimized design is developed.

The durability of timber is highly dependent on the design as can be made up from Setra [8] and RISE [9]. Limiting water ingress and thus humidity decreases fungal attacks, which in term lead to degradation and decreased mechanical performance. Protecting the load carrying structure from direct sunlight also has substantial effects on the durability of the elements.

A study by Kropf [10] shows that, in practice, bridges with load carrying structures underneath the deck provide better long-term durability performance as opposed to bridges where the load carrying structures are above the deck.

For these reasons, only bridge designs, where the load carrying system is located underneath the deck will be considered.
In order to limit the scope of the study, no hybrid members will be considered for the bridge design. It is paramount that the interaction between the different materials is investigated for such members and this would extend the thesis beyond a reasonable limit.

Design 1: Steel to Timber

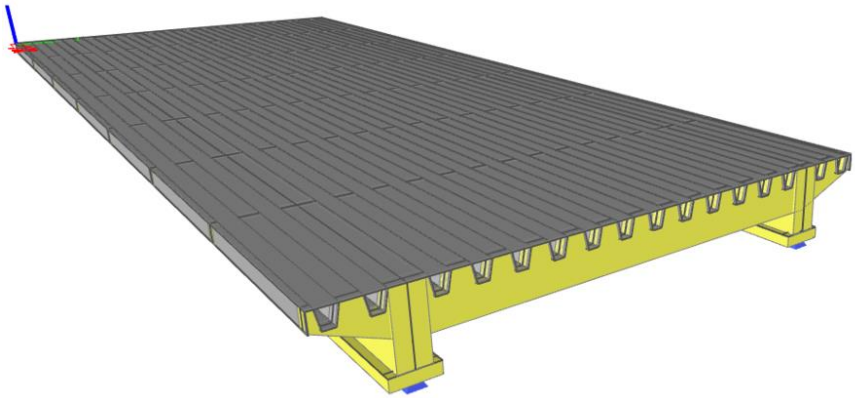

Figure 6.17: Bridge Design 1, overview

Pros and Cons:

+ Little welding, fewer fatigue details in steel

- Complicated connections between OSD and Cross beams, incompatibility of material expansion behaviours, torsion in beams; may require discrete lateral bracing, cantilevering beam must be properly secured with a moment resisting joint

In this bridge design, the orthotropic deck remains and functions as the top flange of the main beams. The steel plated girder design is simply translated to timber.

Swelling of the main beams in the global transverse direction of the bridge can be accommodated by rigidly attaching the deck to the cross beams in the transverse direction and allowing for transverse movement in the main beam connections.

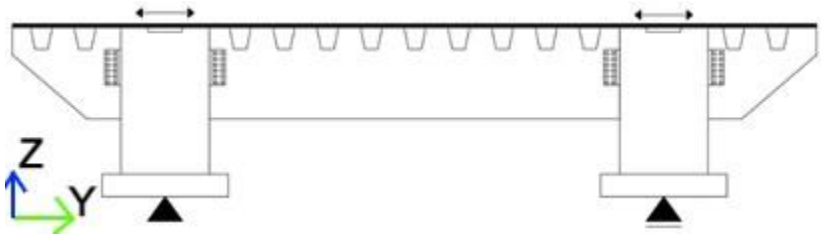

Figure 6.18: Transverse movement due to transverse swelling of the main beams

Swelling of the cross beams in their local transverse direction, can also be accommodated by rigidly attaching the deck to the main beams in the global longitudinal direction and allowing for movement in the same direction in the cross beam to deck connection and cross beam to main beam connection.

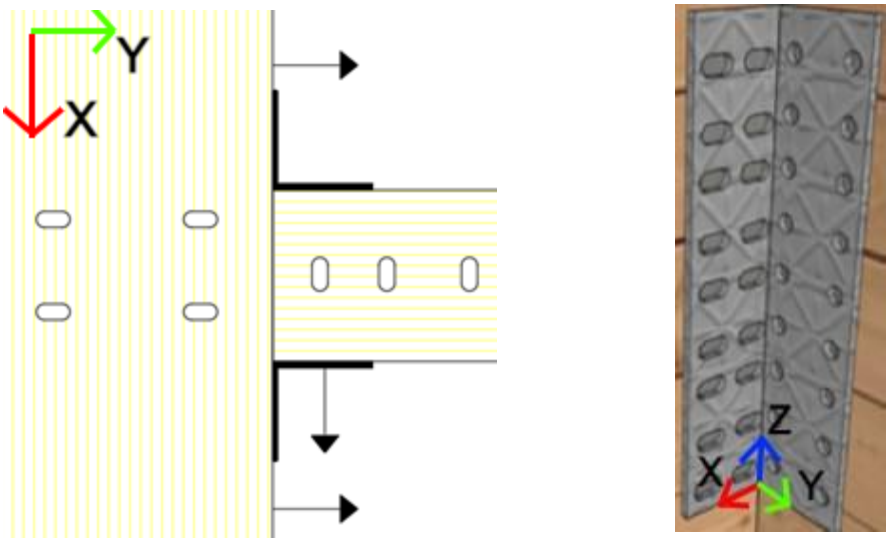

Figures 6.19a, b: Deck to main beam and cross beam connections, cross beam to main beam connections

Up and down swelling of the cross beams would lead to uneven displacement in the deck. This can be solved by making the top part of the cross beams out of steel. The steel used will, however, entail additional welding.

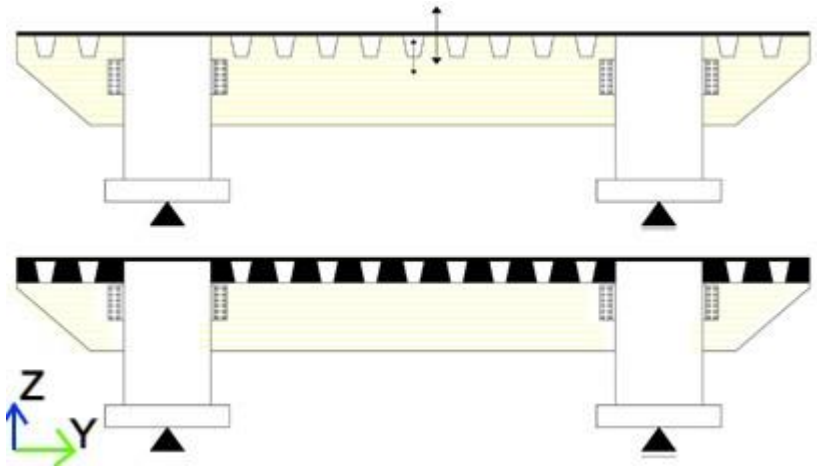

Figure 6.20: Fully timber and timber- steel cross beams

All other movements cannot be accommodated while retaining composite action of the timber elements and the steel deck. Expansion of the deck plate in longitudinal direction would be hindered by its connection to the main beams and expansion in transverse direction- by the connection to the cross beams.

The inverse holds true for longitudinal expansion of the main- and cross beams and the deck plate. With high humidity, the longitudinal swelling of the timber elements would be hindered by the steel deck.

These prevented expansions could lead to cracking in the timber at the connection between itself and the steel deck.

Design 2: Decoupling of Steel and Timber

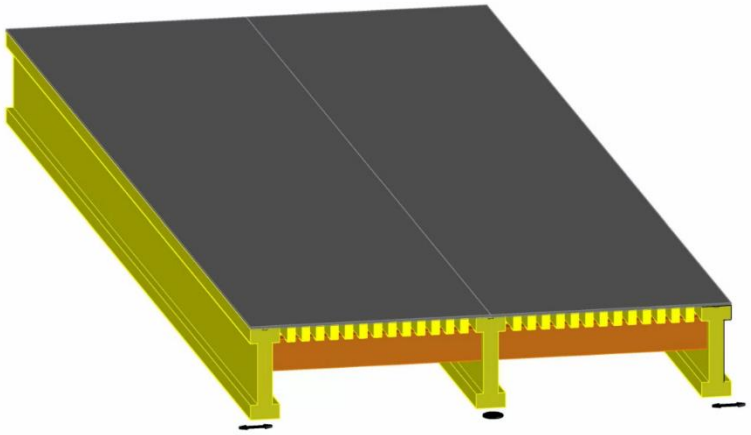

Figure 6.21: No composite action bridge design

Pros and Cons:
+ Little welding, fewer fatigue details in steel
- No composite action, may require large dimensions of the timber members, torsion in beams; may require discrete lateral bracing.

Having the steel deck rest on top of the rest of the superstructure eliminates the incompatible expansion behaviours of the two materials. This can be done with two main beams, with cantilevering cross beams, requiring moment resisting connections. Applying three main beams would reduce the loads on each beam and negate the need for moment resisting connections between the main- and inner cross beams.

Transverse expansion of the cross beams can be accommodated by applying angle brackets with oval holes on the main beam side on one side of the cross beams. The other side of the cross beam to main beam connection can be executed with regular angle brackets. The bracket type with oval holes is illustrated in figures 6.19a, b.

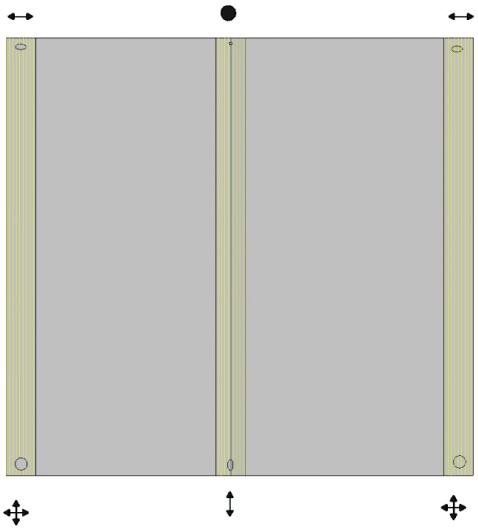

Figure 6.22: Movement directions of deck plate in x-y plane

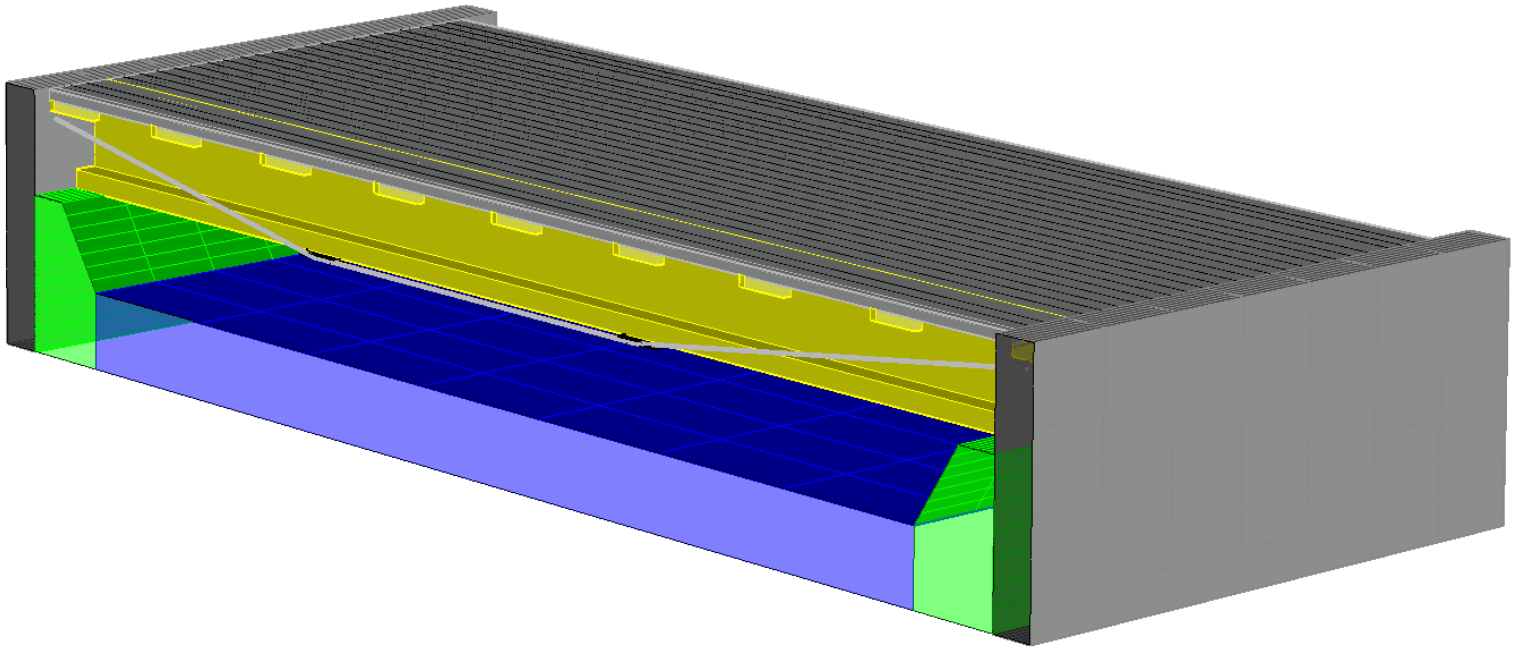

Figure 6.23: Cable supported timber girder bridge; horizontal cable forces taken by anchors in abutments

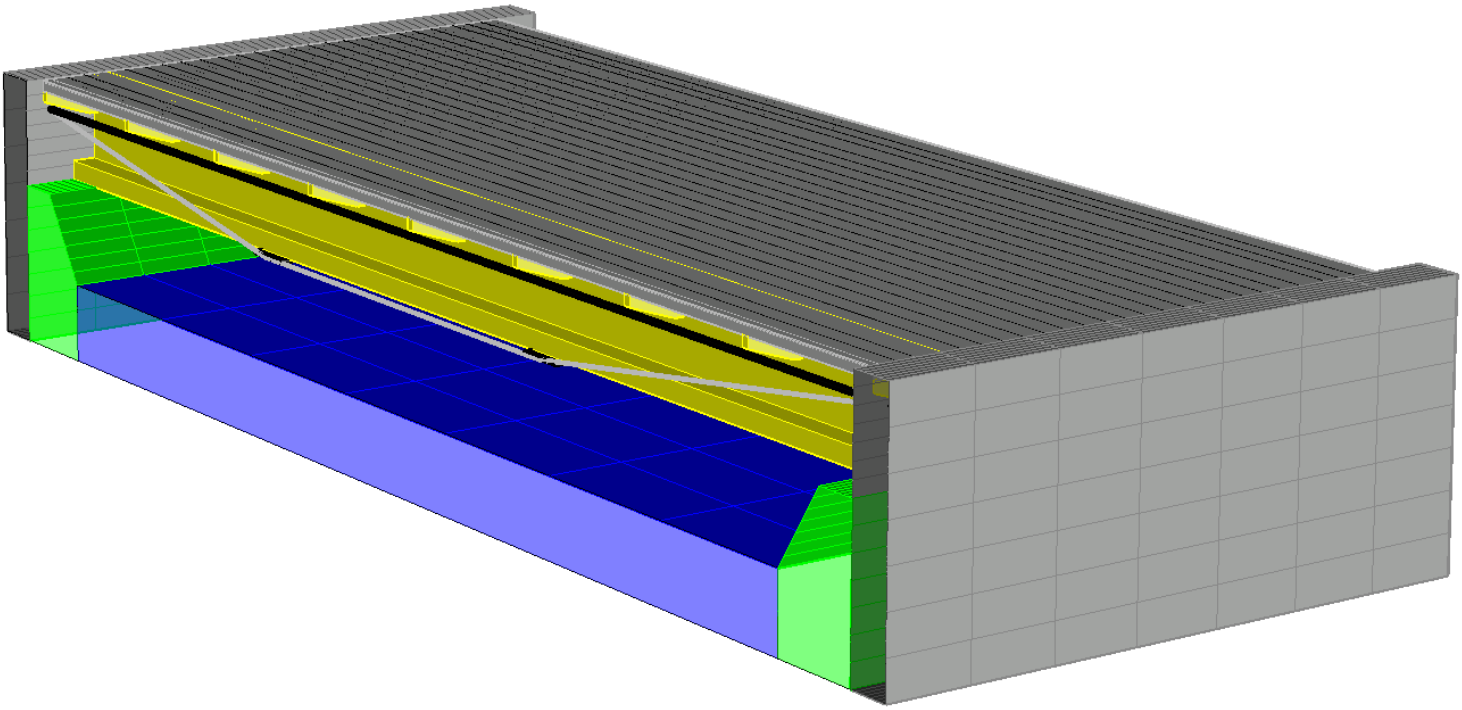

Figure 6.24: Cable supported timber girder bridge; horizontal cable forces taken by cylindrical compression rod

Pros and Cons:

+Partial decoupling of timber and steel expansion behaviors, utilizing steel in tension to a high degree, little welding, vertical deformation of the bridge
- Anchors/ compression rod needed in abutments leading to potentially difficult details, torsion in beams; may require lateral bracing, moment resisting joint required

This design bears resemblance to prestressed concrete beams. Where it differs from those, is that horizontal resultant forces in the cable ends are either balanced by anchors in the abutments or a compression rod. This rod subsequently carries the resultant horizontal force to the abutments in the form of compression, this isn't done by the longitudinal timber elements.

Along each main beam, cables are run on either side of it. These cables go from being positioned high at the abutments, to a metal plate attached to the bottom of the bottom flange of the main beam.

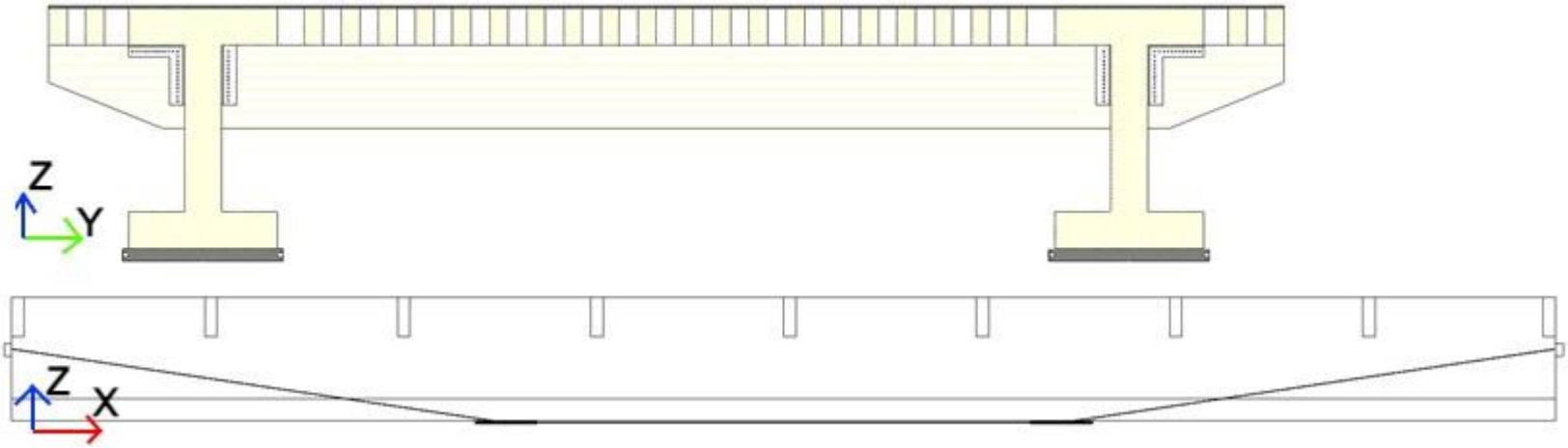

Figure 6.25a, b: Transverse cross section of bridge at metal plate position, longitudinal cross section of bridge (Cables attached to abutments version)

A one-piece deck is laid on top of the bridge in the same way as a single side of the deck of design 2.
The angle of the cable from the metal plates to the abutments/ compression rod needs to be accommodated by the cross beams. This can be done with a cutout, through which the cable can be run, in the necessary cross beams.

Longitudinal swelling of the main beams will slightly extend horizontal part of the cable, resulting in upwards forces on the plates. It is not expected that this would be of great influence.

6.4.3 Choice for further design

There is a practically infinite amount of possible bridge designs.
It is chosen not to further develop designs incorporating composite behaviour of wood and steel, but to combine the two materials in a manner which decouples their expansion behaviours.

This is done to set a limit to the scope of the thesis.
Although combining wood and steel for composite behaviour is a research worthy topic, it is of the belief of the author that detailed analysis of such involvement is required, that it would not fit in this thesis.
Furthermore, an apter use of steel- timber composites would be for elements that are used indoor, under more controlled conditions.

6.5 Timber Bridge Member (ULS) Design

In this chapter, preliminary verifications of designs 2 and 3 from the previous paragraph will be produced. Subsequently, in the following chapter, a final timber bridge design will be made.
As was the case with the steel bridge design, the timber version of the bridge will not be exposed to exceptional loads, such as explosions and collisions with ships.

6.5.1 FE Modelling

In this paragraph model information is presented. This information is divided into generally applicable and specific for bridge design 2 or 3.

General Information

- 1D elements are used: Allows quick calculation and iteration of member sizes.
  SCIA Engineer includes Eurocode checks for 1D members, verifying members by hand is therefore not necessary.
- Linear solver: Speeds up calculation, useful for obtaining general dimensions quickly.
- Mesh: Maximum element length set to 10 cm
- Load panel: Surface loads are applied to the 1D members using load panels which transfer loads to longitudinal members only.
- Load spread: A spread with ratio of 1:1 (45°) for wheel loads, due to the 15 cm thick asphalt layer is applied.

- Hinged connections are applied between secondary longitudinal members and cross beams
- Support lengths: Secondary longitudinal beam support lengths are set to the width of cross beams.
- System strength increase factor of 1,1 is applied to secondary longitudinal beams.
- Buckling strengths are calculated with non- sway conditions.

Design 2

- Cross beams connected to main beams with hinges.
- Support lengths main beams set to 800 mm.

Design 3

- Inner cross beams connected to main beams with hinges, outer cross beams connected with moment resisting connections.
- Upward cable support reactions in mid span modelled as restricted z displacement at $\frac{1}{3}l$ and $\frac{2}{3}l$ of the main beams.

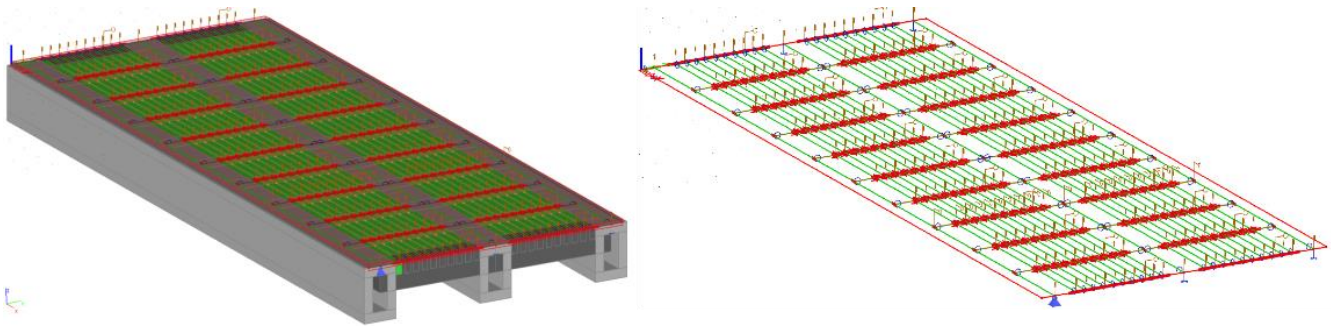

Figure 6.26 a, b: Timber Bridge Design 2: Rendered geometry and 1D plain view

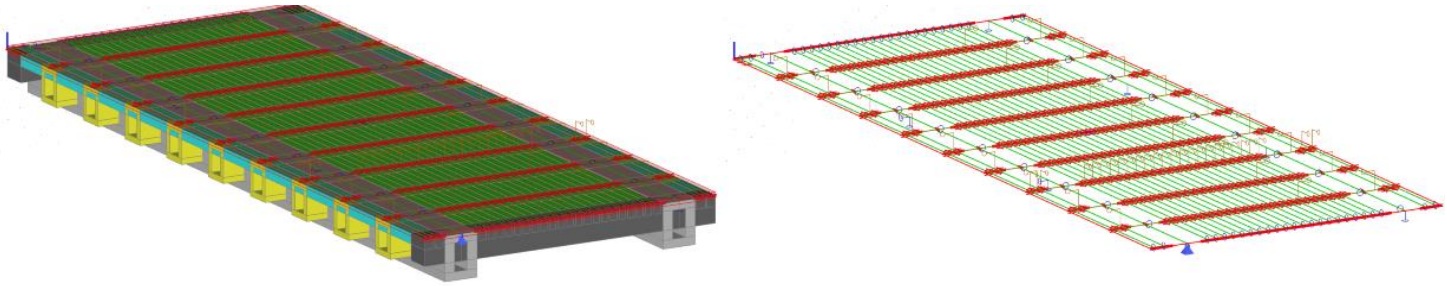

6.27 a, b: Timber Bridge Design 3: Rendered geometry and 1D plain view

6.5.2 Loads and Combinations

The tandem systems of LM1 are set at critical positions:
- At mid span, between cross beams
- At mid span, over cross beams
- Over and close to the one to final cross beams
- At mid span, in the outer end span
- Over and close to the final cross beams

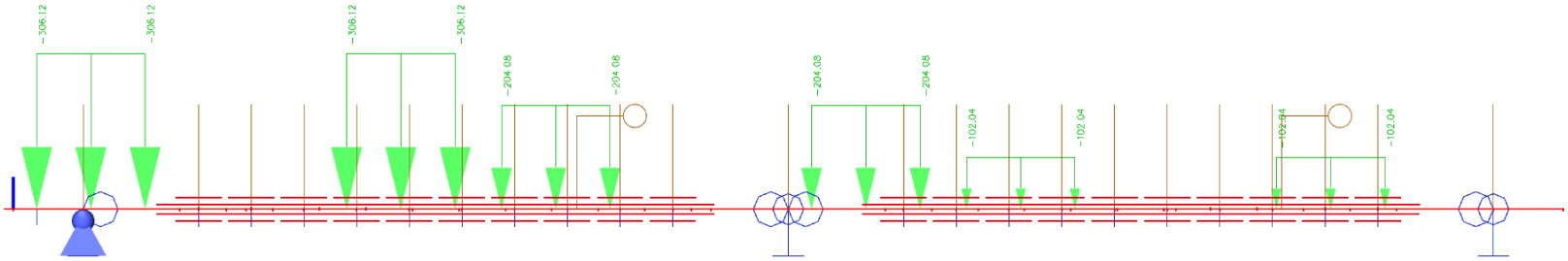

Figure 6.28: Tandem systems from LM1 applied on design 2

Horizontal wind loads are applied directly on the longitudinal main beams via line loads. Combinations follow from EN 1990 and are identical to the ones specified in paragraph 3.2, save for the modelling of temperature differences between the deck and the rest of the superstructure. This is left out as it is not of influence, since the steel and timber are decoupled.

6.5.3 Bridge sizing

Design 2

- Main longitudinal girder centre to centre spacing: 438 cm
- Secondary longitudinal girder centre to centre spacing: 34 cm
- Cross girder centre to centre spacing: 250 cm
- Weight of timber in superstructure: 107 tons

The bridge dimensions used in design 2 are illustrated in figure 7.29 a to c, dimensions are in mm.

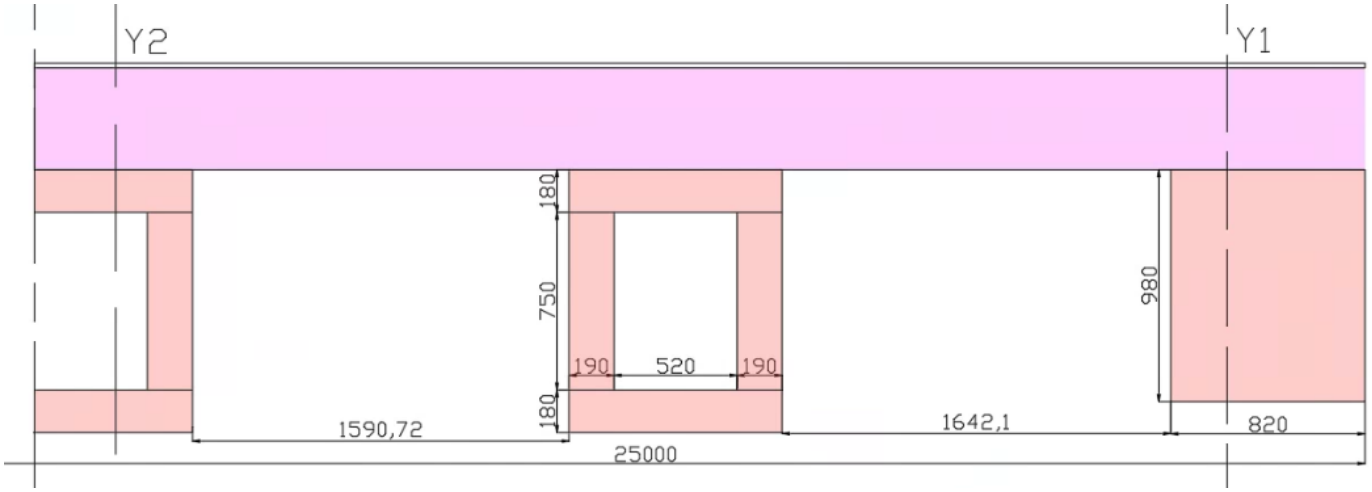

Figure 6.29a: Design 2, longitudinal cross section (Section X-X)

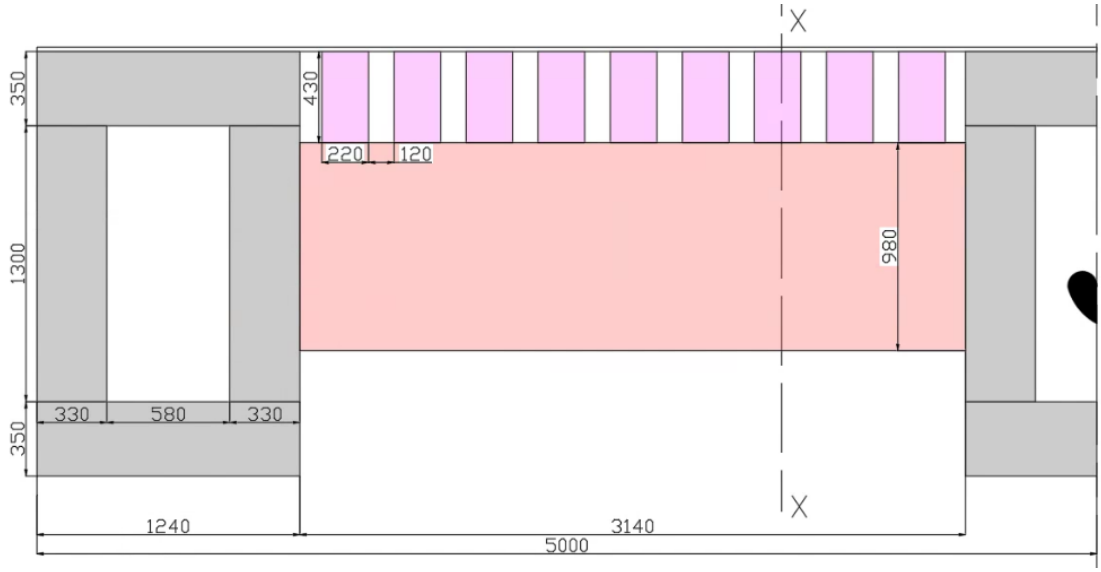

Figure 6.29b: Design 2, transverse cross section at end cross girders (Section Y1-Y1)

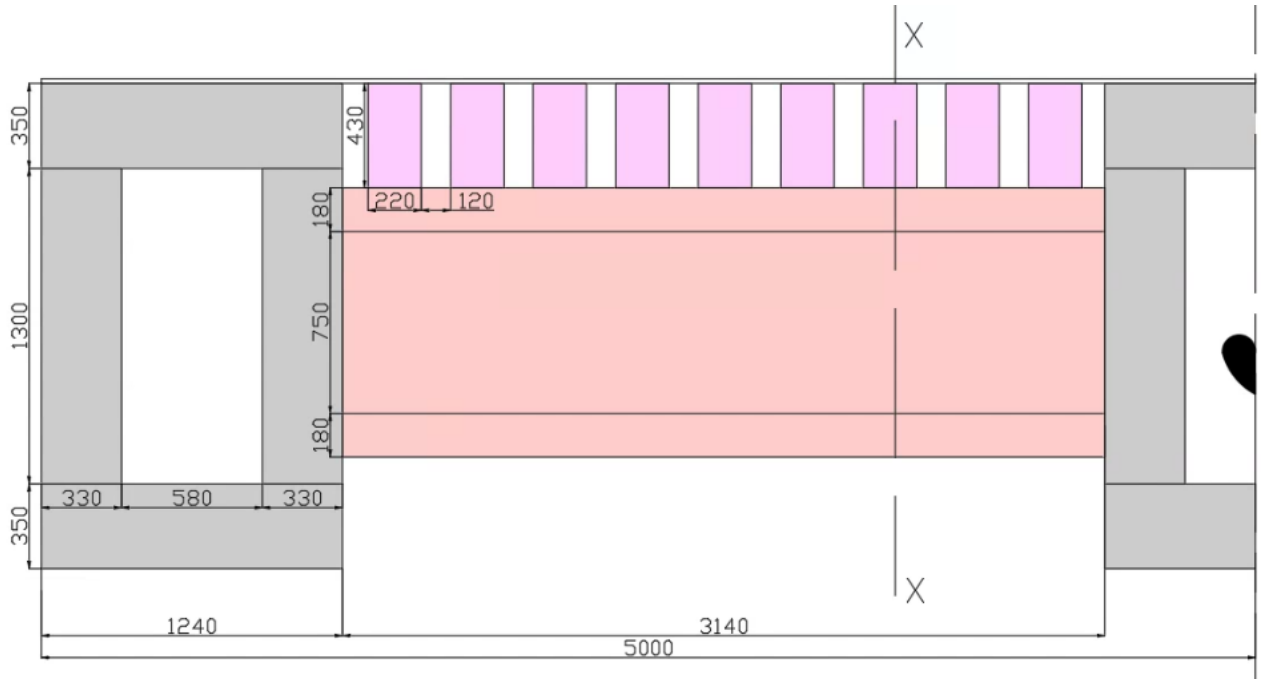

Figure 6.29c: Design 2, transverse cross section at mid cross girders (Section Y2-Y2)

Design 3

- Main longitudinal girder centre to centre spacing: 750 cm
- Cantilever part cross girder from centre main beam: 125 cm
- Secondary longitudinal girder centre to centre spacing, between main girders: 30 cm
- Secondary longitudinal girder centre to centre spacing, over cantilever: 35 cm
- Cross girder centre to centre spacing: 250 cm
- Weight of timber in superstructure: 74 tons

The cross sections used in design 3 are illustrated in figure 6.30 a to c, dimensions are in mm.

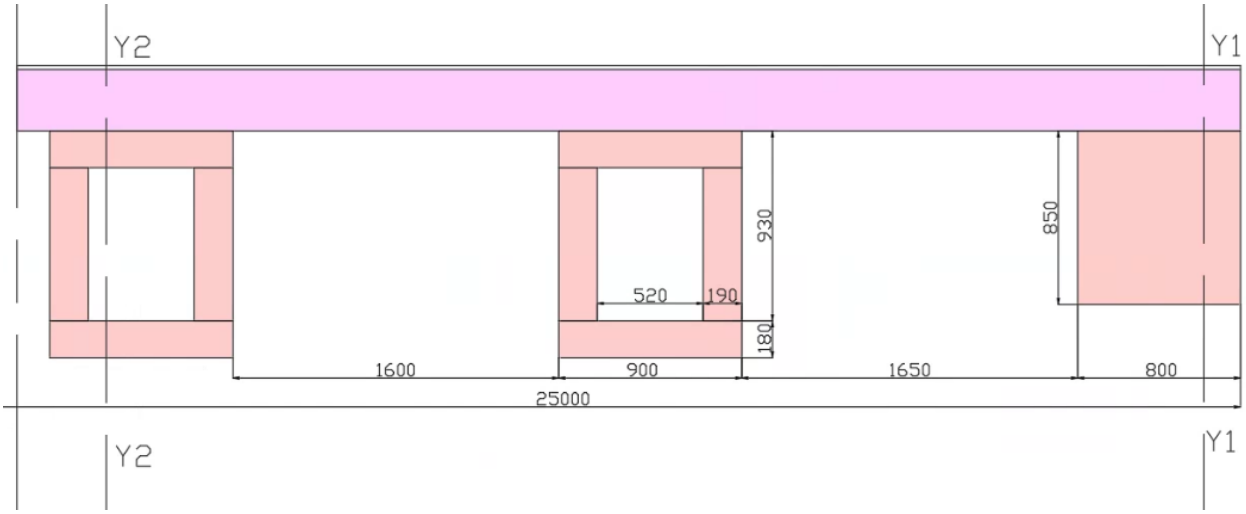

Figure 6.30a: Design 3, longitudinal cross section (Section X-X)

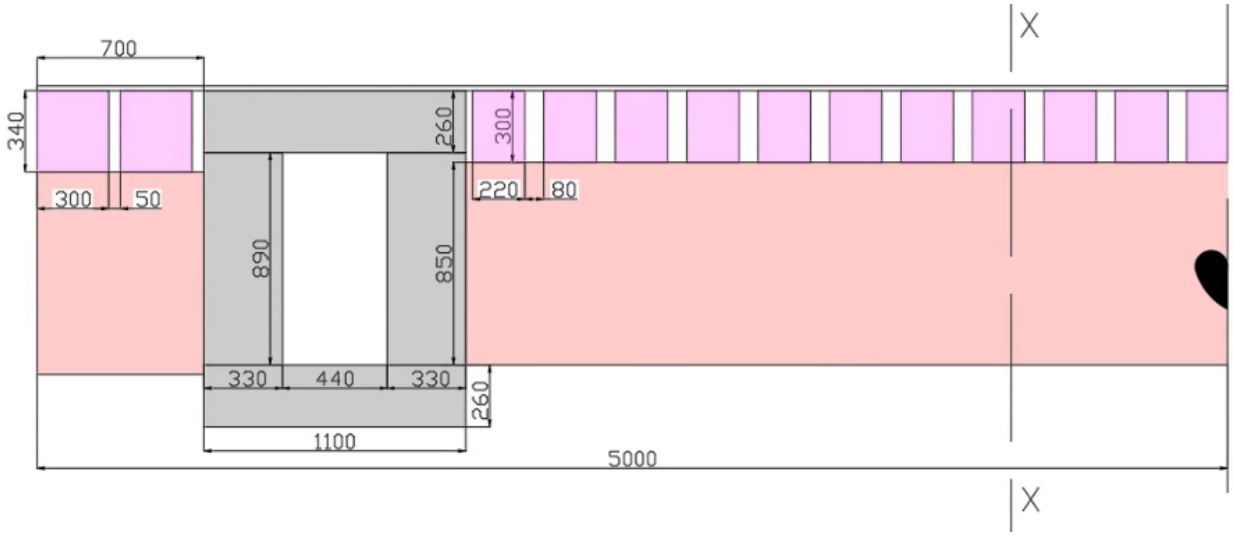

Figure 6.30b: Design 3, transverse cross section at end cross girder (Section Y1-Y1)

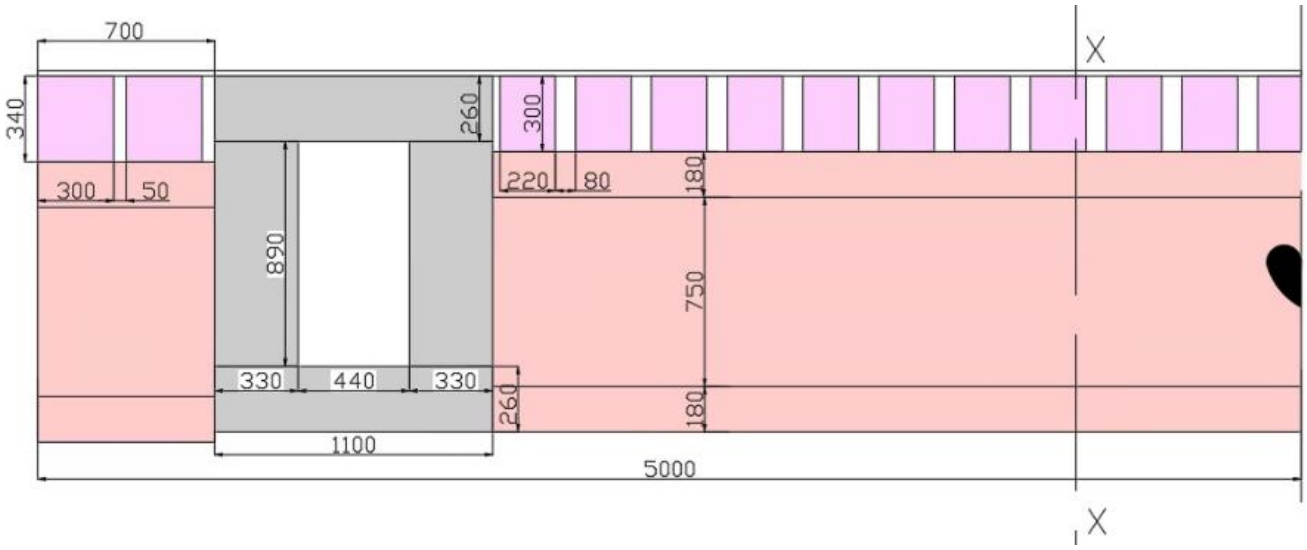

Figure 6.30c: Design 3, transverse cross section at mid cross girder (Section Y1-Y1)

6.5.4 Results

Member	UC Shear/ Torsion	Location UC Shear/ Torsion	UC Bending/ Axial Force	Location UC Bending/ Axial Force
Secondary longitudinal beams	0,97	Next to final support	0,56	Ultimate local span, close to mid-span
Inner Cross beams	0,96	Connection with main beam	0,32	Mid span
Outer Cross beams	0,84	Connection with main beam	0,24	Mid span
Main longitudinal beams	0,92	Next to support	0,90	Mid span

Table 6.1: Timber Bridge Design 2 Unity checks

Member	UC Shear/ Torsion	Location UC Shear/ Torsion	UC Bending/ Axial Force	Location UC Bending/ Axial Force
Inner secondary longitudinal beams	0,95	Next to final support	0,81	Ultimate local span, close to mid-span
Outer secondary longitudinal beams	0,38	Next to final support	0,80	Ultimate local span, close to mid-span
Inner Cross beams	1	Connection with main beam, non-cantilevering part	0,36	Mid span, non-cantilevering part
Outer Cross beams	0,86	Connection with main beam, non-cantilevering part	0,34	Mid span, non-cantilevering part
Main longitudinal beams	0,80	Next to support	0,34	Ultimate local span, close to mid-span

Table 6.2: Timber Bridge Design 3 Unity checks

6.5.5 Discussion

Design comparisons

When it comes to the timber part of the design variants, design 3 requires less material.
The engineering of it, however, is more involved than that of design 2 due to the cable system.

Model limitations

The 1D element model, in the state as described in this chapter, is not fit to use in a detailed design, but has proven useful for obtaining global dimensions and finding bottlenecks.
The actual member lengths of the cross beams are shorter than modelled. In the model, the cross beams span from centre to centre of the main beams, which would not be the case in reality. This is because the width of the main girders is substantial and cannot be neglected.

Secondary longitudinal beams

The secondary longitudinal beams, with their current format and spacing, appear to be well suited.
A point of note is that buckling must be restrained at the cross girders. If not, it becomes normative over shear.
The beam size, however, is relatively large. Using discrete members as secondary longitudinal beams necessitates the large sizes.

Cross beams

The normative unity check for all cross beams is that for shear/ torsion. The bending capacity of the cross section is hardly utilized. Ratios of the unity checks for bending/ axial force and shear/ torsion are about 1 to 3.
Shear reinforcement at critical areas or the use of a non-prismatic cross section could both be used to obtain more balanced sets of unity checks, warranting the use of less material.
For design 3, moment resisting connections must be achieved, entailing additional costs when compared to pinned connections.

Main longitudinal beams

The main longitudinal beams in design 2 have relatively balanced unity checks for shear/ torsion and bending/ axial force. This isn't the case for the beams in design 3 where the ratio between these checks is 2,3 to 1.

Cross section limitations

Shear torsion are the main points of concern, because of this box- and solid sections are fitting types for the use in this bridge.

Most members have relatively unbalanced unity checks. This can be alleviated by local reinforcement and further optimization of the dimensions of the concerned member.
For example, the critical shear and torsion strength can be increased by use of long self-tapping screws as shown by Dietsch and Brandner in [5]. An increase in shear strength can warrant the use of smaller cross sections, resulting in a higher unity check for bending.

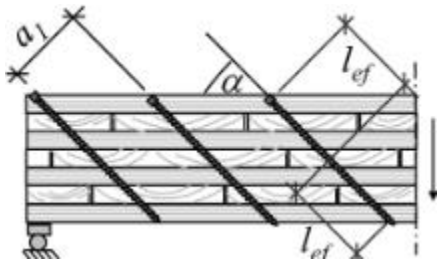

Figure 6.31: Self tapping screws for shear reinforcement, from [5]

Local strengthening can also be done with glued in rods (GIR). Such a rod has similar behaviour to a rebar in concrete as stated by Steiger in [6].

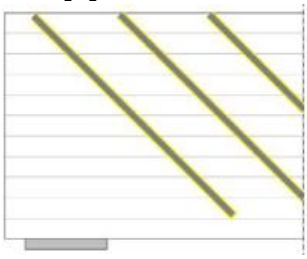

Figure 6.32: Glued in rods for shear reinforcement, from [6]

The abovementioned screws or rods can be placed in the walls of the box sections. Local reinforcement at supports, where high compression stresses occur perpendicular to the grain can also be beneficial. This is especially relevant in the case the abutments or mid span cable supports don't offer a long enough support length along the main beams.

For any and all reinforcement of wood with steel elements, stresses due to expansion behavior must be accounted for.

Deck

Using secondary beams with a steel deck on top does not yield benefits. The load spread due to the steel deck is negligible and no composite action is achieved. Furthermore, the weight of the steel deck is relatively large compared to the lighter timber members.

Amount of Material

Only the timber parts of the superstructures have been compared, the additional steel deck and cable support system aren't included in the bill of material. The additional engineering cost of the cable system also is not accounted for. This makes for a simplified comparison of the two bridge versions. In the final design, at least the material use for the cable system must be taken into account.

7 Design of Definitive Timber Bridge

In this chapter, notes from chapter 6 are processed and a design, accounting for the weaknesses discovered in the previous chapter, is produced. Results will be presented and discussed throughout the chapter. Intermediate results and Eurocode equations used to obtain these are shown in appendix D.

7.1 Bottlenecks To Be Addressed

Model limitations

In order to obtain accurate spans, (nearly) infinitely stiff 1D members, with negligible weight are used to connect the main beams to the rest of the members.

This approach accurately takes into account the thickness of the main beams, while at the same time retaining the actions on said beam from the other elements.

Deck

As mentioned, a steel deck does not benefit the design. Applying a glulam deck system is a more sensible solution. This deck can be placed on top of the cross beams and between the main beams (figure 7.1a) or on top of the cross beams and the main beams (figure 7.1b). Furthermore, due to the lamination effect, a high effective width can be achieved and therefore a less deep deck beams would be needed.

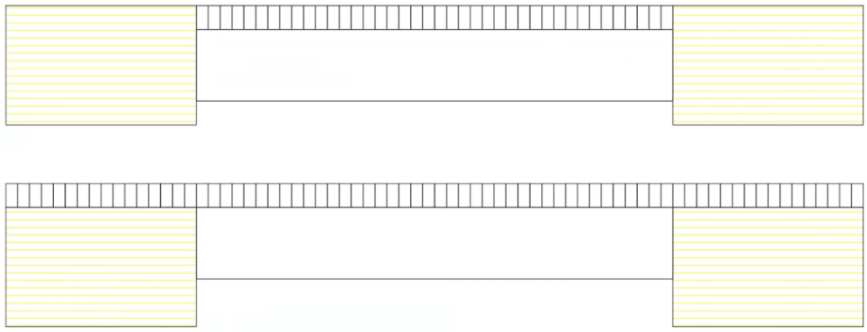

Figures 7.1a, b: Timber deck between cross girders, on top of cross girders

Cable supports

By increasing the effective angle at which the support cables attach to the main beams, tension stresses in said cable would decrease, along with horizontal forces in the abutments or steel compression rods. This increase in depth can be realized with rods, vertically protruding from the bottom of the main longitudinal beams.

Anchoring the cables in the abutments would require a high capacity to be available in the soil. This isn't the case in the Netherlands, where rock deposits are practically non- existent.
Anchoring the cables to the main beams would do away with the necessity for soil with a high capacity or the need for a compression rod.
A larger main beam cross section would be required to provide additional capacity for the horizontal reactions of the cable ends.
A much smaller capacity in the horizontal direction would be required in the abutments, as the cable reactions in the main beam ends would largely balance out themselves.

Placing the cable supports at optimized lengths along the beam, would also yield the greatest benefits when it comes to reducing moment peaks.

The cable stiffness must be accounted for; the designs in chapter 6 allowed for global dimensioning, under the assumption that the cables are infinitely stiff and that loading type does not influence the support reactions provided by the cables.
This isn't the case and these supports need to either be modelled with a certain stiffness, dependant on the loading, or the entire cable system must be included.

Torsion

High torsional moments are found in the longitudinal- and cross beams. A higher number of main beams with smaller dimensions can alleviate this issue, leading to a cross section with more balanced unity checks.

7.2 Design Concept and Methodology

A visualization of the bridge as described according to the aforementioned points is presented in figure 7.2. A choice is made for a longitudinal deck system laid between the main beams with the top of the deck at the same height as the top of the main longitudinal beams. The lamination direction is illustrated with red lines along the beams. Potential necessary multiple adjacent lamellas aren't shown at this stage.

As the cables are anchored to the main beams, there is a relationship between creep deformations of the timber and the prestressing force in the cable. As beam deforms, some cable action will be lost, which must then be regained by periodically restressing the cables.
This relationship falls out of the scope of the case study and the cables are assumed to be directly activated under downwards displacements of the main beams

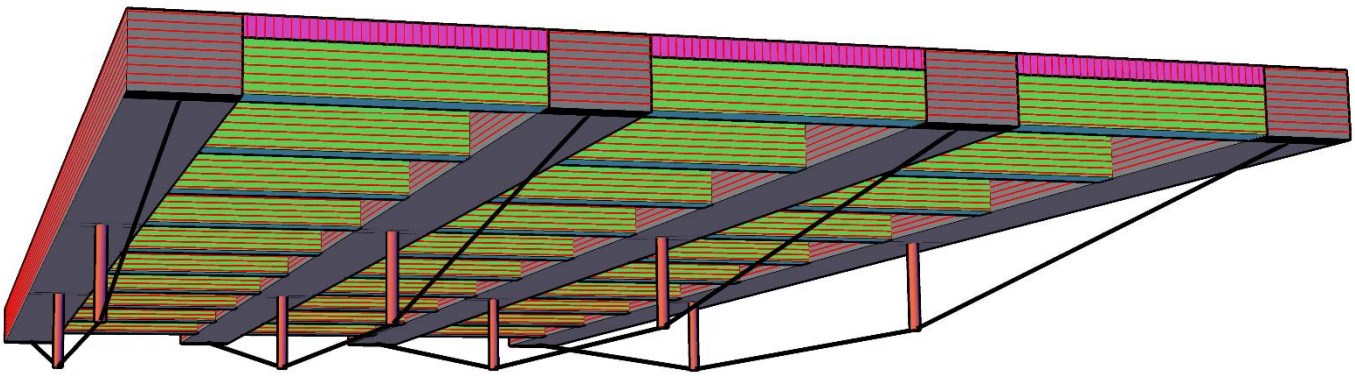

Figure 7.2: Timber bridge concept

Firstly, the deck will be calculated according to the simplified method as detailed in EN 1995-2. Secondly, the location of the vertical supports in the main beams' span will be optimized. Subsequently, the dimensioning of the structure will be done, assuming rigid support conditions at the vertical steel rods connected to the cables. Afterwards, the bridge will be modelled and analysed in its entirety, including the cable system.

7.3 Global Design

Bridge Dimensions

Several iterations, with various combinations of different member sizes, are performed. The global bridge dimensions follow from figures 7.3a, b. The layout of the structure can be seen in figure 8.2. The total length and width of the bridge are respectively, 25 and 10 meters.
The total weight of the timber in the superstructure is **43,34** tons, assuming the average density of 445 $\frac{kg}{m^3}$ for GL 26h as specified in EN 14080

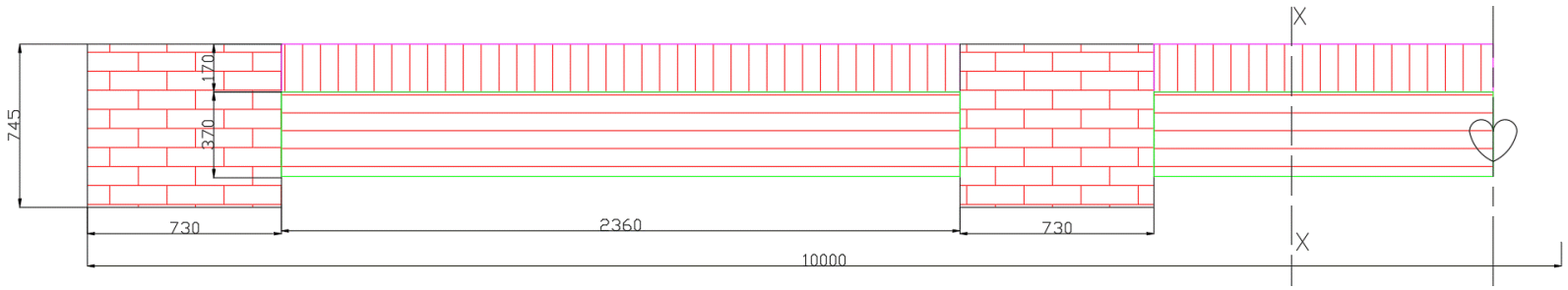

Figure 7.3a: Transverse cross section, at cross beam location, dimensions in mm (Section Y-Y)

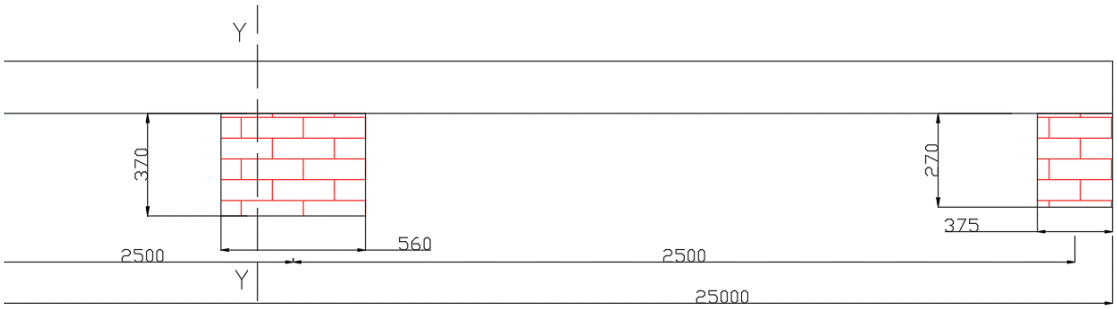

Figure 7.3b: Longitudinal cross section, in local span, dimensions in mm (Section X-X)

7.3.1 Timber Deck

Modelling

- Glulam timber of 170 mm depth
- Load spread from EN 1991-2, 4.3.6 and EN 1995-2, 5.1.2, 5.1.3 as shown in figure 7.4

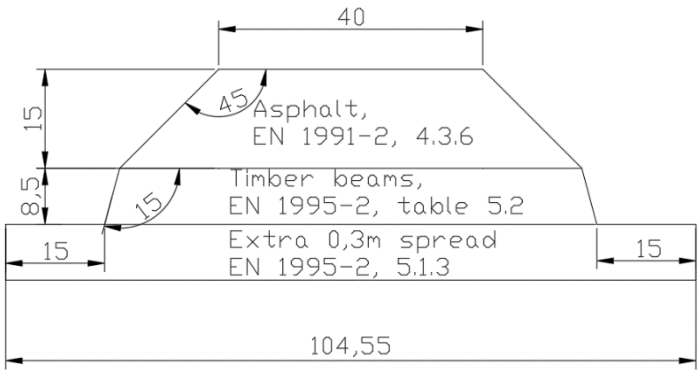

Figure 7.4: Wheel load spread, lengths in mm, angles in degrees

- Nominal centre to centre transverse spacing between two-wheel loads from different lanes is 1 meter, but may be reduced to 0,5 meters for local checks.
- Nominal spacings will be considered for the deck as reduction for local checks is expected to be above main beam and not glulam deck.
- Modelled as a GL 26h beam with dimensions:

  $$length * width * depth = 25\,meters * 1{,}045\,meters * 0{,}17\,meters$$

  Supports in z- direction and buckling restraints placed with spacing of 2,5 meters (centre to centre spacing of cross beams)

Loading

- A single wheel load, from the most heavily loaded lane as a surface load, placed along the beam with a step of 1 meter to obtain envelope

- Distributed loads from LM1 and distributed dead loads from asphalt and self-weight as surface loads

- Braking and acceleration force as line loads

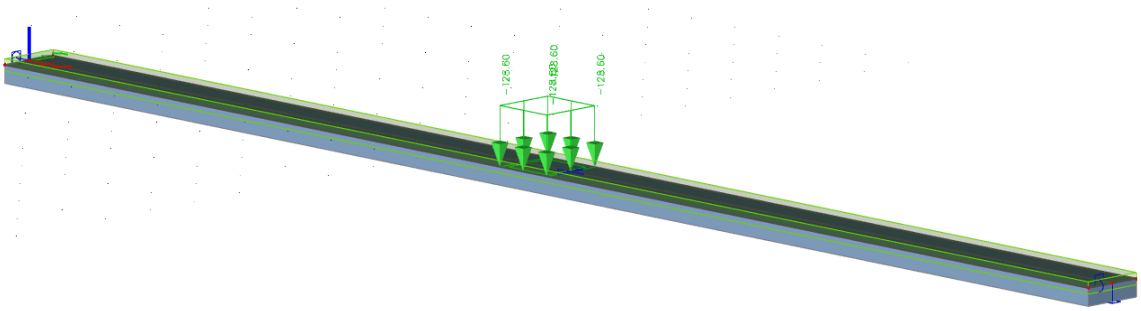

Figure 7.5: Wheel Load modeled in SCIA Engineer

ULS Results

The results for the deck are summarized in table 7.1.

Type of Check	Value	Location
Bending/ Axial Force	0,92	Ultimate local span, close to mid-span
Shear/ Torsion Check	0,63	Over cross beam
Compression perpendicular to the grain	0,29	Over cross beam

Table 7.1: Normative ULS unity checks of timber deck

SLS Results

Normative displacements occur in the local middle span.

$Service\ class\ 3 \qquad k_{def} = 2 \qquad l = 2500\ mm$

$u_{inst} = 5{,}7\ mm = \frac{1}{440} l \qquad within \quad \frac{l}{400}\ to\ \frac{l}{500} \quad (From\ EN\ 1995-2, Table\ 7.1)$

$u_{inst,G} = 0{,}1\ mm \qquad u_{fin,G} = u_{inst,G} * (1 + k_{def}) = 0{,}1 * (1+2) = 0{,}3\ mm$

$$u_{fin,Q1} = u_{inst,G} * (1 + \psi_{2,1} * k_{def}) = 5{,}7 * (1 + 0{,}4 * 2) \approx 10{,}3\ mm$$

$u_{fin} = u_{fin,G} + u_{fin,Q1} + \Sigma u_{fin,Qi} = 0{,}3 + 10{,}3 = 10{,}6\ mm = \frac{l}{253} \quad within\ \frac{l}{150}\ to\ \frac{l}{300}$

$(From\ EN\ 1995-1-1, table\ 7.2)$

7.3.2 Cable Supports placement

The most optimal placement of the vertical rods belonging to the cable support system is established by loading a beam on four supports with a moving unit load, having a step of 1 meter. The supports are placed at different positions and the envelopes from the moving unit load are compared.

The most efficient position of the rods is at **7,8** meters from either end, resulting in the bending moment envelope as shown in figure 7.6.

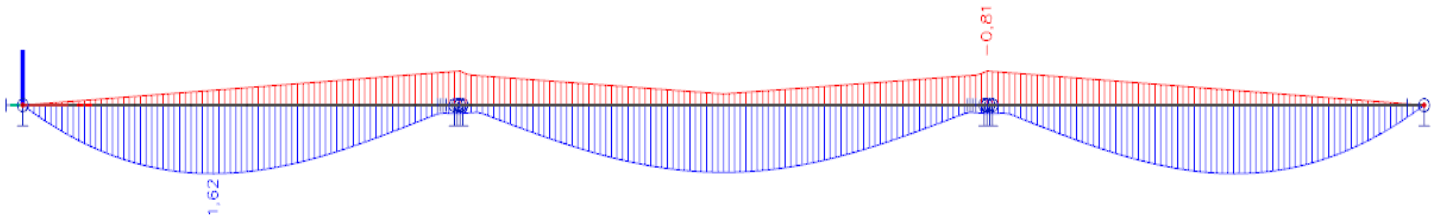

Figure 7.6: Bending moment envelope of a 25-meter beam, midspan supports at 7,8 meters from each end

7.3.3 Global Cross Section Design

Modelling

The bridge is modelled in SCIA Engineer similarly to the way stated in paragraph 6.5.
Additional details or points differing from the description in paragraph 6.5 are presented:

- Additional dead weight on the cross beams, representing the glulam deck, equal to:

$$\rho_{g,mean} * \mathrm{h} * \frac{\mathrm{g}}{1000} = 445 * 0{,}17 * \frac{9{,}81}{1000} = 0{,}74 \frac{kN}{m^2}$$

- Separate load panels on main beams and cross beams to ensure accurate load distribution

- Use of (nearly) infinitely stiff and light dummy elements connecting members to each other to accurately represent member sizes and retain accurate force distribution
- Tandem systems modelled as “driving” along bridge lanes, step of 0,5 meters

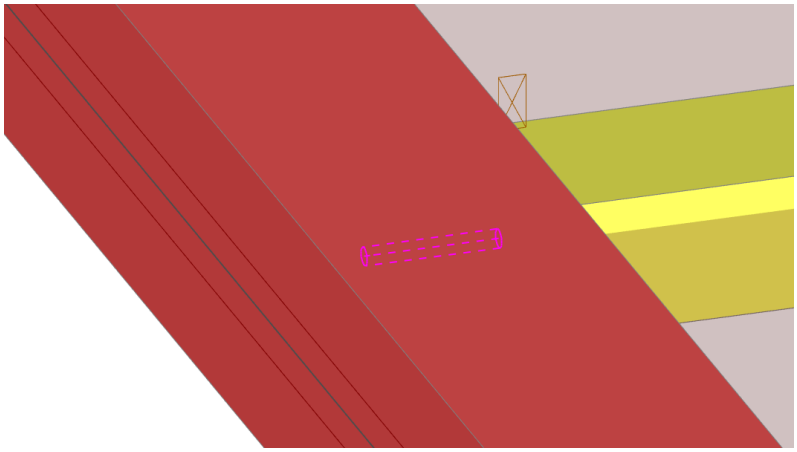

Figure 7.7: Load panels specific to members and stiff 1D connecting element

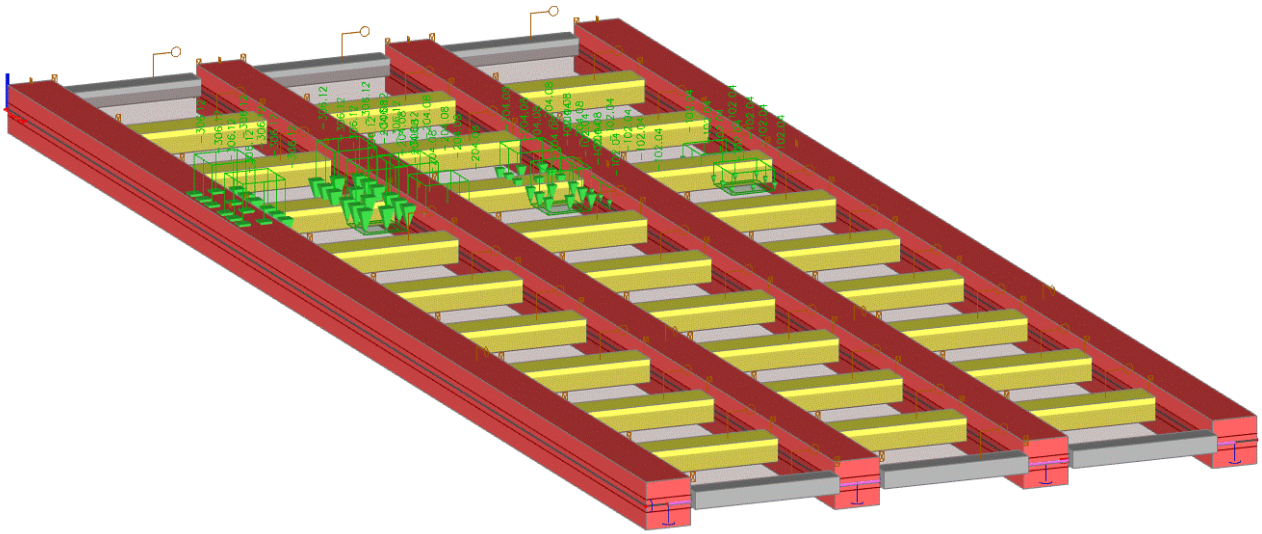

Figure 7.8: Tandem systems from load model 1 placed on bridge.

ULS Results

The ULS results for the structure are presented in table 7.2. As previously stated, the intermediate results and the Eurocode equations used can be found in appendix D.

Member	Type of Check	Value	Location
Normative Main Beam (Middle Beam)	Bending/ Axial	0,97	2,5 meters from end (between abutment and cable support)
Normative Main Beam	Shear/ Torsion	1.0	Over cable support
Normative Main Beam	Compression perpendicular to the grain	0,99	At abutment, support length 400 mm
Normative Outer Cross Beam (Under first lane)	Bending/ Axial	0,96	At mid- span
Normative Outer Cross Beam	Shear/ Torsion	0,99	At support
Normative Outer Cross Beam	Compression perpendicular to the grain	0,96	At support, support length 260 mm
Normative Inner Cross Beam (First cross beam, under lane 1)	Bending/ Axial	0,75	At mid- span
Normative Inner Cross Beam	Shear/ Torsion	0,96	At support
Normative Inner Cross Beam	Compression perpendicular to the grain	0,99	At support, support length 340 mm

Table 7.2: Normative ULS unity checks of timber superstructure

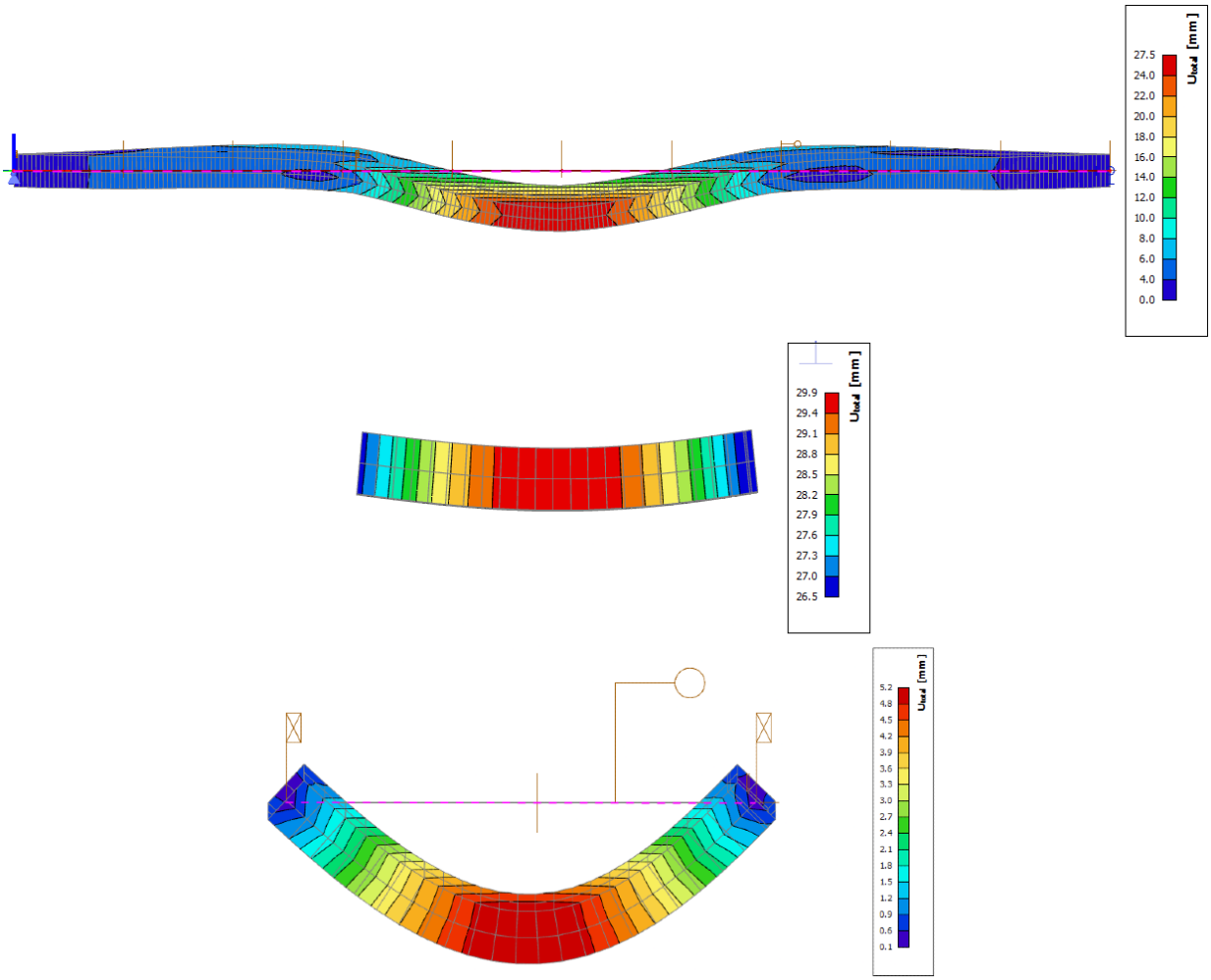

Figure 7.9 a, b, c: Instant deflection of Main-, inner cross-, and outer cross beam

Normative global displacements occur in the mid- span of the bridge.
Results for instant displacements and permanent displacements of the bridge are presented in tables 7.3 and 7.4 respectively.
Calculations are performed as detailed in subparagraph 7.3.1.

$$Service\ class\ 3 \qquad k_{def} = 2$$

$Member$	$l\ (m)$	$u_{inst}\ (mm)$	$limit\ (mm)$	$SLS\ Satisfied$
$Main\ Beam$	25	27,5	Max 62,5	Yes
$Inner\ Cross\ Beam$	2,36	3,3	Max 5,9	Yes
$Outer\ Cross\ Beam$	2,36	4,8	Max 5,9	Yes

Table 7.3: Normative instant SLS results for bridge members

$Member$	$l\ (m)$	$u_{fin,G}\ (mm)$	$u_{fin,Q1}\ (mm)$	$u_{fin}\ (mm)$	$limits(mm)$	$SLS\ Satisfied$
$Main\ Beam$	25	5,4	49,5	54,9	Max 166,6(6)	Yes
$Inner\ Cross\ Beam$	2,36	4,8	5,94	10,74	Max 15,73(3)	Yes
$Outer\ Cross\ Beam$	2,36	0,3	8,64	8,94	Max 15,73(3)	Yes

Table 7.4: Normative final SLS results for bridge members

7.4 Discussion

Deck

As expected, using a timber deck is a sensible solution. The steel deck is assumed to have no composite action with the rest of the timber superstructure. This offers no benefits and drastically increases the weight of the structure, when compared to the timber deck used for the design in chapter 6.

Timber Beams

With the bridge version, developed in this chapter, the members have much more balanced utilization ratios. The shear and bending capacity are both well utilized in the various members, unlike the designs in chapter 6.

Cable supports

The cable supports are currently assumed to rigidly support the main longitudinal beams. In reality this isn't the case.
The supports would act as springs with a certain stiffness, dependent on the loading conditions; the response of these springs would depend on the position of the loading effects.
An increase in the sagging and decrease the hogging bending moment can be expected.

A larger bending moment capacity would therefore be needed in the longitudinal main beams.
The cable supports acting as a spring would also increase the deformation in SLS.

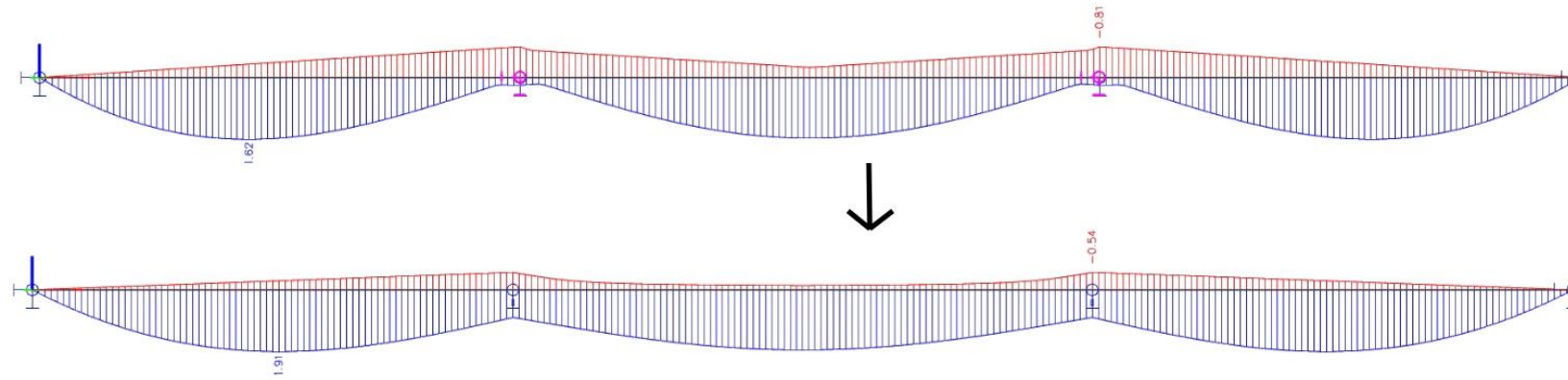

Figure 7.10: Bending moment envelope from infinitely stiff to finitely stiff cables

The horizontal support reactions of the cables are to be accounted for as well. Horizontal forces at the cable ends can be taken up by anchors or by the main beams themselves.

Dutch soil, generally, does not foster the use of anchors.
Attaching the cable ends to the main beam ends is a viable solution for reducing the horizontal resultant force in the abutments. The bridge is then mostly self-anchored.
In such case, the resultant horizontal support reactions can be taken up by the abutments on one side of the bridge.
Sufficient capacity for horizontal forces must be present in the abutments on said side of the bridge.
The same holds for the capacity of the beams which would take up (parts of) the cable horizontal reactions.

7.5 Application of Cable System

In this paragraph, the modelling of the full bridge will be presented and discussed.
The cable system will be fully implemented and an accurate force distribution for the complete design will be obtained. With these results, the connections will be designed.

The bridge is modelled as in paragraph 7.3, with the only difference being that a second order calculation is performed instead of a first order one. This is done in order to accurately represent potential sway of the compression rods under the bridge.

7.5.1 Design

Dimensions of the bridge elements, save for the cable placement are shown in figures 7.12a, b.

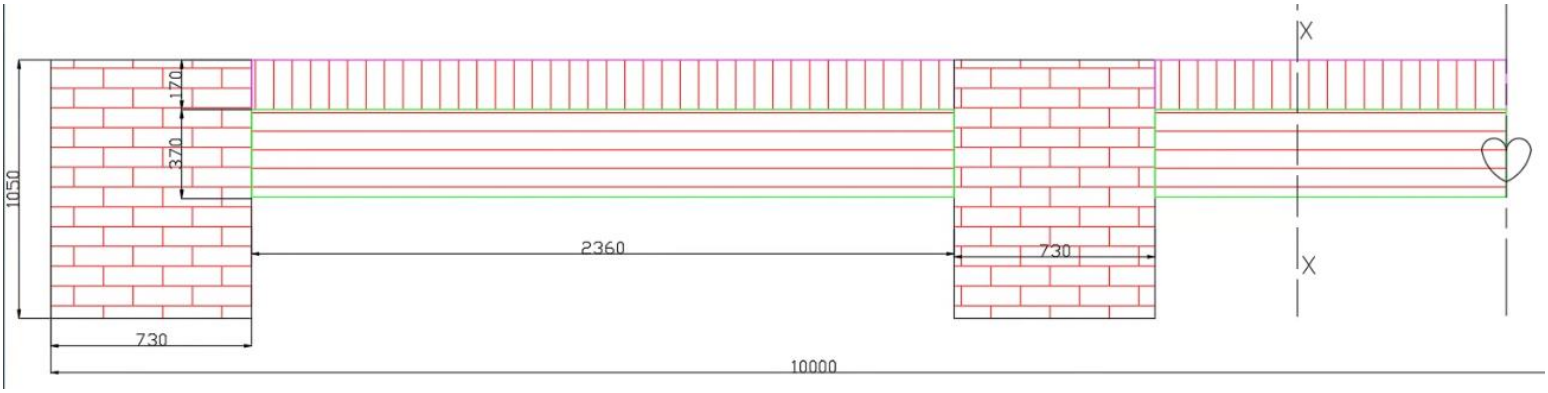

Figure 7.12a: Transverse cross section, at cross beam location (Section Y-Y)

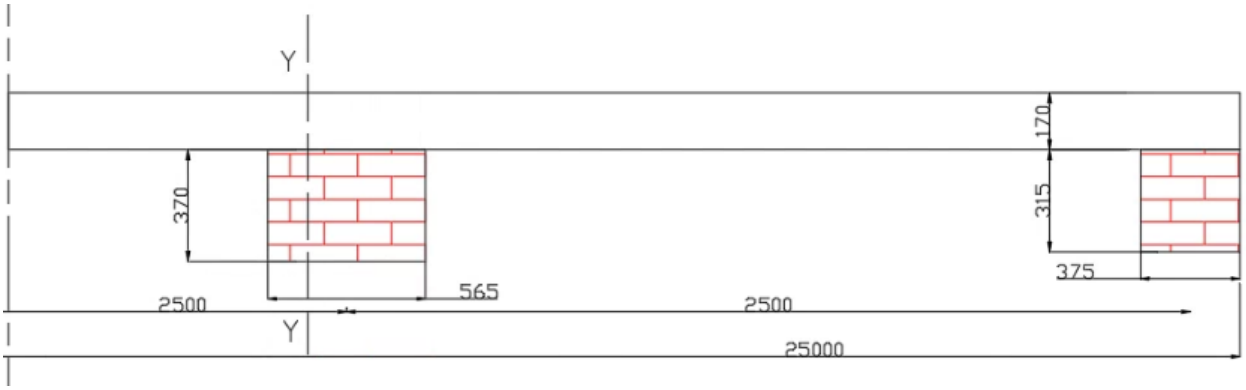

Figure 7.12b: Longitudinal cross section, in local span (Section X-X)

Lamination

The deck- and block glulam set-up is shown in figure 7.13

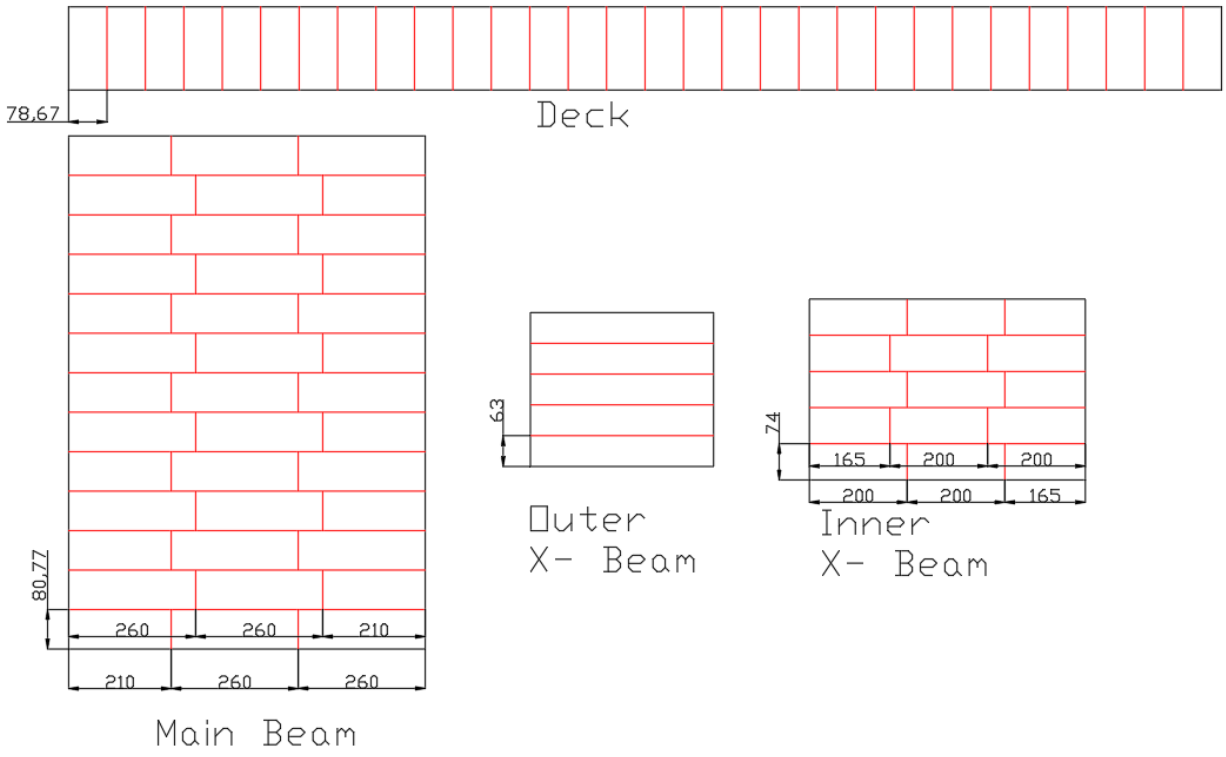

Figure 7.13: Lamina sizes per bridge element

A glue line thickness of 0,5 mm is assumed as used in experiments in [24].

Cables

There are some factors, specific to structural cables, that need to be accounted for.

- Higher strength, but lower ductility than steel. Cables typically experience breakage at 4% strain [11].
- No yield plateau, but limit of proportionality after which plastic deformations occur. Reached at 0,1% proof stress, corresponding with 65% to 70% of the tensile strength [12].
- Wires used in cables have an E modulus of ≈ 205 GPa.
- E moduli of cables vary depending on the configuration of wires and strands, decreasing with increasing spirality.
- Due to the relatively high ratio of strength to stiffness, often making deformations governing.
- Relaxation of cables occurs under certain stress levels under permanent loading. This level is 0,45f_{uk} according to Gimsing and Georgakis [12].

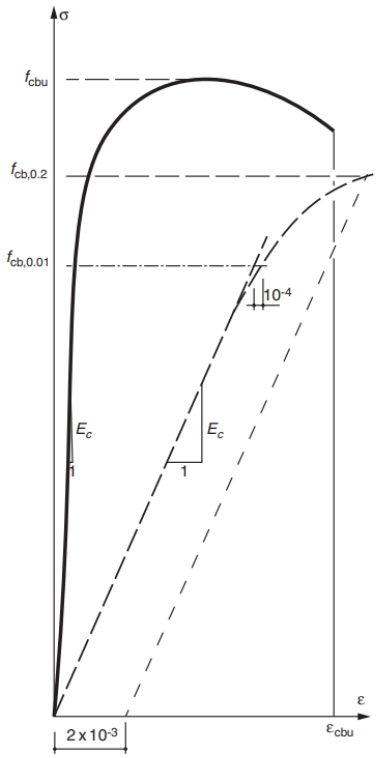

Figure 7.14: Stress- Strain relationship of wires, used in cables, from [12]

The cable system, as shown in figure 7.15 consists of locked coil cables with an E modulus of 180 GPa of class 1370. The choice for this cable system is made for the following reasons:

- Locked coil cables are relatively tightly packed, resulting in a smaller cross diameter and therefore allowing for placement at a larger angle.
- Locked coil cable inner wires are physically isolated from the environment, leading to an increased durability.
- Diagonal orientation of the cables stabilizes the compression rods

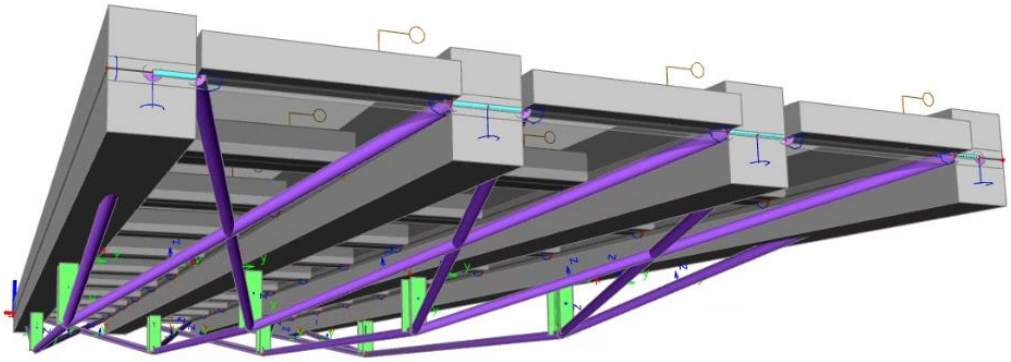

Figure 7.15: Inclined cable system SCIA model

The cables are modelled with geometry as shown in figure 7.16 and have a diameter of 169 mm.

The cables are modelled as discrete 1D tensile elements.
To accurately represent reality, the horizontal elements have the same cross sections as the diagonal ones, but have double the stiffness.

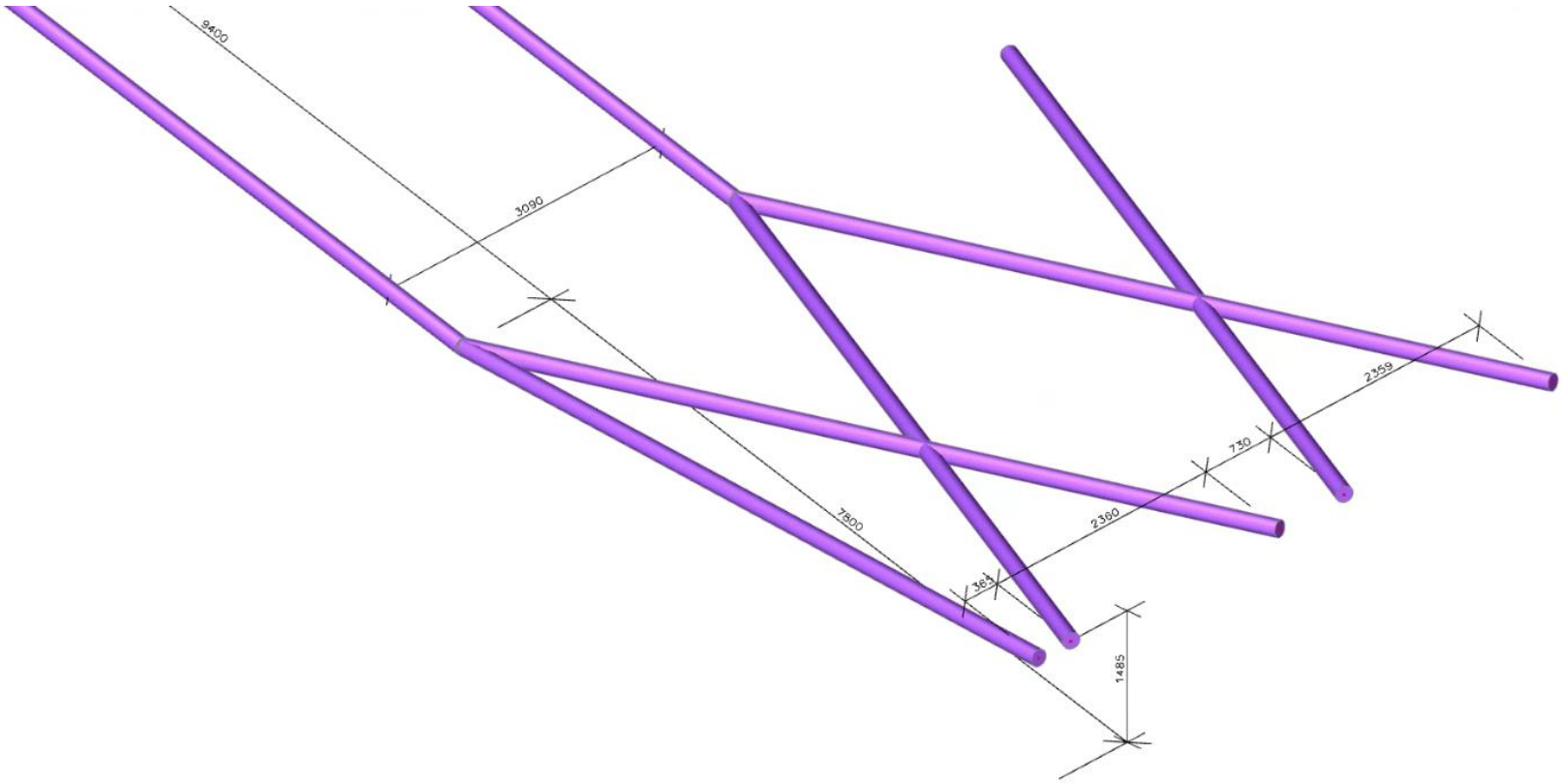

Figure 7.16: Inclined cable system, dimensions in mm

The crossing cables are accommodated with a tensile structure connector. A principal example of such a connector, produced by Macalloy, is shown in figure 7.17. This connector will not be further expanded on.

Figure 7.17: Tensile connector, from [https://www.archiexpo.com/prod/macalloy/product-61092-1557754.html]

The cable ends are attached to steel plates inside the main beams with steel plates as shown in figure 7.18.

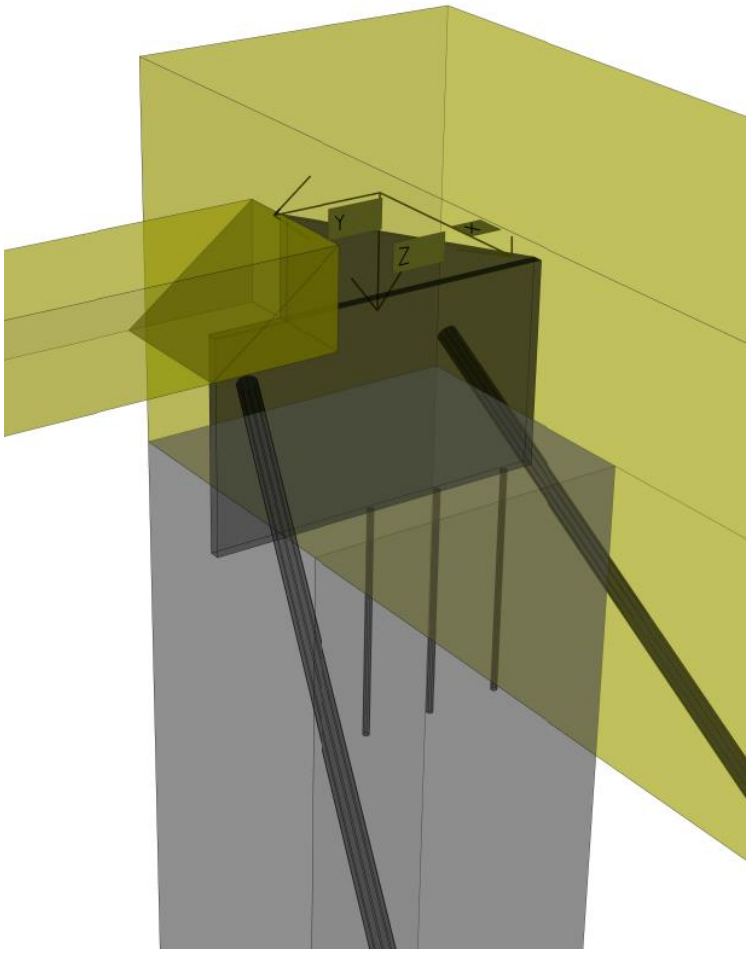

Figure 7.18: Anchor plate concept: outer main beam, all horizontal movement restrained

This force transfer of the datil works according to the following path:

- Tensile force in cable end, X component results in compression in main beam and tension/ compression in abutment with restrained longitudinal movement.
- Tensile force in cable end, Y component results in compression in outer cross beam and tension/ compression in abutments with restrained transverse movement
- Tensile force in cable end, Z component results in compression in abutment.

- Supports on one side of the beams have restricted movement in longitudinal direction.
- Supports on both sides of one outer main beam have restricted movement in transverse direction.

The assembly of this connection differs depending on whether an inner or outer main beam is concerned.

The outer main beams, have one cable running through them. The production of such a detail can be achieved by gluing the steel plate and running the cable through a predrilled hole inside the incomplete main beam.
Subsequently the remainder of the main beam is glued to the back of the plate to complete the element.
This is shown in figure 7.19

The plates in the inner main beams can be slid and glued into a pre-cut slot in the beams, after which the cables are attached to them.
This is done as the cables are attached to either side of the plate. No predrilling of a cable route in the inner beams is necessary.
This is illustrated in figure 7.20

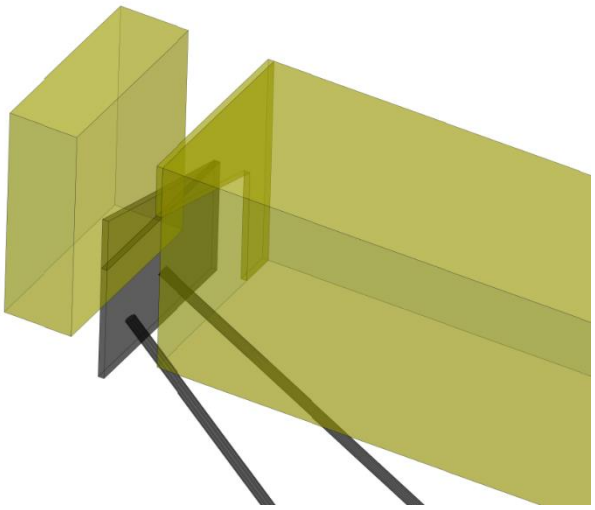

Figure 7.19: Outer beam anchor plate assembly

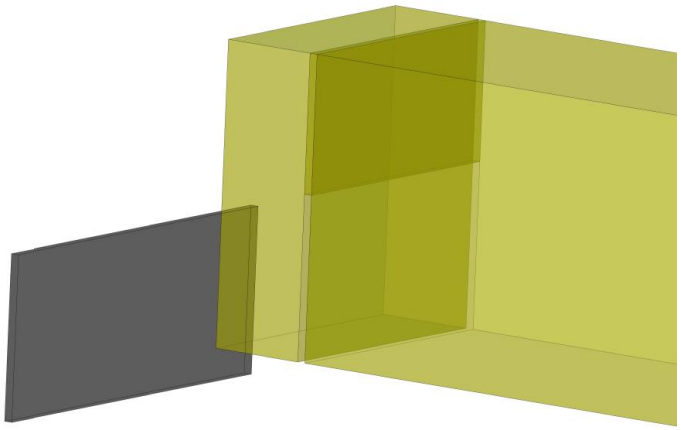

Figure 7:20 Inner beam anchor plate assembly

Compression rod

The compression rod is an HEA450 beam made from S355.

- The compression rod is subjected to shear forces acting in both local x and y direction as shown in figure 7.21a.
- The rod is attached to the main beam with a moment resisting connection, resulting in translation and rotation of the main beam.
- A sway mechanism is considered for the buckling analysis

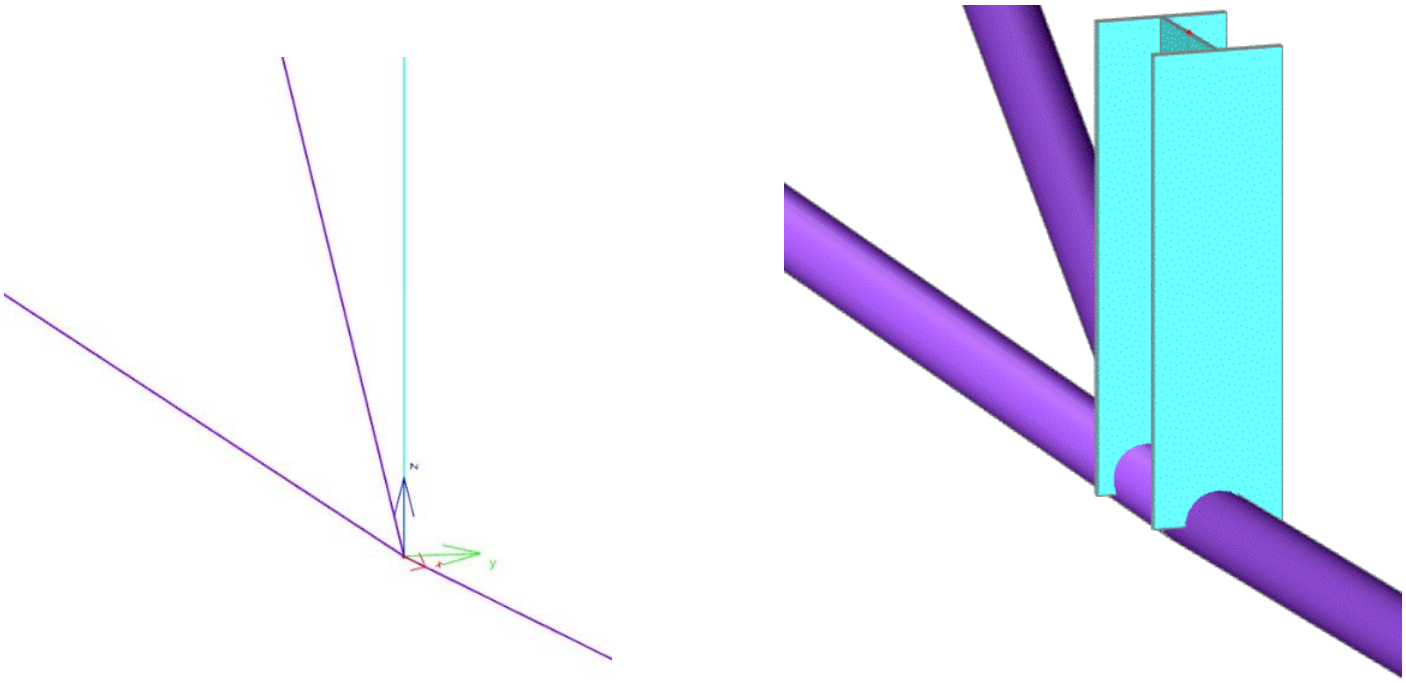

Figures 7.21a, b: Compression rod, axes and profile view

Saddle

The saddle connects the compression rod to the cables.

- The cables have a total angle within the saddle of 14°.
- The saddle has a zinc- metallized surface, providing a maximum mean friction coefficient of 0,6 [13]
- A cable clamp is present to provide sufficient friction between the saddle and the cables.

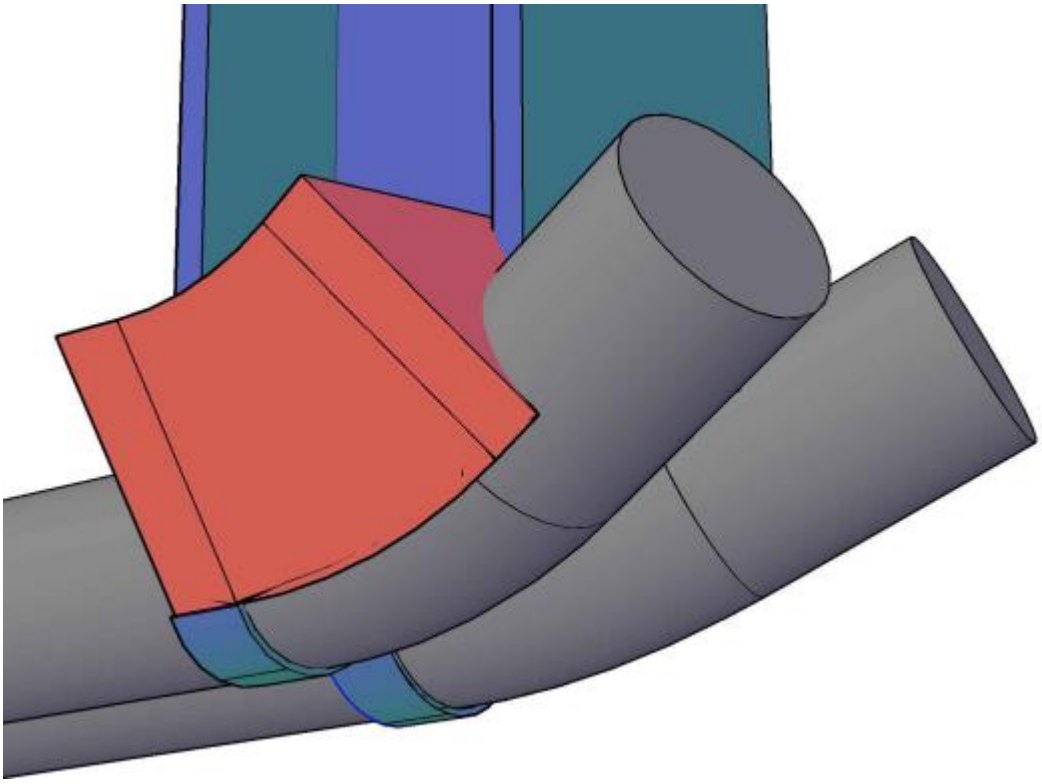

Figure 7.22: Saddle with clamp.

7.5.2 ULS Results

The ULS results of the complete bridge design are presented in this subparagraph. The equations used to obtain the results for the timber members are identical to the ones used in paragraph 7.3.

Appendix D is expanded with the equations and intermediate results of the compression rod. The short verification of the cable is performed within the main text.

The ULS results are presented in this subparagraph. Intermediate results in table form, along with equation numbers from EC 5-1-1 used can be found in appendix D.

Timber Members

Member	Type of Check	Value	Location
Normative Main Beam (Outer Beam)	Bending/ Axial	0,98	Mid span
Normative Main Beam	Shear/ Torsion	0,67	Over cable support
Normative Main Beam	Compression perpendicular to the grain	0,98	At abutment, support length 470 mm
Normative Outer Cross Beam (Under first lane)	Bending/ Axial	0,94	At mid- span
Normative Outer Cross Beam	Shear/ Torsion	0,85	At support
Normative Outer Cross Beam	Compression perpendicular to the grain	0,98	At support, support length 260 mm
Normative Inner Cross Beam (First cross beam, under lane 1)	Bending/ Axial	0,77	At mid- span
Normative Inner Cross Beam	Shear/ Torsion	0,98	At support
Normative Inner Cross Beam	Compression perpendicular to the grain	0,98	At support, support length 340 mm

Table 7.5: Normative ULS unity checks of timber superstructure, including cable system

Cables

The maximum force carried by a single cable, occurs in the first diagonal member, going through the outer main beam. This force results in a tensile stress of 150,1 MPa.

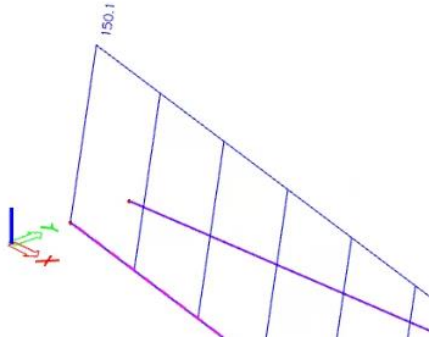

Figure 7.23: Maximum force in cable

$$\frac{f_{u,k}}{\gamma_{M2}} = \frac{1370}{1{,}25} = 1096\ MPa$$

$$UC = \frac{150{,}1}{1096} = 0{,}14$$

$$Relaxation\ limit = 0{,}45 * 1371 = 616{,}5\ MPa \gg 150{,}1\ MPa$$

Saddle clamping force

$$F_{ed1} = 2061{,}3\ kN \qquad F_{ed2} = 1777{,}6\ kN \qquad \mu = 0{,}6$$

$$\boldsymbol{Max\ cable\ force\ ratio\ without\ clamp}: \boldsymbol{e^{(\frac{\mu * \alpha}{\gamma_{m,fr}})} = e^{(\frac{0{,}6 * 0{,}244}{1{,}65})} = 1{,}093}$$

$$Occuring\ cable\ force\ ratio = \frac{2061{,}3}{1777{,}66} = 1{,}16 > 1{,}093 \quad Clamp\ is\ necessary$$

$$k = 2, full\ friction\ between\ cable\ and\ saddle$$

$$Required\ clamping\ force = \frac{F_{ed1} - \frac{k * F_r * \mu}{\gamma_{m,fr}}}{F_{ed2}} = 1{,}093 => F_r = 163\ kN$$

Compression rod

$$Von\ Mises\ Stresses\ at\ top\ (at\ connection\ to\ main\ beam)\ \sigma_{eq,d} = 336{,}6\ kN$$

$$UC = \frac{\sigma_{eq}}{f_{yd}} = \frac{336{,}6}{355} = 0{,}95$$

7.5.3 SLS Results

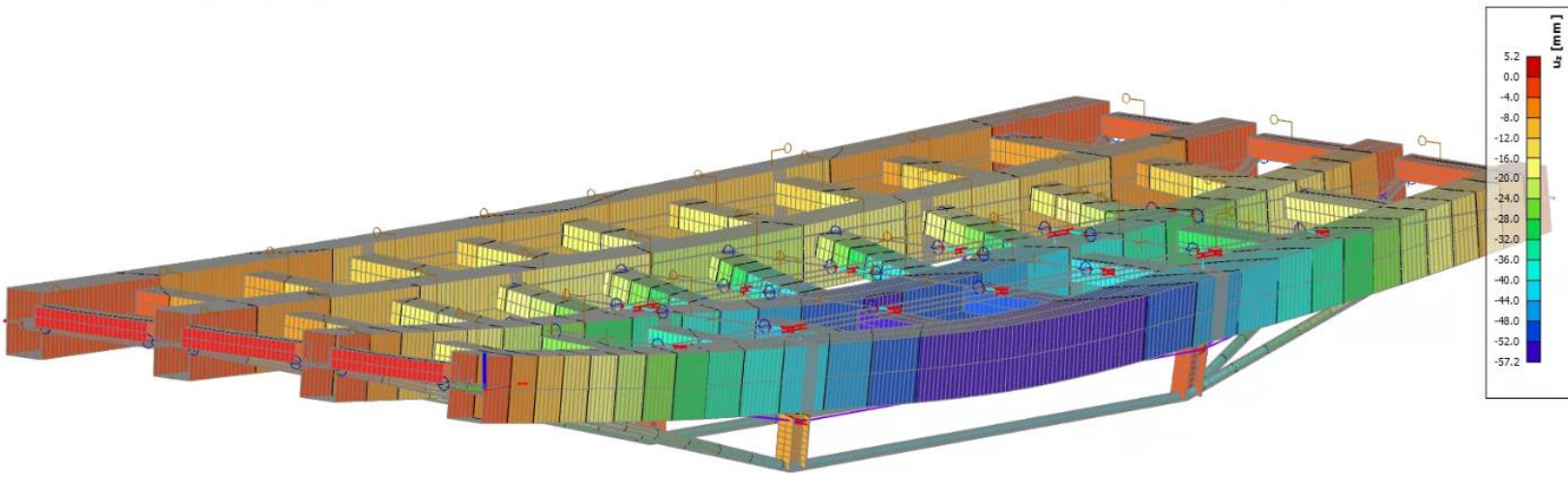

Figure 7.24: Maximum displacement of bridge due to characteristic traffic loading.

$$Service\ class\ 3 \qquad k_{def} = 2$$

$Member$	$l\ (m)$	$u_{inst}\ (mm)$	$limit\ (mm)$	$SLS\ Satisfied$
$Main\ Beam$	25	56,6	Max 62,5	Yes
$Inner\ Cross\ Beam$	2,36	3,4	Max 5,9	Yes
$Outer\ Cross\ Beam$	2,36	3,1	Max 5,9	Yes

Table 7.6: Normative instant SLS results for bridge members

$Member$	$l\ (m)$	$u_{fin,G}\ (mm)$	$u_{fin,Q1}\ (mm)$	$u_{fin}\ (mm)$	$limits(mm)$	$SLS\ Satisfied$
$Main\ Beam$	25	51	101,9	152,9	Max 166,6(6)	Yes
$Inner\ Cross\ Beam$	2,36	9,6	6,1	15,7	Max 15,73(3)	Yes
$Outer\ Cross\ Beam$	2,36	3,6	5,6	9,2	Max 15,73(3)	Yes

Table 7.7: Normative final SLS results for bridge members

7.5.4 Discussion

ULS

- Main Beams experience increased normal forces due to cable ends being attached to beam ends, buckling becomes normative
- Horizontal cable reactions are assumed to act in the centre of timber cross sections.
  If cables would act lower in the cross sections, a favourably acting moment would be exerted on the beams similar to the prestressing of concrete.
  The effective depth of the cable system would be less efficient, producing smaller support reactions in the compression rods.

- Outer cross beams transfer horizontal components of cable forces. They are subjected to high compression forces perpendicular to the grain, requiring a larger cross section.

- The cable deformations are normative. Due to the strength to elasticity ratio of the cables, they must remain under stressed in order to provide adequate support to the compression rods.

SLS

- The SLS requirements for the main beams are narrowly satisfied. This result is expected since the cable supports aren't infinitely stiff as modelled in paragraph 8.3.
- The inner cross beams are skewed under loading. The normative inner cross beam is between two main beams with different deflections, making for a sag. The cross beam suffices nonetheless.
- The outer cross beams easily satisfy the SLS conditions. The beams are oversized with regards to SLS. Due to the small depth of the superstructure a large increase in cable force is present under heavier loads. A component of this cable force must be transferred through the outer cross beams.

7.6 Joints

7.6.1 Cross Beams to Main beam

The cross beam to main beam connection is assumed to be attached with a hinge. For this, joist hangers are to be used.

Points of note for this type of connections are:

- They cause tension perpendicular to the grain in one of the connecting members. Tension perpendicular to the grain is a very brittle failure mechanism and it must be avoided.
- EC 5-1-1 does not cover these connections, the German NA does. Equations used to verify such details are provided by H. J. Blaß and C. Sandhaas in [20].
- Connectors as shown in figures 8.22 and 8.23 are commercially available in grade S250 GD, with a zinc coating (+Z). Higher grades, causing lower ductility in the bracket, are possible.

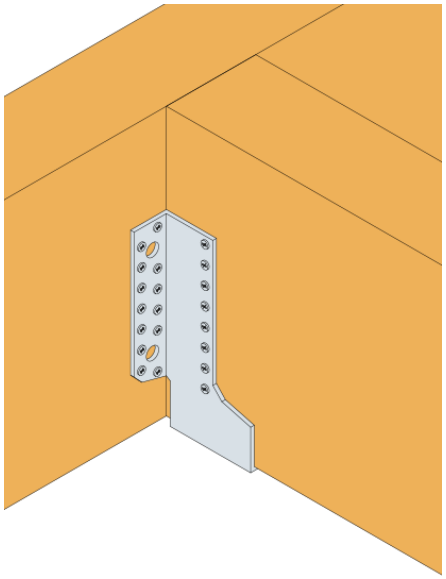

Figure 7.26: Beam joist hanger example, from

[https://www.strongtie.nl/nl-NL/producten/grote-ophangbeugel-met-naar-buiten-stande-flenzen-gle-4]

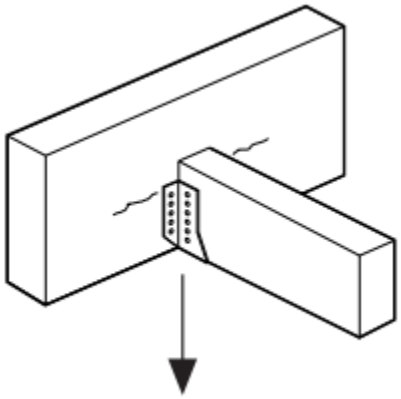

Figure 7.27: Failure due to splitting, illustrated, from [20, p. 442]

The cross beams are connected to the main beams with brackets as visualized in figure 7.28. The rods connecting the back plate to the main beam are glued into the main beam.

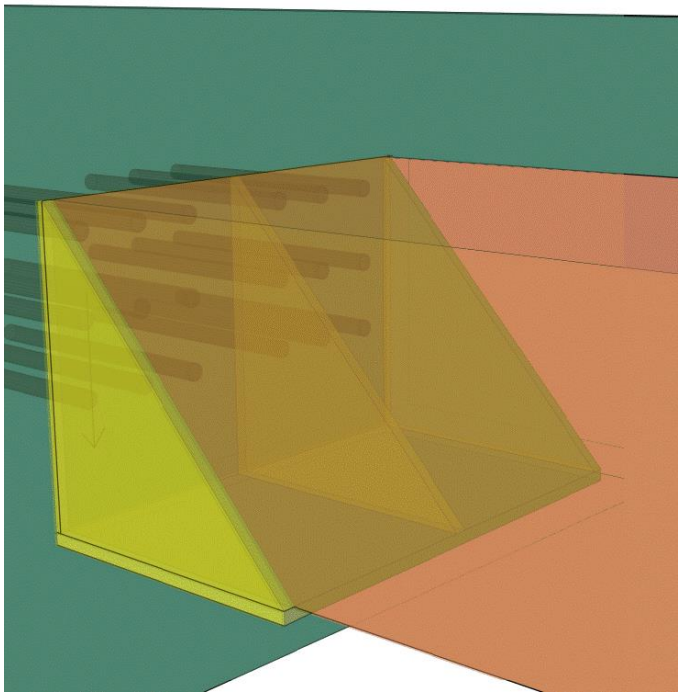

Figure 7.28: Cross girder (brown) to outer main beam (green) connection concept

Design and Modelling

The forces to be transferred are guiding to the design of the connector brackets. These are inventoried in table 8.6

$Member$	$Vz\ (kN)$	$N+\ (positive)(kN)$
$Outer\ cross\ beam$	$ULS = 238{,}94 \quad SLS = 128{,}25$	$-$
$Final\ two\ inner\ cross\ beams$	$ULS = 340{,}77 \quad SLS = 229{,}7$	$ULS = 192{,}76 \quad SLS = 117{,}51$
$Other\ inner\ cross\ beams$	$ULS = 323{,}46 \quad SLS = 216{,}8$	$-$

Table 7.6: Forces to be transferred by cross- beam connectors

The cross-beam connector, transferring tensile normal forces does so with a pin through the vertical plates going through the cross beam.

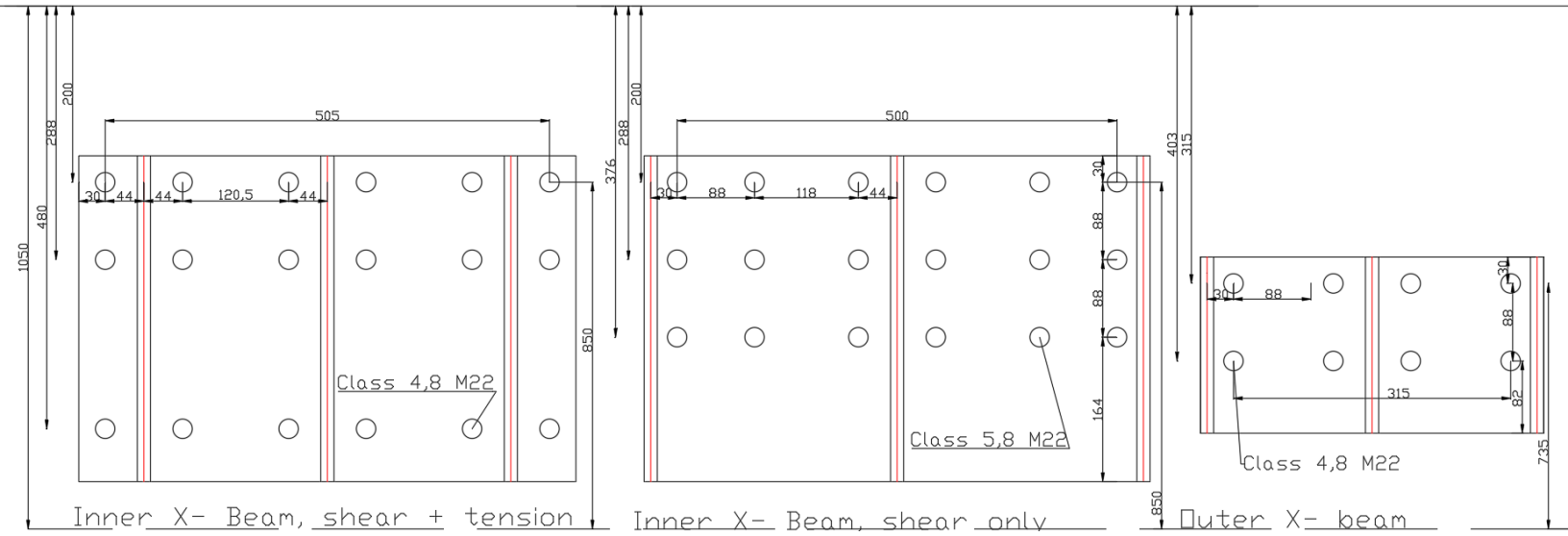

Figure 7.29: Cross beam brackets, main beam face, dimensions in mm

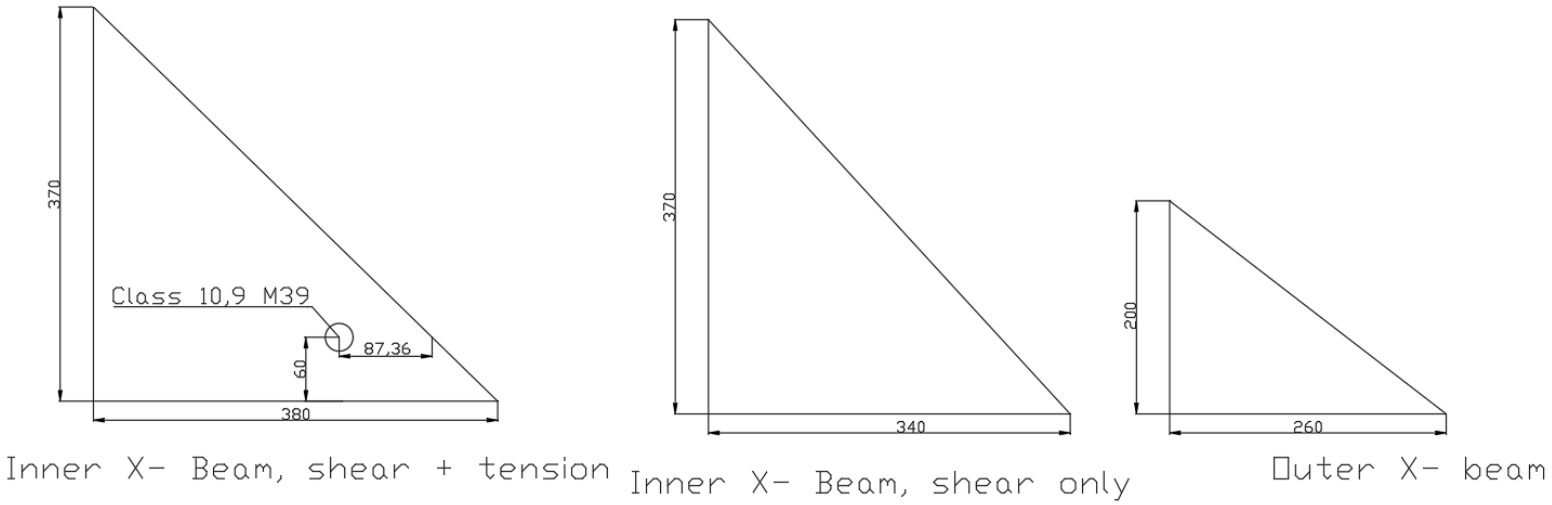

Figure 7.30: Cross beam brackets, cross beam face, dimensions in mm

The following assumptions and parameters with regards to the connections and their modelling hold true:

- S250GD+Z steel grade is used.
- Brackets have a thickness of 15 mm.
- Fastener spacings adhere to requirements (EN 1995-1-1, paragraph 8.2 for timber and EN 1993-1-8, table 3.3 for steel).
- Glued in rod fasteners in the main beam have an embedment depth of 340 mm.
- Full rope effect is taken into account (no extraction of the fasteners).
- For the tensile normal force in the concerning cross beams: $\frac{1}{2}$ of the tensile force is transferred through the middle plate, while the outer plates carry $\frac{1}{4}$ each.

- SCIA plate model with 2 mm element size.
- Material non linearity with a hardening modulus of 2,1 GPa is applied.
- The vertical ULS and SLS loads are modelled as distributed forces across the bottom plate of the bracket.
- Imposed horizontal loads are modelled by line loads across half the pin fastener holes.
- Fasteners are modelled as Z supports across the top half of the hole diameter and X- and Y- supports across the entire hole diameter.
- Plate displacements in the direction of wood contact are prevented by surface supports with stiffness equal to the E- modulus of GL 26h, following from EN 14080.

- Forces on the fasteners are obtained from the FE model and used for analytical verifications of the fasteners.

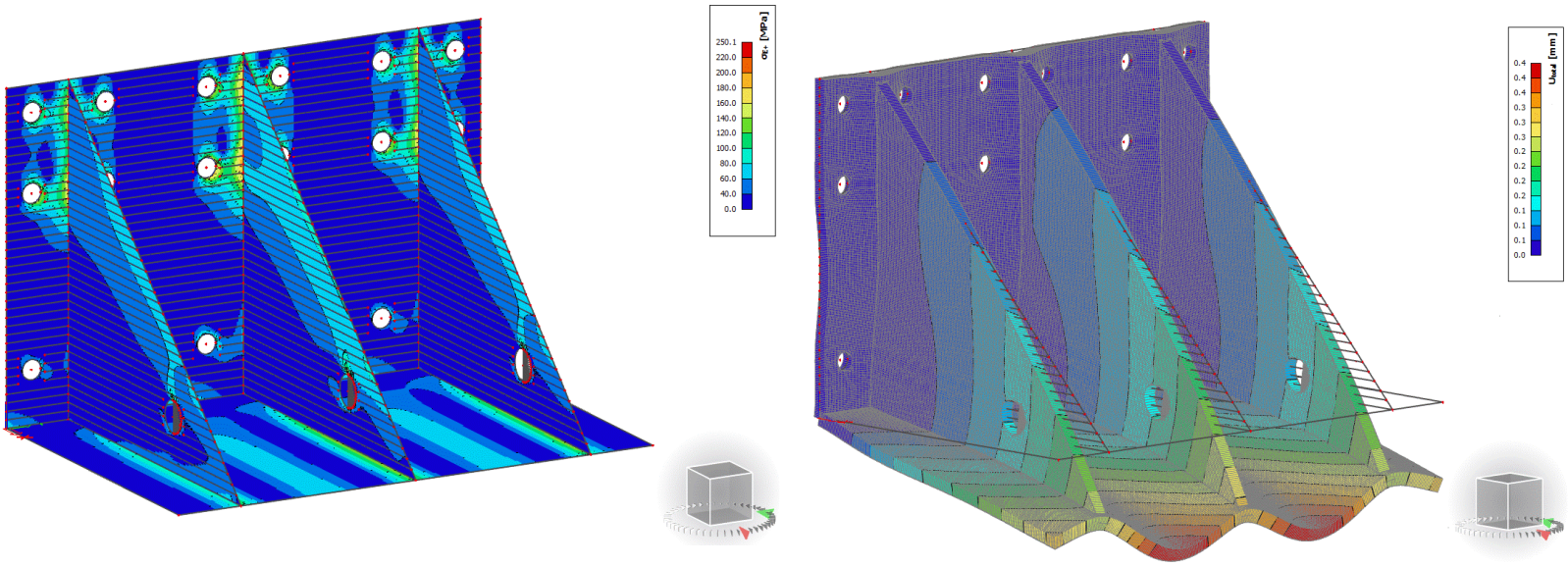

Figures 7.31a, b: Shear and normal force inner x-beam bracket equivalent stress and deformation under predominantly shear loading in ULS

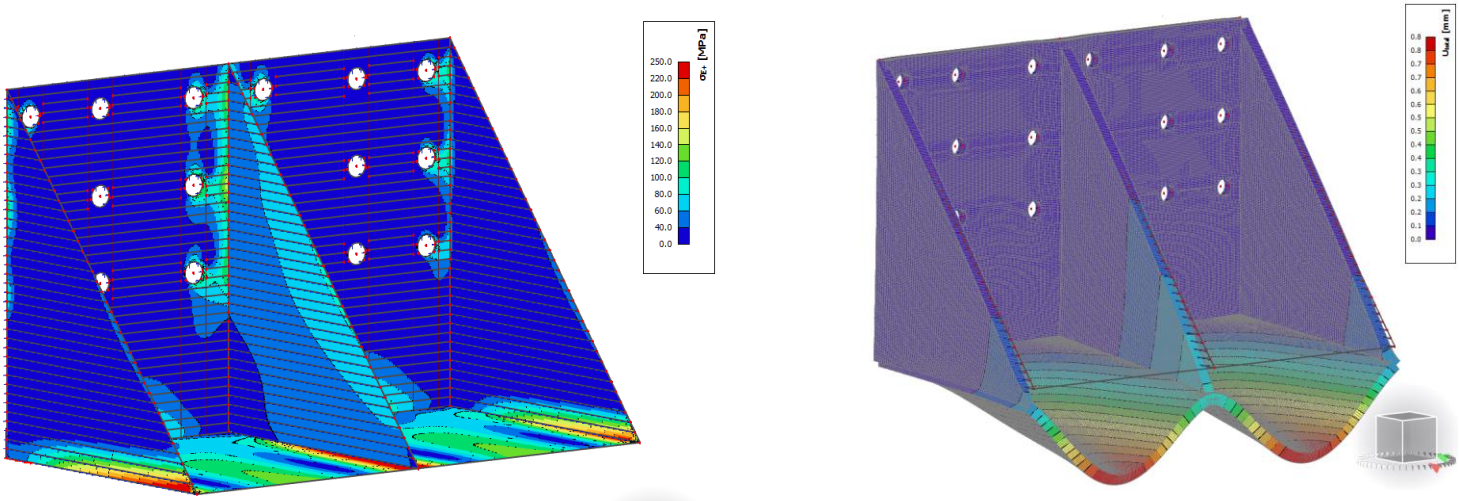

Figures 7.32a, b: Shear Only inner x-beam bracket, equivalent stress and deformation in ULS

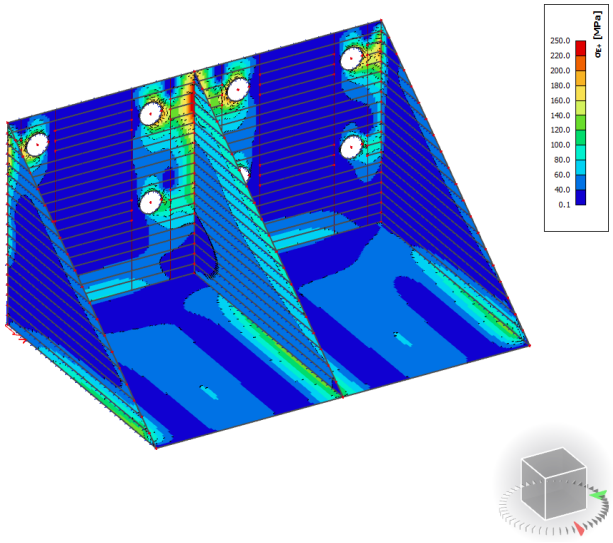

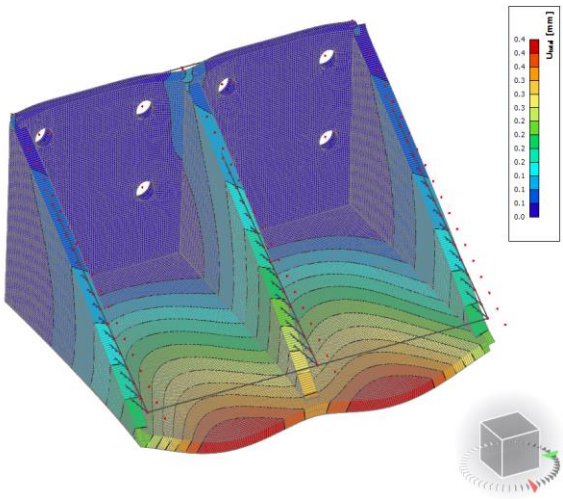

Figures 7.33a, b: Outer x-beam bracket, equivalent stress and deformation in ULS

Analytical Calculations and Results

The inner beam connection is worked out. The results of the other details are calculated in an identical manner. All equations used are shown in appendix E1 in python code form.
The unity checks are summarized in table 7.7.

$M39\ Dowel\ shear\ joint\ check\ according\ to\ EC\ 5-1-1$

$$d = 39 \quad f_{u,k} = 1000\ MPa \quad \alpha_1 = 0° \quad \rho = 445\frac{kg}{m^3} \quad t_1 = 208{,}5\ mm \quad t_2 = 178{,}25\ mm \quad t = 15mm$$

$$F_{v,ed1} = 96{,}38\ kN \quad F_{ax,2} = 40{,}19\ kN \quad Ax = 1\ (no\ extraction) \quad \gamma_{m2} = 1{,}25 \quad k_2 = 0{,}9 \quad \gamma_{m,c} = 1{,}3$$

$$predrilled\ hole$$

$$M_{y,rk} = 0{,}3 * f_{u,k} * d^{2,6} = 4{,}11\ kNm \qquad f_{h,k} = 0{,}082 * (1 - 0{,}01 * d) * \rho = 22{,}26\ MPa$$

$$Failure\ mechanism\ f: F_{v,rk,f} = f_{h,k} * t1 * d \quad F_{v,rd,f} = \frac{F_{v,rk,f}}{\gamma_c} = 139{,}2\ kN$$

$$Failure\ mechanism\ g: F_{v,rk,g} = f_{h,k} * t1 * d * \left(\sqrt{2 + \frac{4 * M_{y,rk}}{f_{h,k} * d * t1^2}} - 1\right)$$

$$F_{v,rd,g} = \frac{F_{v,rk,g} + Ax * 0{,}25 * F_{v,rk,g}}{\gamma_c} = 97{,}58\ kN$$

$$Failure\ mechanism\ h: F_{v,rk,h} = 2{,}3 * \sqrt{M_{y,rk} * f_{h,k} * d}$$

$$F_{v,rd,h} = \frac{F_{v,rk,h} + Ax * 0{,}25 * F_{v,rk,h}}{\gamma_c} = 124\ kN$$

$$F_{v,rd} = \min\left(F_{v,rd,f}, F_{v,rd,g}, F_{v,rd,h}\right) = F_{v,rd,g} = 97{,}58\ kN \quad Non - brittle\ failure\ mechanism$$

$$UC = \frac{F_{v,ed1}}{F_{v,rd,g}} = \frac{96{,}38}{97{,}58} = 0{,}99$$

$M39\ Dowel\ steel\ check\ according\ to\ EN\ 1993-1-8, 3.6.1$

$$F_{v,rd} = \frac{\alpha * f_{u,k} * 0{,}25 * \pi * d^2}{\gamma_2} = 162{,}86\ kN$$

$$F_{t,rd} = \frac{k_2 * f_{u,k} * A}{\gamma_2} = 293{,}15\ kN$$

$$UC = \frac{F_{v,ed}}{F_{v,rd}} + \frac{F_{ax,ed}}{1{,}4 * F_{t,rd}} = 0{,}44$$

$M22\ Dowel\ shear\ joint\ check\ according\ to\ EC\ 5-1-1$

$$d = 22 \quad f_{u,k} = 400\ MPa \quad \alpha_1 = 0° \quad \rho = 445\frac{kg}{m^3} \quad t_1 = 320\ mm \quad t = 15mm$$

$$F_{v,ed} = 26{,}245\ kN \quad F_{ax,ed} = 12{,}78\ kN \quad Ax = 1\ (no\ extraction) \quad \gamma_{m2} = 1{,}25 \quad k_2 = 0{,}9 \quad \gamma_{m,c} = 1{,}3$$

$$predrilled\ hole$$

$$M_{y,rk} = 0{,}3 * f_{u,k} * d^{2,6} = 0{,}93\ kNm \qquad f_{h,k} = 0{,}082 * (1 - 0{,}01 * d) * \rho = 28{,}46\ MPa$$

$$0{,}5 * d < t < d$$

$$Considering\ failure\ mechanisms\ c, alongisde\ linear\ interpolation\ between\ a-d\ and\ b-e$$

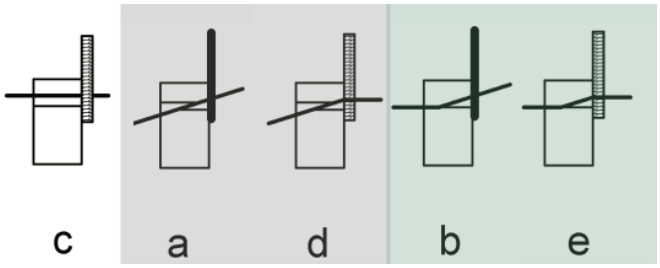

Figure 7.34: (Combination) of failure mechanisms to be considered, from [EN 1995-1-1, figure 8.3]

$$Failure\ mechanism\ c: \qquad F_{v,rk,c} = f_{h,k} * t1 * d \qquad F_{v,rd,c} = \frac{F_{v,rk,c}}{\gamma_{m,c}} = 154{,}13\ kN$$

$$Failure\ mechanism\ a: \ F_{v,rk,a} = 0{,}4 * f_{h,k} * t1 * d \quad F_{v,rd,a} = \frac{F_{v,rk,a} + Ax * 0{,}25 * F_{v,rk,a}}{\gamma_{m,c}} = 61{,}65\ kN$$

$$Failure\ mechanism\ d: \qquad F_{v,rk,d} = f_{h,k} * t1 * d * \left(\sqrt{2 + \frac{4 * M_{y,rk}}{f_{hk} * d * t1^2}} - 1\right)$$

$$F_{v,rd,d} = \frac{F_{v,rk,d} + Ax * 0{,}25 * F_{v,rk,d}}{\gamma_{m,c}} = 81{,}37\ kN$$

$$Mechanisms\ a-d\ interpolated\ F_{v,rd,a-d} = F_{v,rd,a} + (t - 0{,}5 * d) * \frac{F_{v,rd,d} - F_{v,rd,a}}{d - 0{,}5 * d} = 68{,}83\ kN$$

$$Failure\ mechanism\ b: \qquad F_{v,rk,b} = 1{,}15 * \sqrt{2 * M_{y,rk} * f_{h,k} * d}$$

$$F_{v,rd,b} = \frac{F_{v,rk,b} + Ax * 0{,}25 * F_{v,rk,b}}{\gamma_{m,c}} = 23{,}84\ kN$$

$$Failure\ mechanism\ e: \quad F_{v,rk,e} = 2{,}3 * \sqrt{M_{y,rk} * f_{h,k} * d}$$

$$F_{v,rd,e} = \frac{F_{v,rk,e} + Ax * 0{,}25 * F_{v,rk,e}}{\gamma_{m,c}} = 47{,}68\ kN$$

$$Mechanisms\ b-e\ interpolated\ F_{v,rd,b-e} = F_{v,rd,e} + (t - 0{,}5 * d) * \frac{F_{v,rd,e} - F_{v,rd,b}}{d - 0{,}5 * d} = 32{,}51\ kN$$

$$F_{v,rd} = \min\left(F_{v,rd,c}, F_{v,rd,a-d}, F_{v,rd,b-e}\right) = F_{v,rd,a-d} = 32{,}51\ kN \quad Non-brittle\ failure\ mechanism$$

$$UC = \frac{F_{v,ed}}{F_{v,rd,a-d}} = \frac{26{,}245}{32{,}51} = 0{,}81$$

M22 Dowel steel check according to EN $1993-1-8, 3.6.1$

$$F_{v,rd} = \frac{\alpha * f_{u,k} * 0{,}25 * \pi * d^2}{\gamma_2} = 60{,}82\ kN$$

$$F_{t,rd} = \frac{k_2 * f_{u,k} * A}{\gamma_2} = 87{,}26\ kN$$

$$UC = \frac{F_{v,ed}}{F_{v,rd}} + \frac{F_{ax,ed}}{1{,}4 * F_{t,rd}} = 0{,}54$$

Main beam tension to tensile cross beam perpendicular to the grain check according to $[20], E11$

$$F_{ed} = 340{,}77\ kN \quad \alpha_r = 505\ mm \quad number\ of\ fastener\ rows\ (n) = 3 \quad h_1 = 320\ mm$$

$$h_e = 800\ mm \quad h_i = 200, 288, 480\ mm \quad h = 1050 \quad t_{ef} = 150\ mm \quad f_{t,90} = \frac{0{,}5}{1{,}25} * 0{,}9 = 0{,}36\ MPa$$

$$k_s = 0{,}7 + 1{,}4 * \left(\frac{a_r}{h}\right) = 1{,}37 \quad k_r = \frac{n}{\sum_{i=1}^{n}\left(\frac{h_1}{h_i}\right)^2} = 1{,}81$$

$$F_{90,rd} = k_s * k_r * \left(6{,}5 + 18 * \left(\frac{h_e}{h}\right)^2\right) * \left(t_{ef} * h\right)^{0{,}8} * f_{t,90} = 432{,}12\ kN$$

$$UC = \frac{F_{ed}}{F_{90,rd}} = 0{,}79$$

$$Axially\ loaded\ glued-in\ rods, according\ to\ [20], E10.3$$

$$F_{ax} = 24\ kN \quad d = 22\ mm \quad f_{yd} = \frac{f_{yk}}{\gamma_{m2}} = \frac{1000}{1{,}25} = 800\ MPa \quad A = 380{,}13\ mm^2 \quad l_{ad} = 320\ mm$$

$$l_{ad} < 250, thus \quad f_{k1,k} = 4{,}0 \quad f_{k1,d} = \frac{f_{k1,k}}{\gamma_m} = \frac{4}{1{,}3} = 3{,}1$$

$$F_{ax,rd,1} = A * f_{y,d} = 304{,}1\ kN \qquad F_{ax,rd,2} = \pi * d * l_{ad} * f_{k1,d} = 62{,}1\ kN$$

$$UC = \frac{24}{62{,}1} = 0{,}39$$

Type of Verification	Final Inner X- Beams	Remainder of Inner X-Beams	Outer X-Beams
M39 Timber to Steel shear joint: EN 1995, 8.2.3	0,99; 0,91*	-	-
M39 Timber to Steel bolt failure: EN 1993-1-8, 3.6.1	0,44	-	-
M22 Timber to Steel shear joint: EN 1995-1-1, 8.2.3	0,81**	0,93**	0.95**
M22 Timber to Steel bolt failure: EN 1993-1-8, 3.6.1	0,54	0,4	0,65
Main beam tension perpendicular to the grain: [20], E11	0,79	0,85	0,89
Axially loaded GIR: [20], E10.3	0,39	0,33	0,49

Table 7.7: Unity checks for analytical equations

* 0,99 for middle plate, 0,91 for outer plates

** The unity check is based solely on the EC equations. According to [20], the embedment strength for glued-in dowels perpendicular to the grain can be increased. Therefore, the considered unity check is additionally conservative.

Discussion

With regards to the numerical results:

- The bracket which transfers tension as well as shear force experiences some yielding around the pin holes under ULS loading.
- The other brackets experience some yielding at the plate interfaces under ULS loading.
- No yielding occurs in SLS loading.

As stated, the forces on the dowels obtained from the FE model are then used for analytical verifications of the timber.

- The connection suffices on all validations.
- The unity check for tension perpendicular to the grain has a lower unity check than the fastener failure, no brittle failure due to tension perpendicular to the grain occurs.
- The normative failure mechanism for the fasteners are ductile ones, no brittle failure occurs due to them.

7.6.2 Cables to Beam and Abutment

The detail principle is explained in subparagraph 7.5.1.
The connection, as illustrated in figure 7.18, will be designed.
This detail transfers the highest horizontal forces to the abutment and will therefore be worked out.
The other details can be based on the dimensions of this, normative one.

Design and Modelling

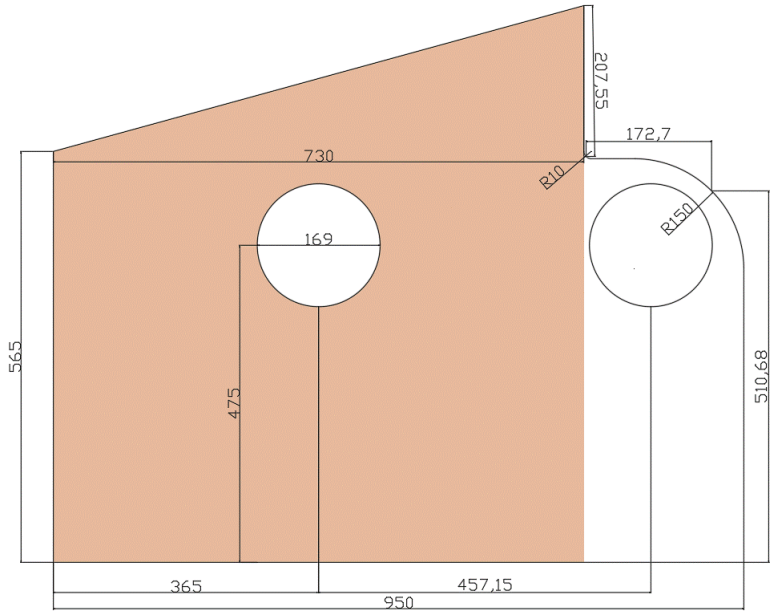

Figure 7.35: Outer beam plate, dimensions in mm, hatched area located inside main beam

- The plate is subjected to a normative combination of cable forces from the cables of 2178 kN for the cable positioned in the global longitudinal plane and 3037 kN for the cable positioned out of the global longitudinal plane.
- S355 steel grade is used.
- The plate has a thickness of 10 cm.

- SCIA plate model with 2mm element size.
- Material non linearity with a hardening modulus of 2,1 GPa is applied.
- Cable loads are modelled as surface loads, acting in their orientation, over the surface area of the cables.
- The abutment restrictions in Y and X direction are modelled as a singular hinge in the middle of the bottom ridge of the plate.
- The abutment restriction in Z direction is modelled as a line support across the bottom of the plate.
- Plate displacements in the direction of wood contact are prevented by surface supports with stiffness equal to the E- modulus of GL 26h, following from EN 14080.

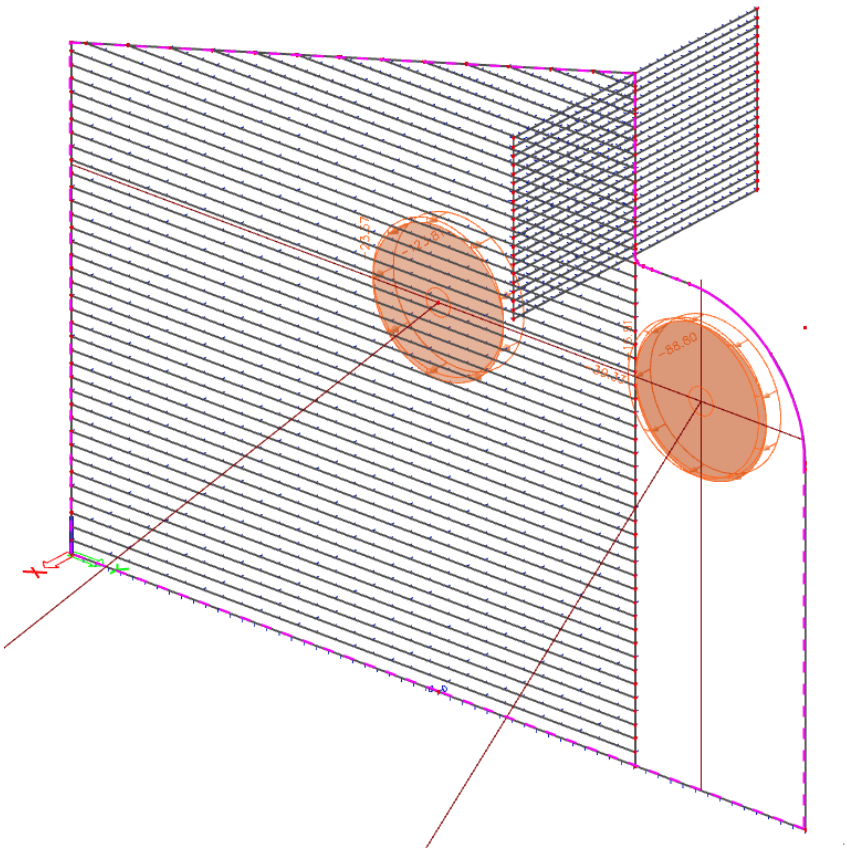

Figure 7.36: SCIA model of critical detail

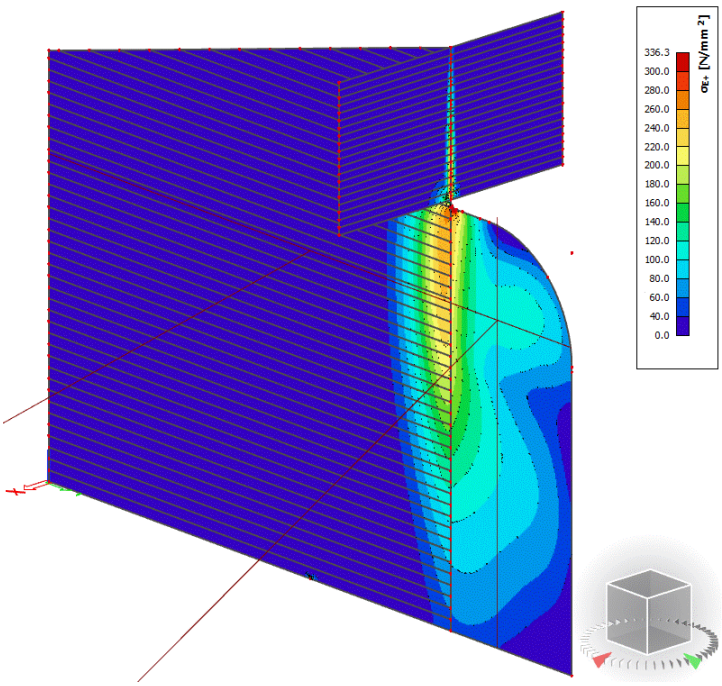

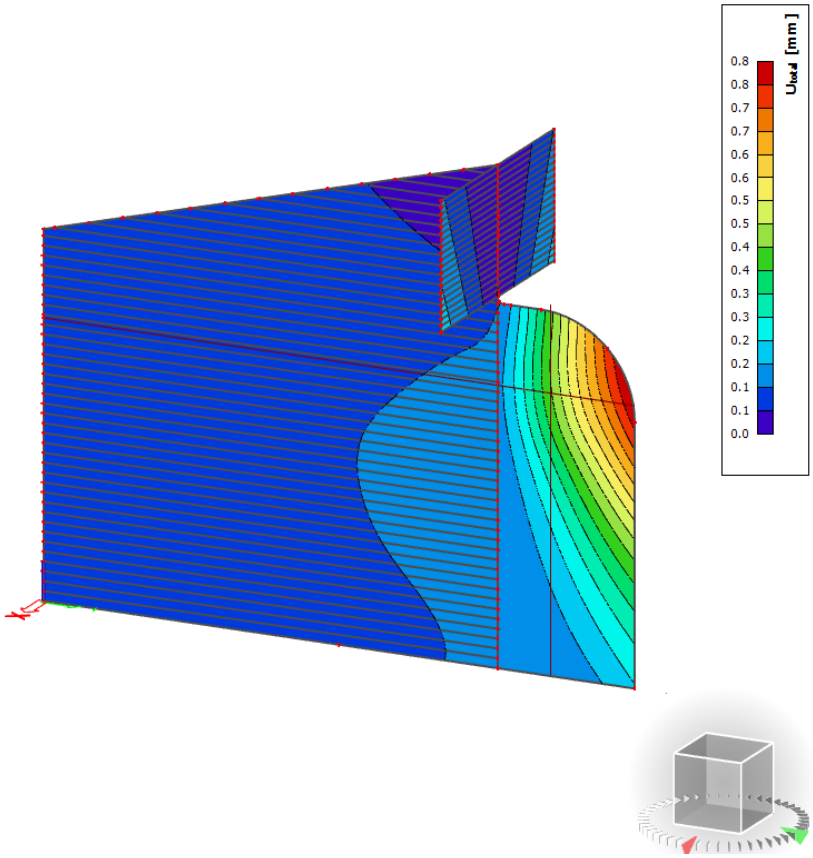

Figures 7.37a, b: Equivalent stresses in anchor plates and total displacement in plates

- The plate experiences some yielding in ULS in the corner where room is made for the cross-beam connector. The stresses in this area can be reduced with a more gradual transition.
- No yielding and much smaller displacements are observed under SLS loading.
  The SLS loads are drastically smaller than those in ULS, due to the small vertical span of the cables.
- The forces are modelled as acting 5 cm under the vertical centre of the beam.
  For the global behaviour of the structure, this would entail slightly less efficient support reactions from the compression rods, but a favourable moment acting on the main beam ends.

7.6.3 HEA 450 to Main Beam

A moment resisting connection between the compression rod (HEA 450) and the main timber beams is needed. The joint type chosen is shown in figure 7.38.

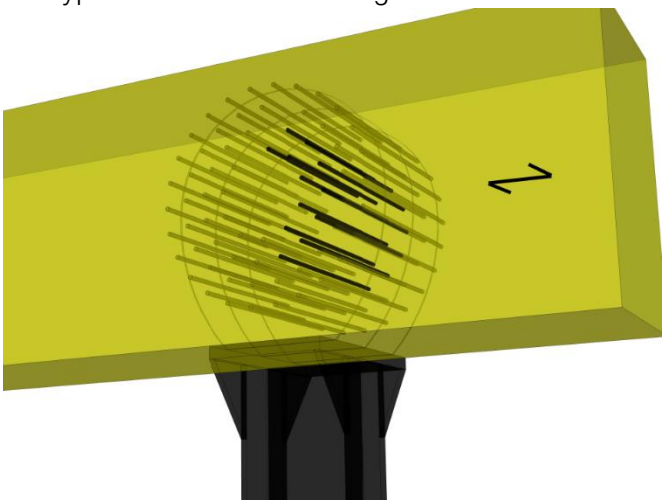

Figure 7.38: Moment resisting joint applied

Design and Modelling

- The HEA 450 compression rod has widened flanges with their top being the length of the main beam width.
- The compression rod is welded onto a 40 mm horizontal plate at the bottom of the main beam.
- Three vertical plates of a 25mm width and a centre to centre spacing of 245 mm are inserted into the main beam.
- M16, class 10.9 dowels are inserted through the width of the main beam and the vertical plates.
- The dowels are positioned in circles width diameters of 810, 650, 490, and 330 mm and are fastened at their ends, allowing for full rope effect.
- Spacings of the dowels adhere to table E14- 24 from [20].

- SCIA shell model with element size of 2 mm.
- Stiffness of dowel connection calculated according to E14 of [20].
- Moments and shear forces out of the longitudinal global plane are negligible comparing to ones in plane and are therefore not accounted for.
- It is assumed that shear forces are transferred only by the web of the HEA profile.
- Normal forces from moments are assumed to be transferred only through the HEA flanges.

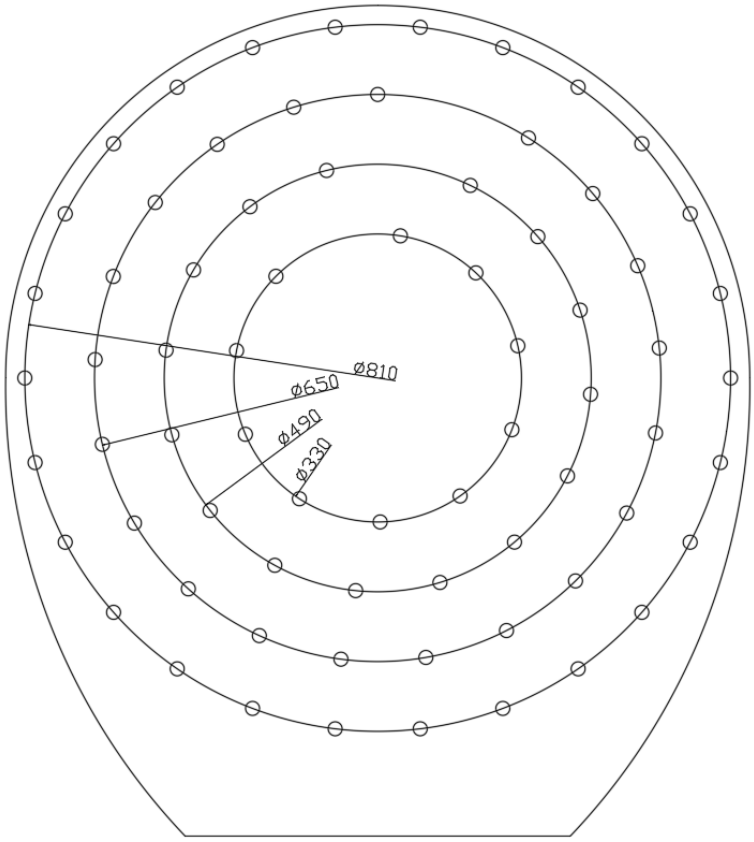

Figure 7.39: Diameters of moment resisting circles

FE Results

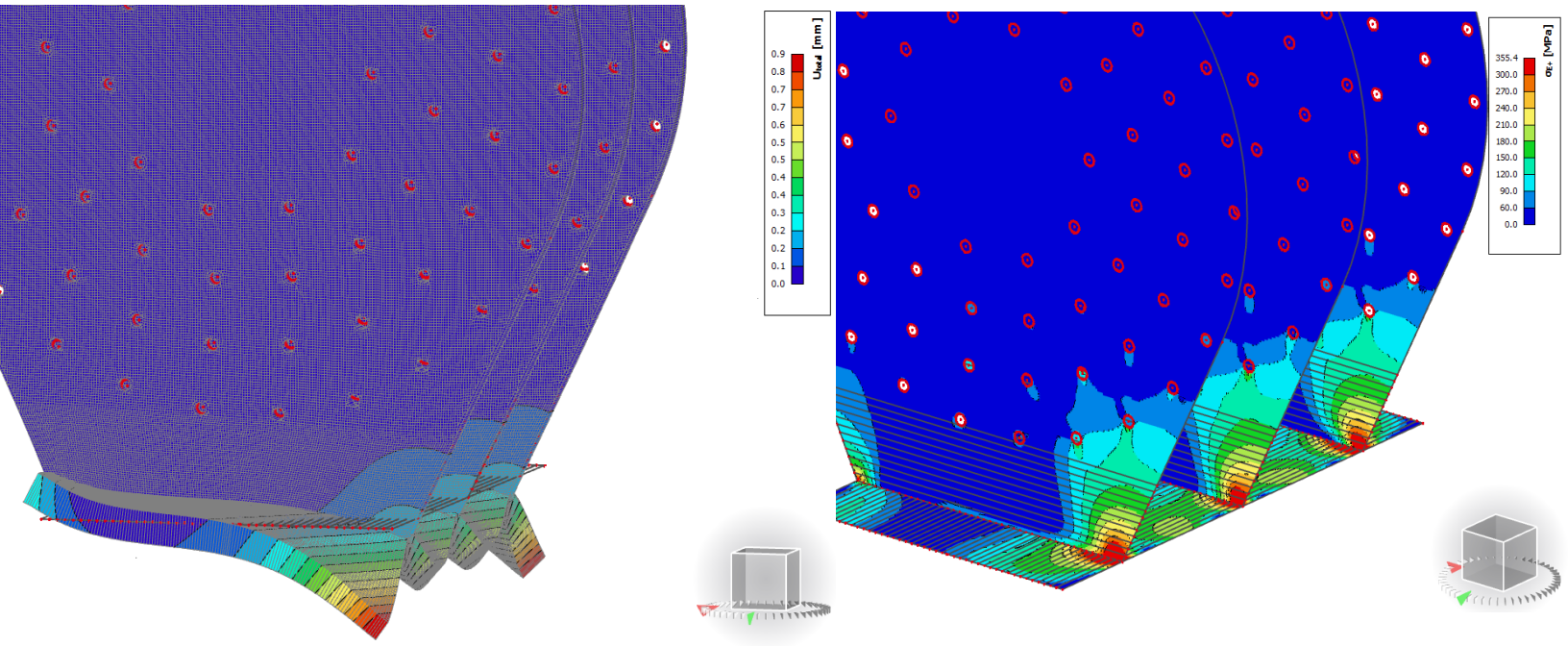

Figures 7.40a, b: Displacement and equivalent stress under ULS.

The calculation for determining the stiffness of the connection and the forces on the dowels will be worked out. The verification of the dowels is identical to the one performed within the cross- beam connections subparagraph and will not be repeated in the main text.
Results are found in table 7.8.
All equations used, including the ones for the verification of the dowels in this connection, can be found in appendix E2 in python code form.

It is assumed that all forces are transferred to the dowels in the analytical solution. In reality some of the compressive normal force, acting in the HEA profile, is transferred through the horizontal plate. The dowel verification presented is therefore a conservative one.

Dowels per circle determination

$$M = 1067{,}27\ kNm \quad V = 717{,}32\ kN \quad N = 629{,}78\ kN \quad \rho = 445\ kg/m^3$$

$$d = 16\ mm \quad R_4 = 405\ mm \quad R_3 = 325\ mm \quad R_2 = 245\ mm \quad R_1 = 165\ mm$$

$$C_4 = 2 * \pi * R_4 = 2544{,}69\ mm \quad C_3 = 2042{,}04\ mm \quad C_2 = 1539{,}38\ mm \quad C_1 = 1036{,}73\ mm$$

$$n_4 = int\left(\frac{C_4}{6 * d}\right) = 26 \quad n_3 = 21 \quad n_2 = 16 \quad n_1 = 10 \quad n = n_1 + n_2 + n_3 + n_4 = 73$$

Spring stiffness of joint

$$K_{ser} = 2 * \left(\frac{1}{23}\right) * \rho^{1{,}5} * d \quad K = \frac{2}{3} * K_{ser} = 8707\,\frac{N}{mm}$$

$$K_r = N_4 * K * (R_4^2) + N_3 * K * (R_3^2) + N_2 * K * (R_2^2) + N_1 * K * (R_1^2)$$

$$K_r = 67.178{,}57\,\frac{kNm}{rad} \quad per\ shear\ plane$$

$$K_{total} = shear\ planes * K_r = 6 * K_r = 40.3071{,}4\,\frac{kNm}{rad}$$

Normative force on dowel in outer circle

$$F_{moment} = \frac{K * R_4}{K_r} * M = 18{,}67\ kN$$

$$F_{normal+shear} = \sqrt{\left(\frac{V}{n}\right)^2 + \left(\frac{N}{n}\right)^2}$$

$$F_{total} = F_{moment} + F_{normal+shear} = 28{,}91\ kN$$

Result type	Value
Dowels in circles 4,3,2,1	26, 21, 16, 10
Stiffness per dowel per shear plane	8707,05 Nmm/rad
Rotational stiffness per shear plane	67179 kNm/rad
UC- Johansen Normative fastener	0,98
UC fastener failure	0,17

Table 7.8: Analytical results moment resisting connection

Discussion

- Some yielding occurs in both the horizontal and vertical plates of the steel part of the connection under ULS
- In SLS a single element reaches 350 MPa, while neighbouring elements remain close to, but under this value. The element has a single sharp angle, potentially leading to this value.
- High local stresses are likely to be lower in reality as more spreading of the imposed loads is expected.

- The normative failure mode for the dowels is a ductile one.
- The rotational spring is applied in the global bridge model, leading to an increased unity check for bending and normal force. This increase is marginal, resulting a unity check of 0.99 as opposed to 0.98 when the connection is assumed to be fully rigid.

7.7 Fatigue

Fatigue in wood is often assumed to be a non-issue. This is not the case.
In this paragraph a fatigue validation of the wood members will be performed according to EC5-2, annex A and subsequently be reflected on.

7.7.1 Eurocode Method Procedure

The Eurocode validation method is based on a fatigue load with a constant amplitude, simulating the full load spectrum. The procedure for applying this method and the influences incorporated are as follows:

- Determine stress range relative to material strength factor $\kappa = \frac{|\sigma_{d,max} - \sigma_{d,\min}|}{f_k/\gamma_{M,fat}}$.
- Compare factor κ with provided limits for various types of loading in EC 5-2, annex A.1.
  If the calculated factor is larger than the provided limits, a fatigue verification must be performed, otherwise member/ detail suffices fatigue validation.
  The provided factors can be seen as cut-off or endurance limits.
- Determine strength reduction factor due to fatigue κ_{fat}. This factor depends on the number of stress cycles (N_{obs}), stress range (R), lifetime (t_L), consequence due to failure (β), and factors ($a, b,$) dependent on the type of loading.
- Determine the fatigue strength $f_{fat,d} = k_{fat} * \frac{f_k}{\gamma_{M,fat}}$.
- Calculate unity check $\frac{\sigma_{d,max}}{f_{fat,d}}$.
- If the member or detail does not suffice the conditions imposed by the endurance limit or the verification equation, perform additional specific research.

7.7.2 Eurocode Method Application

In this subparagraph, the members will be validated according to the EC 5-2 method.
The results will subsequently be reflected upon.

The full validation of the main beam bottom fibers for bending/ tension is shown in the main text.
Intermediate values of the validation of the other timber members are shown in tables 8.9 and 8.10.

Stresses in the members are obtained from the global bridge model, including the spring connections between the compression rods and the main beams.

These stresses result from FLM 3 applied on the structure as shown in subparagraph 5.2.6, save for the equivalent damage factors, which are specific to steel bridges.

$$Bottom\ of\ main\ beam - Bending/Tension$$

$$Normative\ cross\ section: at\ compression\ rod\ support$$

$$\sigma_{d,max} = 5{,}9\ MPa \quad \sigma_{d,min} = -2{,}1 \quad \kappa_{limit} = 0{,}2 \quad \gamma_{M,fat} = 1 \quad \beta = 3\ (high\ consequence)$$

$$a = 9{,}5 \quad b = 1{,}1 \quad N_{obs} = 5e5 \quad t_L = 100\ years$$

$$\kappa = \frac{|\sigma_{d,max} - \sigma_{d,\min}|}{f_k/\gamma_{M,fat}} = \kappa = \frac{|5{,}9 - -2{,}1|}{26/1} \approx 0{,}31 > 0{,}2 \quad verification\ is\ necessary$$

$$R = \frac{\sigma_{d,min}}{\sigma_{d,max}} \approx= \frac{-2{,}1}{5{,}9} \approx -0{,}36$$

$$k_{fat} = 1 - \frac{1-R}{a*(b-R)}\log(\beta * N_{obs} * t_L) = 1 - \frac{1+0{,}36}{9{,}5*(1{,}1+0{,}36)}\log(3*5e5*100) \approx 0{,}20$$

$$f_{fat,d} = k_{fat} * \frac{f_k}{\gamma_{M,fat}} = 0{,}20 * \frac{26}{1} = 5{,}2$$

$$UC = \frac{\sigma_{d,max}}{f_{fat,d}} = \frac{5{,}9}{5{,}2} \approx 1{,}13$$

$Member\ and\ fibre\ location$	$Location\ normative$ $Cross\ section$	$\sigma_{d,max}, \sigma_{d,min}$ (MPa)		κ	R	k_{fat}	$f_{fat,d}\ (MPa)$	UC
$Normative\ Main\ Beam\ top\ fibre$	$Compression\ rod\ support$	$-9{,}1$	$-0{,}2$	$0{,}36$	$-0{,}02$	$0{,}21$	$5{,}62$	$1{,}63$
$Normative\ Inner\ X-beam\ bottom\ fibre$	$Mid-span$	$7{,}8$	$0{,}3$	$0{,}29$	$0{,}038$	$0{,}22$	$5{,}73$	$1{,}31$
$Normative\ Inner\ X-beam\ top\ fibre$	$Mid-span$	$-8{,}2$	$-0{,}3$	$0{,}3$	$0{,}036$	$0{,}27$	$7{,}03$	$1{,}17$
$Normative\ Outer\ X-beam\ bottom\ fibre$	$Mid-span$	$-3{,}4$	$2{,}2$	$0{,}22$	$-0{,}65$	$0{,}19$	$4{,}9$	$0{,}69$
$Normative\ Outer\ X-beam\ top\ fibre$	$Mid-span$	$-7{,}9$	$-3{,}6$	$0{,}17$	$0{,}46$	$-$	$-$	0^*

*Table 7.9: Fatigue results of members due to bending, *κ under endurance limit*

The fatigue calculation regarding shear capacity is performed in the same fashion as the one for bending/ tension, save for the constants, and is therefore not shown.

The differing constants used for the validation are as follows:

$$\kappa_{limit} = 0{,}2 \quad a = 6{,}7 \quad b = 1{,}3$$

$Member$	$Location\ normative$ $Cross\ section$	$\tau_{d,max}, \tau_{d,min}$ (MPa)		κ	R	k_{fat}	$f_{fat,d}\ (MPa)$	UC
$Normative\ Main\ Beam$	$Compression\ rod\ support$	$1{,}4$	$0{,}4$	$0{,}28$	$0{,}28$	$0{,}14$	$0{,}49$	$2{,}84$
$Normative\ Inner\ X-beam$	$Support$	$1{,}47$	$0{,}04$	$0{,}41$	$0{,}027$	$-0{,}05$	$-$	∞
$Normative\ Outer\ X-beam$	$Support$	$0{,}53$	$0{,}0278$	$0{,}14$	$0{,}52$	$-$	$-$	0^*

*Table 7.10: Fatigue results of members due shear force. *κ under endurance limit*

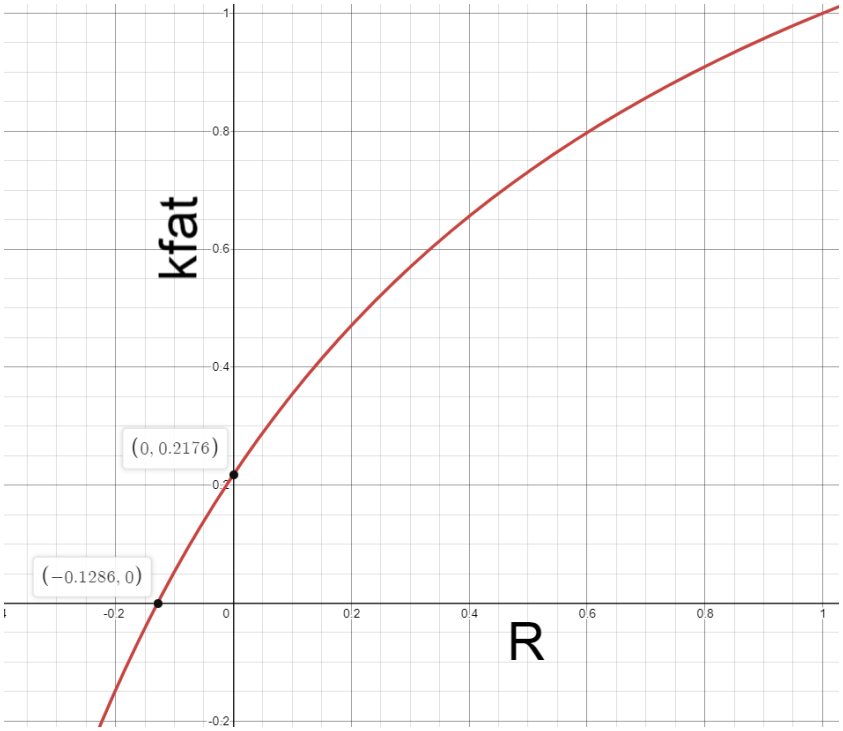

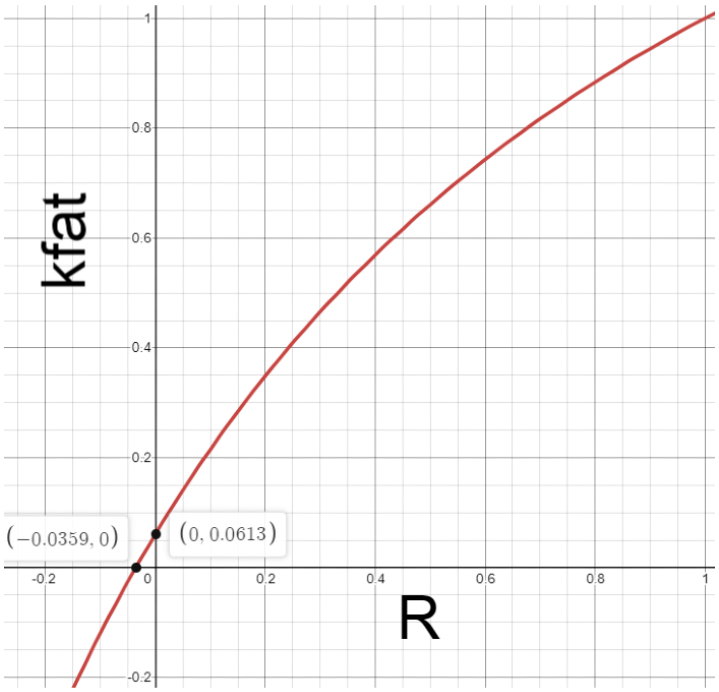

Figures 7.41a, b: Fatigue reduction factor (k_{fat}) vs stress ratio for bending/ tension (a) and shear (b)

7.7.3 Discussion

Duration of Loading and Environmental Influences

The Eurocode method only partially incorporate the duration under loading. This is done in the simplified verification.
The endurance limits (κ), used in the validation, do not account for the duration of loading in any way.

This is counterintuitive, as the effect of duration under loading is taken into account in strength calculations with the k_{mod} factor. It is also with disagreement with Clorius, et al. [43],[47].

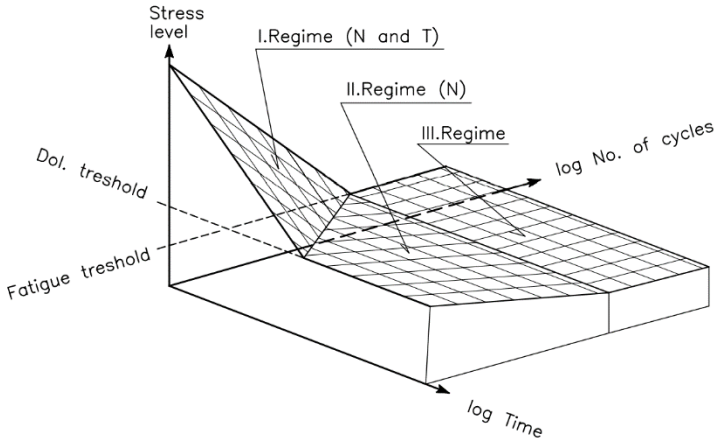

Figure 7.42: Stress cycles vs time under loading failure criterium, from [43, p.4]

The k_{mod} factor also accounts for the influence humidity plays on the mechanical properties of timber in strength validations. Environmental influences aren't considered in the fatigue validation of timber members and details, while relative humidity is shown to be of influence in [43].

Glulam vs Solid Timber

The EC 5-2 method does not differentiate between glued laminated- and solid timber members. Naturally, no distinction is made between different adhesive types, used in the production of glulam.

Bachtiar, et al. [55] tested glued lap joints with different adhesives under high- and low cycle fatigue. It was found that more ductile adhesives, dissipating more energy, provided better high cycle fatigue resistance. The opposite was found true for low cycle fatigue.

Clarc, et al. [68] found that for mode II fracture, more brittle adhesives performed better under fatigue loading, when a crack was present.

Obtained Results for Bridge Members

As previously stated, the outer cross beams are oversized for SLS.
Evidently, their large size allows them to resist the fatigue loading sufficiently to obtain a lifetime of 100 years.

The other members do not suffice. Optimizations of these elements would necessitate radical design changes necessitating larger cross sections to be used.
With regards to the main beams specifically, an increased depth would increase the beam moment capacity and thus reduce stresses in that way. Due to the limited construction depth however, this would also decrease the efficiency of the cable system, reducing the support reactions in mid span and thus increasing the acting moments.
Due to the limited construction depth, it is likely the cable system would offer little to no benefits with an increased main beam height.

Renewed EC 5-2 Draft

The EC 5-2 draft, from 2021-04-06 does away with the endurance limits (κ) and specifies conditions for which a fatigue verification for bridges and/or bridge members may be omitted. These conditions are not applicable to the bridge designed in this thesis.

The simplified fatigue verification provided in the EC 5-2 draft provides the strength reduction factors (k_{fat}) for a limited number of loading types. Its calculation, incorporating the number of stress cycles like in the current EC 5-2, is no longer necessary.

Instead, the verification method is only applicable to $2 * 10^6$ stress cycles per lane per year and a design lifetime of 100 years or less. A maximum of two lanes is also set for the bridge.

The fatigue verification is therefore not applicable to the bridge designed in this thesis. Furthermore, due to the assumptions of a higher number of stress cycles than applicable in the case study, the reduction factors provided are stricter than the ones obtained in subparagraph 7.7.2.

In its current form, the new EC 5-2 draft imposes more stringent requirements in the fatigue verification regarding the bridges, requiring research specific to the member or detail concerned.

8 Bridge Comparison and Reflection

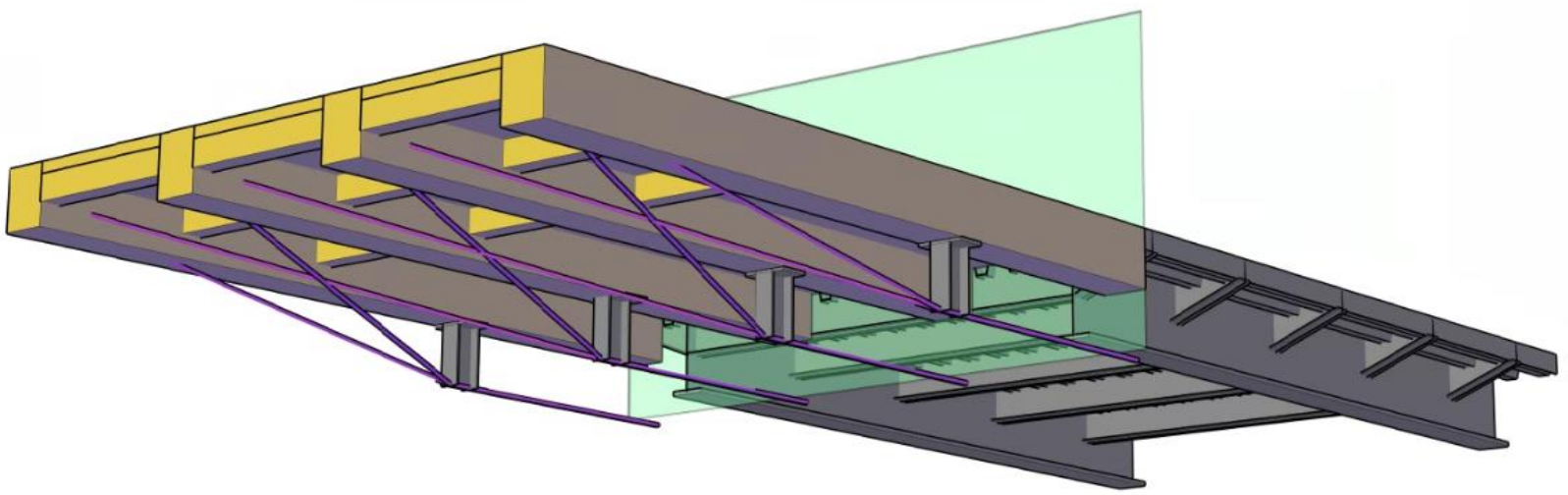

Figure 8.1: Timber and steel bridges to be compared

In this chapter, the designs resulting from the previous sections are compared.
Durability and environmental impact are quantified within a limited scope.
This is followed by introducing alternatives for the timber bridge, which do away with the relatively stringent boundary condition of a shallow construction depth.
A single design, replacing the cable system with hybrid steel- timber main beams is produced in addition.
Afterwards, the obtained results are discussed.

8.1 Durability

The durability of the bridges will be analysed in this paragraph.

8.1.1 Durability of Steel Bridge

The steel bridge variant is classified in category C3 as per ISO 12944-2 as stated in paragraph 3.1. Table C.3 of ISO 12944-5 provides various paint systems with their respective durability various from low to very high. These consist of different primers, binders, number of coats and thickness of the film.

Paint system C3.09 from ISO 12944-5 is chosen. From reference projects at IV- Infra, a repainting increment of 15 years is assumed. This results the bridge needing repainting 6 times over its lifetime of 100 years.

8.1.2 Timber Durability Metrics

Wood, as a natural material, is sensitive to organic degradation. Variability of the material per species and within species makes it comparatively more difficult to predict the durability performance of timber members. Nevertheless, there is a multitude of methods to do so.

A comprehensive overview and comparison of some of these methods can be found in van de Loo [58].

In his thesis, van de Loo compares the Timber Service Life Design Guide [59], used in Australia, with the RISE [9] guidelines, originating from Sweden as a part of the Durable Timber Bridges project. This is done using real life examples.
Both methods are found to have good accuracy with regards to predicting the service life of timber bridges.

The RISE guidelines separate the exposure and resistance. These are respectively based on the climate and wood species, including the potential preservative treatment. These guidelines are based on the Meyer-Veltrup model [62].
The exposure doses for the Netherlands, published in [9], were confirmed by van de Loo [58]. Factors, taking account of the local climate, detailing and severity category, are also included in the design value for the exposure. These factors are based on case studies performed within the DuraTB research programme. The results obtained in these case studies can be found in [9].

To obtain the relationship between exposure and resistance, tests according to EN 252 were run.

Isaksson, et al. [60] report the findings of these tests for Scots pine sapwood and Douglas fir heartwood. These tests were run for 4 to 8 years and at 24 different locations in Europe.
High degrees of determination between the modelled relationship and the field tests were obtained for both species. Some outliers were situated in Southern European countries, where brown rot was prevalent throughout the samples.

A paper published by Humar, et al. [61] further corroborates the accuracy of the exposure doses provided in the RISE guidelines [9].

In a more recent study, Brischke, et al. [63] state, in the state of art, that the model has been validated for other wood species and treatments in various studies, including Humar, et al. [61].

Expansion of the model with additional species and treatments is presented in [63]. It was found that the model achieved greater accuracy for untreated wood. This is due to the additional variability in the influences of the treatments, i.e., concentration of the preservative, treatment intensity, etc.

The model is generally considered somewhat conservative; a timber element is considered to have failed upon the onset of decay. It must therefore be stressed that when lifetime prediction is discussed in the following subparagraphs, the onset of decay is concerned and not necessarily a failure of an element.

Furthermore, the case studies, which the factors are based on, have a low strength of evidence with regards to details with a high predicted lifetime.

While multiple methods, with a reasonably accuracy, are available, the Swedish factor method (RISE) is chosen as the timber durability metric to be used.

8.1.3 Lifetime Prediction Timber Bridge Details

In this subparagraph the RISE guidelines [9] are applied on the bridge elements and their lifetime is predicted.

- The Douglas fir material resistance, D_{Rd} is equal to 1716 days.
- Exposure dose for the Netherlands D_{E0} of 40 to 46 days; 43 days is assumed.
- Severity class of bridge is high, γ_d is equal to 1

The values of the various factors and the predicted lifetime of bridge elements expected to be critical are shown in table 8.1, while the calculation process is shown in appendix G for the main beam to HEA connection.

$Detail$	$Local\ exposure\ conditions\ factor\ k_{E1}$	$Degree\ of\ sheltering\ factor\ k_{E2}$	$Distance\ from\ ground\ factor\ k_{E3}$	$Effect\ of\ detail\ design\ factor\ k_{E4}$	$Predicted\ lifetime\ in\ years$
$Outer\ main\ beam\ to\ HEA$	1	1	1	1,25	32
$Main\ beam\ to\ abutment$	1	1		1,5	26,6
$Cross\ beam\ connector,\ plate\ against\ main\ beam$	0,9	0,8	1	1,25	44,3
$Cross\ beam\ connector,\ plate\ supporting\ cross\ beam$	0,9	0,8	1	1,25/ 1,5	44,3/ 37
$Timber\ deck\ to\ cross\ beams$	0,9	0,8	1	1,25/ 1,5	44,3/ 37

Table 8.1: Exposure factors and predicted lifetime of timber bridge elements

Discussion Timber Lifetime

- It can be argued that the factors presented in the RISE guidelines do not sufficiently encompass the full bridge design. If the bridge is well protected and no water can possibly get to the elements, a higher durability may be possible regardless of the amount of rain. This especially relates to factors k_{E1} k_{E2}, which depend on the exposure to rain. Factor k_{E4} also does not provide a detail design class where a detail is exposed to no water.
- The effect of rainfall is overrepresented. If the bridge elements considered would be placed in Porto, where more rainfall and a lower relative humidity are present compared to Leiden, the elements would have a substantially lower lifetime prediction. This is illogical as the rain has little to no effect on the bridge details as they are fully sheltered.
- Preventing water ingress with a fitting varnish can increase the lifetime of an element. Painting however, is not accounted for in the RISE guidelines.

- The predicted lifetimes for details situated fully under the deck with complete coverage and thus no rain exposure have a higher lifetime than the outer main beams, which are exposed to rain.
- The durability of the bridge can be improved by protecting the outer main beams from direct rain with rain covers.

- The fact that high durability can be obtained for details protected from direct rainfall is evident from historic timber bridges, which are still standing today.
  The Rheinbrücke on the German- Swiss border dates from 1700 in its current form.
  It is known that one of its spans was rebuilt in 1926-27 [71].
  The chapel bridge in Lucerne, Switzerland had been around since 1333 until burned down in 1993. It was rebuilt in 1994 and is still standing today [8].

8.2 Environmental Cost Indicator

In this paragraph the eco- costs of the bridge variants are calculated within the scope as defined in paragraph 2.5.1.

8.2.1 Steel Bridge

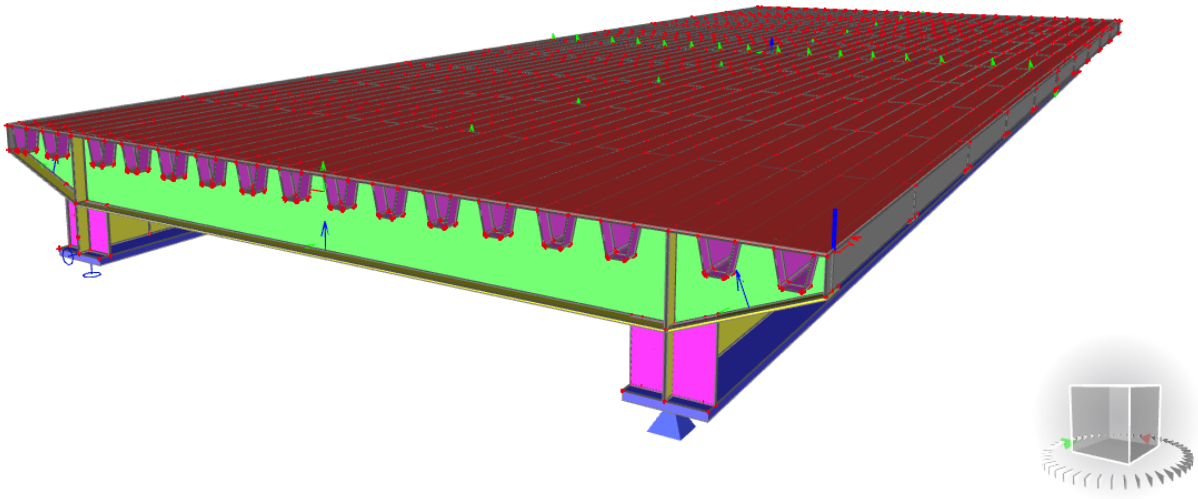

Figure 8.2: Steel Bridge Design

The values for the different materials used throughout the lifetime of the steel bridge, along with motivation behind them, is shown in table 9.2. More detail

Material	*Amount*	*Cost Indicator* (€)	*Motivation*
$S355\ Steel\ (FE470)$	$117e3\ kg$	23.400	$21\%\ secondary\ steel\ (average\ trade\ mix\ in\ the\ Netherlands)$ [48]
$MAG\ Weld$	$1.556{,}2\ m$	242,78	$Fillet\ welds\ between\ all\ connected\ elements.\ Two\ sided\ fillet\ welds\ everywhere\ besides\ trough\ to\ deck\ connection.\ One\ sided\ fillet\ welds\ there.\ Throat\ thickness\ of\ 6{,}3\ mm\ is\ assumed\ for\ all\ welds\ as\ that\ is\ slightly\ above\ the\ minimum\ recommended\ throat\ size\ for\ 12\ to\ 20\ mm\ thick\ elements.$ [64]. $Eco-costs\ based\ on\ consumption\ of\ GMAW\ solid\ wire\ electrode\ in\ \frac{kg}{m},\ which\ follows\ from$ [65].
$Paint\ System\ C3.09\ Primer$	$6.736{,}8\ m^2$	7.612,6	$60\ to\ 80\ \mu m\ thick\ zinc\ primer$
$Paint\ System\ C3.09\ Solvent\ based\ paint$	$3{,}26\ kg$	4.920	$Film\ thickness\ from\ ISO\ 12944-5\ Paint\ density\ from$ [69]

Table 8.2: Eco- costs of Steel Bridge Variant per Material/ Treatment

The total eco- costs of the steel bridge are € 36.175,4.

8.2.2 Timber Bridge

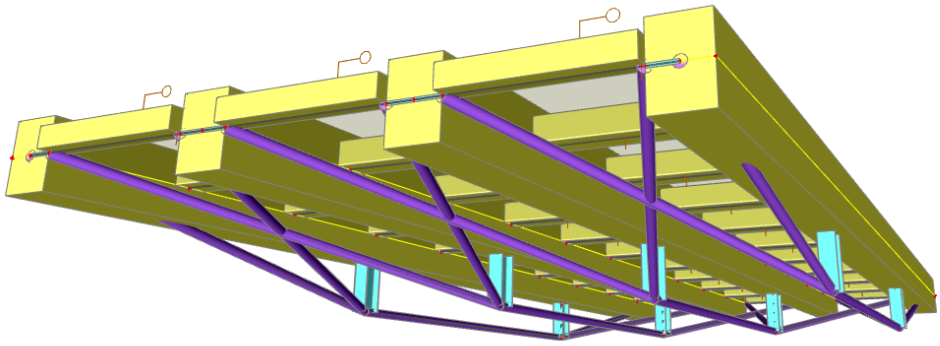

Figure 8.3: Timber Bridge Design

Material or Treatment	Amount	Cost Indicator (€)	Motivation
FSC, PEFC Larch	54 tons	2.036,4	IDEMAT does not contain values for Douglas fir. Other wood types from European FSC, PEFC forests are availible and have similar or identical eco – costs. The most similar species is European larch.
Melamine Formaldehyde Resin	2080,3 kg	1539,4	MF Resin with a thickness of 0,5 mm is used to produce the glulam members.
S250 Steel (FE360)	3987 kg	797,4	Used for connector brackets.
Hot dip Zinc Galvanization	35,43 m^2	60,6	Coating of the brackets.
S355 Steel (FE470)	8672,1 kg	1734,4	Used in Steel plates in abutments, HEA 450 profile, and HEA to Main Beam connectors.
42CrMo4 Steel	1244,8 kg	336,1	Used in all fasteners. Conservative assumption that all fasteners have chemical composition leading to class 10.9. Composition from [66].
55CrV4 Steel	32,8 tons	13.450,6	Composition used to produce steel for cables of class 1370 [12, p. 86], [67].

Table 8.3: ECI values of Timber Bridge per Material/ Treatment

The eco- cost of the welding needed for the bridge connectors is negligible and has therefore been disregarded.

The total eco- costs of the timber bridge are € 19.954,9.
The predicted lifetime of the main beams is 26,6 years, as per subparagraph 8.1.3.
If the entire bridge superstructure, save for the support cables, were to be replaced 3 times, in order to reach a design lifetime of 106 years, the total eco- costs would reach € 45.972,1.
The cable system is not accounted for as locked coil cables have an inherent high durability and are assumed to last the entire service life.

8.3 Potential alternatives

The timber bridge alternatives are mostly limited by the imposed boundary conditions.
The cable system used in this case study is novel and can offer a reasonable improvement to a multi girder bridge.

Three alternative designs, not adhering to the set construction depth limit are presented in this subparagraph.
Hybrid timber- steel girders are considered as well. With this alternative, the interface between the timber and steel is assumed as infinitely stiff and no difference in expansion behavior is considered.

These alternative designs are not analyzed in detail, but regardless present a more efficient use of the materials.

Internal force envelopes of a main beam in these designs, resulting from ULS loading, can be found in appendix H, along with envelopes from the original timber bridge design.

8.3.1 Higher Construction Depth

The only change made to the design is the increase of the length of the HEA compression members by 3 meters, including matching cable length and orientation.

No verifications are performed; this quick conceptual analysis serves only to demonstrate the benefits of a larger construction depth.
It must be noted that due to their considerably larger length, the HEA profiles will need to be laterally supported by additional stability members.
The internal forces of the outer main beam from the design with an increased depth will be compared to those of the outer main beam from the original final timber bridge design.

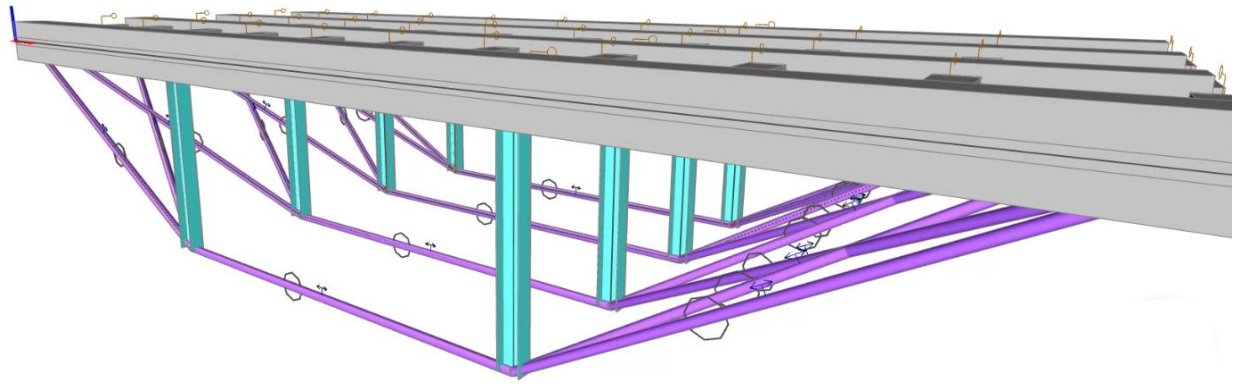

Figure 8.4 Extended compression members

The results are as can be expected:

- The hogging bending moment is notably bigger, while the sagging bending moment is smaller in the larger depth model.
- The shear force distributions of both designs are relatively similar.
- The normal forces in the larger depth design are drastically smaller than the ones in the smaller depth design.

This demonstrates the added efficiency of a larger construction depth.

8.3.2 Hinged Connections of Compression Profiles

The connections between the HEA profiles and the main beams are designed as moment resisting. Producing the connections as hinged increases the sagging bending moment and induces a slight increase of the normal force in the ends of the main beams.

This is in line with what is expected:

- The main beam bends downwards under traffic loading.
- Due to the stiff connection between itself and the HEA profile, the compression rod is subjected to an imposed rotation following from the rotation of the main beam.
- This rotation results in extra extension and thus tensile force in the cable between the two HEA profiles.
- This extra tension results in a shear force in the HEA profiles, which transfers to the main beam as a normal force. The extra tension force naturally also results in an additional moment transferred to the main beam. This moment counteracts the maximum sagging bending moment in the main beam. This principle is shown in figures 9.6a and b.

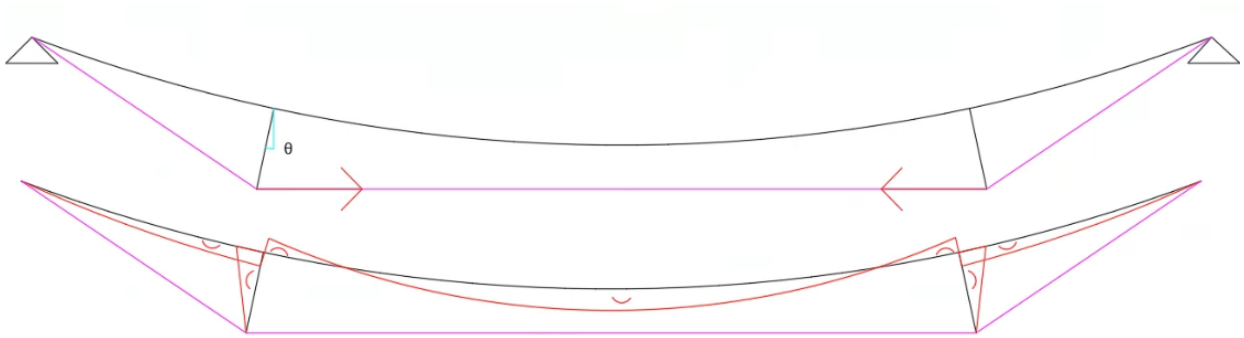

Figures 8.5a, b: Additional tensile force in horizontal cable due to rotation of compression rods (a), Principal moment distribution in longitudinal direction(b)

Any and all rotation of the HEA profile, as shown in figures 8.5a, b, in the design with hinged connections, is due to the cable forces on either side of the HEA profile pulling on it. Naturally no moment is transferred to the main beam with that design.

The increase in internal forces is not drastic when the hinged connections are applied.
However, it must be noted that the critical main beam, in the design with moment resistant connections, is close to failure with a unity check of 0,99.
It is likely that the slight increase in forces would result in a unity check higher than 1.
This would necessitate the implementation of a larger cross section. If the height of this cross section is increased, the angle of the cable connection would decrease due to the construction depth limit of 2 meters.
This would make the system less efficient and result in a higher normal force applied at the beam ends.

Furthermore, it is likely that a saddle clamp would not be necessary due to more balanced forces in the inclined and horizontal parts of the cable.

8.3.3 Higher Construction Depth and Hinged Connections

Applying a higher construction depth alongside hinged connections between the HEA profiles and the main beams allows for an efficient use of the cables as well as the implementation of a cheaper and less involved execution with regards to connections.

As expected, the internal forces in the main beams are reduced to a value slightly lower than that of the high depth bridge version with moment resistant connections.

As previously stated, the high steel compression rods would require additional stabilization in the transverse bridge direction to prevent buckling.

8.3.4 Timber- Steel Hybrid Main Beams

The main timber beams, with dimensions identical to the ones in the final timber bridge design are combined with a standard HEB 800 profile, made from S355. The interface between the timber and steel is assumed as infinitely stiff. A quick analysis is performed, considering only the stress distributions over the beam length, no buckling phenomena are considered.

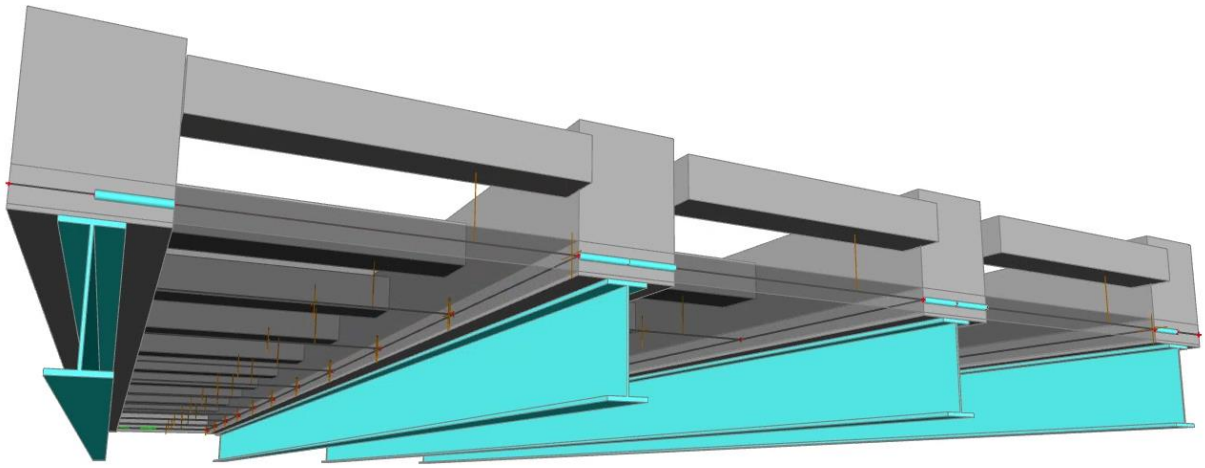

Figure 8.6a: Timber- steel hybrid main beam bridge version.

The normative stresses are normal stresses due to bending and occur at mid span. The discussed stress distribution is shown in appendix H, the bill of material for the main beams can also been found there.

A lower material use is obtained with the use of hybrid main beams when compared to the application of the cable system as described in chapter 7.
It must be noted that no fasteners or a glue line, at the timber to steel interface, are accounted for in the bill of material.

8.4 Discussion

The results obtained from this and previous chapters are to be discussed in this subparagraph per topic. From this discussion, a conclusion to the research questions will be drawn.

Bridge systems

The steel girder bridge is a widely applied solution; construction manuals and codes cover such bridges sufficiently to allow designers to create a safe design.
The dimensions of the steel bridge design produced in this thesis are based on fatigue requirements, which are often normative for such structures.

Multiple timber bridge systems were considered. A system which (partially) decouples the expansion behaviours of the timber and steel was chosen for further development to limit the scope of the study.

Elaborate anchoring of the steel cable system to the timber elements is required for this bridge. This will potentially raise the price of the timber bridge beyond an economically sensible limit.
The system proposed in this thesis would be more fitting in a landscape where rock deposits are present in the soil and larger construction depths are available.
The rocks would allow for anchoring of the steel cables and the larger construction depths would allow for a more efficient force distribution by the cables as demonstrated.
The more efficient force distribution would also permit the use of considerably cross sections.

Hybrid timber beams offer a well suited alternative when construction depth is limited, as in this thesis. The interface between the steel and timber, however, must be investigated.
A balance between stiffness, to resist creep, and ductility, to accommodate the distinct expansion behaviors of the materials.

Durability

The durability of the steel bridge variant, with regards to corrosion, is considered with an approximation of repainting frequency used in tenders at IV- Infra.
It is expected that this bridge will reach its desired lifetime.

Douglas fir is a relatively durable timber species, as detailed in paragraph 2.2. The expected lifetime of timber details, as shown in subparagraph 9.1.3, do not exceed 50 years.
As previously stated, the RISE guidelines [9] predict the time until the onset of decay and do not consider protection by varnishing.
Details of the bridge can be improved by physical protection, but a predicted lifetime of over 50 years is not reasonable within the prescribed RISE limitations.
The accuracy of the RISE predictions regarding this specific bridge is debatable, as the bridge is located under the deck and is therefore covered from rain.

Fatigue

As touched upon, design codes thoroughly cover the design of steel structures. This holds true for fatigue design. All relevant details of the bridge are directly verified with fatigue detail categories, as provided in EC 3-1-9 and the Dutch NA to EC 3-2.

EC 5-2 imposes vast limitations to the fatigue of timber bridge elements and details.
Adapting the bridge design, by changing the member sizes to ones with sufficient fatigue resistance, would entail drastic increases in cross section dimensions.
Employing the use of the cable system, from this thesis, would become unsensible due to the limited construction depth.

Erection

The steel bridge has a relatively high weight compared to the timber variant, necessitating the use of heavier machinery for its installation.

The assembly of the timber bridge is relatively straightforward. The various elements can be placed and connected with fasteners relatively quickly. Only little welding is necessary for the details.
The detailing of the cable system can prove to be a substantial problem that needs to be overcome.

Environmental impact

The material use in the steel bridge design constitutes the highest part of the structure's environmental impact. As the industry transitions to more recycled steel, its toll on the environment is expected to decrease.

The high strength steel in the cable system of the timber bridge accounts for a large percentage of the bridge's eco- costs.
Two values are given for the total eco- costs of the timber bridge:
One for a single application of all the elements and one for replacing the entire superstructure three times due to durability limitations.

It is likely the RISE guidelines do not fully encompass the bridge, as designed in this thesis. Therefore, replacement of the members, with the stipulated frequency, is unreasonable and so are the eco- costs associated with this replacement.

9 Conclusion and Recommendations

This thesis has focused on the comparison between steel and timber- steel hybrid bridges, by way of a case study with a scope limited by a set of boundary conditions:

- The bridge is a part of a trunk road, entailing 0,5 million heavy vehicles per year.
- The span has been limited to 25 meters; a common length for this type of bridge.
- The width has been set to 10 meters, encompassing 3 theoretical traffic lanes.
- The construction depth of the superstructure has been limited to 2 meters to accommodate waterway traffic and connecting road inclination.

Based on the case study performed the research questions can be answered and recommendations for future research and the application of timber in roadway bridges can be made.

9.1 Conclusion

What are the specific limitations and challenges of timber when compared to steel?

- The fatigue resistance is a hurdle with regards to both timber and steel.
  The implications when it comes to timber members are more dire than when it comes to steel.
  With steel, a slight increase in plate thickness can notably increase fatigue resistance and not affect other dimensions in a significant way.
  Timber member sizes for heavy traffic bridges are orders of magnitude larger than those of steel bridges in terms of volume. If dimensions are increased, to comply with fatigue requirements, substantial changes in design may be necessary. This is discussed in subparagraph 7.3.3 in the context of the case study.

- The durability of timber members in bridges and the prediction thereof are limiting factors.
  Detailing is of grave importance; this is evident from the variation in predicted lifetime of the different details of the timber bridge.
  Deterioration of steel on the other hand is a topic within which there is ample experience in the field. Paint systems, as specified in ISO norms, are widely applied and lifetime predictions following from these paint systems are generally uncontested.

What is the cause of these limitations?

- Stringent limits are imposed on cyclically loaded timber members and details.
  A number of variables are not directly accounted for in the EC 5-2 validation and it therefore needs to be relatively conservative.
  The effects of duration of loading are only taken into account partially.
  No difference is made between solid wood and glulam. Naturally, the effect of the adhesive type is also not taken into account.

- Timber, as a natural material, is inherently sensitive to organic degradation.
  Degradation of steel occurs in the form of oxidisation.
  Both materials tend to experience accelerated deterioration in relatively wetter environments.
  While the RISE guidelines, which quantify the durability of timber details in bridges, are held in high regard, they do not cover all design situations.
  In the case of the bridge, designed in this thesis, no rain can reach the timber members and details between the main beams. This is not fully reflected in the RISE guidelines and the prediction can therefore be overly conservative.

What incentives are there for the use of timber in bridges as opposed to steel?

- Timber elements are often lighter than steel ones and are therefore require less heavy machinery to be used during assembly.
  The use of fasteners in the connections also allows for the bridge to be assembled on site. This eases transportation as members can be delivered separately.

- A lower environmental impact can be achieved.
  The wood and adhesive used in this case study represent a relatively small part of the total timber bridge.
  For bridges with small amounts of heavy traffic and thus fewer fatigue stress cycles, wooden elements would benefit the environmental impact of the structure.
  When relying on current norms, this is especially true for bridges where a comparatively shorter service life is required, depending on the detailing, protection, and accuracy of the durability estimation method.

What design aspects are of relevance, when designing a bridge with timber?

Design Aspect	(Partial) Causes	Relation to case study
Construction depth	Follows from the area where the bridge is to be applied	A steel bridge with the stipulated span and construction depth can be designed in an efficient fashion. This is not the case with the timber version of the bridge; a larger construction depth would greatly increase the efficiency of the design. Such a design should be therefore be applied when fitting boundary conditions are present.
Fatigue Resistance	Many variables accounted for in too few factors, some variables not represented at all	S-N curves and guidance, along with detail classes allow for extensive design of steel bridges. Timber fatigue is related to more than stress cycles and their magnitude. This is not fully covered in design norms. In order to produce a bridge compliant with the Eurocode, members should be subjected to favorable loading types, be oversized for ULS/ SLS loading, and ideally be subjected to a relatively low amount of heavy traffic.
Insufficient Durability	Inherent to material variability, lack of knowledge/ insufficient guidance.	Steel has been widely applied in heavy traffic bridges. Guidance and experience regarding its durability are more widespread than that of timber and its degradation is normalized. Although there are old timber structures, with bridges among them, still standing, quantifying wood degradation is more challenging than steel. Naturally, timber elements should be kept as dry as possible, which is reflected in guides and norms.

Table 9.1: Identified Design aspect

9.2 Recommendations

- Perform research into the influences of timber fatigue. Consider whether environmental effects and the effects of the presence of glue/ type of glue need to be accounted for fatigue validations. This can be done similarly to the k_{mod} factor.

- Perform research into timber durability in outside use. Producing accurate quantitative results with regards to timber member durability is needed for more application cases. The effects of painting on preservation must also be included.

- Perform research into timber- steel hybrid members in outside use. Expansion differences between the materials must not result in failure at the interface, but this interface must allow for sufficient cooperation between the timber and steel. A balance between the two must be sought.

References

1. Blaß, H. J., & Sandhaas, C. (2017). Timber Engineering – Principles for Design. KIT Scientific Publishing.

2. Riola-Parada, F. (2016, December). Timber-Steel Hybrid Beams for Multi-Storey Buildings. https://www.researchgate.net/publication/331355241_Timber-Steel_Hybrid_Beams_for_Multi-Storey_Buildings

3. van Aken, B. (2017, June). Hollow core cross-laminated timber. http://resolver.tudelft.nl/uuid:601f038b-d231-47e9-85a4-8d7eba44acd1

4. Kliger, R., Al-Emrani, M., Johansson, M., & Crocetti, R. (2008, January). Strengthening timber with CFRP or steel plates - Short and long-term performance. Researchgate. https://www.researchgate.net/publication/287575564_Strengthening_timber_with_CFRP_or_steel_plates_-_Short_and_long-term_performance

5. Dietsch, P., & Brandner, R. (2015). Self-tapping screws and threaded rods as reinforcement for structural timber elements – A state-of-the-art report. Construction and Building Materials, 97, 78–89. https://doi.org/10.1016/j.conbuildmat.2015.04.028

6. Steiger, R., Serrano, E., Stepinac, M., Rajčić, V., O'Neill, C., McPolin, D., & Widmann, R. (2015). Strengthening of timber structures with glued-in rods. Construction and Building Materials, 97, 90–105. https://doi.org/10.1016/j.conbuildmat.2015.03.097

7. Dietsch, P. (2017). Effect of reinforcement on shrinkage stresses in timber members. Construction and Building Materials, 150, 903–915. https://doi.org/10.1016/j.conbuildmat.2017.06.033

8. Setra: Service d'études sur les transports, les routes et leurs aménagements. (2007). Timber Bridges - How to ensure their durability (Revised 2014). https://www.cerema.fr/fr/centre-ressources/boutique/technical-guide-timber-bridges-how-ensure-their-durability

9. RISE, Pousette, A., & Malo, K. A. (2017). Durable Timber Bridges Final Report and Guidelines. http://www.diva-portal.org/smash/record.jsf?pid=diva2%3A1116787&dswid=8802

10. Kropf, F. W. (1996). Durability and detail design - the result of 15 years of systematic improvements. National conference on wood transportation structures. https://trid.trb.org/view/482240

11. Pipinato, A. (2015). Innovative Bridge Design Handbook: Construction, Rehabilitation and Maintenance (1st ed.). Butterworth-Heinemann.

12. Gimsing, N. J., & Georgakis, C. T. (2012). Cable Supported Bridges: Concept and Design (3rd ed.). Wiley.

13. Takena, K., Sasaki, M., Hata, K., & Hasegawa, K. (1992). Slip Behavior of Cable Against Saddle in Suspension Bridges. Journal of Structural Engineering, 118(2), 377–391. https://doi.org/10.1061/(asce)0733-9445(1992)118:2(377)

14. Hobbacher, A. F. (2008). Recommendations for Fatigue Design of Welded Joints and Components. Springer Publishing.

15. Rijkswaterstaat. (2017, April). Richtlijn Ontwerp Kunstwerken (1.4). RWS GPO.

16. Bastin, J. F., Finegold, Y., Garcia, C., Mollicone, D., Rezende, M., Routh, D., Zohner, C. M., & Crowther, T. W. (2019). The global tree restoration potential. Science, 365(6448), 76–79. https://doi.org/10.1126/science.aax0848

17. Nabuurs, G. J., Lindner, M., Verkerk, P. J., Gunia, K., Deda, P., Michalak, R., & Grassi, G. (2013). First signs of carbon sink saturation in European forest biomass. Nature Climate Change, 3(9), 792–796. https://doi.org/10.1038/nclimate1853

18. European Forest Institute. (2014). Future of the European Forest-Based Sector: Structural Changes Towards Bioeconomy.

19. Gustavsson, L., Haus, S., Lundblad, M., Lundström, A., Ortiz, C. A., Sathre, R., Truong, N. L., & Wikberg, P. E. (2017). Climate change effects of forestry and substitution of carbon-intensive materials and fossil fuels. Renewable and Sustainable Energy Reviews, 67, 612–624. https://doi.org/10.1016/j.rser.2016.09.056

20. Blaß, H. J., & Sandhaas, C. (2017). Timber Engineering – Principles for Design. KIT Scientific Publishing

21. Bois, C. & CEI Bois. (2006). Tackle Climate Change. European parliament.

22. Pieter Smitbrug - de langste fietsbrug van Europa. (2021, March 22). Hout in de GWW. https://www.houtindegww.nl/project/de-blauwe-loper/

23. Harrington, J. J. (2002, September). Hierarchical modelling of softwood hygro-elastic properties.

24. Aicher, S., & Stapf, G. (2014). Block Blued Glulam - Bridges, Beams and Arches. World Conference on Timber Engineering.

25. Spiecker, H., Lindner, M., & Schuler, J. K. (2019). Douglas-fir. European Forest Institute.

26. A. Bindewald, H. Michiels. (2016). Quantifying invasiveness of Douglas fir on the basis of natural regeneration in south-western Germany (p.330-343) in Introduced Tree Species in European Forests. European Forest Institute.

27. N. Schmalfuss, L. Vitkova. (2016). Douglas fir Freiburg City Forest: an introduced tree species in the light of multifunctional management objectives (p. 320-342) in Introduced Tree Species in European Forests. European Forest Institute.

28. Eberhard, B. R., Eckhart, T., & Hasenauer, H. (2021). Evaluating Strategies for the Management of Douglas-Fir in Central Europe. Forests, 12(8), 1040. https://doi.org/10.3390/f12081040

29. Vejpustková, M., & Člhák, T. (2019). Climate Response of Douglas Fir Reveals Recently Increased Sensitivity to Drought Stress in Central Europe. Forests, 10(2), 97. https://doi.org/10.3390/f10020097

30. USDA & US Forest Service. (2015). Predicting Douglas- Fir's Response to a Warming Climate.

31. Anne-Sophie Sergent, Philippe Rozenberg, Benoit Marçais, Yves Lefevre, Jean- Charles Bastien, et al.. Vulnerability of Douglas-fir in a changing climate: study of decline in France after the extreme 2003's drought. Opportunity and risks for douglas-fir in a changing climate, Oct 2010, Freiburg, Germany. 83 p. ffhal-02757012f

32. Kutnik, M., Lepetit, S., & le Neve, S. (2011, May). Performance of Douglas fir in real outdoor use conditions. The International Research Group on Wood Protection, Queenstown, New Zealand.

33. Highley, T. (1995). Comparative durability of untreated wood in use above ground. International Biodeterioration & Biodegradation, 35(4), 409–419. https://doi.org/10.1016/0964-8305(95)00063-1

34. Wang, E., Chen, T., Karalus, A., Sutherland, J., & Pang, S. (2009). Stability properties and performance of Douglas- fir and comparisons with radiata pine.

35. Henin, J. M., Pollet, C., Jourez, B., & Hébert, J. (2018). Impact of Tree Growth Rate on the Mechanical Properties of Douglas Fir Lumber in Belgium. Forests, 9(6), 342. https://doi.org/10.3390/f9060342

36. France Douglas. DOUGLAS FIR, A NATURAL CHOICE FOR CONSTRUCTION. https://www.frenchtimber.com/wp-content/uploads/2014/12/DOUGLAS_catalogue_210x280_EN-V4.pdf

37. Simpson Strong-Tie. (2017). European Technical Assessment ETA-08/0053 of 22/09/2017.

38. Simpson Strong-Tie, Dutch joist hanger catalogue. https://www.strongtie.nl/nl-NL/productlijnen/verbindingen-hout/ophangbeugels

39. S220GD, S250GD, S280GD, S320GD, S350GD. SSAB. https://www.ssab.com/products/steel-categories/metal-coated-steels/steelselector/metal-coated-structural-steels

40. Team, E. Table of design properties for metric steel bolts M5 to M39 - Eurocode 3. EurocodeApplied.Com. https://eurocodeapplied.com/design/en1993/bolt-design-properties

41. Brookhuis Applied Data Intelligence. (2021, March). CEN TC124 WG2 TG1 APPROVED GRADING REPORT (AGR / ITT) mtgBATCH 962 and mtgBATCH 966.

42. M.P. Ansell, Fatigue design for timber and wood- based materials .(1995). in Blass, H. J.. Timber Engineering. Centrum Hout.

43. Clorius, C. O. (2001). Fatigue in Wood: An investigation in tension perpendicular to the grain. Technical University of Denmark. BYG-Rapport No. R-038

44. Clorius, C. O., Pedersen, M. U., Hoffmeyer, P., & Damkilde, L. (2000). Compressive fatigue in wood. Wood Science and Technology, 34(1), 21–37. https://doi.org/10.1007/s002260050005

45. Nielsen, L. F. (2000). Lifetime and residual strength of wood subjected to static and variable load. Holz Als Roh- Und Werkstoff, 58(1–2), 81–90. https://doi.org/10.1007/s001070050391

46. Fuglsang Nielsen, L. (2000). Lifetime and residual strength of wood subjected to static and variable load. Part II: Applications and design. Holz Als Roh- Und Werkstoff, 58(3), 141–152. https://doi.org/10.1007/s001070050405

47. Clorius, C. O., Pedersen, M. U., Hoffmeyer, P., & Damkilde, L. (2009). An experimentally validated fatigue model for wood subjected to tension perpendicular to the grain. Wood Science and Technology, 43(3–4), 343–357. https://doi.org/10.1007/s00226-009-0244-7

48. Eco Costs Value. (2021, June 5). Eco-costs. Sustainability Impact Metrics. https://www.ecocostsvalue.com/eco-costs/

49. Liu, J. Y., & Ross, R. J. (1996). Energy Criterion for Fatigue Strength of Wood Structural Members. Journal of Engineering Materials and Technology, 118(3), 375–378. https://doi.org/10.1115/1.2806823

50. Dourado, N., de Moura, M., & de Jesus, A. (2019). Fatigue-fracture characterization of wood under mode I loading. International Journal of Fatigue, 121, 265–271. https://doi.org/10.1016/j.ijfatigue.2018.12.012

51. KNMI - Daggegevens van het weer in Nederland. (2021). KNMI. https://www.knmi.nl/nederland-nu/klimatologie/daggegevens

52. Hedlin, C. P. (1967). Sorption Isotherms of Twelve Woods at Subfreezing Temperatures. Forest Products Journal, 43–48.

53. Bergman, R. (2010). Drying and Control of Moisture Content and Dimensional Changes. Algrove Publishing.

54. Nguyen, D. M., Care, S., Courtier-Murias, D., Zhou, M., & Coussot, P. (2020). Mechanisms of liquid imbibition in Douglas-fir inferred from 1H nuclear magnetic resonance methods. Holzforschung, 75(3), 225–236. https://doi.org/10.1515/hf-2020-0051

55. Bachtiar, E. V., Clerc, G., Brunner, A. J., Kaliske, M., & Niemz, P. (2017). Static and dynamic tensile shear test of glued lap wooden joint with four different types of adhesives. Holzforschung, 71(5), 391–396. https://doi.org/10.1515/hf-2016-0154

56. Majano-Majano, A., Lara-Bocanegra, A. J., Xavier, J., & Morais, J. (2020). Experimental Evaluation of Mode II fracture Properties of Eucalyptus globulus L. Materials, 13(3), 745. https://doi.org/10.3390/ma13030745

57. Majano-Majano, A., Lara-Bocanegra, A., Xavier, J., & Morais, J. (2018). Measuring the Cohesive Law in Mode I Loading of Eucalyptus globulus. Materials, 12(1), 23. https://doi.org/10.3390/ma12010023

58. van de Loo, J. (2020, March). Estimating the (remaining) service life of timber bridges with the use of factors methods. http://resolver.tudelft.nl/uuid:bd5b73a9-851a-49f8-8969-26b43cf74311

59. MacKenzie, C. E., Wang, C. H., Leicester, R. H., Foliente, G. C., Nguyen, M. N., Forest and Wood Products Australia, & Timber Queensland. (2007). Timber Service Life Design (Revised 2013). Forest and Wood Products Australia.

60. Isaksson, T., Brischke, C., & Thelandersson, S. (2012). Development of decay performance models for outdoor timber structures. Materials and Structures, 46(7), 1209–1225. https://doi.org/10.1617/s11527-012-9965-4

61. Humar, M., Kržišnik, D., Lesar, B., & Brischke, C. (2019). The Performance of Wood Decking after Five Years of Exposure: Verification of the Combined Effect of Wetting Ability and Durability. Forests, 10(10), 903. https://doi.org/10.3390/f10100903

62. Meyer-Veltrup, L., Brischke, C., Alfredsen, G., Humar, M., Flæte, P. O., Isaksson, T., Brelid, P. L., Westin, M., & Jermer, J. (2017). The combined effect of wetting ability and durability on outdoor performance of wood: development and verification of a new prediction approach. Wood Science and Technology, 51(3), 615–637. https://doi.org/10.1007/s00226-017-0893-x

63. Brischke, C., Alfredsen, G., Humar, M., Conti, E., Cookson, L., Emmerich, L., Flæte, P. O., Fortino, S., Francis, L., Hundhausen, U., Irbe, I., Jacobs, K., Klamer, M., Kržišnik, D., Lesar, B., Melcher, E., Meyer-Veltrup, L., Morrell, J. J., Norton, J., . . . Suttie, E. (2021b). Modelling the Material Resistance of Wood—Part 2: Validation and Optimization of the Meyer-Veltrup Model. Forests, 12(5), 576. https://doi.org/10.3390/f12050576

64. How do you determine the minimum size of a fillet weld?. TWI. https://www.twi-global.com/technical-knowledge/faqs/faq-how-do-you-determine-the-minimum-size-of-a-fillet-weld

65. Handbook - Calculations. ESAB. https://www.esabna.com/euweb/fm_handbook/577fm8_4.htm

66. OVAKO steel navigator. Steel Navigator. https://steelnavigator.ovako.com/steel-grades/42crmo4/

67. Sompoliński, V. P. 51CrV4, 50CrV4, 1.8159, AISI 6150 - alloy steel. Virgamet. https://virgamet.com/strips-coils-51crv4-50crv4-58crv4-59crv4-50cv4-51cv4-spring-steel

68. Clerc, G., Brunner, A. J., Niemz, P., & van de Kuilen, J. W. G. (2019). Feasibility study on Hartman–Schijve data analysis for mode II fatigue fracture of adhesively bonded wood joints. International Journal of Fracture, 221(2), 123–140. https://doi.org/10.1007/s10704-019-00414-5

69. Jotafix PU Topcoat. (2018, September 6). Jotun Coatings. https://www.jotun.com/Datasheets/Download?url=%2FTDS%2FTDS__36902__Jotafix+PU+Topcoat__Euk__GB.pdf

70. AZoM. (2013, June 12). Melamine Formaldehyde - MF Melamine Cellulose Filled. AZoM.Com. https://www.azom.com/article.aspx?ArticleID=693

71. Caston, P.S. (2009). Historic Wooden Covered Bridge Trusses in Germany.

Appendices

Appendix A: Python scripts for determination of effective cross section, steel design

Calculation of buckling of subpanels, subjected to pure compression (stiffener web)

In [1]:
```
import numpy as np
```

In [2]:
```
#Invoer
b = 308 # Panneel lengte in mm
t = 7 # Panneel dikte in mm
fy = 355 # Vloeisterkte in MPa
pos = 1 # 1 is inwendige plaat, 2 is uitkragend
psi = 1 # kleine spanning/ grote spanning (tabel 4.1 of 4.2 1993-1-5)

ksig = 0 #plooifactor, tabel 4.1 of 4.2 in 1993-1-5, voor inwendig of uitkragend respectievelijk, laat op 0 als je psi is al inge


#NL bijlage van EN 1993-2\
#doorsneden en staven
ym0= 1.0 # weerstand van vloeigrens wat betreft plooien
ym1= 1.0 # weerstand van staven tegen instabiliteit bepaald bij toetsing
ym2= 1.25 # weerstand van doorsneden in trek tot aan breuk
# verbindingen
ym22= 1.25 # bouten, klinknagels, pennen, lassen, stuik van platen
ym3 = 1.25 #glijweerstand in UGT (cat C)
ym3ser= 1.10 # glijweerstand in BGT
```

In [3]:
```
eps = np.sqrt(235/fy)
print("epsilon is", eps)
if ksig ==0:
    if psi ==1:
        ksig = 4
    if 0 < psi< 1:
        ksig = 8.2/(1.05 + psi)
    if psi ==0:
        ksig = 7.81
    if -1< psi < 0:
        ksig = 7.81- 6.29*psi +9.78 * (psi**2)
    if psi == -1:
        ksig = 23.9
    if -1 > psi >= -3:
        ksig = 5.98 * (1-psi)**2
    print ("ksig (plooifactor)=",ksig)
```

```
epsilon is 0.813616513467
ksig (plooifactor)= 4
```

In [4]:
```
lamdarel= (b/ t)/ (28.4*eps*np.sqrt(ksig))
print("Relatieve slankheid lamdarel=",lamdarel)
print("")
rho = 0 # reductiefactor
if pos ==1:
    if lamdarel <= 0.5 + np.sqrt(0.085 - 0.055*psi):
        rho =1
    if lamdarel >0.5 + np.sqrt(0.085 - 0.055*psi):
        rho = (lamdarel - 0.055 * (3+psi))/ (lamdarel**2)
        if rho > 1:
            rho =1

if pos == 2:
    if lamdarel <= 0.748:
        rho = 1
    if lamdarel > 0.748:
        rho = (lamdarel - 0.188)/ (lamdarel**2)
print('Reductiefactor rho=',rho)
```

```
Relatieve slankheid lamdarel= 0.952104430653

Reductiefactor rho= 0.807614044657
```

Plate like buckling behaviour (inner plate)

In [5]:
```
###PLATELIKE BEHAVIOUR
Ac = 1.199447*10**5 # mm2, Totale oppervlakte van alle verstijfde delen, behalve diegene ondersteund door hoofdligger
Aceffloc = 1.8471*10**5 ## mm2, Totale effectieve oppervlakte
tp = 18 #mm dikte dekplaat
b= 7500 #mm afstand tussen hoofdliggers (breedte plaat)
a = 3571 #mm afstand tussen dwarsliggers (lengte plaat)
v = 0.3 #Poission, staal = 0.3
E = 210*10**3 # MPA, elasticiteitsmodulus
Isl = 2.1395*10**9 # mm4, traagheidsmoment volledig verstijfde plaat
Asl = 64895.08 #Oppervlakte alle langsverstijfers in veld

#Einde invoer
Ip = (b*tp**3)/(12*(1-(v**2)))
print("Traagheidsmoment plaatbuiging (dekplaat)=", Ip/(10**6),"*10^6 mm4")
betac = Aceffloc/Ac #verhouding
print('beta,c, verhouding netto en totale oppervlakte, slankheid=',betac)
re = Isl/Ip #bijlage A
rel = (re)**0.25
print('relatieve buigsijfheid=',re, 'en wortel 4=',rel)
alfa= a/b #aspect ratio
print ("Aspect ratio alpha=",alfa)
Ap = b *tp #oppervlakte dekplaat in veld
rela = Asl/Ap #relatieve axiale stijfheid
print("Relatieve axiale stijfheid=", rela)
print("")

ksigp = 0 #plooicoefficient, ook te achterhalen via FEM of tabellen
if alfa <= rel:
    print("alfa <= relatieve buigstijfheid^0.25")
    ksigp = (2*(((1+(alfa**2))**2)+re-1))/((alfa**2)*(psi+1)*(1+rela))
if alfa > rel:
    print("alfa > relatieve buigstijfheid^0.25")
    ksigp = (4*(1+np.sqrt(re)))/((psi+1)*(1+rela))
print("plooicoefficient, ksig,p=", ksigp)
print("")
sige = ((np.pi**2)*E*tp**2)/(12*(1-(v**2))*b**2) # Euler buckling stress
print("Euler knik spanning =",sige,"MPa")
sigcrp = ksigp *sige # critical buckling stress
print("kritische plooi (plaat) =",sigcrp, "MPa")
lamdapp = np.sqrt((betac*fy)/sigcrp)
print ("relatieve slankheid plaat=", lamdapp)

if lamdapp <= 0.5 + np.sqrt(0.085 - 0.055*psi):
    rho =1
    print("Geen reductie door plaat plooi, rho=", rho)
if lamdapp >0.5 + np.sqrt(0.085 - 0.055*psi):
    rho = (lamdarel - 0.055 * (3+psi))/ (lamdapp**2)
    if rho > 1:
        rho =1
    print("Reductie door plaat plooi toepassen, rho=",rho)
```

```
Traagheidsmoment plaatbuiging (dekplaat)= 4.0054945054945055 *10^6 mm4
beta,c, verhouding netto en totale oppervlakte, slankheid= 1.5399596647455036
relatieve buigsijfheid= 534.1412894375857 en wortel 4= 4.807441825998535
Aspect ratio alpha= 0.47613333333333335
Relatieve axiale stijfheid= 0.4807042962962963

alfa <= relatieve buigstijfheid^0.25
plooicoefficient, ksig,p= 1592.7253214481761

Euler knik spanning = 1.0932484875052826 MPa
kritische plooi (plaat) = 1741.2445486845836 MPa
relatieve slankheid plaat= 0.560323664282
Geen reductie door plaat plooi, rho= 1
```

Columnlike buckling, inner stiffeners

In [6]:
```
##Columnlike behaviour, verstijfde plaat
Asl= 16205.9158 # mm2, oppervlakte trog en meewerkende breedte dek
Asleff = 15393 #mm2, oppervlakte trog met reductie panelen

Isl =  1.7829*10**8 #mm4, traagheidsmoment trog en meewerkende breedte dek
knik = 0.34 # imperfectiefactor knikkromme a = 0.21 ,b =0.34 (gesloten profielen), c = 0.49 (open profielen), d=0.76
e= 125.54 #mm Figuur A.1 en paragraap 4.5.3 van EN 1993-1-5

##Einde invoer
sigcrc= ((np.pi**2)* E * Isl)/(Asl*a**2) #kritieke spanning verstijfde plaat
print("kritieke spanning, verstijfde plaat=",sigcrc, "MPa")
betacc = Asleff/Asl
print("beta,c, verhouding gereduceerde en bruto doorsnede =",betacc)
lamdar= np.sqrt((betacc*fy)/sigcrc)
print('relatieve slankheid kolom, lamda c =', lamdar)
i = np.sqrt(Isl/Asl)
print("reduction factor i =", i,'mm')
print("")
alfae = knik + 0.09/(i/e) #imperfectie factor
print('alfae =', alfae)
fi = 0.5 * (1 + alfae*(lamdar - 0.2 )+ (lamdar**2)) #initiele scheefstand
print('fi=', fi)
ksic = 1/(fi+np.sqrt((fi**2)-(lamdar**2))) #reductie factor ksi
print("ksi, kolom =",ksic)
```

```
kritieke spanning, verstijfde plaat= 1788.1038841842326 MPa
beta,c, verhouding gereduceerde en bruto doorsnede = 0.9498383300251381
relatieve slankheid kolom, lamda c = 0.434252821459
reduction factor i = 104.88821713 mm

alfae = 0.447720393283
fi= 0.646727639148
ksi, kolom = 0.88811664001
```

Interaction of platelike and columnlike buckling behaviour for inner part

In [7]:
```
##Interaction platelike and columnlike
epsi = sigcrp/sigcrc -1
if 0 <= epsi<=1:
    print("epsi=", epsi)
if epsi < 0:
    print("epsi=",epsi)
    epsi = 0
    print("epsi gelijkgesteld aan 0")
    print("columnlike buckling")
if epsi > 1:
    print("epsi=",epsi)
    epsi = 1
    print("epsi gelijkgesteld aan 1")
    print("platelike buckling")
print("")
rhoc = (rho- ksic)*epsi*(2-epsi)+ ksic #totale reductie combi plooi en kolomknik
print('reductie=', rhoc)
```

```
epsi= -0.02620615944863136
epsi gelijkgesteld aan 0
columnlike buckling

reductie= 0.88811664001
```

Global shear lag effects, inner plate

In [8]:
```
##Shear lag simply supported
Le = 25000 #mm, afstand tussen ondersteuningen
Asl0 = 6*5407.9223 #mm, oppervlakte langsverstijfers (dus zonder dek) in b0, zie EN 1993-1-5, paragraaf 3.2.1
b0 = 3750 #mm, uitkraging flens of halve breedte inwendig element

#Einde invoer

alfa0= np.sqrt(1+(Asl0)/(b0*tp))
print("alfa0 =", alfa0)
kappa = (alfa0*b0)/Le
print("kappa=", kappa)
if kappa <= 0.02:
    beta = 1
if 0.02 <= kappa <= 0.70:
    beta= 1/(1+6.4*kappa**2)
if kappa >0.70:
    beta = 1/ (5.9 * kappa)
print("")
print("beta in overspanning=", beta)
beta0 = (0.55 +0.025/kappa)* beta
if beta0 >beta:
    print("beta0 is eigenlijk =",beta0, 'maar')
    print('beta0 wordt gereduceerd naar beta')
    beta0= beta
print ('beta0 in oplegging=', beta0)
print("")
beff=beta*b0 #beff in overspanning
beffs= beta0*b0  #beff in steunpunt
print("b,eff, in overspanning=", beff,'mm')
print('b,eff, in oplegging=', beffs,'mm')
print("")
print("Plastisch")
betap = beta**kappa # Toe te passen op gereduceerde doorsnede
beta0p= beta0**kappa #Insgelijks
print('reductiefactoren voor respectievelijk overspanning en steunpunt, beta en beta0=')
print(betap, beta0p)
```

```
alfa0 = 1.21684189788
kappa= 0.182526284683

beta in overspanning= 0.824251859979
beta0 in oplegging= 0.566233476914

b,eff, in overspanning= 3090.94447492 mm
b,eff, in oplegging= 2123.37553843 mm

Plastisch
reductiefactoren voor respectievelijk overspanning en steunpunt, beta en beta0=
0.965336509989 0.901395102298
```

Global shear lag and buckling of plate interaction

In [9]:
```
# Global reduction shear lag and buckling
bedgeff = 300 #mm, som van effecieve plaatvelden (druk) ondersteund door aangrezende plaatelement EN 1993-1-5 paragraaf 4.5
Aceff = rhoc * Aceffloc + bedgeff * tp
print ("effectieve op druk belaste doorsnede =", Aceff/1000, '*10 ^3 mm2')
Aeff = Aceff * (beta**kappa)
if Aeff < Aceff * beta:
    Aeff = Aceff*beta
    print("Aeff gereduceerd volgens EN 1993-1-5, 3.3")

Aeff2= Aceff * (beta0 **kappa)
if Aeff2 < Aceff * beta0:
    Aeff = Aceff*beta0
    print("Aeff gereduceerd volgens EN 1993-1-5, 3.3")

print("")
print("Effectieve doorsnede shear lag en plooi in veld= ", Aeff/1000,'* 10^3 mm2')
print("Effectieve doorsnede shear lag en plooi bij steunpunt= ", Aeff2/1000,'* 10^3 mm2')
```

```
effectieve op druk belaste doorsnede = 169.444024576 *10 ^3 mm2

Effectieve doorsnede shear lag en plooi in veld=  163.570503323 * 10^3 mm2
Effectieve doorsnede shear lag en plooi bij steunpunt=  152.736013867 * 10^3 mm2
```

Local shear lag effects (deck plate, end span, inner plate)

In [10]:
```
#Local shear lag troughs# End span
L1 = 3035.71428572 #mm, afstand tussen nulpunten dwarsliggers 0.7 voor overspanning in veld # 0.85 voor eindoverspanning
L2 = L1 #Same
b0l = 150 #mm uitkraging flens of halve breedte intern element

#Einde invoer

alfa0l= 1 # Vast op 1, geen verstijfers op platen die deel van de trog zijn
print("alfa0 =", alfa0l)
kappal = (alfa0l*b0l)/L1
print("kappa=", kappal)
if kappal <= 0.02:
    betal = 1
if 0.02 <= kappal <= 0.70:
    betal= 1/(1+6.4*kappal**2)
if kappal >0.70:
    betal = 1/ (5.9 * kappal)
print("")
print("beta in overspanning=", betal)
beta0l = (0.55 +0.025/kappal)* betal
if beta0l >betal:
    print("beta0 is eigenlijk =",beta0l, 'maar')
    print('beta0 wordt gereduceerd naar beta')
    beta0l= betal
print ('beta0 in oplegging=', beta0l)
print("")
beffl=betal*b0l #beff in overspanning
beffsl= beta0l*b0l  #beff in steunpunt
print("b,eff, in overspanning=", beffl,'mm')
print('b,eff, in oplegging=', beffsl,'mm')
print("")
print("Plastisch")
betapl = betal**kappal # Toe te passen op gereduceerde doorsnede
beta0pl= beta0l**kappal #Insgelijks
print('reductiefactoren voor respectievelijk overspanning en steunpunt, beta en beta0=')
print(betapl, beta0pl)
```

```
alfa0 = 1
kappa= 0.032945129886174575

beta in overspanning= 0.9931014780509314
beta0 is eigenlijk = 1.2998084557784861 maar
beta0 wordt gereduceerd naar beta
beta0 in oplegging= 0.9931014780509314

b,eff, in overspanning= 99.31014780509314 mm
b,eff, in oplegging= 99.31014780509314 mm

Plastisch
reductiefactoren voor respectievelijk overspanning en steunpunt, beta en beta0=
0.9997719657552371 0.9997719657552371
```

Appendix B: Python scripts for steel shear, steel design

Longitudinal shear check

In [2]:

```
#Weerstand tegen afschuiving lijf
a = 3571.42857143 # mm afstand tussen dwarsverstijvingen # 0 indien geen
hw = 1863.5 # mm Hoogte van lijf
hf = 1900 # mm Hoogte van lijf tussen hartlijnen flenzen
Isl = 0 # mm4 Treegheidsmoment om z-z as van langsverstijvingen (figuur 5.3(b) van 1993-1-5) # 0 laten indien geen
t = 20 # mm Dikte plaat
ts= 20 # mm Dikte dwars
E = 210*10**3 # E modulus in MPa
v= 0.3 #Poisson
fy = 345 # MPa, voor S355, t <=16mm is 355, 16< t <=40 is 345, 40< t <= 63 is 335.
Ved = 2036.70 *10**3 # N, dwarskracht
ni = 1.2 # 1.2 voor t/m S460, daarboven 1.0
verst= 0 #verstijfte plaat (0 voor niet, 1 voor wel)
verv = 0 #start of vervormbare verstijving van de oplegging, 0 voor vervormbaar, 1 voor stijf
ym0= 1 #factor = 1 in NB
ym1= 1 #factor = 1 in NB

#Einde invoer
eps = np.sqrt(235/fy)
print("epsilon=",eps)
ktsl = 0
if Isl != 0:
    ktsl = 9 * ((hw/a)**2) * (((Isl)/((t**3)*hw))**3)**0.25
    if ktsl < (2.1/t) * ((Isl/ hw)**0.33333333333333333):
        print("ktsl reduced")
        ktsl = (2.1/t) * ((Isl/ hw)**0.33333333333333333)
    print("ktsl=", ktsl)
hoog= a/hw
if hoog < 1:

    print("a/hw=", hoog)
    kt = 4 + 5.34 * ((hw/a)**2) + ktsl
    print("plooicoefficent, kt=", kt)
if hoog >= 1:
    print("a/hw=", hoog)
    kt = 5.34 + 4 * ((hw/a)**2) + ktsl
    print("plooicoefficent, kt=", kt)

sige= ((np.pi**2)*E*(t**2))/((12*(1-(v**2)))*(hw**2))
print("sigma,e=", sige, "MPa")
print("")
Aw = t * hw
print("Oppervlakte lijf=",Aw,"mm2")
Ted= Ved / Aw
UC1= Ted/ (fy/(ym0*np.sqrt(3)))
print("Tau,ed=",Ted,"MPa")
print("UC=",UC1)

tcr = kt * sige
print("Kritische spanning=", tcr, "MPa")
if verst ==0:
    if hw/t > (72*eps)/ni:
        print("weerstand tegen plooien moet worden gechekt en verstijfers bij de oplegging zijn nodig")
        print("")
        lamda = hw/(86.4*t*eps)
        print("gewijzigde slankheid, lamdaw =",lamda)
    if hw/t <= (72*eps)/ni:
        print("weerstand tegen plooien hoeft niet gechekt te worden")

if verst ==1:
    if hw/t > ((31*eps)/ni)*np.sqrt(kt):
        print("weerstand tegen plooien moet worden gechekt en verstijfers bij de oplegging zijn nodig")
        print("")
        lamda = hw/(37.4*t*eps*np.sqrt(kt))
        rint("gewijzigde slankheid, lamdaw =",lamda)
    if hw/t <= ((31*eps)/ni)*np.sqrt(kt):
        print("weerstand tegen plooien hoeft niet gechekt te worden")

if lamda < 0.83 /ni:
    ksi = ni
if 0.83 /ni <= lamda < 1.08:
    ksi = 0.83/lamda
if verv ==0:
    if 1.08 <= lamda:
        ksi = 0.83/ lamda
if verv ==1:
    if 1.08 <= lamda:
        ksi= 1.37/(0.7+lamda)
print("bijdrage van lijfe, ksiw =",ksi)
Vwrd = (ksi*fy*Aw)/(ym1*np.sqrt(3))
print("Weerstand tegen afschuiving vanuit lijf, Vw,rd=",Vwrd/1000,"kN")
```

```
epsilon= 0.825323827531
a/hw= 1.9165165395385029
plooicoefficent, kt= 6.429017473599129
sigma,e= 21.8623880644239 MPa

Oppervlakte lijf= 37270.0 mm2
Tau,ed= 54.6471693050711 MPa
UC= 0.274352677467
Kritische spanning= 140.5536748807863 MPa
weerstand tegen plooien moet worden gechekt en verstijfers bij de oplegging zijn nodig

gewijzigde slankheid, lamdaw = 1.30665602504
bijdrage van lijfe, ksiw = 0.635209254842
Weerstand tegen afschuiving vanuit lijf, Vw,rd= 4715.57522704 kN
```

Longitudinal shear check, with and without flanges

In [3]:
```
#Weerstand tegen afschuiving flenzen indien geen moment aanwezig, indien wel, 5.4 van 1993-1-5
bf = 555 #mm Breedte flens
tf = 55 #mm hoogte flens
fyf = 335 #MPa vloeigrens flens
## Einde invoer
eps1= np.sqrt(235/fyf)
if bf >2*15*eps1*tf:
    bf = 2*15*epi1*tf
    print("bf gereduceerd naar bf=",bf,'mm')

c = a*(0.25+(1.6*bf*(tf**2)*fyf)/(t*(hw**2)*fy))
print("c=",c,'mm')

Vfrd= ((bf*(tf**2)*fyf)/(c*ym1))
print("Weerstand tegen afschuiving vanuit flenzen, Vf,rd=", Vfrd/1000, 'kN')
```

```
c= 1026.9844593105115 mm
Weerstand tegen afschuiving vanuit flenzen, Vf,rd= 547.6452149797817 kN
```

In [4]:
```
Vrdtot = Vwrd + Vfrd
print("Totale weerstand tegen afschuiving=", Vrdtot/1000, 'kN')
UC2 = Ved/Vrdtot
UC3 = Ved/ Vwrd
print("UC met flens=", UC2)
print("UC zonder flens=",UC3)
```

```
Totale weerstand tegen afschuiving= 5263.22044202 kN
UC met flens= 0.386968401274
UC zonder flens= 0.431909131323
```

Appendix C: Fatigue verification of Steel Bridge details

$\lambda = 2\ \gamma_{Mf} = 1{,}35\ or\ 1{,}15\ voor\ osd$

Cross beam at stiffener

Detail-categorie	Constructie-detail	Beschrijving	Eisen
80	9	**Locatie** Verbinding van de verstijver aan de dwarsdrager **Scheurtype** Scheur in de dwarsdrager bij doorgestoken verstijver **Scheurgroei** In de lijfplaat van de dwarsdrager vanuit de teen van de las	**Spanningswisseling** $\Delta\sigma$ Berekend als nominale spanning in het lijf van de dwarsdrager ter plaatse van de teen van de las door buiging uit het vlak van het lijf van de dwarsdrager als gevolg van de doorbuiging van de verstijver gecombineerd met de vierendeeleffecten in het vlak van de dwarsdrager $a_{min} \geq 5$ mm, of groter indien noodzakelijk voor de sterkte van de las **Voorbewerking** Spleet $h_1 \leq 1{,}0$ mm **Lassen** Handlas; lasaanzetten op de koudvervormde delen zijn niet toegelaten **NDO** visueel en MT 100 %

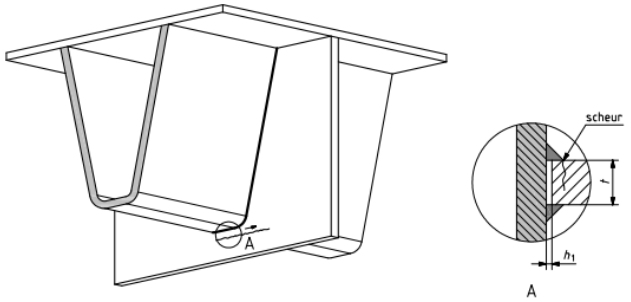

0.737*80 = 58,96 MPa

58.96/(1,35*2) = 21,833 MPa

Nom. Max, +Principal stress

Nom. Min, +Principal stress

Range 13,7 MPa

$$\left(\frac{21{,}833}{13{,}7}\right)^5 * 5 * 10^6 = 51{,}4 * 10^6 < 50 * 10^6$$

UC = 50/51,4= 0,97

Bottom of trough at cross beam

80	$t \leq 12$mm	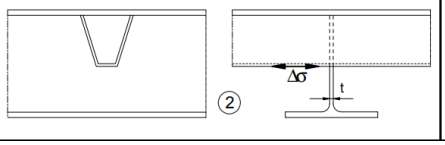	2) Doorgaande langsverstijver, zonder uitsparingen in de dwarsdrager.	2) Toetsing gebaseerd op het normaalspanningsinterval $\Delta\sigma$ in de langsverstijver.
71	$t > 12$mm			

0,737*71 = 52.327 MPa

52,327/(1,15*2) = 22,751 MPa

−7.4	3.8
−8.7	3.2
−9.6	3.1
−10.2	3.2
−10.7	3.2
−11.1	3.1
−11.4	3.0
−11.9	2.7
−12.4	2.4
−13.0	1.9
−13.8	1.2
−14.7	0.2

Nom. Min and Max respectively, longitudinal direction stress

2nd cross beam normative

Stress range =13,825

$$\left(\frac{22.751}{13,825}\right)^5 * 5 * 10^6 = 60,35 * 10^6 > 50 * 10^6$$

UC= 50/60,35=0,83

Deck between cross girders

0,737*125 = 92,125 MPa

92,125/(1,15*2) = 40,05435 MPa

Detail-categorie	Constructie-detail	Beschrijving	Eisen
125	1	**Locatie** Scheur in de dekplaat op een locatie tussen de dwarsdragers **Scheurtype** Scheur geïnitieerd vanuit de las tussen de dekplaat en de verstijvers; kan aan beide zijden ontstaan **Scheurgroei** Door de dikte van de dekplaat vanuit de las	**Spanningswisseling** $\Delta\sigma$ Berekend als nominale lokale spanning aan de onderzijde van de dekplaat op het scheurinitiatiepunt, berekend met een 3D-model $a_{min} \leq t + 1$ mm **Voorbewerking** Verstijverbeen afschuinen tot een lasopeningshoek van 50°. Bij OP-lassen tot $t \leq 6$mm geen afschuining **Spleet** $h_1 = 0$ mm; over 10 % van de lengte is $h_1 < 0,5$ mm toegelaten **MDF** $h_2 \leq 1,0$ mm **NDO** visueel: 100 %; MT: alle lasaanzetten + 10 % van de laslengte als steekproef te kiezen op basis van de visuele inspectie **Lasgeometrie** De las moet vloeiend aanliggen aan het dek en het verstijverbeen **Lasoverhoogte** $h_3 \geq 2$

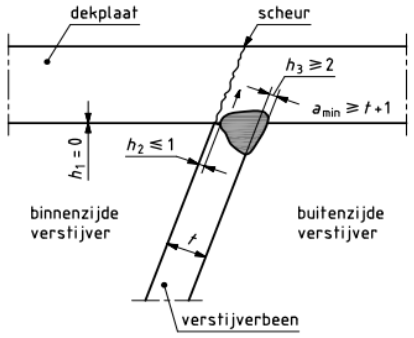

Nom. Max. stress, transverse direction, bottom of deck

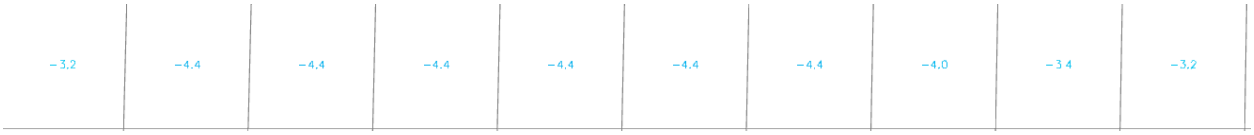

Nom. Min. stress, transverse direction, bottom of deck

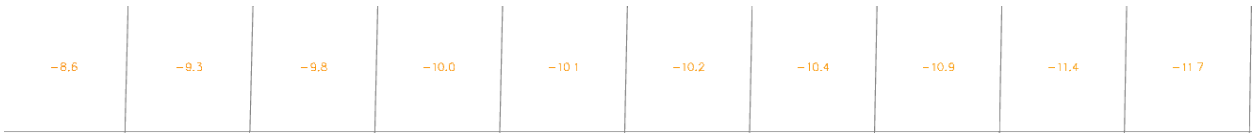

Range = 8 MPa

$$\left(\frac{40,05435}{8}\right)^{5} * 5 * 10^{6} = 1,57 * 10^{10} \gg 50 * 10^{6}$$

UC= infinite, under cut-off limit

Deck above cross beam

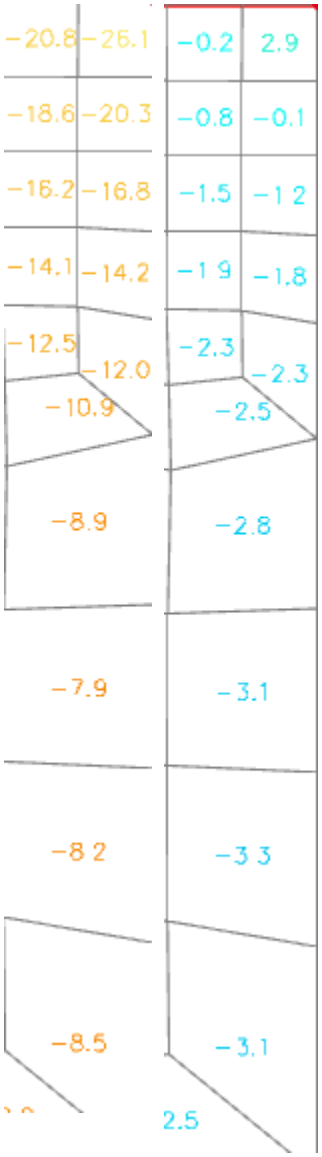

Max and Min. stress respectively, transverse direction, bottom of deck

0,737*125 = 92,125 MPa

92,125/ (1,15*2) = 40,05435 MPa

Range = 23,7 (HSS method)

$$\left(\frac{40{,}05435}{23{,}7}\right)^{5} * 5 * 10^{6} = 68{,}85 * 10^{6} > 50 * 10^{6}$$

UC = 50/68,85 = 0,73

Detail-categorie	Constructie-detail	Beschrijving	Eisen
125	2	**Locatie** Dekplaat boven de kruising tussen de verstijverbenen en de dwarsdrager **Scheurtype** Scheur geïnitieerd vanuit de las tussen de dekplaat en de verstijver **Scheurgroei** Door de dikte van de dekplaat vanuit de wortel van de las	**Spanningswisseling** $\Delta\sigma$ Berekend als lokale 'hot spot stress'-spanning aan de onderzijde van de dekplaat op het scheurinitiatiepunt, berekend met een 3D-model of de lokale nominale spanning vermenigvuldigd met een SCF-factor uit een vereenvoudigd 2D-model overeenkomstig de aanpak van figuur NB.5 $a_{min} \leq t + 1$ mm **Voorbewerking** Verstijverbeen afschuinen tot een lasopeningshoek van 50°. Bij OP-lassen tot $t \leq 6$ mm geen afschuining **Spleet** h_1 = 0 mm; over 10 % van de lengte is h_1 = < 0,5 mm toegelaten **MDF** $h_2 \leq 1{,}0$ mm **NDO** visueel: 100 %; MT: 100 % waar de las van de verstijver aan de dwarsdrager en dekplaat en de las van de dwarsdrager aan de dekplaat samenkomen (x-y-z-aansluiting) en ter plaatse van lasaanzetten **Lasgeometrie** De las moet vloeiend aanliggen aan het dek en het verstijverbeen **Lasoverhoogte** $h_3 \geq 2$

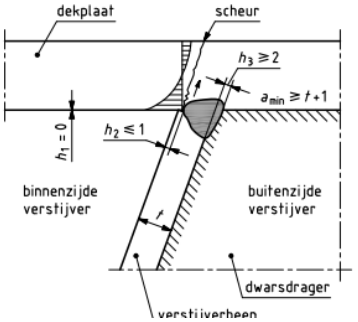

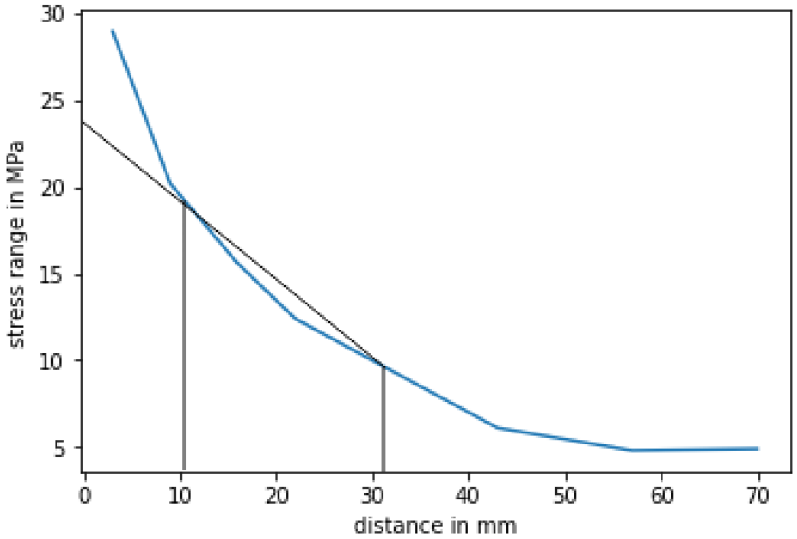

Main Beam- Flange to Web Connection

0,737*125 = 92,125 MPa

92,125/(1,35*2) = 34,12037 MPa

30.8	30.8	53.1	53.1
30.8	30.8	52.8	52.9
30.8	30.8	52.6	52.6
30.8	30.8	52.4	52.4
30.9	30.9	52.2	52.2
30.9	30.9	52.0	52.1
31.0	31.0	51.9	51.9
31.1	31.1	51.8	51.8
31.1	31.1	51.6	51.6
31.0	31.0	51.2	51.2
31.0	31.0	50.9	50.9
31.0	31.0	50.6	50.6
31.0	31.0	50.3	50.3
30.9	30.9	50.0	50.0
30.9	30.9	49.8	49.8
30.9	30.9	49.5	49.5

Min. and Max. Stress in Longitudinal direction

Stress range = 20,5 MPa

Detail-categorie	Cons
125	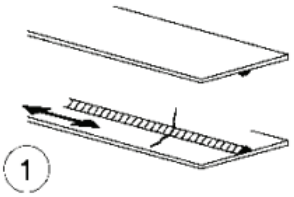

$$\left(\frac{34{,}12037}{20{,}5}\right)^{5} * 5 * 10^{6} = 63{,}87 * 10^{6} > 50 * 10^{6}$$

UC = 50/63,87 = 0,78

Cross beam- Flange to Web Connection

Mid Cross beam

Min. and Max. Stress in transverse direction

0,737*125 = 92,125 MPa

92,125/(1,35*2) = 34,12037 MPa

Stress range 20,97 MPa

$$\left(\frac{34{,}12037}{20{,}97}\right)^5 * 5 * 10^6 = 57{,}023 * 10^6 > 50 * 10^6$$

UC = 50/57= 0,88

Outer Cross beam

Min. and Max. Stress in Transverse direction

Stress range 21,48

$$\left(\frac{34{,}12037}{21{,}48}\right)^5 * 5 * 10^6 = 50{,}57 * 10^6 > 50 * 10^6$$

UC = 50/ 50,57= 0,99

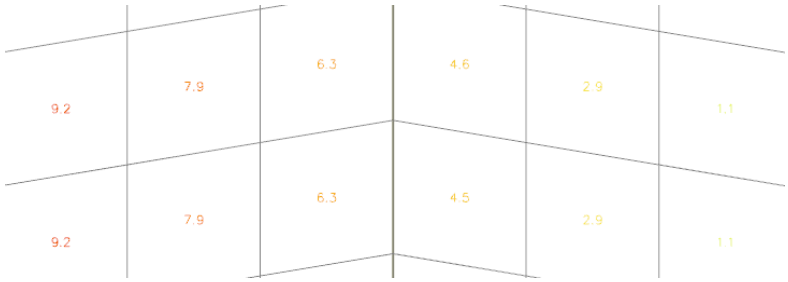

Cross beam flange to Main beam web connection

0,737*80 = 58,96 MPa

58,96/(1,35*2) = 21,84 MPa

End cross beam normative,

Stress range under 8 MPa, lower than cut-off limit

UC = Inifnite

Detail-categorie	Constructiedetail	
80	ℓ < 50 mm	alle t [mm]
71	50 < ℓ ≤ 80	alle t
63	80 < ℓ ≤ 100	alle t
56	100 < ℓ ≤ 120	alle t
56	ℓ > 120	t ≤ 20
50	120 < ℓ ≤ 200 ℓ > 200	t > 20 20 < t ≤30
45	200 < ℓ ≤ 300 ℓ > 300	t > 30 30 < t ≤ 50

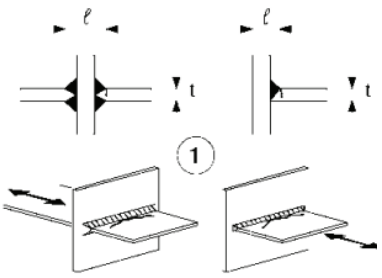

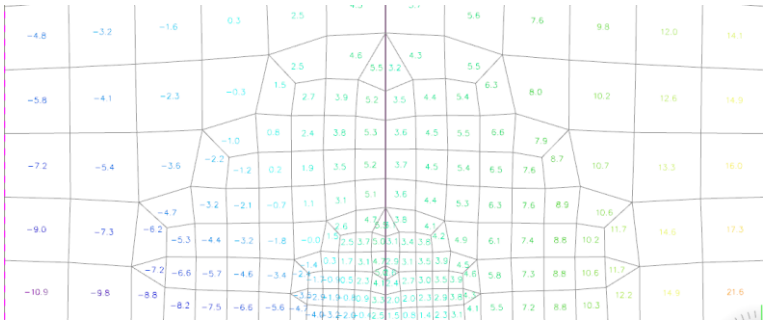

Deck to Cross beam connection

0,737*80 = 58,96 MPa

58,96/(1,15*2) = 25,63 MPa

80	$\ell \leq 50$ mm	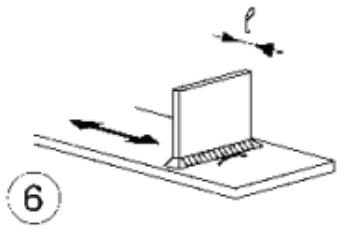

Stress range = 13,7 MPa

Under cut-off limit

UC= Infinite

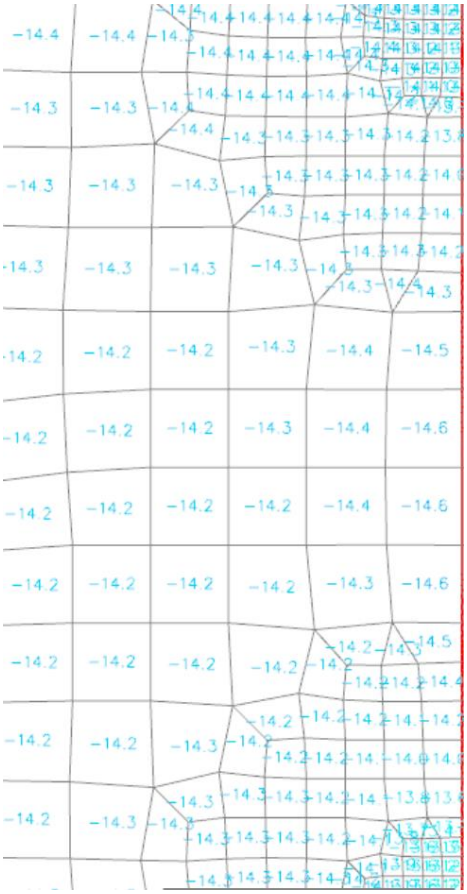

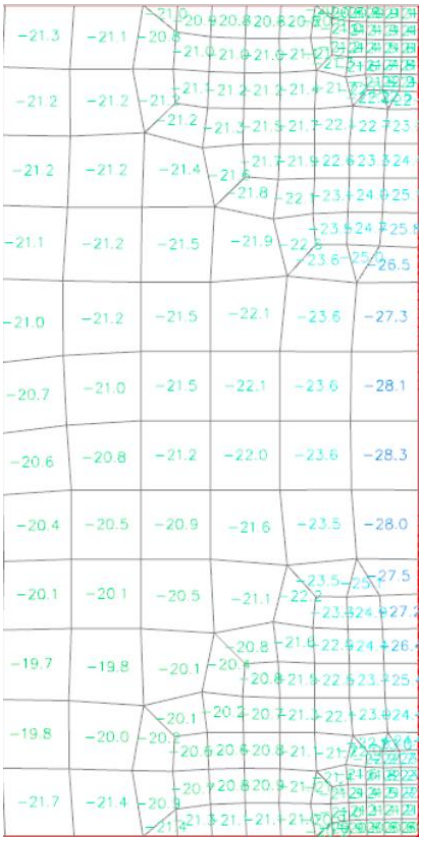

Appendix D: Member Checks of Final Timber Bridge

Deck- Bending/ Axial force check

Basisgegevens		
Partiële veiligheidsfactor \ \ gamma_ {M} voor Gelijmd gelamineerd hout	1.25	

Materiaalgegevens		
Buigend (fm,k)	26.0	MPa
Spanning (ft,0,k)	20.8	MPa
Spanning (ft,90,k)	0.5	MPa
Compressie (fc,0,k)	26.0	MPa
Compressie (fc,90,k)	2.5	MPa
Afschuiving (fv,k)	3.5	MPa
Houtsoort	Gelijmd gelamineerd	

Let op: Volgens EN 1995-1-1 artikel 6.6 wordt de ontwerp sterkte van deze staaf verhoogd met een systeem kracht factor k_ {sys} van 1.10

De kritische controle is op positie **1.200** m.

Interne krachten		
NEd	488.38	kN
Vy,Ed	-2.74	kN
Vz,Ed	0.00	kN
TEd	0.00	kNm
My,Ed	0.00	kNm
Mz,Ed	77.91	kNm

Opmerking: Asdefinitie:
- y-hoofdas in deze normcontrole verwijst naar de z-hoofdas in SCIA Engineer
- z-hoofdas in deze normcontrole verwijst naar de y-hoofdas in SCIA Engineer

Modificatiefactor	
Service Klasse	3
Belastingsduur	Onmiddellijk
Modificatie factor kmod	0.90

Buiging
Volgens EN 1995-1-1 artikel 6.1.6 en formule (6.11),(6.12)

σm,z,d	15.5	MPa
kh,z	1.00	
fm,z,d	20.6	MPa
km	0.70	

Eenheidscontrole (6.11) = 0.00 + 0.53 = 0.53 -
Eenheidscontrole (6.12) = 0.00 + 0.75 = 0.75 -

Gecombineerd Buig- en Axiale trek
Volgens EN 1995-1-1 artikel 6.2.3 en formule (6.17),(6.18)

ft,0,d	16.5	MPa
fm,z,d	20.6	MPa
km	0.70	

Eenheidscontrole (6.17) = 0.17 + 0.00 + 0.53 = 0.69 -
Eenheidscontrole (6.18) = 0.17 + 0.00 + 0.75 = 0.92 -

De staaf voldoet aan de doorsnedecontrole.

..:: STABILITEITSCONTROLE ::..

De staaf voldoet aan de stabiliteitscontrole.

Deck- Shear/ Torsion Check

Basisgegevens		
Partiële veiligheidsfactor \ \ gamma_ {M} voor Gelijmd gelamineerd hout	1.25	

Materiaalgegevens		
Buigend (fm,k)	26.0	MPa
Spanning (ft,0,k)	20.8	MPa
Spanning (ft,90,k)	0.5	MPa
Compressie (fc,0,k)	26.0	MPa
Compressie (fc,90,k)	2.5	MPa
Afschuiving (fv,k)	3.5	MPa
Houtsoort	Gelijmd gelamineerd	

Let op: Volgens EN 1995-1-1 artikel 6.6 wordt de ontwerp sterkte van deze staaf verhoogd met een systeem kracht factor k_ {sys} van 1.10

De kritische controle is op positie **0.000** m.

Interne krachten		
NEd	513.00	kN
Vy,Ed	207.15	kN
Vz,Ed	0.00	kN
TEd	0.00	kNm
My,Ed	0.00	kNm
Mz,Ed	-43.61	kNm

Opmerking: Asdefinitie:
- y-hoofdas in deze normcontrole verwijst naar de z-hoofdas in SCIA Engineer
- z-hoofdas in deze normcontrole verwijst naar de y-hoofdas in SCIA Engineer

Modificatiefactor	
Service Klasse	3
Belastingsduur	Onmiddellijk
Modificatie factor kmod	0.90

Afschuiving
Volgens EN 1995-1-1 artikel 6.1.7 en formule (6.13)

kcr	1.00	
τy,d	1.7	MPa
fv,d	2.8	MPa
Eenheidscontrole τy	0.63	-

Deck- Compression perpendicular to the grain

In [1]:
```
import numpy as np
Fc90= 207.15 #kN, Force perpendicular to grain
b= 1045.5 #mm, Width of beam
l = 375 #mm, Contact length
kc90= 1 #factor, see EN 1995-1-1, 6.1.5
fc90d= 1.8 # Design value compression strength perp. to the grain

sig90d = ((Fc90*1000)/(l*b))
print("Pressure parallel to the grain=",sig90d,'MPa')
UC=(sig90d)/(kc90*fc90d)
print("UC=",UC)
```

```
Pressure parallel to the grain= 0.5283596365375418 MPa
UC= 0.29353131140974546
```

Main Beam- Bending/ Axial force check

Basisgegevens	
Partiële veiligheidsfactor \ \ gamma_ {M} voor Gelijmd gelamineerd hout	1.25

Materiaalgegevens		
Buigend (fm,k)	26.0	MPa
Spanning (ft,0,k)	20.8	MPa
Spanning (ft,90,k)	0.5	MPa
Compressie (fc,0,k)	26.0	MPa
Compressie (fc,90,k)	2.5	MPa
Afschuiving (fv,k)	3.5	MPa
Houtsoort	Gelijmd gelamineerd	

De kritische controle is op positie **2.500** m.

Interne krachten		
NEd	350.35	kN
Vy,Ed	2.44	kN
Vz,Ed	-77.06	kN
TEd	-39.16	kNm
My,Ed	1167.73	kNm
Mz,Ed	-3.21	kNm

Modificatiefactor	
Service Klasse	3
Belastingsduur	Onmiddellijk
Modificatie factor kmod	0.90

Buiging

Volgens EN 1995-1-1 artikel 6.1.6 en formule (6.11),(6.12)

σm,y,d	17.3	MPa
kh,y	1.00	
fm,y,d	18.7	MPa
σm,z,d	0.0	MPa
kh,z	1.00	
fm,z,d	18.7	MPa
km	0.70	

Eenheidscontrole (6.11) = 0.92 + 0.00 = 0.93 -
Eenheidscontrole (6.12) = 0.65 + 0.00 = 0.65 -

Gecombineerd Buig- en Axiale trek

Volgens EN 1995-1-1 artikel 6.2.3 en formule (6.17),(6.18)

ft,0,d	15.0	MPa
fm,y,d	18.7	MPa
fm,z,d	18.7	MPa
km	0.70	

Eenheidscontrole (6.17) = 0.04 + 0.92 + 0.00 = 0.97 -
Eenheidscontrole (6.18) = 0.04 + 0.65 + 0.00 = 0.69 -

De staaf voldoet aan de doorsnedecontrole.

..:: STABILITEITSCONTROLE ::..

Balken onderworpen aan buiging of gecombineerde buiging en compressie

Volgens EN 1995-1-1 artikel 6.3.3 en formule (6.33),(6.35)

Kip Parameters		
Elastisch kritisch moment My,crit	111637.52	kNm
Kritische buigspanning σm,crit	1653.2	MPa
Relatieve slankheid λrel,m	0.13	-
Reductie factor kcrit	1.00	-

Eenheidscontrole (6.33) = 0.92 -

My,crit Parameters		
G0,05	631.3	MPa
LTB lengte L	2.500	m
Lef/L	0.90	
Effectieve lengte Lef	2.250	m
Invloed van lastpositie	geen invloed	

De staaf voldoet aan de stabiliteitscontrole.

Main Beam- Shear/ Torsion Check

Basisgegevens	
Partiële veiligheidsfactor \ \ gamma_ {M} voor Gelijmd gelamineerd hout	1.25

Materiaalgegevens		
Buigend (fm,k)	26.0	MPa
Spanning (ft,0,k)	20.8	MPa
Spanning (ft,90,k)	0.5	MPa
Compressie (fc,0,k)	26.0	MPa
Compressie (fc,90,k)	2.5	MPa
Afschuiving (fv,k)	3.5	MPa
Houtsoort	Gelijmd gelamineerd	

De kritische controle is op positie **7.800** m.

Interne krachten		
NEd	252.85	kN
Vy,Ed	-0.59	kN
Vz,Ed	-896.99	kN
TEd	7.42	kNm
My,Ed	-594.92	kNm
Mz,Ed	-0.35	kNm

Modificatiefactor	
Service Klasse	3
Belastingsduur	Onmiddellijk
Modificatie factor kmod	0.90

Afschuiving

Volgens EN 1995-1-1 artikel 6.1.7 en formule (6.13)

kcr	1.00	
τy,d	0.0	MPa
τz,d	2.5	MPa
fv,d	2.5	MPa
Eenheidscontrole τy	0.00	-
Eenheidscontrole τz	0.98	-
Eenheidscontrole Interactie	0.96	-

Opmerking: De interactie vergelijking is toegevoegd als een NCCI.

Torsie

Volgens EN 1995-1-1 artikel 6.1.8 en formule (6.14)

τtor,d	0.1	MPa
kshape	1.05	
fv,d	2.5	MPa
Eenheidscontrole	0.03	-
Eenheidscontrole Interactie Afschuiving	1.00	-

Main Beam- Compression perpendicular to the grain, edge of beam

Naam	dx [m]	Belasting	N [kN]	V_y [kN]	V_z [kN]	M_x [kNm]	M_y [kNm]	M_z [kNm]
S2	0.000	23/1	**365.91**	0.09	27.60	3.90	0.32	-0.06
S2	0.000	12-2/2	**401.86**	2.65	180.01	4.44	-0.78	-2.94
S2	0.000	2/3	399.90	-2.82	382.96	**37.26**	-0.74	2.04
S2	0.000	7-2/4	401.75	2.31	419.34	**0.63**	-1.83	-3.17
S2	0.000	3/5	399.95	-3.16	**518.43**	19.10	-1.59	1.94

```
import numpy as np
Fc90= 518.43 #kN, Force perpendicular to grain
b= 730 #mm, Width of beam
l = 400 #mm, Contact length
kc90= 1 #factor, see EN 1995-1-1, 6.1.5
fc90d= 1.8 # Design value compression strength perp. to the grain

sig90d = ((Fc90*1000)/(l*b))
print("Pressure parallel to the grain=",sig90d,'MPa')
UC=(sig90d)/(kc90*fc90d)
print("UC=",UC)
```

```
Pressure parallel to the grain= 1.7754452054794518 MPa
UC= 0.9863584474885844
```

Outer Cross Beam- Bending/ Axial force check

Basisgegevens	
Partiële veiligheidsfactor \ \ gamma_ {M} voor Gelijmd gelamineerd hout	1.25

Materiaalgegevens		
Buigend (fm,k)	26.0	MPa
Spanning (ft,0,k)	20.8	MPa
Spanning (ft,90,k)	0.5	MPa
Compressie (fc,0,k)	26.0	MPa
Compressie (fc,90,k)	2.5	MPa
Afschuiving (fv,k)	3.5	MPa
Houtsoort	Gelijmd gelamineerd	

De kritische controle is op positie **1.261** m.

Interne krachten		
NEd	-9.12	kN
Vy,Ed	3.36	kN
Vz,Ed	-0.96	kN
TEd	-0.19	kNm
My,Ed	0.36	kNm
Mz,Ed	81.16	kNm

Opmerking: Asdefinitie:
- y-hoofdas in deze normcontrole verwijst naar de z-hoofdas in SCI
- z-hoofdas in deze normcontrole verwijst naar de y-hoofdas in SCI

Modificatiefactor		
Service Klasse	3	
Belastingsduur	Onmiddellijk	
Modificatie factor kmod	0.90	

Buiging
Volgens EN 1995-1-1 artikel 6.1.6 en formule (6.11),(6.12)

σm,y,d	0.1	MPa
kh,y	1.05	
fm,y,d	19.6	MPa
σm,z,d	17.8	MPa
kh,z	1.00	
fm,z,d	18.7	MPa
km	0.70	

Eenheidscontrole (6.11) = 0.00 + 0.67 = 0.67 -
Eenheidscontrole (6.12) = 0.00 + 0.95 = 0.95 -

Compressie parallel aan de vezel
Volgens EN 1995-1-1 artikel 6.1.4 en formule (6.2)

σc,0,d	0.1	MPa
fc,0,d	18.7	MPa
Eenheidscontrole	0.00	-

Gecombineerde Buiging en Axiale druk
Volgens EN 1995-1-1 artikel 6.2.4 en formule (6.19),(6.20)

fc,0,d	18.7	MPa
fm,y,d	19.6	MPa
fm,z,d	18.7	MPa
km	0.70	

Eenheidscontrole (6.19) = 0.00 + 0.00 + 0.67 = 0.67 -
Eenheidscontrole (6.20) = 0.00 + 0.00 + 0.95 = 0.95 -

De staaf voldoet aan de doorsnedecontrole.

..:: STABILITEITSCONTROLE ::..

Kolommen onderworpen aan compressie of gecombineerde compressie en buiging
Volgens EN 1995-1-1 artikel 6.3.2 en formule (6.23),(6.24)

Knikparameters	yy	zz	
Zijd. flex. type	Zijdelings stijf	Zijdelings flexibel	
Systeemlengte L	2.360	2.360	m
Knikfactor k	0.65	1.00	
Kniklengte Lcr	1.544	2.360	m
Slankheid λ	14.27	30.27	-
Relatieve slankheid λ	0.23	0.49	-
Limietslankheid	0.30	0.30	-
Imperfectie βc	0.10	0.10	-
Reductie factor kc	1.00	0.98	-

Eenheidscontrole (6.23) = 0.00 + 0.00 + 0.67 = 0.67 -
Eenheidscontrole (6.24) = 0.00 + 0.00 + 0.95 = 0.96 -

Outer Cross Beam- Shear/ Torsion check

Basisgegevens	
Partiële veiligheidsfactor \ \ gamma_ {M} voor Gelijmd gelamineerd hout	1.25

Materiaalgegevens		
Buigend (fm,k)	26.0	MPa
Spanning (ft,0,k)	20.8	MPa
Spanning (ft,90,k)	0.5	MPa
Compressie (fc,0,k)	26.0	MPa
Compressie (fc,90,k)	2.5	MPa
Afschuiving (fv,k)	3.5	MPa
Houtsoort	Gelijmd gelamineerd	

De kritische controle is op positie **2.360** m.

Interne krachten		
NEd	-8.92	kN
Vy,Ed	-168.38	kN
Vz,Ed	-1.64	kN
TEd	-0.19	kNm
My,Ed	-1.07	kNm
Mz,Ed	0.00	kNm

Opmerking: Asdefinitie:
- y-hoofdas in deze normcontrole verwijst naar de z-hoofdas in SCIA Engineer
- z-hoofdas in deze normcontrole verwijst naar de y-hoofdas in SCIA Engineer

Modificatiefactor	
Service Klasse	3
Belastingsduur	Onmiddellijk
Modificatie factor kmod	0.90

Afschuiving
Volgens EN 1995-1-1 artikel 6.1.7 en formule (6.13)

kcr	1.00	
τy,d	2.5	MPa
τz,d	0.0	MPa
fv,d	2.5	MPa
Eenheidscontrole τy	0.99	-
Eenheidscontrole τz	0.01	-
Eenheidscontrole Interactie	0.98	-

Torsie
Volgens EN 1995-1-1 artikel 6.1.8 en formule (6.14)

τtor,d	0.0	MPa
kshape	1.07	
fv,d	2.5	MPa
Eenheidscontrole	0.01	-
Eenheidscontrole Interactie Afschuiving	0.99	-

Opmerking: De interactie vergelijking is toegevoegd als een NCCI.

Outer Cross Beam- Compression perpendicular to the grain

```
import numpy as np
Fc90= 168.38 #kN, Force perpendicular to grain
b= 375 #mm, Width of beam
l = 260 #mm, Contact length
kc90= 1 #factor, see EN 1995-1-1, 6.1.5
fc90d= 1.8 # Design value compression strength perp. to the grain

sig90d = ((Fc90*1000)/(l*b))
print("Pressure parallel to the grain=",sig90d,'MPa')
UC=(sig90d)/(kc90*fc90d)
print("UC=",UC)
```

```
Pressure parallel to the grain= 1.726974358974359 MPa
UC= 0.9594301994301994
```

Inner Cross Beam- Bending/ Axial force check

Basisgegevens		
Partiële veiligheidsfactor \ \ gamma_ {M} voor Gelijmd gelamineerd hout	1.25	

Materiaalgegevens		
Buigend (fm,k)	26.0	MPa
Spanning (ft,0,k)	20.8	MPa
Spanning (ft,90,k)	0.5	MPa
Compressie (fc,0,k)	26.0	MPa
Compressie (fc,90,k)	2.5	MPa
Afschuiving (fv,k)	3.5	MPa
Houtsoort	Gelijmd gelamineerd	

De kritische controle is op positie **1.261** m.

Interne krachten		
NEd	-3.29	kN
Vy,Ed	-0.15	kN
Vz,Ed	-0.40	kN
TEd	-0.84	kNm
My,Ed	1.58	kNm
Mz,Ed	178.18	kNm

Opmerking: Asdefinitie:
- y-hoofdas in deze normcontrole verwijst naar de z-hoofdas in SCIA Engi
- z-hoofdas in deze normcontrole verwijst naar de y-hoofdas in SCIA Engi

Modificatiefactor	
Service Klasse	3
Belastingsduur	Onmiddellijk
Modificatie factor kmod	0.90

Buiging

Volgens EN 1995-1-1 artikel 6.1.6 en formule (6.11),(6.12)

σm,y,d	0.1	MPa
kh,y	1.01	
fm,y,d	18.8	MPa
σm,z,d	13.9	MPa
kh,z	1.00	
fm,z,d	18.7	MPa
km	0.70	

Eenheidscontrole (6.11) = 0.00 + 0.52 = 0.53 -
Eenheidscontrole (6.12) = 0.00 + 0.74 = 0.75 -

Gecombineerde Buiging en Axiale druk

Volgens EN 1995-1-1 artikel 6.2.4 en formule (6.19),(6.20)

fc,0,d	18.7	MPa
fm,y,d	18.8	MPa
fm,z,d	18.7	MPa
km	0.70	

Kolommen onderworpen aan compressie of gecombineerde compressie en buiging

Volgens EN 1995-1-1 artikel 6.3.2 en formule (6.23),(6.24)

Knikparameters	yy	zz	
Zijd. flex. type	Zijdelings stijf	Zijdelings flexibel	
Systeemlengte L	2.360	2.360	m
Knikfactor k	0.68	1.00	
Kniklengte Lcr	1.613	2.360	m
Slankheid λ	9.98	22.09	-
Relatieve slankheid λ	0.16	0.36	-
Limietslankheid	0.30	0.30	-
Imperfectie βc	0.10	0.10	-
Reductie factor kc	1.00	0.99	-

Eenheidscontrole (6.23) = 0.00 + 0.00 + 0.52 = 0.53 -
Eenheidscontrole (6.24) = 0.00 + 0.00 + 0.74 = 0.75 -

Balken onderworpen aan buiging of gecombineerde buiging en compressie

Volgens EN 1995-1-1 artikel 6.3.3 en formule (6.33),(6.35)

Kip Parameters		
Elastisch kritisch moment My,crit	13560.09	kNm
Kritische buigspanning σm,crit	701.2	MPa
Relatieve slankheid λrel,m	0.19	-
Reductie factor kcrit	1.00	-

Eenheidscontrole (6.33) = 0.00 -
Eenheidscontrole (6.35) = 0.00 + 0.00 = 0.00 -

My,crit Parameters		
G0,05	631.3	MPa
LTB lengte L	2.360	m
Lef/L	0.90	
Effectieve lengte Lef	2.124	m
Invloed van lastpositie	geen invloed	

Inner Cross Beam- Shear/ Torsion check

Combinatiesleutel
Checkings / 1.25*BG1 + 1.25*Spread + 1.50*Spread1 + 1.20*Rem_versnelling + 1.50*Lanes_4 + 1.65*Wind_Z + 1.65*Wind_Langs + 1.65*Wind_dwars_1

Basisgegevens	
Partiële veiligheidsfactor \ \ gamma_ {M} voor Gelijmd gelamineerd hout	1.25

Materiaalgegevens		
Buigend (fm,k)	26.0	MPa
Spanning (ft,0,k)	20.8	MPa
Spanning (ft,90,k)	0.5	MPa
Compressie (fc,0,k)	26.0	MPa
Compressie (fc,90,k)	2.5	MPa
Afschuiving (fv,k)	3.5	MPa
Houtsoort	Gelijmd gelamineerd	

De kritische controle is op positie **2.360** m.

Interne krachten		
NEd	-3.23	kN
Vy,Ed	-340.57	kN
Vz,Ed	2.70	kN
TEd	-0.84	kNm
My,Ed	5.20	kNm
Mz,Ed	0.00	kNm

Opmerking: Asdefinitie:
- y-hoofdas in deze normcontrole verwijst naar de z-hoofdas in SCIA Engineer
- z-hoofdas in deze normcontrole verwijst naar de y-hoofdas in SCIA Engineer

Modificatiefactor	
Service Klasse	3
Belastingscuur	Onmiddellijk
Modificatie factor kmod	0.90

Afschuiving
Volgens EN 1995-1-1 artikel 6.1.7 en formule (6.13)

kcr	1.00	
τy,d	2.5	MPa
τz,d	0.0	MPa
fv,d	2.5	MPa
Eenheidscontrole τy	0.98	-
Eenheidscontrole τz	0.01	-
Eenheidscontrole Interactie	0.96	

Opmerking: De interactie vergelijking is toegevoegd als een NCCI.

Torsie
Volgens EN 1995-1-1 artikel 6.1.8 en formule (6.14)

τtor,d	0.0	MPa
kshape	1.08	
fv,d	2.5	MPa
Eenheidscontrole	0.02	-
Eenheidscontrole Interactie Afschuiving	0.97	-

Opmerking: De interactie vergelijking is toegevoegd als een NCCI.

Inner Cross Beam- Compression perpendicular to the grain

```
import numpy as np
Fc90= 340.57 #kN, Force perpendicular to grain
b= 560 #mm, Width of beam
l = 340 #mm, Contact length
kc90= 1 #factor, see EN 1995-1-1, 6.1.5
fc90d= 1.8 # Design value compression strength perp. to the grain

sig90d = ((Fc90*1000)/(l*b))
print("Pressure parallel to the grain=",sig90d,'MPa')
UC=(sig90d)/(kc90*fc90d)
print("UC=",UC)
```

```
Pressure parallel to the grain= 1.7887079831932773 MPa
UC= 0.9937266573295984
```

Compression rod- Cross section checks

Partiële veiligheidsfactoren	
γ_{M0} voor weerstand van doorsneden	1.00
γ_{M1} voor weerstand tegen instabiliteit	1.00
γ_{M2} voor weerstand van netto-doorsneden	1.25

Materiaal			
Vloeisterkte	f_y	355.0	MPa
Treksterkte	f_u	490.0	MPa
Bouwwijze		Gewalst	

...::DOORSNEDECONTROLE::...

De kritische controle is op positie 0.960 m

Interne krachten		Berekende	Eenheid
Normaalkracht	N_{Ed}	-587.01	kN
Dwarskracht	$V_{y,Ed}$	9.12	kN
Dwarskracht	$V_{z,Ed}$	1088.69	kN
Torsie	T_{Ed}	0.00	kNm
Buigend moment	$M_{y,Ed}$	0.00	kNm
Buigend moment	$M_{z,Ed}$	0.00	kNm

Classificatie voor doorsnede-ontwerp
Classificatie volgens EN 1993-1-1 Artikel 5.5.2
Classificatie van interne en uitkragende onderdelen volgens EN 1993-1-1 tabel 5.2 blad 1 en 2

Id	Type	c [mm]	t [mm]	σ_1 [kN/m²]	σ_2 [kN/m²]	ψ [-]	k_σ [-]	ρ [-]	c/t [-]	Limiet klasse 1 [-]	Limiet klasse 2 [-]	Limiet klasse 3 [-]	Klasse
1	SO	116	26	2.693e+04	2.693e+04	1.00	0.43	1.00	4.46	7.32	8.14	11.39	1
3	SO	116	26	2.693e+04	2.693e+04	1.00	0.43	1.00	4.46	7.32	8.14	11.39	1
4	I	344	14	2.693e+04	2.693e+04	1.00		1.00	24.57	22.78	27.66	30.92	2
5	SO	116	26	2.693e+04	2.693e+04	1.00	0.43	1.00	4.46	7.32	8.14	11.39	1
7	SO	116	26	2.693e+04	2.693e+04	1.00	0.43	1.00	4.46	7.32	8.14	11.39	1

Opmerking: De classificatielimieten zijn ingesteld volgens Semi-Comp+.
De doorsnede is geclassificeerd als klasse 2

Drukcontrole
Volgens EN 1993-1-1 artikel 6.2.4 en formule (6.9)

Oppervlakte van de doorsnede	A	2.1800e-02	m^2
Drukweerstand	$N_{c,Rd}$	7739.00	kN
Eenheidscontrole		0.08	-

Dwarskrachtcontrole voor V_y
Volgens EN 1993-1-1 artikel 6.2.6 en formule (6.17)

Correctiefactor voor dwarskracht	η	1.20	
Afschuifoppervlak	A_v	1.6174e-02	m^2
Plastische dwarskrachtweerstand voor V_y	$V_{pl,y,Rd}$	3315.01	kN
Eenheidscontrole		0.00	-

Drukcontrole
Volgens EN 1993-1-1 artikel 6.2.4 en formule (6.9)

Oppervlakte van de doorsnede	A	2.1800e-02	m^2
Drukweerstand	$N_{c,Rd}$	7739.00	kN
Eenheidscontrole		0.08	-

Dwarskrachtcontrole voor V_y
Volgens EN 1993-1-1 artikel 6.2.6 en formule (6.17)

Correctiefactor voor dwarskracht	η	1.20	
Afschuifoppervlak	A_v	1.6174e-02	m^2
Plastische dwarskrachtweerstand voor V_y	$V_{pl,y,Rd}$	3315.01	kN
Eenheidscontrole		0.00	-

Dwarskrachtcontrole voor V_z
Volgens EN 1993-1-1 artikel 6.2.6 en formule (6.17)

Correctiefactor voor dwarskracht	η	1.20	
Afschuifoppervlak	A_v	7.9680e-03	m^2
Plastische dwarskrachtweerstand voor V_z	$V_{pl,z,Rd}$	1633.12	kN
Eenheidscontrole		0.67	-

Controle voor gecombineerde buiging, axiale kracht en Dwarskracht
Volgens EN 1993-1-1 artikel 6.2.1(5) en formule (6.1)

Elastische toetsing			
Vezel		8	
Normaalspanning ten gevolge van de normaal kracht N	$\sigma_{N,Ed}$	26.9	MPa
Normaalspanning ten gevolge van het buigend moment M_y	$\sigma_{My,Ed}$	0.0	MPa
Normaalspanning ten gevolge van het buigend moment M_z	$\sigma_{Mz,Ed}$	0.0	MPa
Totale longitudinale spanning	$\sigma_{tot,Ed}$	26.9	MPa
Dwarskrachtspanning vanwege de dwarskracht in dwarsrichting V_y	$\tau_{Vy,Ed}$	0.0	MPa
Dwarskrachtspanning vanwege de dwarskracht in dwarsrichting V_z	$\tau_{Vz,Ed}$	193.7	MPa
Dwarskrachtspanning vanwege gelijkmatige (St. Venant) torsie	$\tau_{t,Ed}$	0.0	MPa
Totale schuifspanning	$\tau_{tot,Ed}$	193.7	MPa
Som van de Von Mises spanning	$\sigma_{von\ Mises,Ed}$	336.6	MPa
Eenheidscontrole		0.95	-

Compression rod- Stability Checks

Beslissende positie voor stabiliteitsclassificatie: 0.864 m
Classificatie volgens EN 1993-1-1 Artikel 5.5.2
Classificatie van interne en uitkragende onderdelen volgens EN 1993-1-1 tabel 5.2 blad 1 en 2

Id	Type	c [mm]	t [mm]	σ_1 [kN/m²]	σ_2 [kN/m²]	Ψ [-]	k_σ [-]	α [-]	c/t [-]	Limiet klasse 1 [-]	Limiet klasse 2 [-]	Limiet klasse 3 [-]	Klasse
1	SO	116	26	5.494e+04	5.580e+04	0.98	0.43	1.00	4.46	7.32	8.14	11.22	1
3	SO	116	26	5.443e+04	5.356e+04	0.98	0.44	1.00	4.46	7.32	8.14	11.29	1
4	I	344	14	4.944e+04	4.394e+03	0.09		1.00	24.57	22.78	27.66	45.21	2
5	SO	116	26	-1.098e+03	-1.965e+03								
7	SO	116	26	-5.899e+02	2.774e+02	-2.13	1.33	0.32	4.46	22.89	25.44	19.73	1

Opmerking: De classificatielimieten zijn ingesteld volgens Semi-Comp+.
De doorsnede is geclassificeerd als klasse 2

Buigingsknikcontrole
Volgens EN 1993-1-1 artikel 6.3.1.1 en formule (6.46)

Knikparameters		yy	zz	
Zijd. flex. type		Zijdelings flexibel	Zijdelings flexibel	
Systeemlengte	L	0.960	0.960	m
Knikfactor	k	10.00	5.68	
Kniklengte	l_{cr}	9.600	5.455	m
Kritische Euler last	N_{cr}	17965.92	8163.13	kN
Slankheid	λ	50.15	74.40	
Relatieve slankheid	λ_{rel}	0.66	0.97	
Limietslankheid	$\lambda_{rel,0}$	0.20	0.20	
Knikcurve		a	b	
Imperfectie	α	0.21	0.34	
Reductie factor	χ	0.87	0.61	
Knikweerstand	$N_{b,Rd}$	6712.15	4750.25	kN

Buigingsknikverificatie			
Oppervlakte van de doorsnede	A	2.1800e-02	m^2
Knikweerstand	$N_{b,Rd}$	4750.25	kN
Eenheidscontrole		0.12	-

Torsieknikcontrole
Volgens EN 1993-1-1 artikel 6.3.1.1 en formule (6.46)
Opmerking: Voor deze I-sectie de Torsieknikweerstand is hoger dan de weerstand van Buigknik. Om deze reden is de Torsieknik niet afgedrukt in de uitvoer.

Gecombineerde buig- en axiale drukcontrole
Volgens EN 1993-1-1 artikel 6.3.3 en formule (6.61),(6.62)

Buig- en axiale drukcontrole paramaters			
Interactie methode		alternatieve methode 2	
Oppervlakte van de doorsnede	A	2.1800e-02	m^2
Plastische doorsnedemodulus	$W_{pl,y}$	3.9820e-03	m^3
Plastische doorsnedemodulus	$W_{pl,z}$	1.1980e-03	m^3
Ontwerpdrukkracht	N_{Ed}	587.01	kN
Ontwerp buigend moment (maximum)	$M_{y,Ed}$	-1045.76	kNm
Ontwerp buigend moment (maximum)	$M_{z,Ed}$	-8.74	kNm

Buig- en axiale drukcontrole paramaters			
Karakteristieke drukweerstand	N_{Rk}	7739.00	kN
Karakteristieke momentweerstand	$M_{y,Rk}$	1413.61	kNm
Karakteristieke momentweerstand	$M_{z,Rk}$	425.29	kNm
Reductie factor	χ_y	0.87	
Reductie factor	χ_z	0.61	
Gewijzigde reductiefactor	$\chi_{LT,mod}$	1.00	
Interactiefactor	k_{yy}	0.94	
Interactiefactor	k_{yz}	0.63	
Interactiefactor	k_{zy}	0.56	
Interactiefactor	k_{zz}	1.05	

Maximum moment $M_{y,Ed}$ is afgeleid van balk S683 positie 0.000 m.
Maximum moment $M_{z,Ed}$ is afgeleid van balk S683 positie 0.000 m.

Interactie methode 2 parameters		
Methode voor interactiefactoren		Tabel B.1
Zijdelings flexibel type y		Zijdelings flexibel
Equivalente moment factor	C_{my}	0.90
Zijdelings flexibel type z		Zijdelings flexibel
Equivalente moment factor	C_{mz}	0.90
Resulterend belastingtype LT		lineair moment M
Ratio van uiteinde momenten	ψ_{LT}	0.00
Equivalente moment factor	C_{mLT}	0.60

Eenheidscontrole (6.61) = 0.09 + 0.69 + 0.01 = 0.79 -
Eenheidscontrole (6.62) = 0.12 + 0.42 + 0.02 = 0.56 -

Plooicontrole
Volgens EN 1993-1-5 artikel 5 & 7.1 en formule (5.10) & (7.1)

Plooiparameters			
Knik veldlengte	a	0.960	m
Lijf		niet-verstijfd	
Lijfhoogte	h_w	398	mm
Lijfdikte	t	14	mm
Materiaal coefficiënt	ε	0.81	
Correctiefactor voor dwarskracht	η	1.20	

Plooiverificatie			
Lijf slankheid		h_w/t	28.43
Lijfslankheid limiet			48.82

Opmerking: De slankheid van het lijf is zo dat de Plooi effecten kunnen worden genegeerd volgens EN 1993-1-5 artikel 5.1(2).

De staaf voldoet aan de stabiliteitscontrole.

Appendix E1: Timber Bridge Design Joints – Cross girder to main girder

Timber- Steel shear: Johansen M39

```
import numpy as np

pre = 1 #predrilled 1= yes, 0= no
d = 39 #mm diamter bolt
fuk = 1000 #MPa ultimate strength dowel
a1=  0 # Radians, grain angle
rho = 445 #density of woodses
t1= 208.5 #embedment depth
t2 = 178.25 #embedment depth, one side plate
t= 15 #mm Thickness of plate
FvEd= 96.38 #kN
FaxEd= 0 #kN
FvEd2 = 40.19 #kN
Faxrk = 1 # 1 for no extraction
alphav = 0.5 # Table 3.4 from EN 1993-1-8
ym2 = 1.25 #safety factor Steel ULS connections
k2 = 0.9 #Table 3.4 from EN 1993-1-8
Ax = 1 # No extraction as attached at ends

boltcheck = 1 # 1 for check of bolt on tension+shear
```

```
Myrk = 0.3*fuk*(d**2.6)
As = 0.25 * np.pi * (d **2)

if pre ==0:
    fhk = 0.082*rho*(d**(-0.3))
if pre == 1:
    fhk = 0.082*(1-0.01*d)*rho

print("Stuiksterkte, fhk=",fhk,'MPa')

k90= 1.35+0.015*d

fh1k= fhk/(k90*((np.sin(a1))**2)+((np.cos(a1))**2))
print("embedment strength 1=",fh1k,"MPa")
```

```
Stuiksterkte, fhk= 22.2589 MPa
embedment strength 1= 22.2589 MPa
```

```
Fvrkf = fh1k*t1*d
Fvrdf = Fvrkf/1300
print("Failure mode f=",Fvrdf,'kN')
Fvrkg= fh1k*t1*d*(((2+(4*Myrk)/(fh1k*d*(t1**2)))**0.5)-1)
Fvrkg = Fvrkg + 0.25*Ax*Fvrkg
Fvrdg= Fvrkg/1300
print("Failure mode g=",Fvrdg,'kN')
Fvrkh = 2.3 * ((Myrk*fh1k*d)**0.5)
Fvrkh = Fvrkg + 0.25*Ax*Fvrkh
Fvrdh = Fvrkh/1300
print("Failure mode h=",Fvrdh,'kN')

UC = FvEd/(min(Fvrdg,Fvrdh, Fvrdf))
print(UC)
```

```
Failure mode f= 139.2294195 kN
Failure mode g= 97.5766591817 kN
Failure mode h= 123.997903169 kN
0.987736214872
```

```
Fvrkf = fh1k*t2*d
Fvrkf = 0.25*Ax*Fvrkf + Fvrkf
Fvrdf = Fvrkf/1300
print("Failure mode f=",Fvrdf,'kN')
Fvrkg= fh1k*t2*d*(((2+(4*Myrk)/(fh1k*d*(t2**2)))**0.5)-1)
Fvrkg = Fvrkg + 0.25*Ax*Fvrkg
Fvrdg= Fvrkg/1300
print("Failure mode g=",Fvrdg,'kN')
Fvrkh = 2.3 * ((Myrk*fh1k*d)**0.5)
Fvrkh = Fvrkg + 0.25*Ax*Fvrkh
Fvrdh = Fvrkh/1300
print("Failure mode k=",Fvrdh,'kN')

UC = FvEd2/(min(Fvrdg,Fvrdh, Fvrdf))
print(UC)
```

```
Failure mode f= 148.786834688 kN
Failure mode g= 90.944898655 kN
Failure mode k= 117.366142642 kN
0.441915935851
```

M39 bolt check

```
# Check, EN 1993-1-8, 3.6.1; bolt subjected to shear and tensile force
if boltcheck ==1:
    Fvrdb =  ((alphav*fuk*(0.25*np.pi*(d**2)))/ym2)/1000
    print("Bolt shear resistance=", Fvrdb,"kN")
    Ftrd = (k2*fuk*As)/(ym2*1000)
    print("Bolt tensile resistance=",Ftrd,'kN')
    UC1 = FvEd/Fvrdb + (FaxEd/(1.4*Ftrd))
    print("Unity check, bolt on shear and tension=",UC1)
```

```
Bolt shear resistance= 162.86016316209486 kN
Bolt tensile resistance= 293.1482936917708 kN
Unity check, bolt on shear and tension= 0.436877862692452
```

Timber-Steel shear: Johansen M22:

```
import numpy as np

pre = 1 #predrilled 1= yes, 0= no
d = 22 #mm diamter bolt
fuk = 400 #MPa ultimate strength dowel
a1=  0 # Radians, grain angle
rho = 445 #density of woodses
t1= 320 #embedment depth
t= 15 #mm Thickness of plate
FvEd= 26.245 #kN
FaxEd= 12.78 #kN
Faxrk = 1 # 1 for no extraction
alphav = 0.5 # Table 3.4 from EN 1993-1-8
ym2 = 1.25 #safety factor Steel ULS connections
k2 = 0.9 #Table 3.4 from EN 1993-1-8

boltcheck = 1 # 1 for check of bolt on tension+shear
```

```
Myrk = 0.3*fuk*(d**2.6)

if pre ==0:
    fhk = 0.082*rho*(d**(-0.3))
if pre == 1:
    fhk = 0.082*(1-0.01*d)*rho

print("Stuiksterkte, fhk=",fhk,'MPa')

k90= 1.35+0.015*d

fh1k= fhk/(k90*((np.sin(a1))**2)+((np.cos(a1))**2))
print("embedment strength 1=",fh1k,"MPa")
```

```
Stuiksterkte, fhk= 28.462200000000003 MPa
embedment strength 1= 28.4622 MPa
```

```
Fvrk01 = 0.4 * fh1k*t1*d
Fvrk02 = 1.15 * ((2*Myrk*fh1k*d)**0.5)
Fvrk1 = (fh1k*t1*d)
Fvrk2 = fh1k*t1*d*(((2+(4*Myrk/(fh1k*d*(t1**2))))**0.5)-1)
Fvrk3 = 2.3*((2*Myrk*fh1k*d)**0.5)

if t >= d:
    Fvrd1= Fvrk1/1300
    Fvrd2 = (Fvrk2 + Faxrk*Fvrk2*0.25)/1300
    Fvrd3 = (Fvrk3 + Faxrk* Fvrk3*0.25)/1300
    print("Strengths according to failure mechanisms, including safety factor 1.3")
    print("Failure mode c (brittle)=", Fvrd1,'kN')
    print("Failure mode d (ductile)=", Fvrd2, 'kN')
    print("Failure mode e (ductile)=", Fvrd3, 'kN')
    Fvrd= min(Fvrd1,Fvrd2,Fvrd3)
    if Fvrd == Fvrd1:
        print("brittle failure, adjust and continue")
    UC= FvEd/Fvrd
    print("Unity check timber shear connection=",UC)

if  t <= 0.5*d:
    Fvrd01 = (Fvrk01/1300)
    Fvrd02 = (Fvrk02 + Faxrk*Fvrk02*0.25)/1300
    print("Strengths according to failure mechanisms, including safety factor 1.3")
    print("Failure mode a (ductile)=", Fvrd01,'kN')
    print("Failure mode b (ductile)=", Fvrd02, 'kN')
    Fvrd= min(Fvrd01,Fvrd02)
    UC= FvEd/Fvrd
    print("Unity check timber shear connection=",UC)

if 0.5*d < t <d:

    Fvrd01 = (Fvrk01/1300)
    Fvrd02 = (Fvrk02 + Faxrk*Fvrk02*0.25)/1300
    Fvrd1= Fvrk1/1300
    Fvrd2 = (Fvrk2 + Faxrk*Fvrk2*0.25)/1300
    Fvrd3 = (Fvrk3 + Faxrk* Fvrk3*0.25)/1300
    print("Strengths according to failure mechanisms, including safety factor 1.3")

    Inter1= Fvrd01 + (t- 0.5*d)*((Fvrd2-Fvrd01)/(d- 0.5*d))
    Inter2= Fvrd02 + (t- 0.5*d)*((Fvrd3-Fvrd02)/(d- 0.5*d))

    print("Failure mode c (brittle)=", Fvrd1,'kN')
    print("Failure mode a =", Fvrd01,'kN')
    print("Failure mode d =", Fvrd2,'kN')
    print("Failure mode a and d, linearly interpolated ", Inter1,'kN')
    print("Failure mode b =", Fvrd02,'kN')
    print("Failure mode e =", Fvrd3,'kN')
    print("Failure mode b and e, linearly interpolated ", Inter2,'kN')
    Fvrd = min(Inter1,Inter2)
    UC = FvEd/Fvrd
    print("Unity check timber shear connection=", UC)
```

```
Strengths according to failure mechanisms, including safety factor 1.3
Failure mode c (brittle)= 154.13376 kN
Failure mode a = 61.653504 kN
Failure mode d = 81.3777583841 kN
Failure mode a and d, linearly interpolated  68.8259601397 kN
Failure mode b = 23.8377455896 kN
Failure mode e = 47.6754911792 kN
Failure mode b and e, linearly interpolated  32.5060167131 kN
Unity check timber shear connection= 0.807388989911
```

M22 bolt check

```
# Check, EN 1993-1-8, 3.6.1; bolt subjected to shear and tensile force
if boltcheck ==1:
    Fvrdb =  ((alphav*fuk*(0.25*np.pi*(d**2)))/ym2)/1000
    print("Bolt shear resistance=", Fvrdb,"kN")
    Ftrd = (k2*fuk*As)/(ym2*1000)
    print("Bolt tensile resistance=",Ftrd,'kN')
    UC1 = FvEd/Fvrdb + (FaxEd/(1.4*Ftrd))
    print("Unity check, bolt on shear and tension=",UC1)
```

```
Bolt shear resistance= 60.821233773498406 kN
Bolt tensile resistance= 87.264 kN
Unity check, bolt on shear and tension= 0.5361235788586317
```

Timber, compression perpendicular to the grain, cross beam

```
import numpy as np
Fc90= 340.77 #kN, Force perpendicular to grain
b= 565 #mm, Width of beam
l = 380 #mm, Contact length
kc90= 1 #factor, see EN 1995-1-1, 6.1.5
fc90d= 1.8 # Design value compression strength perp. to the grain

sig90d = ((Fc90*1000)/(l*b))
print("Pressure parallel to the grain=",sig90d,'MPa')
UC=(sig90d)/(kc90*fc90d)
print("UC=",UC)
```

```
Pressure parallel to the grain= 1.5871914299021892 MPa
UC= 0.8817730166123273
```

Timber, tension perpendicular to the grain main beam

```
F = 340.77*1000 #kN Force applied
ar = 505 #distance covered by fasteners in grain direction
n = 3 #number of fastener rows
h1 = 200 # mm highest row of fasteners location
he = 850 # mm, bottom of beam to top fastener row location
hi= np.array([200,288,480]) #mm, row of fasteners to be checked location
h = 1050
tef = 240 #mm penetration depth
ft90 = (0.5/1.25) *0.9 # MPa, including factors

ks = 0.7 + 1.4 * (ar/h)
som = 0
if ks < 1:
    ks = 1
print("ks=", ks)
for i in range(n):
    som = som + ((h1/hi[i])**2)
kr = n/som
print("kr=",kr)

F90rD = ks * kr *(6.5+ 18* ((he/h)**2))*((tef*h)**0.8)*ft90
print("Capacity for wood splitting=",F90rD/1000,'kN')
UC = F/F90rD
print("UC=",UC)
```

```
ks= 1.3733333333333333
kr= 1.81174277726
Capacity for wood splitting= 343.280905579 kN
UC= 0.992685565849
```

Axial pullout strength of bolt in Timber

```python
import numpy as np
Fax= 24 #kN axial load effect
d = 22 # Diameter fastener
fyd = 1000/1.25 # Fastener design strength
A= 0.25*np.pi*d**2
lad = 320 #mm glued in length

if lad <250:
    fk1k= 4
if 250<=lad<500:
    fk1k= 5.25 - 0.005*lad
if 500<= lad <= 1000:
    fk1k= 3.5- 0.0015*lad
fk1d= fk1k/1.3

if lad < max(0.5*d**2, 10*d):
    print("increase glued in length")


Faxrd1 = A*fyd
Faxrd2 = np.pi*d*lad*fk1d
print("Faxrd1=",Faxrd1/1000,'kN')
print("Faxrd2=",Faxrd2/1000,'kN')
UC = Fax/min(Faxrd1/1000,Faxrd2/1000)
print("UC=",UC)
```

```
Faxrd1= 304.106168867492 kN
Faxrd2= 62.097203712802546 kN
UC= 0.38649083316213695
```

Appendix E2: Timber Bridge Design Joints – HEA 450 to Main beam

Spacings of dowels applied

```
d = 16 #mm, diameter dowel
R2 = 405 #mm Large radius
R1 = 325 #mm Small radius
R0 = 245 #mm Smaller radius
R00= 165 #mm Smallest radius


C2 = 2*np.pi*R2
C1 = 2*np.pi*R1
C0 = 2*np.pi*R0
C00 = 2*np.pi*R00



print("large circumference=",C2,'mm')
print("small circiumference=",C1,"mm")
print("smaller circiumference=",C0,"mm")
print("smallest circiumference=",C00,"mm")

N2= C2/(6*d)

N2= int(N2)
print("# Dowels in outer circle=",N2)
N1= C1/(6*d)

N1= int(N1)
print("# Dowels in inner circle=",N1)

N0= C0/(6*d)

N0= int(N0)
print("# Dowels in innerer circle=",N0)

N00= C00/(6*d)

N00= int(N00)
print("# Dowels in innerer circle=",N00)

n = N2+N1+N0+N00
print("Total dowels=",n)
```

```
large circumference= 2544.690049407732 mm
small circiumference= 2042.0352248333654 mm
smaller circiumference= 1539.3804002589986 mm
smallest circiumference= 1036.7255756846316 mm
# Dowels in outer circle= 26
# Dowels in inner circle= 21
# Dowels in innerer circle= 16
# Dowels in innerer circle= 10
Total dowels= 73
```

Forces after spring application in Bridge model

ULS and SLS forces in HEA 450

Staaf	css	dx [m]	Belasting	N [kN]	Vy [kN]	Vz [kN]	Mx [kNm]	My [kNm]	Mz [kNm]
S651	push2 - HEA450	0.000	NC_17-2	**-763.39**	57.00	-85.64	-0.14	82.67	-55.44
S685	push2 - HEA450	0.000	NC_1-1	**-171.26**	50.61	103.54	0.73	-99.48	-48.69
S682	push2 - HEA450	0.000	NC33	-640.80	**-183.19**	75.67	-2.25	-73.14	**176.34**
S685	push2 - HEA450	0.000	NC_10	-273.96	**77.08**	236.28	2.20	-227.13	**-74.24**
S587	push2 - HEA450	0.000	NC30	-555.43	-70.44	**-570.56**	5.97	**549.13**	68.29
S683	push2 - HEA450	0.000	NC_19-2	-632.72	7.88	**725.03**	-2.91	**-698.10**	-7.64
S682	push2 - HEA450	0.000	NC_20-2	-568.67	-145.58	546.76	**-10.48**	-526.27	140.37
S587	push2 - HEA450	0.000	NC29	-570.50	-73.99	-559.82	**5.97**	538.83	71.73

Staaf	css	dx [m]	Belasting	N [kN]	Vy [kN]	Vz [kN]	Mx [kNm]	My [kNm]	Mz [kNm]
S651	push2 - HEA450	0.000	NC_26	**-435.61**	29.64	-131.52	0.00	126.51	-28.66
S655	push2 - HEA450	0.000	NC_24-5	**-61.43**	20.08	-55.32	-0.13	53.12	-19.30
S682	push2 - HEA450	0.000	NC47	-348.53	**-104.68**	8.62	-0.35	-8.34	**100.82**
S685	push2 - HEA450	0.000	NC47	-137.84	**46.42**	55.24	0.32	-53.07	**-44.65**
S587	push2 - HEA450	0.000	NC47	-284.54	-34.70	**-298.38**	**1.69**	**286.83**	33.42
S683	push2 - HEA450	0.000	NC_26	-373.45	2.37	**411.06**	-0.96	**-395.31**	-2.29
S682	push2 - HEA450	0.000	NC_26	-318.49	-83.65	311.11	**-3.47**	-299.10	80.73

ULS and SLS forces in Centre of Main Beam

Staaf	css	dx [m]	Belasting	N [kN]	Vy [kN]	Vz [kN]	Mx [kNm]	My [kNm]	Mz [kNm]
S652	Infinitestiff - Cirkel	0.525	NC_17-2	**-763.17**	-57.00	-85.64	-0.22	-127.73	-85.40
S658	Infinitestiff - Cirkel	0.525	NC_1-1	**-171.20**	-50.61	103.54	1.13	153.84	-75.24
S658	Infinitestiff - Cirkel	0.525	NC_10	-273.87	**-77.08**	236.28	3.41	351.18	**-114.66**
S664	Infinitestiff - Cirkel	0.525	NC33	-641.03	**183.19**	75.67	-3.48	113.03	**271.84**
S650	Infinitestiff - Cirkel	0.525	NC30	-555.33	70.43	**-570.56**	9.22	**-848.66**	105.29
S662	Infinitestiff - Cirkel	0.525	NC_19-2	-632.48	-7.88	**725.03**	-4.49	**1078.74**	-11.78
S664	Infinitestiff - Cirkel	0.525	NC_20-2	-568.82	145.58	546.75	**-16.19**	813.35	216.45
S650	Infinitestiff - Cirkel	0.525	NC29	-570.29	73.99	-559.82	**9.22**	-832.72	110.58

Staaf	css	dx [m]	Belasting	N [kN]	Vy [kN]	Vz [kN]	Mx [kNm]	My [kNm]	Mz [kNm]
S652	Infinitestiff - Cirkel	0.525	NC_26	**-435.38**	-29.64	-131.52	0.00	-195.56	-44.21
S656	Infinitestiff - Cirkel	0.525	NC_24-5	**-61.42**	-20.08	-55.32	-0.20	-82.16	-29.84
S658	Infinitestiff - Cirkel	0.525	NC47	-137.78	**-46.42**	55.24	0.50	82.07	**-69.00**
S664	Infinitestiff - Cirkel	0.525	NC47	-348.66	**104.68**	8.62	-0.54	12.89	**155.65**
S650	Infinitestiff - Cirkel	0.525	NC47	-284.42	34.70	**-298.38**	**2.62**	**-443.48**	51.61
S662	Infinitestiff - Cirkel	0.525	NC_26	-373.37	-2.37	**411.06**	-1.49	**611.11**	-3.53
S664	Infinitestiff - Cirkel	0.525	NC_26	-318.59	83.65	311.10	**-5.36**	462.42	124.65

Spring stiffness, Dowel force determination and Johansen checks

```
M = 1067.269/3 #kNm, moment
V = 717.32 #kN, shear force
N = 629.78/3 #kN, Normal force

Ms= M*10**6
V = V*1000
N = N*1000
```

```
rho = 445 # density of wood
Kser = 2*(1/23)*(rho**1.5)*d
K = (2/3)*Kser
print("Stiffness of dowel plane=",K,"N/mm")
Kr = N2*K*(R2**2)+ N1*K*(R1**2) + N0*K*(R0**2) + N00*K*(R00**2)
print("Rotational stiffness per shear plane=",Kr,"Nmm/rad")

Fm2 = ((K*R2)/(Kr))* Ms
Fm1 = ((K*R1)/(Kr))* Ms
Fm0 = ((K*R0)/(Kr))* Ms
Fm00 = ((K*R00)/(Kr))* Ms


print("")
print("Forces only due to momments")
print("Force in outer circle=",Fm2/1000,'kN')
print("Force in inner circle=",Fm1/1000,'kN')
print("Force in innerer circle=",Fm0/1000,'kN')

print("")
Fm2 = Fm2 + (((V/n)**2) + ((N/n)**2))**0.5
Fm1 = Fm1 + (((V/n)**2) + ((N/n)**2))**0.5
Fm0 = Fm0 + (((V/n)**2) + ((N/n)**2))**0.5
Fm00 = Fm00 + (((V/n)**2) + ((N/n)**2))**0.5


print("Forces total")
print("Force in outer circle=",Fm2/1000,'kN')
print("Force in inner circle=",Fm1/1000,'kN')
print("Force in innerer circle=",Fm0/1000,'kN')
print("Force in innerest circle=",Fm00/1000,'kN')

Kr2 = 6*(N2*K*(R2**2))
Kr1 = 6*(N1*K*(R1**2))
Kr0 =  6*(N0*K*(R0**2))
Kr00 = 6*(N00*K*(R00**2))
print("Largest circle stiffness=", Kr2/1000000,'kNm/rad')
print("Large circle stiffness=",Kr1/1000000,'kNm/rad')
print("Medium circle stiffness=",Kr0/1000000,'kNm/rad')
print("Small circle stiffness=",Kr00/1000000,'kNm/rad')
print("")
print("Total stiffness=",(Kr2+Kr1+Kr0+Kr00)/1000000,'kNm/rad')
```

```
Stiffness of dowel plane= 8707.047219783788 N/mm
Rotational stiffness per shear plane= 67178569795.70034 Nmm/rad

Forces only due to momments
Force in outer circle= 18.67444956045843 kN
Force in inner circle= 14.985669400367877 kN
Force in innerer circle= 11.296889240277322 kN

Forces total
Force in outer circle= 28.912901286525354 kN
Force in inner circle= 25.224121126434802 kN
Force in innerer circle= 21.535340966344243 kN
Force in innerest circle= 17.84656080625369 kN
Largest circle stiffness= 222795.0535551056 kNm/rad
Large circle stiffness= 115879.91468629749 kNm/rad
Medium circle stiffness= 50173.48889928211 kNm/rad
Small circle stiffness= 14222.96163351682 kNm/rad

Total stiffness= 403071.418774202 kNm/rad
```

```
import numpy as np
import matplotlib.pyplot as plt
%matplotlib inline
pre = 1 #predrilled 1= yes, 0= no
d = 16 #mm diamter bolt
fuk = 1000 #MPa ultimate strength dowel
a1=  1.5708 # Radians, grain angle
rho = 445 #density of woodses
t1= 220 #embedment depth
t2 = 730 # Total width of wood element
t= 25 #mm Thickness of plate
FvEd= 28.912901286525354 #kN
FaxEd= 0 #kN
FvEd2 = 60.826 #kN
Faxrk = 1 # 1 for no extraction
alphav = 0.5 # Table 3.4 from EN 1993-1-8
ym2 = 1.25 #safety factor Steel ULS connections
k2 = 0.9 #Table 3.4 from EN 1993-1-8
Ax = 1 # No extraction as attached at ends
```

```
Myrk = 0.3*fuk*(d**2.6)
As = 0.25 * np.pi * (d **2)

if pre ==0:
    fhk = 0.082*rho*(d**(-0.3))
if pre == 1:
    fhk = 0.082*(1-0.01*d)*rho

print("Stuiksterkte, fhk=",fhk,'MPa')

k90= 1.35+0.015*d

fh1k= fhk/(k90*((np.sin(a1))**2)+((np.cos(a1))**2))
print("embedment strength 1=",fh1k,"MPa")
```

```
Fvrkf = fh1k*t1*d
Fvrkf = 0.25*Ax*Fvrkf + Fvrkf
Fvrdf = Fvrkf/1300
print("Failure mode f=",Fvrdf,'kN')
Fvrkg= fh1k*t1*d*(((2+(4*Myrk)/(fh1k*d*(t1**2)))**0.5)-1)
Fvrkg = Fvrkg + 0.25*Ax*Fvrkg
Fvrdg= Fvrkg/1300
print("Failure mode g=",Fvrdg,'kN')
Fvrkh = 2.3 * ((Myrk*fh1k*d)**0.5)
Fvrkh = Fvrkg + 0.25*Ax*Fvrkh
Fvrdh = Fvrkh/1300
print("Failure mode k=",Fvrdh,'kN')

UC = FvEd/(min(Fvrdg,Fvrdh, Fvrdf))
print(UC)
```

```
Failure mode f= 65.2477213356 kN
Failure mode g= 29.498856408 kN
Failure mode k= 34.4445715769 kN
0.980136344494
```

```
# Check, EN 1993-1-8, 3.6.1; bolt subjected to shear and tensile force
if boltcheck ==1:
    Fvrdb =  ((alphav*fuk*(0.25*np.pi*(d**2)))/ym2)/1000
    print("Bolt shear resistance=", Fvrdb,"kN")
    Ftrd = (k2*fuk*As)/(ym2*1000)
    print("Bolt tensile resistance=",Ftrd,'kN')
    UC1 = FvEd/Fvrdb + (FaxEd/(1.4*Ftrd))
    print("Unity check, bolt on shear and tension=",UC1)
```

```
Bolt shear resistance= 407.15040790523716 kN
Bolt tensile resistance= 732.870734229427 kN
Unity check, bolt on shear and tension= 0.17475114507698078
```

Appendix F: Calculation of Timber Bridge Durability

Annual exposure dose and free driving rain for the Netherlands

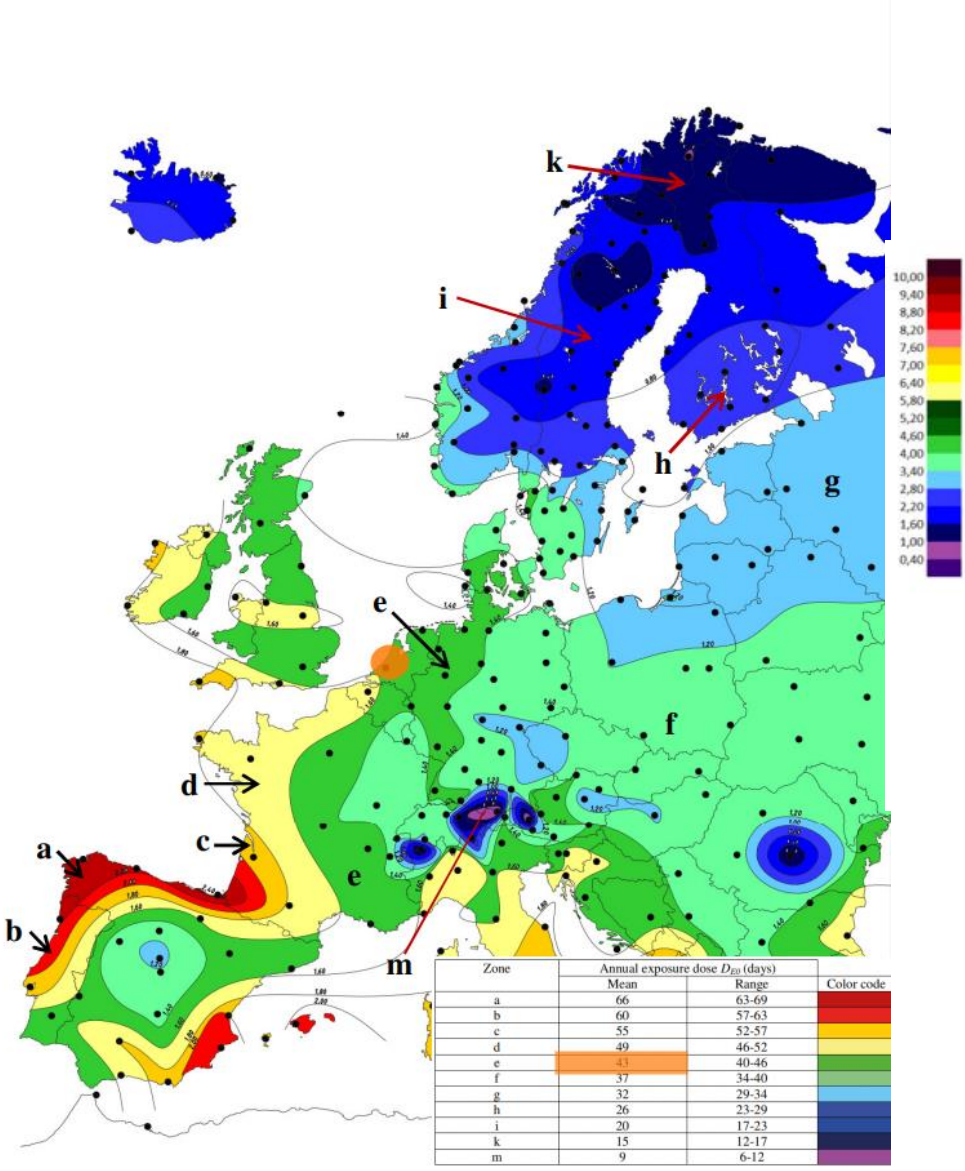

Zone	Annual exposure dose D_{E0} (days)		
	Mean	Range	Color code
a	66	63-69	
b	60	57-63	
c	55	52-57	
d	49	46-52	
e	43	40-46	
f	37	34-40	
g	32	29-34	
h	26	23-29	
i	20	17-23	
k	15	12-17	
m	9	6-12	

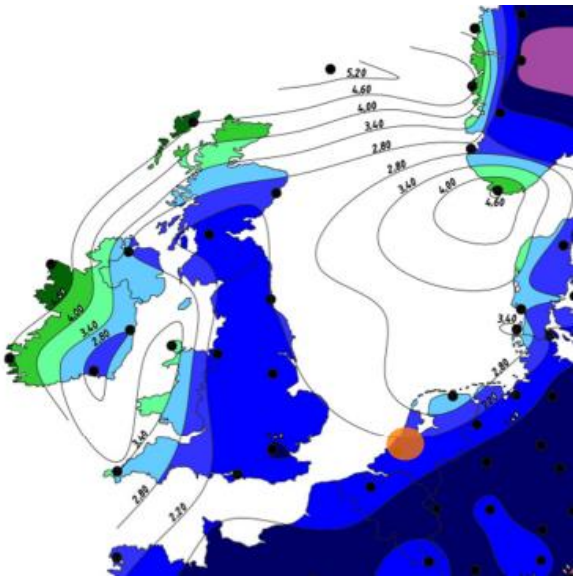

Outer Main beam to HEA connection

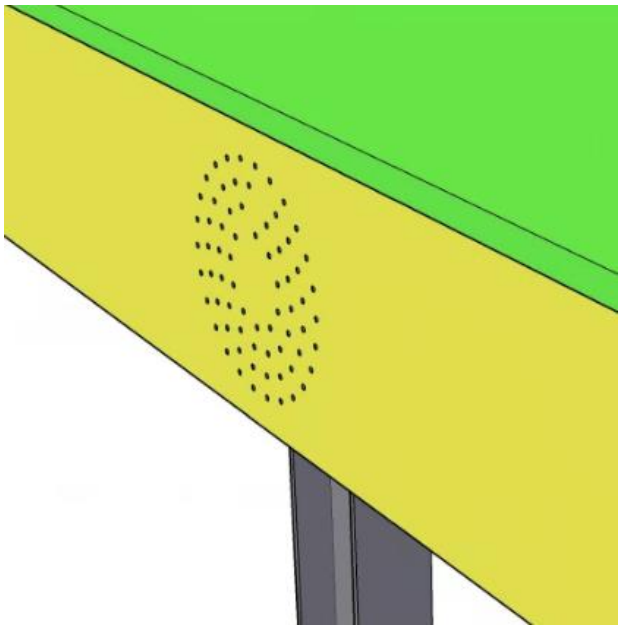

Factor k_{E1}

Degree of exposure	Protective effects are present	Driving rain expected at the site	k_{E1}
Light	Yes	No	0.8
Medium	Yes	Yes	0.9
Medium	No	No	0,9
Severe	No	Yes	1.0

[1]For horizontal rain-exposed surfaces $k_{E1} = 1{,}0$ should be chosen.

Factors $k_{E2},\ k_{E3}$

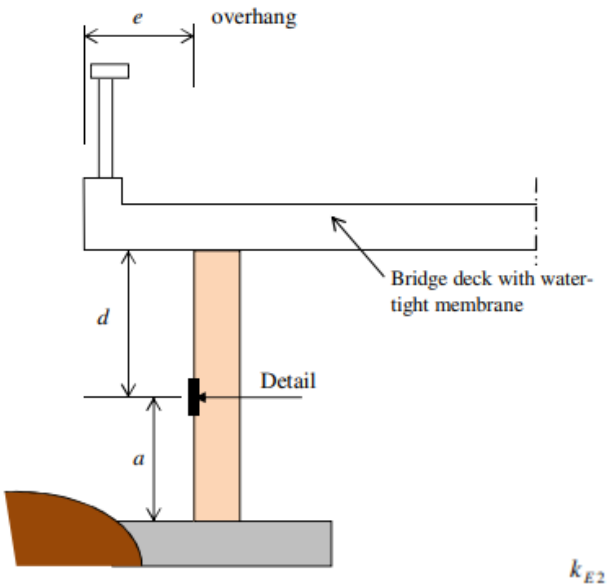

$k_{E2} = 1 - 0{,}2\frac{e}{d}$ if $0 < \frac{e}{d} \leq 1$

$k_{E2} = 0{,}8$ if $\frac{e}{d} > 1$

$k_{E3} = \frac{700 - a}{300}$ if $100 < a \leq 400mm$

$k_{E3} = 1{,}0$ if $a > 400$ mm

$$k_{E2} = 1 - 0{,}2 * \frac{e}{d} \; if \; 0 < \frac{e}{d} \leq 1$$

$$k_{E2} = 0{,}8 \; if \; \frac{e}{d} > 1$$

$$k_{E3} = \frac{700 - a}{300} \; if \; 100 < a \leq 400$$

$$k_{E3} = 1{,}0 \; if \; a > 400 \; mm$$

$$\frac{e}{d} = 0$$

$$a > 400 \; mm$$

$$k_{E2}, = k_{E3} = 1$$

Factor k_{E4}

Class	Description	Example	k_{E4}
Excellent	Design characterized by excellent ventilation (air gap > 10 mm) and no standing water. For example: a vertical surface without connecting members or with sufficient gap between members[1]	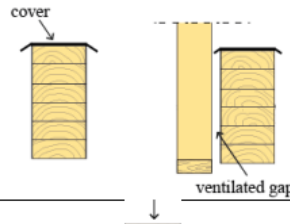	0,8
Good	Design characterized by excellent ventilation but standing water after rain events. For example: horizontal surface without connecting member.		1,0
Medium	Design characterized by poor ventilation but limited exposure to water. For example, vertical contact areas without sufficient air gap.	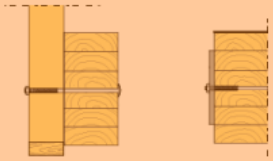	1,25
Fair	Design characterized by poor ventilation and high exposure to water **or** end-grain with good ventilation and limited exposure to water.[1] For example: horizontal contact areas and end-grain with sufficient air gap.	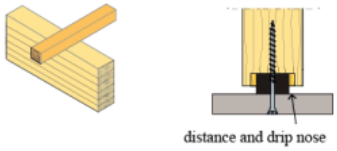	1,5
Poor	Design characterized by exposed end-grain with no ventilation and very high exposure to water. For example: end-grain contact area without air gap.	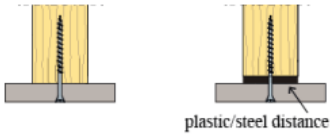	2

[1)] It is assumed that the gap is kept completely free from dirt and vegetation

Design exposure:

$$D_{Ed} = k_{E1} * k_{E2} * k_{E3} * k_{E4} * c_a * \gamma_d * D_{E0} = 1 * 1 * 1 * 1{,}25 * 1 * 43 = 53{,}75\ days$$

Lifetime prediction:

$$\frac{D_{Rd}}{D_{Ed}} = \frac{1716}{53{,}75} \cong 32\ years$$

Appendix G: ECI Calculation

Note that structural steel impact is assumed as 21% secondary steel (average trade mix in the Netherlands)

Steel Bridge

Element	Material/ Treatment	Unit	Unit price (€)	Unit amount	Cost indicator (€)
All Bridge Members	S355/ FE470 Steel	Kilogram	0,20	117e3	23400
Longitudinal Beams	MAG Weld 0,167 kg/m electrode	Meter	0,156	264,4	41,25
Shear Support	MAG Weld 0,167 kg/m electrode	Meter	0,156	12,2	1,9
Troughs	MAG Weld 0,167 kg/m electrode	Meter	0,156	826,6	128,95
Cross Beams	MAG Weld 0,167 kg/m electrode	Meter	0,156	351,8	54,88
End Plates	MAG Weld 0,167 kg/m electrode	Meter	0,156	101,2	15,8
Paint system C3.09	Zn (R) 60 to 80 µm Primer	Square meter	1,13	962,4*7	7612,6
Paint system C3.09	Solvent Based paint, transparent	Kilogram	3,26	215,6*7	4920

Timber Bridge

Element	Material/ Treatment	Unit	Unit price (€)	Unit amount	Cost indicator (€)
All Timber Elements	FSC/ PEFC Larch	Kilogram	0,05	54e3	2704,5
Deck	MF Resin	Kilogram	0,74	171,1	126,62
Main Beams	MF Resin	Kilogram	0,74	1604,7	1187,53
Inner Cross Beams	MF Resin	Kilogram	0,74	272,6	201,72
Outer Cross Beams	MF Resin	Kilogram	0,74	31,9	23,6
Outer Cross Beam Brackets	S250 / FE360 Steel	Kilogram	0,20	174,6	69,8
Outer Cross Beam Brackets	Hot- dip Zinc Galvanizing	Square Meter	1,71	2,96	5,1
Outer Cross Beam Brackets M22 Dowels	42CrMo4 Steel	Kilogram	0,27	85,4	23
Inner Cross Beam Shear Only Brackets	S250/ FE360 Steel	Kilogram	0,20	2046	409,2
Inner Cross Beam Shear Only Brackets	Hot- dip Zinc Galvanizing	Square Meter	1,71	17,37	29,7
Inner Cross Beam Shear Only Brackets M22 Dowels	42CrMo4 Steel	Kilogram	0,27	480,2	129,6
Inner Cross Beam Shear/ Tension Brackets	S250/ FE360 Steel	Kilogram	0,20	1766,4	353,28
Inner Cross Beam Shear/ Tension Brackets	Hot- dip Zinc Galvanizing	Square meter	1,71	15,1	25,77
Inner Cross Beam Shear/ Tension Brackets M22 Dowels	42CrMo4 Steel	Kilogram	0,27	384.1	103,7
Inner Cross Beam Shear/ Tension Brackets M36 Dowels	42CrMo4 Steel	Kilogram	0,27	106,93	28,9
Steel Plates in Abutment	S355/ Fe470 Steel	Kilogram	0,20	3785,6	757,12
Support Cables	55CrV4 Steel	Kilogram	0,41	32,8e3	13450,6
HEA 450 Profiles	S355/ FE470 Steel	Kilogram	0,20	1090,5	218,1
HEA 450 to Main Beam Steel Connector	S355/ FE470 Steel	Kilogram	0,20	3796	759,2
HEA 450 to Main Beam M16 Dowels	42CrMo4 Steel	Kilogram	0,27	668,4	180,5

Appendix H: Alternative Timber Bridge Systems Force/ Stress Distribution

Main beam force distribution envelopes

High depth superstructure

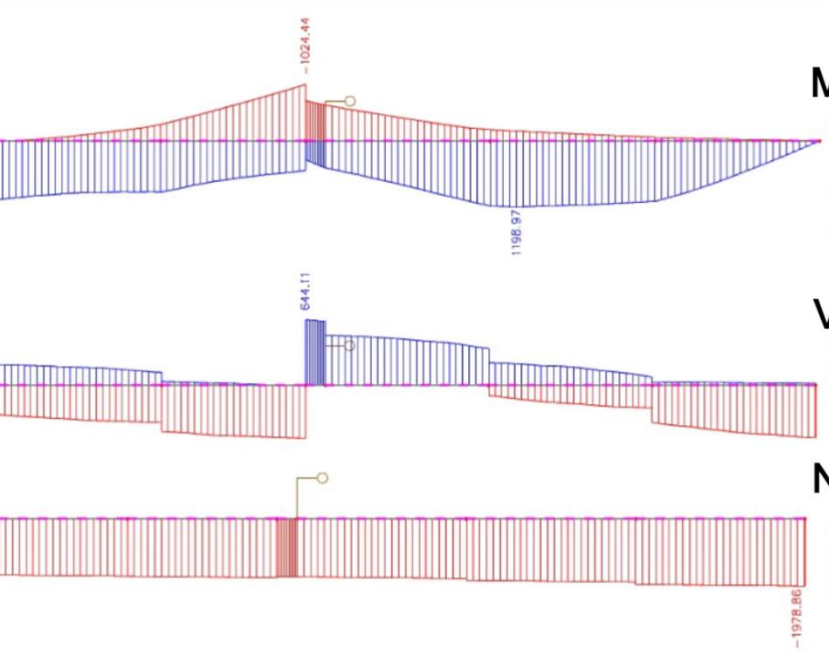

Low depth superstructure

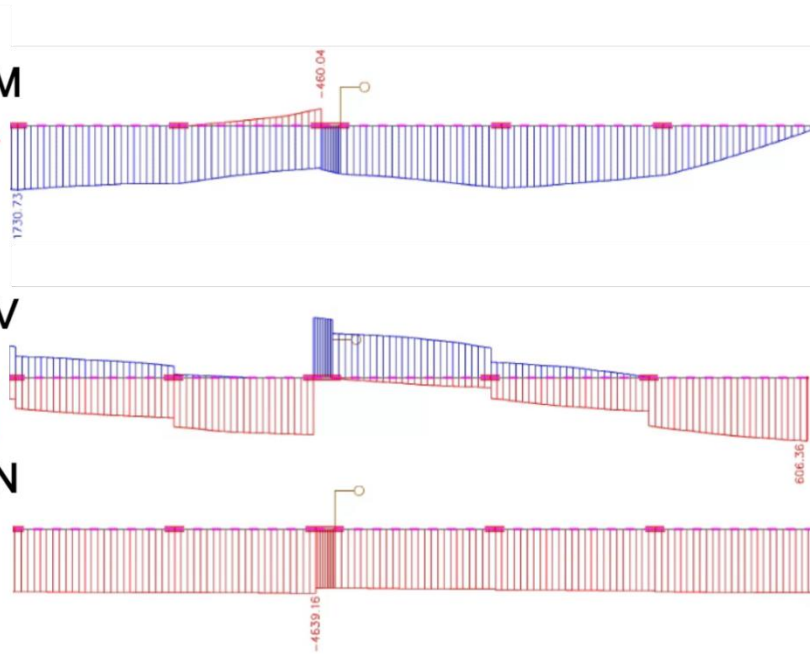

Hinged connection

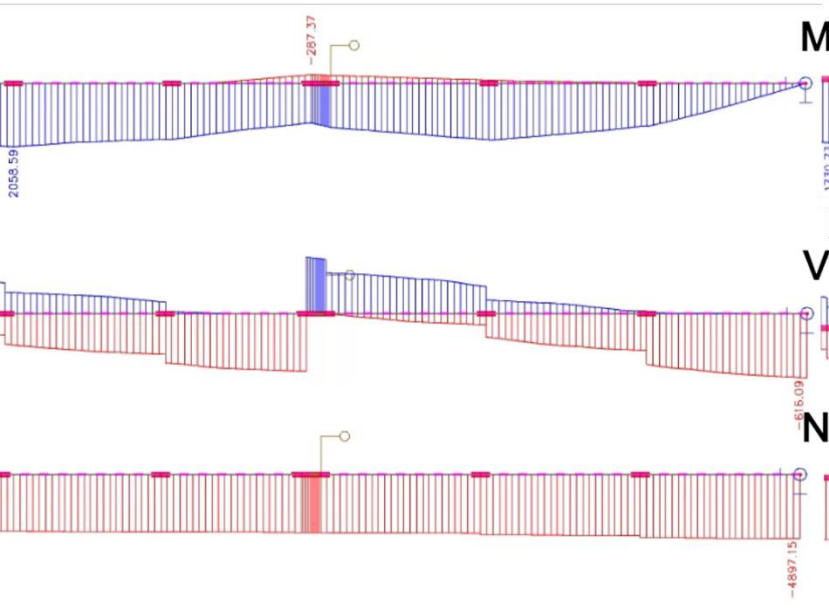

Moment Resisting Connection

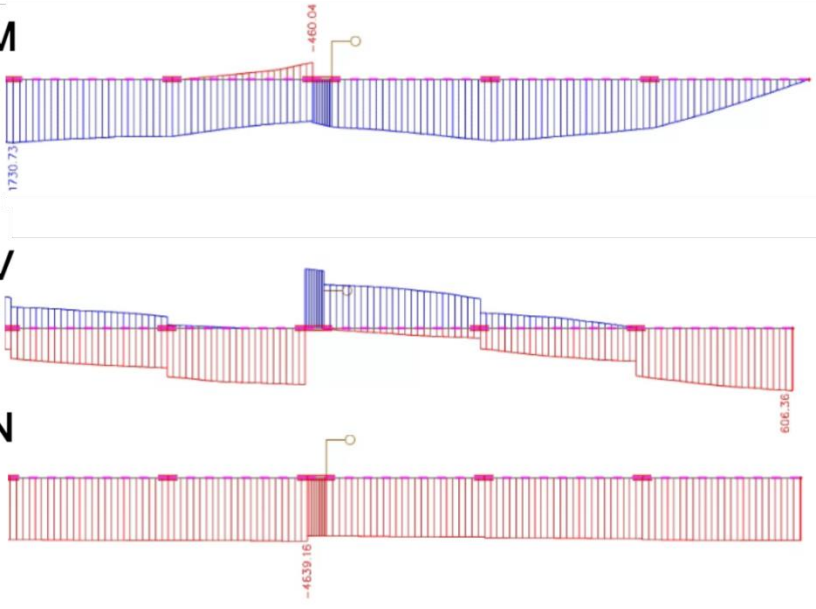

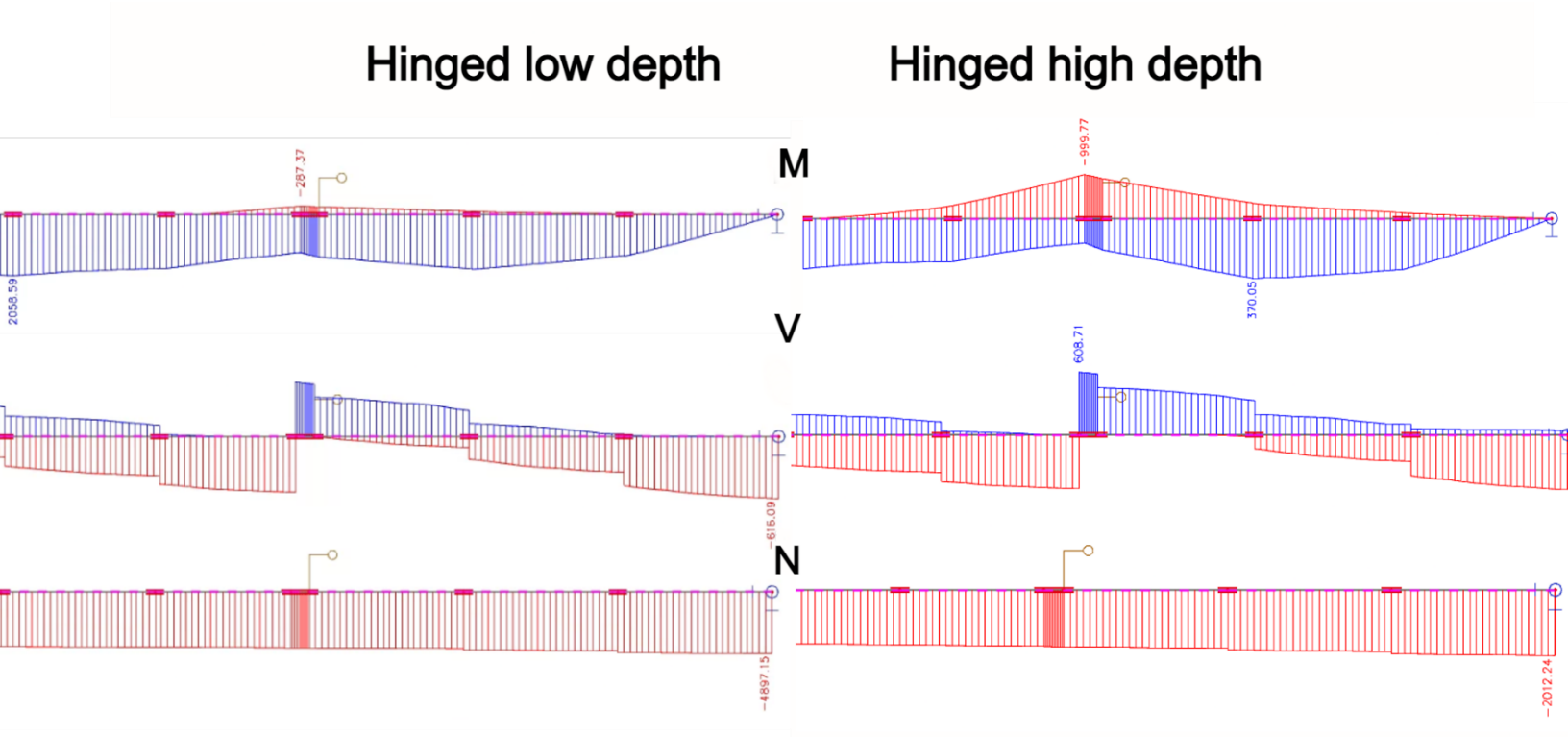

Main beam (hybrid) stress distribution mid span envelope, UC, and bill of material of all main beams

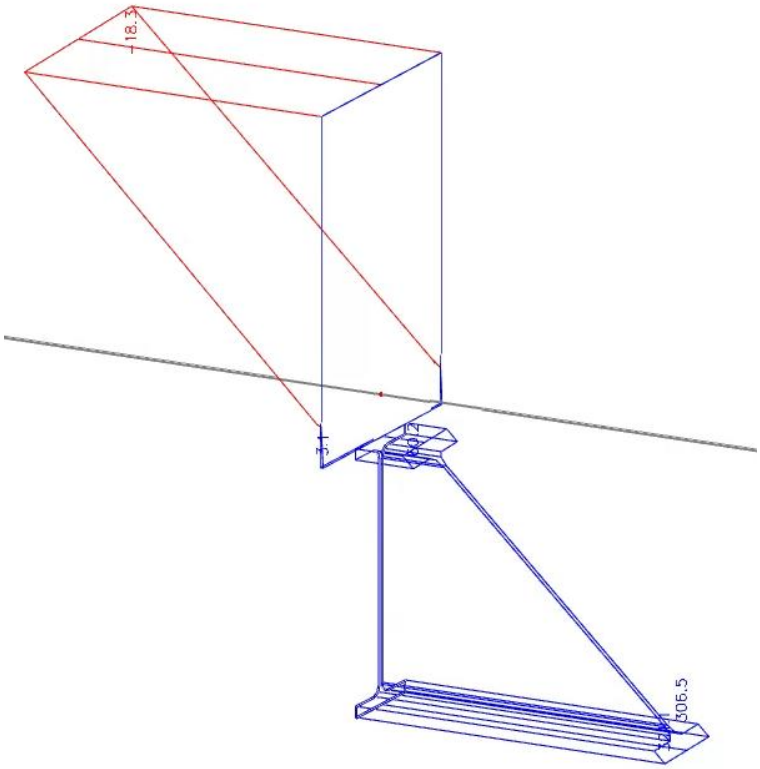

$$UC = \frac{f_{ed}}{\frac{f_k * k_{mod}}{\gamma_m}} = \frac{18{,}3}{\frac{26 * 0{,}9}{1{,}25}} \approx 0{,}98$$

Selectie: S2, S3, S39, S665

Materiaal	Massa [kg]	Oppervlak [m²]	Volume [m³]
Staal	26244.1	0.000	3.3432e+00
Hout	34109.3	567.326	7.6650e+01
Totaal	60353.3	567.326	7.9993e+01